Multi-objective Smart Charge Control of Electric Vehicles

Ridoy Das

A thesis submitted in partial fulfilment
of the requirements of the
University of Northumbria at Newcastle
for the degree of
Doctor of Philosophy

Research undertaken in the Faculty of Engineering and Environment

Department of Mathematics, Physics and Electrical Engineering

December 2019

“Satisfaction lies in the effort, not in the attainment”

- Mahatma Gandhi

“Some attainment every now and then is also appreciated“

- Ridoy Das

Dedication and Appreciation

I would like to dedicate this thesis to my loving parents who have supported me in every moment and guided me through the ups and downs that life brought. I warmly express my appreciation to my partner, Melody, who has patiently endured my variable mood in these tough three years and lovingly told me every time to not give up. My humble gratitude goes to Professor Ghanim Putrus, who relentlessly supervised my work from the very early days and showed me the way of becoming a better researcher. To Richard Kotter, I would like to say thanks for accompanying me through uncountable deadlines and for the inspiring conversations. To Professor Krishna Busawon goes my endless appreciation for guiding me in the path of thorough research and for being more than a supervisor, in fact a true friend. I would also like to thank Dr. Mousa Marzband for supporting me throughout the doctorate. To Edward and Daniel (Xuewu) I express my gratefulness for the help, memorable moments and innumerable laughs.

Declaration

I declare that the work contained in this thesis has not been submitted for any other award and that it is all my own work. I also confirm that this work fully acknowledges opinions, ideas and contributions from the work of others.

Any ethical clearance for the research presented in this thesis has been approved. Approval has been sought and granted by the Faculty Ethics Committee on 20/10/2017

I declare that the Word Count of this Thesis is 62,635 words.

Name: Ridoy Das

Signature: 

Date: 15/06/2020

Acknowledgements

I would like to acknowledge the EU – Interreg North Sear Region programme - Smart clean, Energy and Electric Vehicles for the City (SEEV4-City) project J-No.: 38-2-23-15, for sponsoring this PhD and providing useful data and an experimental ground for the development that supported the current research work.

Abstract

With the increasing integration of electric vehicles and renewable energy sources in electricity networks, key opportunities in terms of a cleaner environment and a sustainable energy portfolio are unlocked. However, the widespread deployment of these two technologies, can entail significant challenges for the electricity grid and in a larger context for the society, when they are not optimally integrated. In this context, smart charging of electric vehicles and vehicle-to-grid technologies are being proposed as crucial solutions to achieve economic, technical and environmental benefits in future smart grids. The implementation of these technologies involves a number of key stakeholders, namely, the end-electricity user, the electric vehicle owner, the system operators and policy makers. For a wider and efficient implementation of the smart grid vision, these stakeholders must be engaged and their aims must be fulfilled. However, the financial, technical and environmental objectives of these stakeholders are often conflicting, which leads to an intricate paradigm requiring efficient and fair policies. With this focus in mind, the present research work develops multi-objective optimisation algorithms to control the charging and discharging process of electric vehicles. Decentralised, hybrid and real-time optimisation algorithms are proposed, modelled, simulated and validated. End user energy cost, battery degradation, grid interaction and CO_2 emissions are optimised in this work and their trade-offs are highlighted. Multi-criteria-decision-making approaches and game theoretical frameworks are developed to conciliate the interests of the involved stakeholders. The results, in the form of optimal electric vehicle charging/discharging schedules, show improvements along all the objectives while complying with the user requirements. The outcome of the present research work serves as a benchmark for informing system operators and policy makers on the necessary measures to ensure an efficient and sustainable implementation of electro-mobility as a fundamental part of current and future smart grids.

Contents

Contents ix
List of Publications xiii
List of Figures xiv
List of Tables xix
Nomenclature 21
Chapter 1 Introduction 23
1.1 Background 23
1.2 Electric vehicle deployment 28
1.3 Renewable energy sources deployment 32
1.4 Lithium-ion batteries for EVs 35
1.5 Scope of research 40
1.6 Aims and objectives of the research work 41
1.7 Original contributions 41
1.8 Outline of the thesis 42
Chapter 2 Assessment of the State-of-the-Art on economic feasibility of V2G and Smart Charging 44
2.1 Introduction 44
2.2 Literature review motivations and structure 45
2.3 Literature review on economic feasibility of V2G 48
2.4 Review of the impact of smart charging and V2G on distribution networks 60
2.5 Transportation compatibility for V2G implementation 63
2.6 Optimisation strategies applied to charging scheduling 65
2.7 Conclusions 68
Chapter 3 Modelling of a synergetic EV-RES integration framework 70
3.1 Introduction 70
3.2 Modelling EV utilisation pattern 75

3.3 Modelling electricity demand and PV generation 84
3.3.1 Modelling of electricity demand 85
3.3.2 Partitioning of electricity demand data using k-means clustering 87
3.3.3 Modelling of PV generation 90
3.3.4 Prediction of PV power output using ANN 90
3.4 Modelling of grid impact in distribution networks 92
3.5 Modelling CO_2 emissions 95
3.6 Modelling ancillary service provision 101
3.7 Conclusions 108
Chapter 4 Modelling Degradation in Lithium-Ion batteries 109
4.1 Introduction 109
4.2 Development of an equivalent circuit model 118
4.2.1 Development of a self-adaptive ECM model 125
4.3 Development of a dynamic empirical capacity fade model for Lithium-Ion batteries 129
4.3.1 Extension to a self-adaptive capacity fade model 148
4.4 Conclusions 150
Chapter 5 Development of an optimisation framework for smart EV charging scheduling 152
5.1 Introduction 152
5.2 Single-objective optimisation 153
5.2.1 Solution of a mathematical optimisation problem 153
5.3 Multi-objective optimisation 157
5.3.2 Multi-criteria-decision-making with analytical hierarchy process 162
5.4 Conclusions 165
Chapter 6 Application of Multi-objective optimisation to electric vehicles in distribution networks 166
6.1 Introduction 166
6.2 Decentralised Multi-Objective optimisation 167
6.2.1 Assumptions for the mathematical model 173
6.2.2 Analytical formulation 175
6.2.3 Energy cost minimisation 176
6.2.4 Battery degradation minimisation 176
6.2.5 Grid net exchange minimisation 176
6.2.6 CO_2 emission minimisation 177

6.2.7 Constraints of the optimisation – EV model 179
6.2.8 Results and discussion 180
6.2.9 Results of case study 3 for cross-case comparison 197
6.3 Game-theoretical Multi-Objective optimisation in a local energy market 198
6.3.1 Methodology 202
6.3.2 Development of a non-cooperative game theoretical energy trading system 208
6.3.3 Results and discussion 210
6.4 Assesment of economic feasibility of V2G services 215
6.5 Conclusions 220
Chapter 7 Implementation of real-time multi-objective optimisation in a micro-grid 223
7.1 Introduction 223
7.2 Design of a real-time controller based on Multi-objective dynamic programming 231
7.3 Graphical user interface 236
7.4 Functional demonstration experiments 238
7.5 Comparison between OMODP and ANEC 243
7.6 Conclusions 246
Chapter 8 Conclusions and future works 247
8.1 Future works 250
References 251
Appendix A Appendix A-1
A.1 Distribution network modelling A-1
A.2 Definition of a mathematical optimisation problem A-5
A.3 Algorithms for mathematical optimisation A-8
A.4 Setting for case study 2 ..... A-10
A.5 Decentralised MOO results A-13

List of Publications

Journals

[P1] **R. Das**, Y. Wang, G. Putrus, R. Kotter, M. Marzband, B. Herteleer and J. Warmerdarm, *Multi-objective Techno–Economic–Environmental Optimisation of Electric Vehicles for Energy Services*, Applied Energy, vol. 257, 2020.

[P2] Y. Wang, **R. Das**, G. Putrus and R. Kotter, *"Economic evaluation of photovoltaic and energy storage technologies for future domestic energy systems – A case study of the UK",* Energy, vol. 203, 2020.

[P3] A. Paladin, **R. Das**, Y. Wang, G. Putrus, R. Turri and R. Kotter, *Micro Market based Optimisation Framework for Decentralised Management of Renewable Energy Sources, Storage and Electric Vehicles*. (submitted to Renewable Energy special issue "RES to drive EVs")

[P4] E. Bentley, R. Kotter, Y. Wang, **R. Das** and G. Putrus, *Pathways to energy autonomy – challenges and opportunities*, Internation Journal of Environmental Studies, Sep 2019.

Conferences

[P5] **R. Das**, Y. Wang, G. Putrus and K. Busawon, *Modelling the State of Charge in Lithium-ion Batteries*, 53rd University Power Engineering Conference (UPEC), Glasgow, Sep 2018.

[P6] M. Nicoli, **R. Das**, Y. Wang, G. Putrus, R. Kotter and R. Turri, *A Smart Grid Modelling Tool for Evaluating Optimal Control of Electric Vehicles*, 53rd University Power Engineering Conference (UPEC), Glasgow, Sep 2018.

[P7] A. A. Al-Karakchi, G. Putrus and **R. Das**, *Smart EV Charging Profiles to Extend Battery Life*, 53rd University Power Engineering Conference (UPEC), Crete, 2017.

[P8] R. Van den Hoed, J. Van der Hoogt, B. Jablonska, E. Van Bergen, R. Prateek, G. Putrus, R. Kotter, **R. Das** and Y. Wang, *Lessons Learnt – A cross-case analysis of six, real-time Smart Charging and V2X Operational Pilots in the North Sea Region*, EVS32, May 2019.

List of Figures

Figure 1.2-1 National EV stock 29
Figure 1.2-2 BEV national stock 29
Figure 1.2-3 New national BEV registrations 30
Figure 1.2-4 Deployment scenarios for global EV stock for 2030 31
Figure 1.2-5 EV numbers in the UK for the four scenarios 31
Figure 1.3-1 Global installed power capacity 33
Figure 1.3-2 UK FIT rate for PV systems up to 10kW 34
Figure 1.4-1 Dimensions of Li-Ion battery performance 36
Figure 1.4-2 Technical specifications of common Lithium-Ion batteries 36
Figure 1.4-3 Breakdown of the costs for the components of a battery pack 37
Figure 1.4-4: Li-ion battery cost history 2011-2016 38
Figure 1.4-5: Li-ion battery cost trends and estimates 39
Figure 1.4-6 Technical characteristics of the most advanced battery technologies for stationary storage purpose [25] 39
Figure 2.3-1 Profits from V2G provision in chronological order 53
Figure 2.3-2 Battery investment costs considered in different studies in chronological order 55
Figure 2.3-3 Service payments considered in research works in chronological order 56
Figure 2.3-4 Clusters of the research works according to different parameters 58
Figure 3.1-1 Stakeholders involved in the electricity system with physical connection, business and policy relationships 71
Figure 3.1-2 Stakeholders involved in the framework of multi-objective optimisation of EV charging 72
Figure 3.1-3 Multi-objective EV-RES integration model 74
Figure 3.2-1 Distribution of daily driven mileage for ten years 2009-2018 76
Figure 3.2-2 Distribution of trip start time throughout an average week from 2014-2018 in the UK 77
Figure 3.2-3 Distribution of trip start time for an average week for 2014-2018 for different purposes in the UK 78

Figure 3.2-4 Distribution of charge start time for different locations in European cities 79
Figure 3.2-5 Distribution of SOC upon plugging-in for European cities 80
Figure 3.2-6 Parameter fitting of departure and arrival probabilities for weekdays, Saturday and Sunday 83
Figure 3.2-7 Parameter fitting for daily travelled miles 84
Figure 3.3-1 Average UK electricity demand profiles for four seasons, weekdays and weekends 86
Figure 3.3-2 Typical single household electricity demand profile 86
Figure 3.3-3 Average variation within clusters for increasing number of clusters 88
Figure 3.3-4 Partition of daily electricity demand in ten clusters 89
Figure 3.3-5 Training results of an ANN for PV generation forecast 91
Figure 3.4-1 Illustration of a typical electricity system 92
Figure 3.4-2 Block model of the distribution network with generation and load buses 94
Figure 3.5-1 CO_2 emission caused by the UK national energy mix 96
Figure 3.5-2 Power generation variation for Coal, Nuclear, CCGT, Wind, Pumped-hydro, Hydro, Biomass and OCGT 99
Figure 3.6-1 Average payment for UK ancillary services in 2018/2019 104
Figure 3.6-2 Droop control for different frequency deviation ranges 105
Figure 3.6-3 Example of frequency regulation provision with smart charging and bidirectional charging 107
Figure 4.1-1 Lithium-ion charging/discharging process 110
Figure 4.1-2 Lithium-ion battery degradation reactions 112
Figure 4.1-3 Adaptive battery degradation model functional diagram 118
Figure 4.2-1 ECM of Lithium-ion battery 119
Figure 4.2-2 One-time constant ECM model 120
Figure 4.2-3 CC-CV charging process 120
Figure 4.2-4 Variation of open-circuit voltage with respect to battery capacity 122
Figure 4.2-5 Output of the ECM model 125
Figure 4.2-6 Internal resistance increase due to battery cycling 126
Figure 4.2-7 Functional diagram for the self-adaptive ECM model 127
Figure 4.2-8 Adaptive ECM model output against real voltage measurement 128
Figure 4.2-9 Fitted ECM parameter increase throughout the life of a battery 128
Figure 4.3-1 Storage degradation coefficient as a function of temperature and SOC 132
Figure 4.3-2 Equivalent accelerated battery degradation curves for different storage states 133
Figure 4.3-3 Example of a daily EV battery utilisation pattern 134

Figure 4.3-4 Experimental setup for battery testing: (a) Arbin charger, (b) Neware charger, (c) environmental chamber, (d) battery typed B, (e) battery type A, (f) sample of cycling data and (g) testing software....137
Figure 4.3-5 Cycling degradation tests for type A cells....138
Figure 4.3-6 Cycling degradation tests for type B cells at different charging rates....139
Figure 4.3-7 Internal resistance for the three type B cells....140
Figure 4.3-8 Behaviour of cycling degradation coefficient with respect to the impacting parameters....141
Figure 4.3-9 Graphical representation of lifetime energy throughput....144
Figure 4.3-10 Average daily temperature and SOC....145
Figure 4.3-11 Minute based current, temperatures and SOCs....146
Figure 4.3-12 Calendar degradation model output....146
Figure 4.3-13 Cycling degradation model output....147
Figure 4.3-14 Comparison between measured SOH and model output....147
Figure 4.3-15 Prediction error of the self-adaptive capacity fade model....150
Figure 5.3-1 Conflicts between two objective functions....158
Figure 5.3-2 Convex Pareto frontier for two objectives....159
Figure 6.2-1 MOTEEO framework for single H-MG....172
Figure 6.2-2 MOTEEO framework for a distribution network....173
Figure 6.2-3 Flowchart of the proposed MOTEEO framework....175
Figure 6.2-4 Generic mathematical functions....178
Figure 6.2-5 EV availability and real-time price....182
Figure 6.2-6 EV scheduling for single-objective optimisations without FFR....185
Figure 6.2-7 EV scheduling for single-objective optimisation with FFR....186
Figure 6.2-8 Pareto front with ANEC without FFR....188
Figure 6.2-9 Pareto front with ANEC method with FFR....189
Figure 6.2-10 MOTEEO scheduling for scenario 2c) winter and spring....193
Figure 6.2-11 MOTEEO scheduling for scenario 2c) summer and autumn....194
Figure 6.3-1 Hybrid framework for the game-theoretical energy trading model....201
Figure 6.3-2 Depiction of the rolling window approach....207
Figure 6.3-3 Charging and discharging schedules of the 5 ESSs....212
Figure 6.3-4 Charging and discharging schedules of the 5 EVs....213
Figure 6.3-5 Wholesale market price (blue) and local market price (red) for one day of operation....214

Figure 6.3-6 Total power exchange of the ED with selfish optimisation and with the energy trading system 215
Figure 6.4-1 Sample of one day of scheduling under BAU and V2G case for all scenarios. 218
Figure 6.4-2 Cost comparison between BAU and V2G cases 219
Figure 7.1-1 Flow diagram for real-time scheduling of a micro-grid 224
Figure 7.1-2 Real-time multi-objective optimisation implementation setup 226
Figure 7.1-3 Bidirectional battery charger 228
Figure 7.1-4 Agilent current measurement probe 228
Figure 7.1-5 Low pass filter 229
Figure 7.2-1 Illustration of SOC states and feasible set 233
Figure 7.3-1 Graphical user interface to control charging in real-time 237
Figure 7.4-1 Real-time charging profile for case study 1 239
Figure 7.4-7.4-2 Pareto frontiers and chosen solutions in case study 1 240
Figure 7.4-3 Real-time charging profile for case study 2 240
Figure 7.4-4 Pareto frontiers and chosen solutions in case study 2 241
Figure 7.4-5 Real-time charging profile for case study 3 241
Figure 7.4-6 Pareto frontiers and chosen solutions in case study 3 242
Figure 7.5-1 Comparison between OMODP and ANEC profiles for a generic real-time operation case 244
Figure 7.5-2 Comparison between the normalised dynamic Pareto fronts achieved with OMODP 244
Figure 7.5-3 Comparison between the computational time of OMODP versus ANEC 245

List of Tables

Table 1.1-1 Different charging rating in Europe 27
Table 1.1-2 Different charging modes available in the market 28
Table 2.3-1 Summary of research works on feasibility of V2G 50
Table 3.2-1 Results of probability distribution parameter fitting 82
Table 3.3-1 Input data for ANN training 90
Table 3.5-1 Average CO_2 emission for different generation types 97
Table 3.6-1 Range of available reserve services in the UK 102
Table 3.6-2 Frequency regulation services in the UK 103
Table 4.2-1 ECM parameters for one period of CC charging 128
Table 4.3-1 Battery type and specifications 135
Table 4.3-2 Battery testing conditions 136
Table 4.3-3 Fitted parameters for the type A battery degradation model 142
Table 5.3-1 Random consistency index for different number of criteria 164
Table 6.2-1 case study and scenarios for MOTEEO 170
Table 6.2-2 Setting for the case study 1 180
Table 6.2-3 Parameters of the case study 2 184
Table 6.2-4 Results of the single-objective optimisations 187
Table 6.2-5 Decision matrix for different DMs 190
Table 6.2-6 Results of the MOTEEO method with the application of AHP 190
Table 6.2-7 Results of the MOTEEO method for eight days 195
Table 6.2-8 Results of the MOTEEO method with a utility function 197
Table 6.3-1 Game-theoretical energy trading case study setting 211
Table 6.3-2 Normalised losses with selfish optimisation and with the energy trading system 215
Table 6.4-1 System components for two comparison cases 216
Table 6.4-2 Assessment parameter categories for assessing economic feasibility of V2G (shaded parameters represent the base scenario) 216
Table 6.4-3 Economic parameters for the scenario analysis 217
Table 6.4-4 Cost breakdown for six V2G scenarios 219

Table 6.4-5 NPV for six V2G scenarios 220
Table 7.1-1 Main specifications of MG components 227
Table 7.1-2 Information provided by the user for MOO 229
Table 7.4-1 Details of the case studies 238
Table 7.5-1 Comparison between OMODP and ANEC's performance along three objectives for case 4 244

Nomenclature

AHP	Analytical Hierarchy Process	EVSE	Electric vehicle supply equipment
ANEC	Augmented Non-dominated epsilon constrained algorithm	FFR	Firm frequency response
ANN	Artificial neural network	FIT	Feed-in tariff
BAU	Business as usual	FR	Frequency regulation
BEV	Battery electric vehicles	GHG	Greenhouse gas
C	Consumer	GPU	Graphics processing unit
CC	Constant current	GUI	Graphical user interface
CCGT	Combined-cycle gas turbine	HEV	Hybrid electric vehicle
CSP	Concentrated solar-thermal power	HV	High voltage
CV	Constant voltage	ICE	Internal combustion engine
DM	Decision maker	IP	Interior point algorithm
DN	Distribution network	KKT	Karush-Kuhn Tucker conditions
DOD	Depth of discharge	LCOE	Levelised cost of energy
DP	Dynamic Programming	LFP	Lithium-iron phosphate
DS	Distribution system	LM	Local market
DSO	Distribution system operator	LMO	Lithium-manganese oxide spinel
ECM	Equivalent circuit model	LTO	Lithium-titanate
ED	Energy district	LV	Low voltage
ESS	Energy storage system	MCDM	Multi-criteria-decision-making
EU	European Union	MMC	Markov Chain Monte Carlo
EV	Electric vehicles	MFR	Mandatory frequency response

MG	Micro-grid	PJM	Pennsylvania-Jersey- Maryland
MMP	Memory base multi-path	PR	Prosumer
MOO	Multi-objective optimisation	PSO	Particle swarm optimisation
MOTEEO	Multi-objective techno-economic-environmental optimisation	PV	Photovoltaic
MPC	Model predictive control	PWM	Pulse width modulation
MV	Medium voltage	RES	Renewable energy source
NCA	Lithium-nickel-cobalt-aluminium	RET	Retailer
NI	Nikaido-Isoda function	SC	Self-consumption
NIRA	Nikaido-Isoda relaxation algorithm	SEI	Solid electrolyte interface
NMC	Lithium-nickel-manganese-cobalt	SOC	State of charge
NPV	Net present value	SOH	State of health
NSR	North Sea region	SS	Self-sufficiency
NTS	National travel survey	STLF	Short-term load forecasting
OCGT	Open-cycle gas turbine	STOR	Short time operating reserve
OCPP	Open charge point protocol	TOU	Time of use
OCV	Open circuit voltage	TSO	Transmission system operator
OEM	Original equipment manufacturer	UK	United Kingdom
OMODP	Online multi-objective dynamic programming	USD	United States Dollar
OSCP	Open smart charging protocol	V2G	Vehicle-to-grid
PEV	Plug-in electric vehicle	V2X	Vehicle-to-everything
PHEV	Plug-in hybrid electric vehicle		

When required, a list of variables has been provided in the relevant Sections.

Chapter 1 Introduction

1.1 Background

In recent years, a significant deployment of Electric Vehicles (EVs), such as cars (including taxis), vans and buses, is witnessed around the world. In most of the mature, industrialized and a range of developing countries, measures to facilitate the penetration of EVs in the car and van market are undertaken. Different countries have set ambitious targets concerning the share of EVs in their national fleets, although new registrations and penetration levels remain comparatively low.

The main drive for wide EV adoption comes from both environmental and public health concerns related to urban pollution, although energy security and geopolitics of energy sources can also be some of the motivations. According to the European Environment Agency [1], the major environmental impacts of internal combustion engine (ICE) vehicles include greenhouse gas (GHG), air pollution, and noise pollution (as well as land consumption for the transportation infrastructure). While GHG emissions from all other major economic sectors have fallen in recent decades, those from transport have increased. In the EU, road transport's GHG emissions are today around 17% above 1990 levels, while the contribution of road transport to total EU, GHG emissions has increased by around half — from 13% of the total in 1990 to almost 20% in 2014 [2]. By the substitution of ICEs (fuelled by benzene petrol or diesel), the aforementioned tailpipe emissions can be completely avoided using full battery EVs.

Furthermore, EVs can be a central enabling feature of smart grids and distributed energy use [3]. To this end, Vehicle-to-Grid (V2G) technologies have been considered as the most

advanced solution in terms of EV integration in the future electricity system [4]. As the penetration of EVs in the national car stocks of many countries is increasing at a relatively high pace [5], albeit from a very low base, with projections showing that this trend will continue, EVs must be integrated in the electricity network in an efficient way, as otherwise there will be stress on the electricity infrastructure. By 2040, 33% of the global light duty vehicle fleet (530 million by 2040) will be composed by EVs [5]. As a consequence, the electricity demand for EV charging will increase on a yearly basis, and this will require additional energy demand, which is estimated to be 1,800TWh by 2040 [5]. This will be a central issue to be addressed by the various national decision makers, balancing the needs of different stakeholders. In this context, a smart grid is argued to be one route to defer grid reinforcements [3].

In the near future, those countries where the EV uptake is growing, will have to meet the EV charging power demand requirement with additional generation assets. V2G technologies promise to alleviate this additional electricity demand, by changing the way in which EVs are perceived, from mere loads to smart storages for the grid [6]. In this context, EVs could be exploited as storage for the grid, to integrate a higher share of intermittent renewable energy sources (RES), such as solar photovoltaic (PV) and wind. The EVs and RESs will behave as part of an agglomeration of generation and storage assets, to provide network services for the grid.

In the V2G concept, EVs establish bidirectional energy exchange with the grid. They not only absorb energy but can also supply part of the stored energy. In the ideal case, EVs will absorb more energy than what is required for transportation requirement, in periods where the electricity is cheap or where the grid is underutilized. Conversely, when the electricity from the grid is costly or the grid is under stress at peak times, a suitable share of that energy will be supplied to the grid.

However, the V2G concept presents some barriers: The charging and discharging process implies an energy loss for the full charge/discharge cycle; with current round-trip (charging and discharging) efficiencies being in the range of 80-90%, the energy lost reduces the profit

margin for the prospective providers. Moreover, the ability to provide V2G services requires additional and more advanced charging infrastructure as compared to the current status, smart communication links with central management systems (and back-office) and the grid aided by a metering system [7]. Hence, the usefulness and profitability of such practice must be carefully assessed with a techno-economic analysis.

To employ V2G, some upgrades in the EV is required; for example, differently designed on-board power electronics for V2G and a real-time control system that allows the stakeholders demanding EV power to access the storage when needed. These additions to the basic EV charging setting translates into additional investment costs.

In addition, in order to participate in V2G services, EVs need to be idle (i.e. parked) and plugged-in at charging stations for periods that vary depending on the service that is opted for. During that time, those EVs will not be used for transportation, and this is in line with the usage patterns of most EVs, which are parked on average for 90-96% of the time on a daily basis according to several studies [8][9][10]. Strategic optimisation models covering a variety EV usage patterns will need to be developed to effectively exploit the whole set of potentially feasible V2G services.

Lithium-Ion batteries are the most popular solution for EVs [5]. However, despite their superior energy efficiency when compared with other batteries (for instance, above 90% [11] against 25-45% of the compressed air energy storage [12]), they have inherent shortcomings. The performance of Li-Ion batteries depends on the temperature, they are prone to self-discharge and crucially their performance degrades with usage [13]. Hence, when EVs are also exploited as storage solutions, their batteries incur extra utilization implied by the additional charging/discharging cycles. This results in a higher depreciation of the battery in time [14]. A range of services with suitable operating conditions [9] should be approached and the operation of the battery should always be optimised in order to minimise degradation.

As can be seen, EVs bring the remarkable opportunity for integrating the transportation and energy systems, but the question of how they should be managed/operated is in no way trivial. Optimal EV utilisation is a task that connects multiple areas, among which power

system operation, economics, energy and environmental sciences, chemical engineering and social sciences are the most essential ones. As the integration of EVs in the electricity network brings together a range of disciplines, multiple stakeholders will have to interact in this ecosystem. Understanding and analysing their behaviour and modelling their priorities is therefore of pivotal importance in a time where EVs have attracted the interest of different communities of users. While cooperation among different stakeholders can bring benefits, sometimes there will be inherent conflicts due to the very nature of the topic, which does not have a unique solution. An immediate example is the conflict that may arise between electricity system operators and EV users, each aiming to achieve divergent objectives. The system operator will pursue technically and economically optimal grid operation whereas the EV user will want to prioritise their transportation requirement while prolonging as much as possible the life of their asset; that is, the EV. The prerogatives of these two stakeholders cannot be simultaneously optimised as the system operator will expect the EV to be available for as long as possible, which may hinder the timing of the trips and the battery will undergo additional utilisation which will most probably lead to extra degradation. Conversely, if the EV user follows their own objectives, the grid may suffer due to the non-optimal operation.

This glimpse into this paradigm, which will be discussed in this thesis, accurately depicts a major challenge that future energy systems will need to resolve. Multiple conflicting objectives from different groups of stakeholders involved in future smart grids will need to be simultaneously optimised to ensure societal benefits. The need of finding a solution to this complex, yet exquisite, multi-faceted problem has motivated the undertaking of the present work.

To this end, multi-objective optimisation (MOO) is a topic that has recently gained considerable interest in the research community. Researchers and scholars have applied MOO in a variety of fields, ranging from economics, finance, engineering to water resource management among others. In this field, the trade-off among several conflicting objectives is mathematically depicted, and a set of optimal solutions is found.

EVs represent a large sector including several categories. There are several definitions around the types of EVs. However, the designation adopted throughout this thesis allows a clear

differentiation between plug-in and non-plug-in vehicles. Hereafter, plug-in electric vehicles (PEV) refer to those that allow grid connection to charge the on-board battery. This category includes battery electric vehicles (BEVs) and plug-in hybrid electric vehicles (PHEVs), with the latter being also supplied by an auxiliary ICE. Given the two types of energy (electricity and fuel) supply, the capacity of the battery of a PHEV is considerably smaller compared to that of a BEV. Outside the group of PEVs, hybrid electric vehicles (HEVs) are also available in the market (these cannot be plugged into the grid and only use regenerative breaking). The initial EV market was mainly composed by HEVs allowing regenerative breaking. However later on, PHEVs and BEVs rapidly took over. It is envisaged that the future EV market (2040 and 2050) will be primarily composed by BEVs as PHEVs are seen as a transition technology [15]. This perspective reinforces the idea of considering only BEVs for this research since it is a cleaner technology (for BEVs, the only power source is the grid electricity, which, in many countries, is cleaner than fossil fuels and offsets CO_2 emitted during battery manufacturing [5]) and more suitable for grid integration, due to the higher battery capacity.

As EVs become more popular, the market for EV charging system has also developed, with several protocols being adopted by the automotive original equipment manufacturers (OEM). The different charging systems can be classified according to the charging power, location of power electronic converter (on-board or off-board), type (AC or DC), and level of protection. Table 1.1-1 and Table 1.1-2 provide a useful classification of the different charging ratings and modes, respectively [16].

Table 1.1-1 Different charging rating in Europe [16]

Charge power	Connection	Power (kW)	Max current (A)	Location
Slow charging	1-phase AC connection	3.7	10-16	Domestic
Semi-fast charging	1-phase or 3-phase AC connection	3.7 - 22	16 - 32	Semi-public
Fast charging	3-phase AC or DC connection	>22	>32	Public

Table 1.1-2 Different charging modes available in the market [16]

Mode 1 (AC)	Slow charging from a standard household-type socket supplying up to 16 A (1-phase). There is a residual current device.
Mode 2 (AC)	Slow charging from a standard household-type socket (1 or 3-phase) up to 32 A per phase. An in-cable control box including restriction of the charging current and protection device is provided.
Mode 3 (AC)	Semi fast charging with dedicated 1 or 3-phase AC socket or EV connector with up to 70 A or 63 A per phase. Continuous protective earth conductor and continuity checking are provided and control of charging current is allowed.
Mode 4 (DC)	Fast DC charging from off-board electric vehicle supply equipment (EVSE). The charging cable is fixed and the charging post has inbuilt protection and control devices. Charging powers up to 120-170 kW.

As can be seen from Table 1.1-2, AC charging relies upon on-board charging equipment, and only provides the grid connection. In this category, two charging levels are available, from the standard domestic plug (level 1) to a maximum 7 kW connection (level 2). DC charging systems convert electricity from AC with off-board equipment and are usually characterised by high power.

1.2 Electric vehicle deployment

Major industrial powers as well as developing countries have identified EVs as essential assets to reduce the carbon footprint of national and global transportation systems, and pave the way for a more sustainable energy landscape. Fostered by the supporting policy, EV uptake soared globally with China, USA, Norway, the Netherlands, Japan and the UK leading the scene [5]. The EV phenomenon has started to take form around 2010, with uptake seeing an exponential growth. Evidence of this can be found in Figure 1.2-1, where the national EV stock is depicted for the UK, the Netherlands, Norway, Germany and Sweden [5].

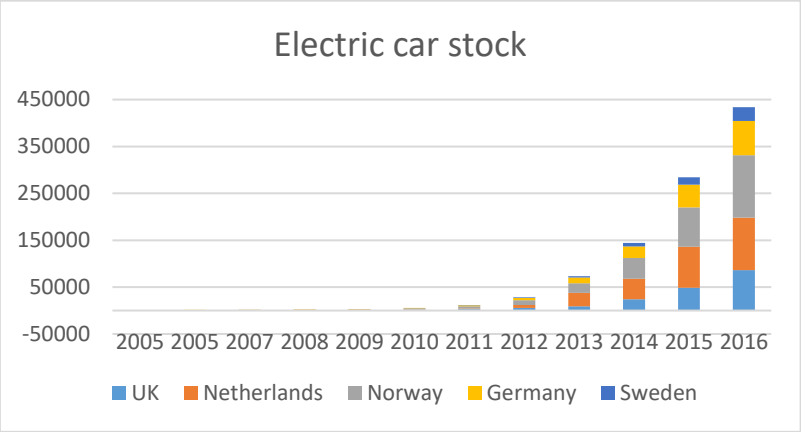

Figure 1.2-1 National EV stock [5]

As for this work, BEVs are more relevant, for the reasons mentioned earlier. Figure 1.2-2 shows the national stock for BEVs in the North Sea region (NSR) countries.

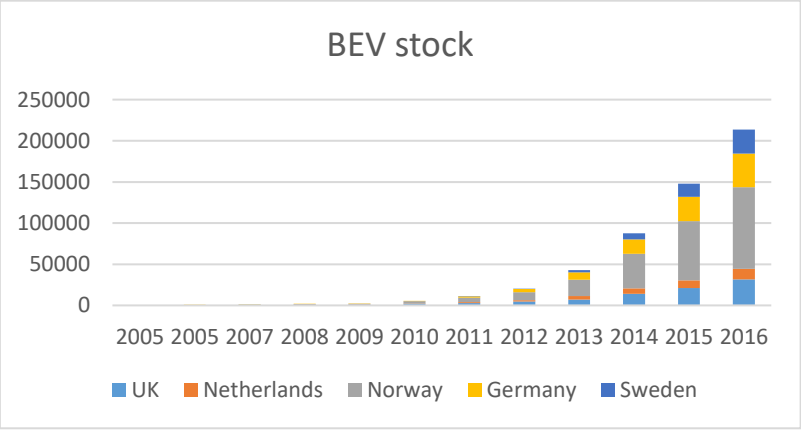

Figure 1.2-2 BEV national stock [5]

As of 2018, BEVs still represented only a fraction of the national EV fleet. This indicates that PHEVs still constitute a big part of the EV stock. However, the preference towards BEVs has already been manifested; the UK and the Netherlands have reduced the economic support towards PHEVs [5]. On the other hand, the number of BEVs has prospered as evidenced by Figure 1.2-3 which shows the new registration of BEVs in the NSR countries of the EU.

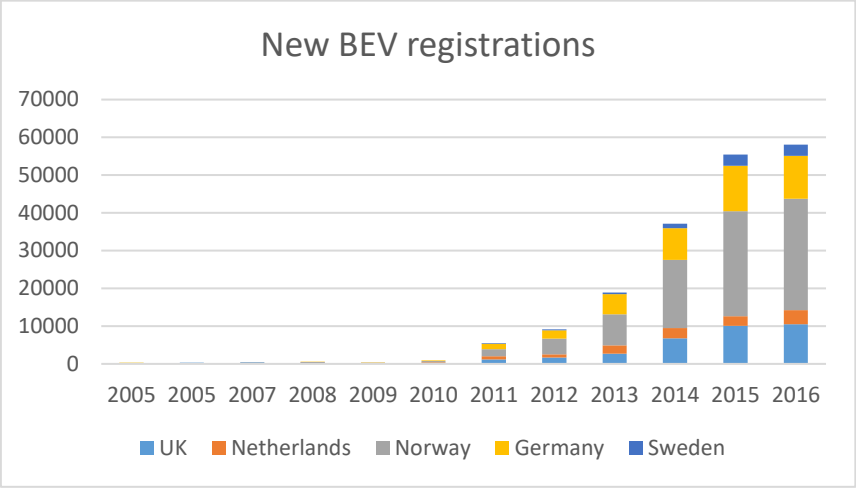

Figure 1.2-3 New national BEV registrations [5]

BEVs have experienced a higher growth than PHEVs since 2013: in 2016 BEVs increased by 62% in the NSR while PHEVs only by 59%. These promising numbers are still relatively modest when compared with the total national fleets of the respective countries. However, there is a global drive to promote BEVs as the ideal transportation solution for the future. Proof of this can be found in the future scenarios developed by several institutions. Some noteworthy research is reported herewith.

The International Energy Agency [5] presented two EV deployment scenarios for 2030; the former depicts the future market based on efforts to meet the goal of reducing the global average temperature increase to below 2°C above preindustrial level and ensuring efforts to limit the temperature increase to 1.5°C above preindustrial level (2DS), while the latter aims at reducing the temperature increase beyond 2°C (B2DS). A reference scenario based on the Paris Agreement on Climate Change is also presented for comparison, as illustrated in Figure 1.2-4.

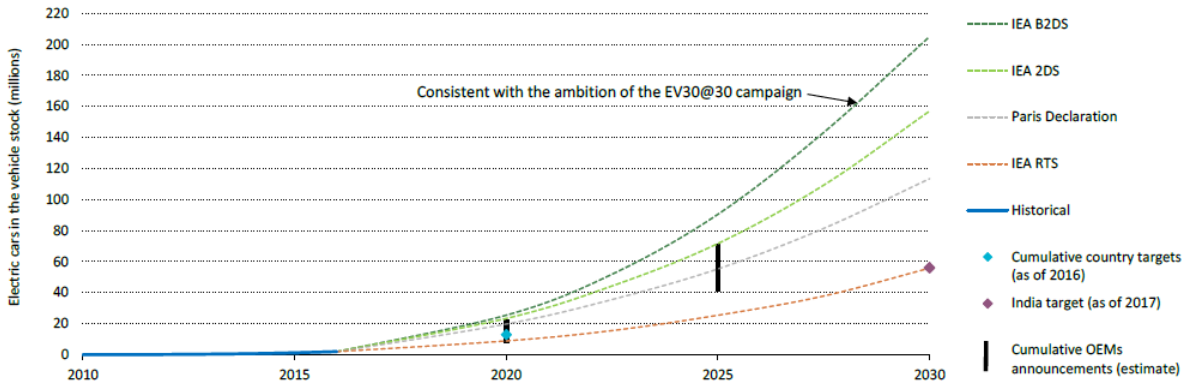

Figure 1.2-4 Deployment scenarios for global EV stock for 2030 [5]

As predicted, the higher is the targeted global warming reduction (see 2DS and B2DS), the higher the number of EVs deployed to meet the goal. Even in the reference scenario in Figure 1.2-4, which is more conservative than the 2DS and the B2DS scenarios, foresees 56 million EVs globally by 2030.

In the UK, National Grid's Future Energy Scenarios 2017 [15] reported that in all the scenarios they developed, there would be between 1.9 and 9.3 million EVs on the UK roads by 2030. Figure 1.2-5 shows the expected numbers of EVs in the UK for every decade until 2050 for four scenarios, each having different rates of development of low-carbon technology and associated user adoption. BEVs are referred to as PEVs in their report.

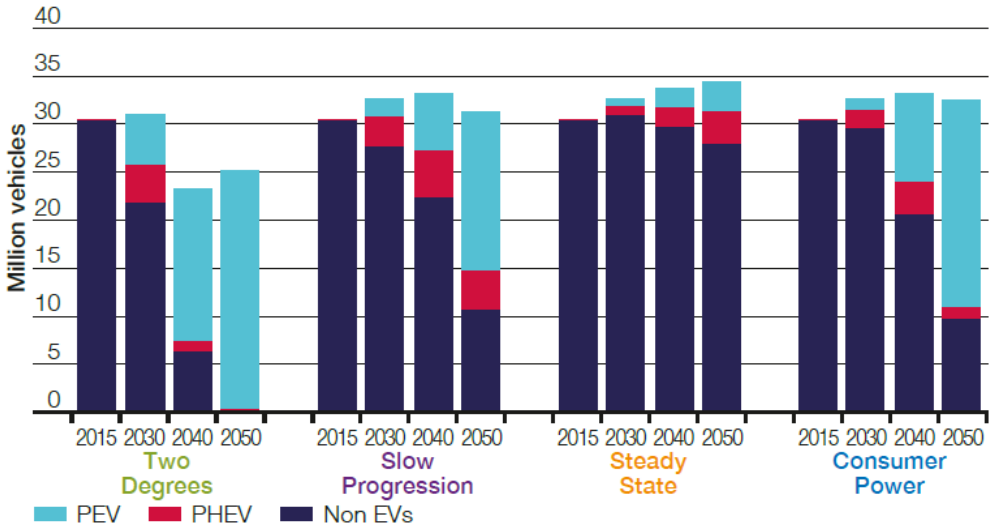

Figure 1.2-5 EV numbers in the UK for the four scenarios [15]

Figure 1.2-5 above reaffirms the two conceptions that have been stressed hitherto: PHEV is a transition technology; therefore, it will be systematically phased out or will play a progressively smaller part in the future national fleet. BEVs are the key EV technology, as only the most pessimistic scenario (Steady State in Figure 1.2-5) shows little increase in their numbers. Following this framing, we will designate BEVs as EVs henceforth and we will set aside PHEVs.

The phenomenon of large-scale EV deployment that has been only briefly highlighted here will certainly bring a number of opportunities, but it will also entail challenges that may radically change the electricity grid as we know it. The very large numbers projected thus far underline an equally massive demand of energy, or even more crucially power. Even with a simple calculation, by taking an average EV battery capacity of 30kWh and an assumed UK EV fleet of 2 million (see the Steady State scenario in Figure 1.2-5), the resulting energy demand amounts to 60 GWh. What may bring a significant challenge is that if nearly all the 60 GWh of charging energy is demanded in the same hour, on average, it would exceed the current daily national peak demand (48.8 GW in 2019 [17]). Under this simplistic assessment, the current generation, transmission and distribution infrastructure would have to be doubled to cope with such power demand. This basic estimate does not account for the power quality concerns, such as voltage profiles and stability of supply. This will be covered in detail in Chapter 3, where the challenges awaiting for the current electricity network will be extensively modelled.

Crucially, some positive prospects may be offered by the concurrent deployment of RES, or - more importantly for the sake of the current work - distributed energy resources (DER). The next few Sections will present the global status on RES deployment and will highlight the complementarities with EVs.

1.3 Renewable energy sources deployment

In the past decades, the world has become increasingly accustomed to RES, which currently constitute a major proportion of the energy mix of several countries among the 169 that have

adopted this technology, with the total installed capacity of 2,378 GW as of 2018 [18]. Out of this capacity, hydropower, wind and solar are leading the sector, followed by bio-power, geothermal, concentrated solar-thermal power (CSP) and tidal. At the end of 2018, RES contribute to 26.2% of the global electricity generation, with wind and solar providing 5.5% and 2.4%, respectively. Figure 1.3-1 shows the globally installed power generation capacities.

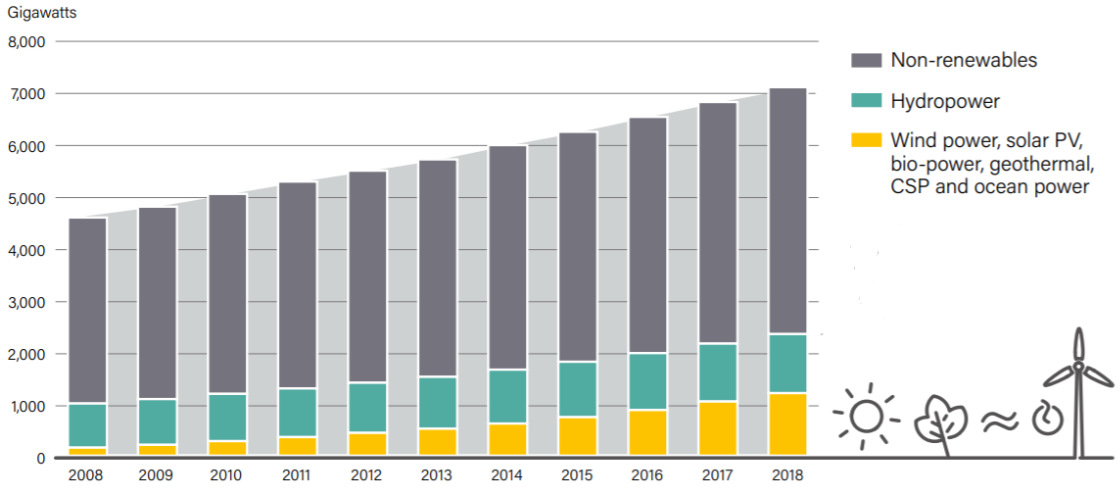

Figure 1.3-1 Global installed power capacity [18]

Especially in the UK, wind is a strong contributor, with a share of 17%, while solar provides 4%. Among the available technologies, PV offers the highest versatility in terms of scalability, as both large plants and distributed systems are installed. In fact, 150 million of people in Africa and Asia make use of off-grid PV systems, with Bangladesh in the lead of the countries with the highest access to off-grid PV.

The installation of PV technology was driven by the generous economic support provided by different governments around the world. Among a number of measures designed to promote PV, Feed-in-tariff (FIT) and Net metering (NM) are the most widely adopted, with the former being implemented in 111 countries, while the latter was adopted in 66 countries, by the end of 2018 [18]. Concurrently, the price of PV energy has fallen in the last decade as the technology becomes more cost efficient. This has led to a decrease in the corresponding

support, as PV systems become more competitive. As an example, Figure 1.3-2 depicts the decline in FIT in the UK along with a similar behaviour of the cost of PV installation [19][20][21].

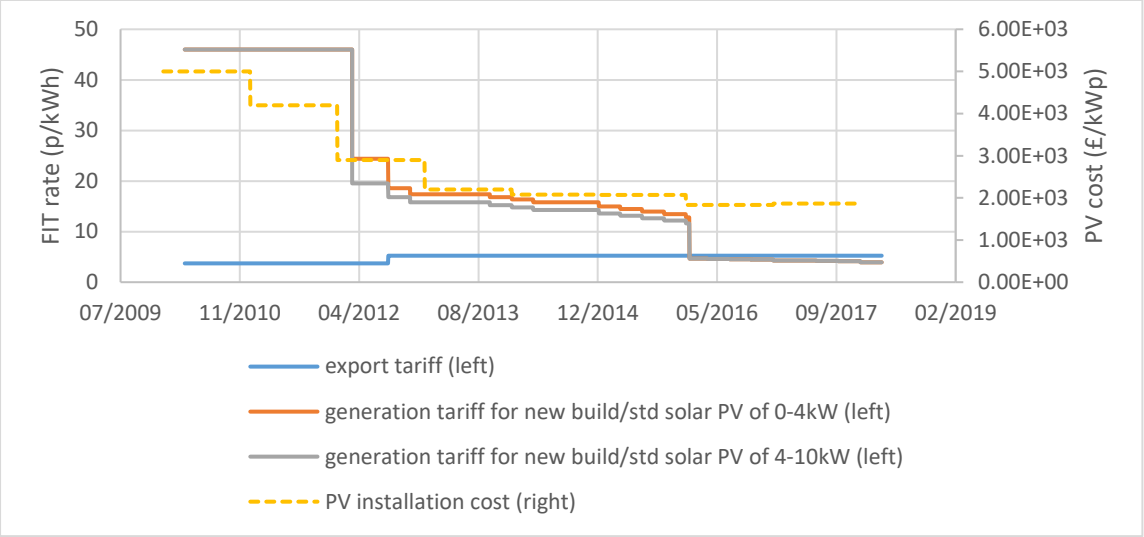

Figure 1.3-2 UK FIT rate for PV systems up to 10kW [19][20][21]

If on one hand these measures encourage improvements in the efficiency of the PV technology (technologies much improve their performance in a competitive market), it may also have the adverse effect of discouraging new installations. As a consequence, yearly installations in 2016 were four times lower compared to the previous year, [22] and the situation is about to become worse. In fact, the UK government has abolished the FIT scheme for new installations from April 2019 [23].

As the investment in distributed PV becomes more challenging, the concept of self-consumption (SC) and self-sufficiency (SS) assume paramount importance. SC refers to processes that allow consumers to generate and utilise their own energy [24], whereas SS means that a certain proportion of the electricity demand is satisfied by the local generation. This demonstrates that EVs and PV systems can mutually benefit each other. EVs could achieve a near zero-carbon footprint by charging primarily from PV and both SC and SS of the PV-EV system could be increased by storing the excess PV energy in the EV battery. To this end, one specific technology, the lithium-ion battery, is currently dominating the scene as

the preferred solution for EV batteries. Therefore, it is worth spending some efforts discussing the advantages, drawbacks brought by the different chemistries within li-ion batteries and future trends.

1.4 Lithium-ion batteries for EVs

EVs consume the energy solely provided by a battery to supply their powertrains, while PHEVs can make use of an auxiliary ICE to travel long distances. Hence, the battery is the most vital part of an EV, because it provides the energy for transportation. To this end, lithium-ion batteries are dominating the market for both transportation as well as the already well-established home electronics and hand-held devices industry. Lithium-ion batteries are complex electrochemical devices that make use of certain chemical reactions to be able to be charged and discharged. More details will be provided in Chapter 4, while this Section reflects on the current lithium-ion battery market and the future trends.

The most promising lithium-ion battery chemistries are lithium-iron phosphate (LFP), lithium-nickel-cobalt-aluminium (NCA), lithium-nickel-manganese-cobalt (NMC), lithium-manganese oxide spinel (LMO) and lithium-titanate (LTO). The performance of these battery types can be compared according to five criteria, which are:

- *Lifespan*; this is the maximum number of charging/discharging cycles.
- *Specific energy*; this is the energy contained per unit mass of a certain substance (J/kg).
- *Specific power;* this is the power contained per unit mass of a certain substance (W/kg).
- *Cost.*
- *Safety*; this is intended as the temperature performance of a substance when subject to high utilisation.

Figure 1.4-1 depicts the performance of the different chemistries along these six dimensions.

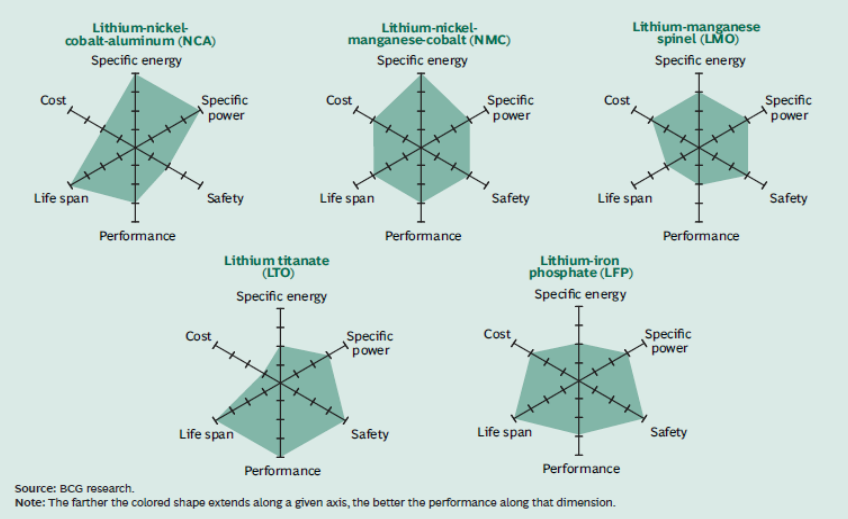

Figure 1.4-1 Dimensions of Li-Ion battery performance [13]

It can be seen that there is no one type that excels along all these dimensions. NMC, LFP and LTO are commonly are adopted in EVs due to their superior performance. More detailed explanation is provided for the different factors:

- *Lifespan*: we refer to Chapter 4 for details regarding this aspect.
- *Specific power*: EVs have superior power performance, which are comparable and even higher than ICE vehicles [13].
- *Specific energy*: this refers the amount of energy per kg in a battery. In Figure 1.4-2, the technical characteristics of common lithium-ion technologies are listed.

	Lithium Titanate	Lithium Nickel Cobalt Aluminum Oxide	Lithium Iron Phosphate	Lithium Nickel Maganese Cobalt Oxide	Lithium Manganese Oxide
Specific energy (capacity)	70-80Wh/kg	200-260Wh/kg	90-120Wh/kg	150-220Wh/kg	100-150Wh/kg
Cycle life	3,000 - 7,000	500	1000-2000	1000-2000	300-700
Thermal runaway	Among the safest Li-ion technologies	150C (302F) typical, high charge promotes thermal runaway	270C (518F) Typically safe regardless of charge level	210C (410F) typical. High charge promotes thermal runaway	250C (482F) typical. High charge promotes thermal runaway
Applications	Distributed storage, EVs	Medical devices, industrial	Portable and stationary	EVs, industrial	Medical, EV, industrial
Note	Long life, fast charge, wide temperature range but low specific energy and expensive	Similar to Ci cobalt	High self discharge relative to others	Market share is increasing	High power but less capacity; safer than Li-cobalt; commonly mixed with NMC to improve performance
Industry participants		Tesla	Alees, Changs Asoending Enterprise Co, Phostech Lithium, Johnson Matthey	Umicore, BASF, Targray, Tesla Energy	Umicore, BASF TODA Battery Materials

Figure 1.4-2 Technical specifications of common Lithium-Ion batteries [25]

Moreover, the energy density, or specific energy, for BEV batteries is reported to have reached near 300Wh/l in 2015 [5].

- *Cost*: the value chain of automotive batteries consists of the production operations carried out on the components such as raw materials for production of the cells, module production into the battery packs, battery-vehicle integration and usage in the lifetime and disposal. Figure 1.4-3 shows a cost breakdown of the different components of a battery pack

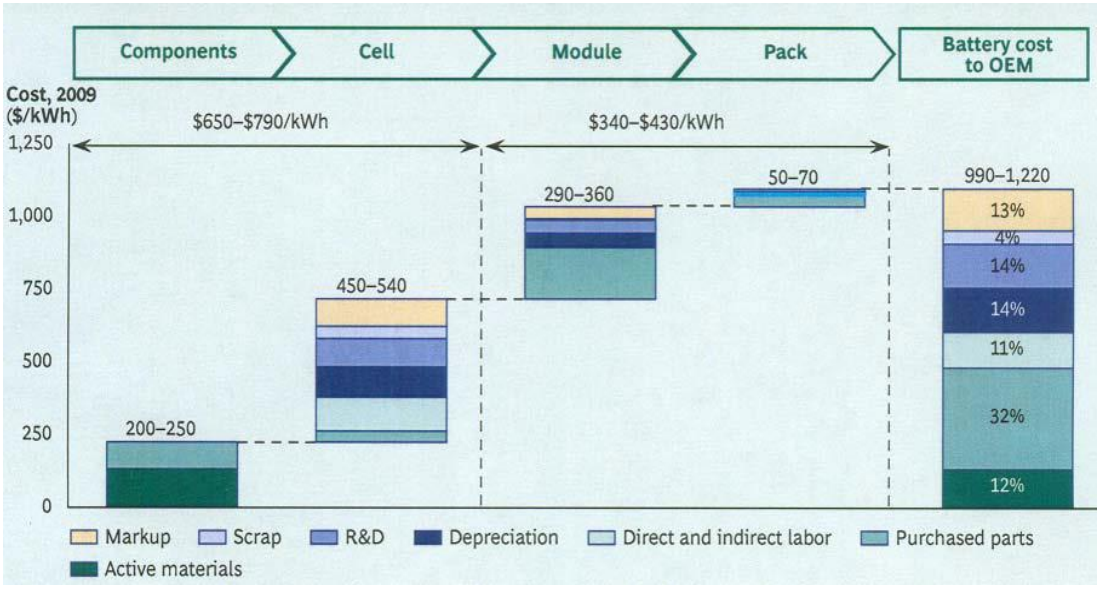

Figure 1.4-3 Breakdown of the costs for the components of a battery pack [13]

The cost of the raw materials is only some 12% of the total cost of the battery pack [13]. Owing to the developments in battery technology, manufacturing costs of EV batteries have fallen significantly in recent years. Figure 1.4-4 depicts the situation of battery costs in USD (United States Dollar) up to 2016. As can be seen, EV battery manufacturing costs have dropped from 1000 USD/kWh in 2008 to below 300 USD/kWh in 2016 for PHEVs, according to US Department of Energy, while for BEVs the cost is even lower. This is because, larger pack size, as it is the case for BEVs compared to PHEVs, leads to reduced cost per kWh [5]. Moreover, original equipment manufacturers (OEMs) like Tesla, Panasonic, GM and LG Chem have announced prices that are in the range of 180-200$/kWh which are significantly lower than the figures previously mentioned. This is

consistent with the values shown in Figure 1.4-4 which shows battery pack prices well below $300/kWh.

Figure 1.4-4: Li-ion battery cost history 2011-2016 [26]

- *Safety*: this is related to preventing thermal runaway with a possible ensuing fire. High discharging rates, overcharging or short circuits, favoured by a positive feedback loop, can cause chemical reactions that release heat and may cause a fire. This is why a cooling system is a fundamental component of any automotive battery pack to ensure a controlled and safe energy release and avoid thermal runaway. There is usually a compromise between the high energy density and inherent battery safety.

Looking at the future, battery pack prices projections indicate a future price below $190/kWh by 2020 and below 100$/kWh by 2030 [27]. Cost reduction is expected from improved production processes and larger scale production. According to [5], battery prices decreased by 35% in 2015 and they predict that by 2040 long-range electric cars will have an EV battery cost that is below $220. Figure 1.4-5 illustrates these considerations.

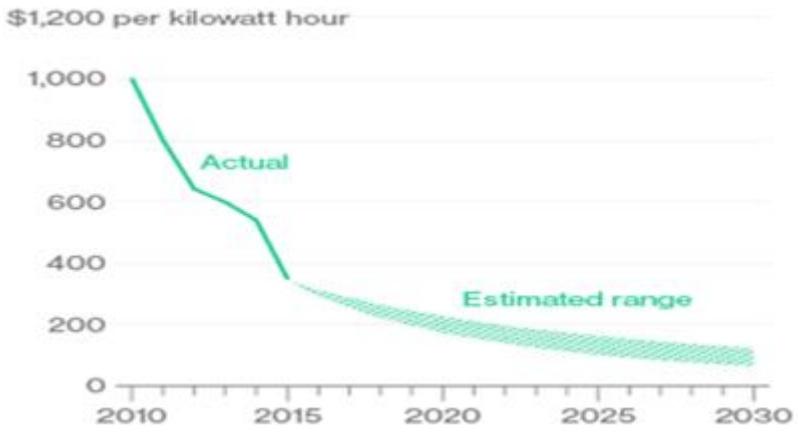

Figure 1.4-5: Li-ion battery cost trends and estimates [28]

Currently, lithium-ion are the most efficient and economic battery types but there are other emerging technologies that show promising performances. Advanced stationary storage solutions are listed in Figure 1.4-6, which gives a detailed insight into their characteristics.

Mature — Level of commercialization — R&D

	Lithium ion (Li ion)	Flow	Sodium Sulfur (NaS)	Emerging
Installed base	150 MW+	50 MW+	450 MW+	N/A
Chemistries	Li Nickel Cobalt Aluminum Oxide; Li Iron Phosphate; Li Nickel Maganese Cobalt Oxide; Li Manganese Oxide	Vanadium redox; Iron-Chromium; Zinc-bromine	NaS	Liquid metal; metal air
Storage duration	Short (1-4 hours)	Medium (4-10 hours)	Medium (4-10 hours)	Short - Long
Lifespan	5 - 15 years	10 - 20 years	10 - 15 years	2 - 10 years
Cycles	2,000 - 10,000	10,000 - 15,000	2,500 - 4,500	Varies
Efficiency	85%-98%	60%-85%	70%-90%	Varies
Energy density	High	High	High	High-Low
Capital cost	$350/kWh - $1000/kWh	$600/kWh - $200/kWh	~$500/kWh	$200/kWh-$1000/kWh
Levelized Cost of Storage	$0.15-$0.75 per kWh	$0.11-$0.28 per kWh	$0.23-$0.57 per kWh	$2-$0.05 per kWh
Key limitations	Safety - risk of igniting	Size, cost	Safety, discharge rate, heat requirement; monitoring needed	Safety, low efficiency

Figure 1.4-6 Technical characteristics of the most advanced battery technologies for stationary storage purpose [25]

As can be seen, there is not one type that satisfies all the ideal requirements: for instance, sodium-sulphur batteries have safety issues but display a considerable discharge rate.

1.5 Scope of research

The main focus of this work is to employ multi-objective optimisation to tackle the problem of optimal electric vehicle charging scheduling. Multi-objective optimisation may not be conceptually hard to grasp, however proposing a workable framework that can be adapted to the problem of optimal electric vehicle charging scheduling is not trivial. In effect, it presents a multi-dimensional problem, where individuals and organisations from different backgrounds, with different behaviours and objectives interact with each other in what could be described, not erroneously, as a game. In fact, it will be shown later in this work that multi-objective optimisation can also be formulated, with appropriate assumptions, as a game among competitive players. Before the implementation phase, the participants of this framework must be accurately modelled and the rules that regulate their interaction must be defined. Moreover, the metrics that evaluate the effectiveness of the proposed framework should be rigorously defined. With this aim in sight, the introduction chapter provided a complete overview of the topic covering electric vehicle integration with its associated opportunities and challenges. In this work, the United Kingdom (UK) will be often considered as a model and working ground for the future wide adoption of EVs. This selection is motivated by the recent position of the UK regarding EV adoption in relation to climate change, as well as urban air pollution. The UK government has announced a ban on new sales of internal combustion engine (ICE) vehicles by 2040 [29]. The immediate consequence of this move is the urgent need for smart solutions to sustainably integrate EVs in the electricity network. This further reinforces the motivation behind this work.

In this research, simulations and control methods have been implemented using the Matlab software. Matlab is an environment for mathematical computation that is widely utilised in the scientific community because it offers a comprehensive suite for science, technology, engineering and mathematics disciplines. It includes up to date software and algorithms for a wide range of mathematical problems including, optimisation, machine learning, control theory, real-time control, parallel and graphics processing unit (GPU) computation. Apart from simulating the developed models, due to the seamless interfacing capability with

external hardware that MATLAB offers, ultimately the real-time charging/discharging controller will also be developed and implemented in a laboratory setup with the MATLAB Support Package for Arduino Hardware [30].

1.6 Aims and objectives of the research work

The aim of the present work is to establish an operational framework for the optimal EV charging, considering the major stakeholders involved in the implementation of smart grids.

Objectives of the research

The objectives of the research are to:

- Develop a mathematical optimisation model applied to the optimal EV charging problem by modelling current and future smart grids.
- Model the crucial objectives including technical, economic and environmental aspects.
- Assessment of the economic feasibility of smart charging and V2G, by varying multiple technical and economic parameters.
- Develop an adaptive, dynamic matematical model to analyse and control degradation of lithium-ion batteries.
- Develop real-time optimisation techniques to optimise the operation of battery chargers, using multi-objective control.
- Provide a practical solution that can help to build the foundation for the sustainable integration of EVs in current and future electricity networks.

1.7 Original contributions

The key contributions of this thesis are summarised as follows:

- Simultaneous optimisation of electricity cost, battery degradation, grid net exchange and CO_2 emissions has been performed.
- A dynamic battery model (using empirical data), depicting the impact of three key stress-factors, has been implemented in order to minimize cycle degradation as a key objective.
- An algorithm to adapt a mathematical degradation model with real-life data influx has been proposed
- The use of EV batteries to provide ancillary services to the grid has been considered as an additional objective and its implications on other objectives has been investigated.
- The conflict of interest among the end electricity user, the EV owner and the system operator has been highlighted and addressed using analytical hierarchy process (AHP) and utility function.
- A game theoretical framework, performing a hybrid control on a micro-grid, to enable energy trading among prosumers and EV users while complying with grid constraints has been proposed.
- Real-time multi-objective optimisation based on a dynamic programming approach has been demonstrated as an efficient way to control EV charging in a decentralised manner.

1.8 Outline of the thesis

The remainder of the thesis is organised as follows:

- In Chapter 2, the most recent advances in the area of EV and RES integration with vehicle-to-grid technology are presented. Subsequently, the research works, that are available in literature, addressing optimal EV charging scheduling aimed at different objectives are reviewed, highlighting the research gaps identified in the current literature. Accordingly, the main contributions of this work are laid out.
- Chapter 3 focuses on the modelling of the key elements of a smart grid, starting from the EV - which is the main focus of this thesis - by looking at travelling patterns. Next residential electricity demand and PV generation profiles are modelled based on the UK data. The methods for quantifying the impact of EV charging in distribution networks

and CO_2 emission quantification methodology are presented next. The provision of ancillary services is then modelled based on the UK data.

- Chapter 4 deals with lithium-ion battery modelling by presenting a behavioural equivalent-circuit-based model and a degradation model. In this chapter, the methodology for developing an empirical battery degradation model, the approaches to make it dynamic and adapt to different batteries and operating conditions are presented.
- In Chapter 5, mathematical optimisation techniques are introduced, elaborating on both single-objective and multi-objective optimisation. Classic and metaheuristic methods for both convex and non-convex problems are presented.
- Chapter 6 presents the two key case studies, defined as decentralised and hybrid optimisation frameworks. In the former, MOO and multi-criteria-decision-making (MCDM) techniques are adopted, while the latter implements a game-theoretical energy-trading model for prosumers and EV users.
- Chapter 7 develops a real-time MOO framework and applies it to a small-scale laboratory setup. The results of three operation cases are presented.
- Finally Chapter 8 looks back at the core objectives of the thesis, the methodologies applied and results obtained, in order to draw meaningful conclusions. This chapter also elaborates on the future implementability scope.

Chapter 2 Assessment of the State-of-the-Art on economic feasibility of V2G and Smart Charging

2.1 Introduction

In this chapter, a review of the published research works on energy and ancillary service provision with EVs is presented. This is to establish the state-of-the-art in terms of EV integration, as well as to survey the major trends in optimisation. Several works have dealt with EV and RES integration by looking at technical, economic and environmental aspects. However, researchers have encountered a number of hurdles while trying to quantify the profitability of V2G, evidenced by the wide span of results, ranging from very promising figures to some that depict V2G as unprofitable. The reason for such variable outcomes is due to the fact that a considerable number of factors come into play to decide the profitability of V2G, among which the most important ones are:

- technical aspects - i.e. technology status and constraints and
- economic parameters - i.e. tariffs, costs and payments, policy implications, supporting regulation.

The environmental benefits of EVs have already been discussed in Chapter 1 and will be briefly touched upon in this review. The previous works on V2G are reviewed, by highlighting both the strengths but also the shortcomings of these studies to identify major gaps in knowledge. Subsequently, the most advanced research works on optimal EV charging scheduling are analysed separating the research on single-objective optimisation from those

related to multi-objective optimisation. A few useful definitions are provided hereby to set the context of this review.

Definition 1. Vehicle to Grid (V2G) is defined as "*a system in which there is capability of controllable-bidirectional electrical energy flow between a vehicle and the electrical grid*" [31].

Definition 2. When the energy flow is established between the vehicle and different archetypes, i.e. single household or a building, this service is called Vehicle to everything (V2X) charging/discharging.

Definition 3. Arbitrage is the "*... purchase of a commodity or derivative in one market and the sale of the same, or similar, commodity or derivative in another market in order to exploit price differentials*" [32].

2.2 Literature review motivations and structure

The motivations, the structure and the elements of the literature review are presented herewith. When dealing with any technology that seeks commercialisation, two fundamental aspects are always examined: technical feasibility and economic viability. These two features represent the core of any successful and sustainable product. In this thesis, the technology in question is the EV, with a focus on advanced charging strategy, hence their technical and economic features must be inspected. As there is both societal and political drive behind the development of EVs, environmental aspects are also taken into account, however, it is undeniable that eco-friendly, but unrealiable and unproductive tehcnologies are short-lived. Hence, a techno-economic feasibility assessment of EV charging strategies is of pivotal importance, and constitutes the motivation behind this review.

EV charging strategies can be classified in uncontrolled ("dumb" or "dump") charging, smart (or "controlled") charging and V2G. The feasibility and benefits of smart charging compared to uncontrolled charging represent common knowledge among researchers and practitioners and include cost savings, grid relief [3], [33] and improvement of battery life. On the other

hand, the benefits of V2G are still today subject of heated debate, as will be evident from the results surveyed in this review. In fact, neither the level of prospective benefits that V2G can bring nor the elements that influence such level have been clearly reported yet. Consequently, individuals, user associations, industry, academia and policy makers are doubtful of the utility of V2G which constitutes the greatest barrier for its wide implementation. There is an evident gap between the results achieved by academic research and industrial pilots and the final verdict on V2G, and this review aims at bringing clarity on the topic. Consequently, more a more in depth analysis is required for V2G rather than for smart charging.

Evidence of the public perplexity on V2G is effectively raised in [34], where 611 German drivers, including conventional ICE and EV drivers, were surveyed on their willingness to participate to V2G services. Although the survey was conducted in 2013, the findings were published in 2018, and the majority of concerns and viewpoints still stand today. The topics covered by the survey were awareness of different EV types, elements that can enhance or limit willingness to participate to V2G, awareness of V2G and concerns and incentives to participate in V2G. They analysed the impact of several aspects characterising V2G services on participation and these were, plug-in restriction, minimum required range, possibility of indicating beginning and end of trips, different levels of monthly payments or one-off payments. The responses showed that most drivers were unaware of V2G, with only 1% declaring of knowing about it and that willingness to use a bidirectional charger was significantly less than that of using a unidirectional or even uncontrolled charger. This underwhelming response was due to the main concerns to V2G related to the prospective shortening of battery life, travelling pattern not being compatible to V2G services and that there will be third-party access to the vehicle which cannot be controlled, in order of importance. Enablers of V2G were overwhelmingly dominated by cost related aspects, i.e. cheaper charging compared to uncontrolled charging, discounts on purchasing an EV or a charging station and an annual bonus. By applying ordinal regression, the authors found the impact of the combinations of these factors: the results indicated that drivers expected high payments (compared to conventional electricity tariffs) to reduce their minimum driving range requirements and allowing an on-board computer.

Addressing a different category of stakeholders, in [35], 227 experts were queried on the benefits of EVs and V2G. Participants from 200 institutions in Denmark, Finland, Iceland, Norway and Sweden, the likes of national and government ministries, universities and research institutions, electricity transmission and distribution utilities, car manufacturers, private companies and industry groups and associations, were interviewed. They gathered the opinions of important names in different fields, such as BMW, Volkswagen, Nissan, E.ON, Tesla Club and pioneers in the field of smart charging and V2G, such as Fortum and Nuvve. Unsurprisingly, the experts perceived the environmental benefits of EVs as major drivers: reduced emissions, followed by reduced noise, better performance and only then economic savings and more integration with renewables were mentioned. Mirroring the outcome of [34], the overall knowledge on V2G was more limited, with only 66% of the experts discussing the benefits of V2G. The majority of the experts identified the possibility of integrating with intermitter renewable energy as a key benefit. Moreover, V2G was comparatively more often linked with domestic solar than wind, with experts saying it is a more intuitive connection. Smart (controlled) charging was seen as the second most popular advantage being also defined as a steppingstone for V2G. Those that were aware of the economic benefits of V2G, agreed on similar levels of earning of around 120 euro/month (107 £/month).

Comparing the findings of the two studies, they surveyed the two sides of the debate, users and specialists. One common aspect is the relatively limited awareness of the V2G concept; even though the material from [34] are based on the situation in 2013, the currently limited number of V2G implementations indicates that awareness did not much improve from then. Understandably, users were mainly concerned about factors that directly relate to them, such as travelling patterns, battery life and cost reduction. Experts were more informed about wider objectives, such as reducing intermittence of RES. In addition, a rather good estimate of potential profits was brought forward. From this brief, yet illuminating scrutiny, two research questions are raised:

- Is V2G currently profitable?
- What are the factors that influence the profitability of V2G and what is their impact?

2.3 Literature review on economic feasibility of V2G

With the aim of responding to the research questions defined in Chapter 2.2, 45 papers have been collected and reviewed. These have been retrieved from the Google Scholar search engine as it collects research papers from the major publishers including IEEE, Elsevier, Nature, Francis and Taylor, Wiley, MDPI among others. The collection research works spans over a period of 13 years, from 2007 to 2019, to provide a chronological roundup of the advancements in this field. A few rules are established for a coherent and rational investigation, for this review and throughout the thesis:

- Some pioneering research works are referred to regardless of the year of publication; this is because such works were the first in initiating the research in that area and they serve as references for the most updated research.
- As indicated in the introduction of this chapter, this review and the thesis will deal with technical and economic aspects in the area of EV charging strategies. While cost factors are heavily influenced by the time of publication, as the economic parameters, policies and market status can change significantly in a matter of few years, technical performance is a does not change significantly in a matter of few years. For instance, if EVs are optimally scheduled to reduce peak electricity demand by 10 kW, the magnitude of this reduction will not change across some decades. On the other hand, economic benefits change as the influencing factors vary in time. We therefore provide a chronological roundup of the works that dealt with economic aspects related to smart charging and V2G, while for technical achievements, i.e. peak shaving, voltage balancing, the time dimension is not a concern.
- Cost values were all converted to British pounds to allow comparative analysis.

Literature [9], [34]-[49], provided some insights on the economic dimension of V2G, while literature [50]-[63] dealt with technical aspects. References [64]-[77] are reviewed on the adopted optimisation strategies. Table 2.3-1 summarises the settings considered in [9], [34]-[49] in chronological order. The factors that are highlighted have been categorised based on criteria set hereby:

- Technological and market considerations
  - Time; as technology advances ad reaches mass production, cost comes down, markets saturates, all leading to different implications on prospective benefits through years.
  - Country, market and service; different countries will have different policies in place and different market structures designed for the various V2G services.
- Case-study setup
  - EV battery capacity; EVs of different categories, with diverse battery capacities can be utilised to provide V2G services, and since service payments are often proportional to the energy exchanged, this factor is crucial in determining potential remunerations.
  - Charger rating; several services, including frequency regulation provide payments that are proportional to the committed power and EV chargers, in combination with on-board power electronics, decide the feasible power level.
- Cost-benefit considerations
  - Battery investment cost; this is one of the most critical factor in determining the prospective benefits. In fact, as increased utilisation from V2G is known to lead to battery wear, the undelying battery cost discerns the economically feasible services.
  - Charger cost; the cost of a V2G charger is a cryptic information and it is a fixed cost that can weigh on the cost-benefit calculation.
  - Electricity tariff and service payment; depending on the type of service, V2G can be employed to reduce electricity bills or provide ancillary services. In the former case, the (avoided) electricity tariff constitute the main revenue stream while in the latter, it is the service payment.
- Considerations on a realistic assessment
  - Battery degradation model; model simulations provide estimates of the real-life operation. By using battery degradation models, a more accurate account of the real cost-benefits can be given.
  - EV availability: as EVs are primarily used for transportation, their unavailability as parked and plugged-in assets will definitely affect the achievable profits.

Table 2.3-1 Summary of research works on feasibility of V2G

Literature	Profits (£/vehicle/year)	Service	Battery capacity (kWh)	Charger rating (kW)	Battery cost (£/kWh)	Charger cost (£)	Electricity tariff (ET) or regulation prices (RP) (£/kWh)	Battery degradation consideration	EV availability consideration
[9] (2007) USA	427-3,555 depending on the committed power	Frequency regulation	11.5, 27.4	2.9, 6.6, 15	277, 479	435	ET = 0.04 RP = 0.006-0.03	Degradation model function of DOD	▪ Commuter fleet with availability during the day and night ▪ Utility fleet available 3 pm to 8 am
[36] (2012) USA	[910 1,529 2090]	Frequency regulation	4.25, 14.5, 40	Char. 60 Dich.120	PHEV 750 BEV 237-395	Not considered	RP=0.03	Degradation according to testing cycles set by OEM	Full availability
[37] (2012) USA	988-1106	Frequency regulation	20, 99	19.2	790-948	1,580-3,160	Not stated, New England regulation market	Degradation model function of DOD	Availability from 8 pm to 8 am
[38] (2014) Germany	108-207	Energy arbitrage	28.3, 35, 53	3.3, 11	119-483	131,476	ET= 0.18 Wholesale price = 0.0612	Degradation model considering power and energy fading	Availability of employed users and retired ones.
[39] (2014) Singapore	Frequency regulation: 600 Primary reserve: 0 Secondary reserve: 21 Contingency reserve: 370	Frequency regulation, primary, secondary and contingency reserve	24	6.6	214	Not considered	RP=0.054, 0.00026, 0.0011, 0.0091	Degradation model function of DOD	Different availability depending on the employment status

[40] (2015) USA	347-1,251	Frequency regulation	7.6, 23, 60	3.3, 6.6, 10	237	830	0.0079-0.0711+0.004	Degradation model function of DOD	15 hours of provision per day (365 days)
[41] (2015) USA	6,909, 6,997	Frequency regulation	80, 108	70	Not considered	23,700	ET=0.079-0.082 RP=0.0237 (std. dev. 0.0103)	Not considered	180 days 5-8 am and 2-5 pm, and 185 days of full 24 h provision
[42] (2015) Singapore	Frequency regulation: 40.3-51.4 Primary reserve: 0 Secondary reserve: 0 Contingency reserve: 13	Frequency regulation, primary, secondary and contingency reserve	20	40	436	Not considered	ET=0.158 (std. dev. 0.0032) RP= 0.0521 (std. dev. 0.0229), 0.0002 (std. dev. 0.0013), 0.0008 (std. dev. 0.0025) and 0.0065 (std. dev. 0.0036)	Comprehensive battery degradation model function of DOD and SOC	Travelling patterns of commuters in Singapore were considered
[43] (2016) USA	1,563, 2,487	Frequency regulation	40, 80	19.2, 25	474	5,451-5,609	ET=0.0632-0.11 RP= 0.013-0.039, 0.0073-0.0239, 0.0093-0.047, 0.0087-0.0301, 0.0084-0.0324, depending on the region	A total battery life cycle for V2G of 2000-6000 cycles is considered	Assumption of 60% of the total available range left for V2G
[44] (2017) USA	1,298	Frequency regulation	16, 24, 35	8, 10, 12	Not considered	Not considered	ET=0.0008-0.0261 RP=0.004-0.0221	Not considered	Travelling patterns generated from statistical data

[45] (2017) USA	73-2,442, depending on the demand profile and EV initial charge	Load levelling	30	1.5, 7.5	Not considered	Not included	Time of Use, not specified	Not included	Daytime availability with long and short duration and night time availability
[46] (2017) UK	167-1,367	Short time operation reserve, energy arbitrage, capacity market and triade avoidance	24	12	160	3,750	ET=0.085 STOR availability payment = 0.0033 -0.0043 STOR utilisation payment=0.167-0.171	A total battery life cycle for V2G of 1020 cycles is considered	Fleet of utility vehicles with availability from 7 am to 11pm
[47] (2018) Japan	Not profitable. Requires breakeven price of 0.44-1.83 £/kWh	Frequency regulation	40	Not specified	283	Not considered	System price=0.071	Degradation model with SOC dependency	Full availability
[48] (2019) China	Not profitable, levelised cost of storage is higher than commercial electricity tariff	PV integration	60	7	130	224	ET=0.09	Model based on utilisation	Availability during the day at working hours
[49] (2019) Australia	135	Electricity cost reduction	23	Not specified	Not specified	Not considered	Peak ET=0.19 Off-peak ET=0.095	Not considered	Residential pattern: EV unavailable during the day on weekends

In Table 2.3-1, shaded boxes indicate that the associated information was not provided/considered in the study. It should be noted that many of the considered features coincide with the main points indicated by [34] (battery cost and degradation, EV availability, cost consideration etc.) and [35] It can be seen from the same table that the chronological roundup starts from [9], where the foundations of V2G implementation for ancillary services were first layed. The V2G concept was first academically introduced in 2005 by Professor Willet Kempton based at the University of Delaware, USA. His team defined the basic setting for the economic viability assessment for EV fleets providing network services. They simulated frequency regulation provision in the Pennsylvania-Jersey-Maryland (PJM) market for a fleet of 250 vehicles, and calculated revenues in the range of USD 427-3,555 per vehicle. It was argued that the wide spectrum of profits is determined by three factors: the rating of the charger, the energy stored in the battery (if the battery of an EV is either empty or full, then it cannot provide the entire regulation up and down service) and the number of available EVs. The upper bound of their calculated profits is comparatively high, when compared with more recent studies, as can be seen from Table 2.3-1 and Figure 2.3-1, where whenever required, profit ranges have been used to report the results.

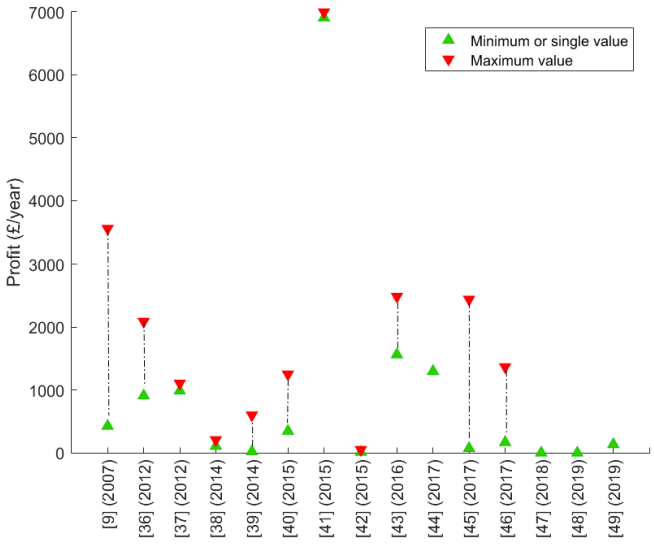

Figure 2.3-1 Profits from V2G provision in chronological order

Only [41] provided a profit higher than [9], which however is due to the high battery capacity of the considered buses (80-108 kWh) and committeed power (chargers rated 70 kW). Even [36], which assessed the economic feasibility of frequency regulation provision in the same market by assuming 24 h EV availability, reported lower profits than [9]. It can be seen from Table 2.3-1 that both works used similar capacity payments but the latter showed much lower profits, despite the very optimistic availability assumption. This is due to the more realistic assumption on battery cost, which was the second highest in [36]; high battery cost weighed heavily on the achievable profits. Interestingly, the highest battery cost was adopted in [37], which also assessed frequency regulation provision and was conducted in the same year as [36], indicating that these values of battery cost represented the most sensible levels at the time. Considering that [9] was published five years earlier than [36] and [37], it can be concluded that the former assumed a rather unrealistic value of battery cost (as well known, manufacturing costs decrease in time driven by increased scale of production). More recent works, for instance from 2016 onwards, exhibit a sharp decline in profits. Comparing the results achieved in [36] and [37] with those from more recent studies, the closest one is [44], published four years later. However, they reported higher profits than the studies in 2012. This may be due to the fact that they did not consider battery degradation in their calculations; considering the same battery investment cost and total V2G cycles as [43], published one year earlier (therefore battery cost should not be much different), namely 474 £/kWh and 4000 cycles respectively, the cost of degradation comes at 0.11 £/kWh, which is more than threefold the service payment they considered, making the service not profitable. In fact [43] resulted as a profitable business case because they employed both higher service payment, battery capacity and committed power. This may indicate that in some USA markets the payments can be less favourable to EV fleets providing frequency regulation now compared to 2012.

In addition, the striking popularity of frequency regulation is evident, with two thirds of the works investigating its profitability. Almost equivalent is the recurrence of the USA in the list of countries (eight times out of fifteen); in fact, all the works that dealt with markets based in the USA chose frequency regulation as prospective service. This highlights the effect that

supporting regulatory and policy frameworks can have on the adoption of technologies. In fact, as stated in [40], the PJM provided two types of signals: the conventional regulation signal, denoted as RegA, for conventional power plants and performance-based regulation signal, denoted as RegD, for assets with fast response capability. The latter provided a capacity payment, that is proportional to the committed time, and a performance payment, proportional to the ratio between the variability of the RegD signal and the variability of the RegA signal. This is particularly favourable towards batteries, which are inherently characterised by superior response capability. In contrast, as stated in [47], in 2018 a frequency regulation market was not yet available in Japan, which contributed to the nil profits stated in the same study. The only other country where frequency regulation has been considered is Singapore, with [39] and [42], both reporting lower profits than works that focused on the USA market. This is due to the comparatively lower payment for ancillary services (especially in [42]).

Figure 2.3-2 represents the battery investment cost utilised in [9], [34]-[49].

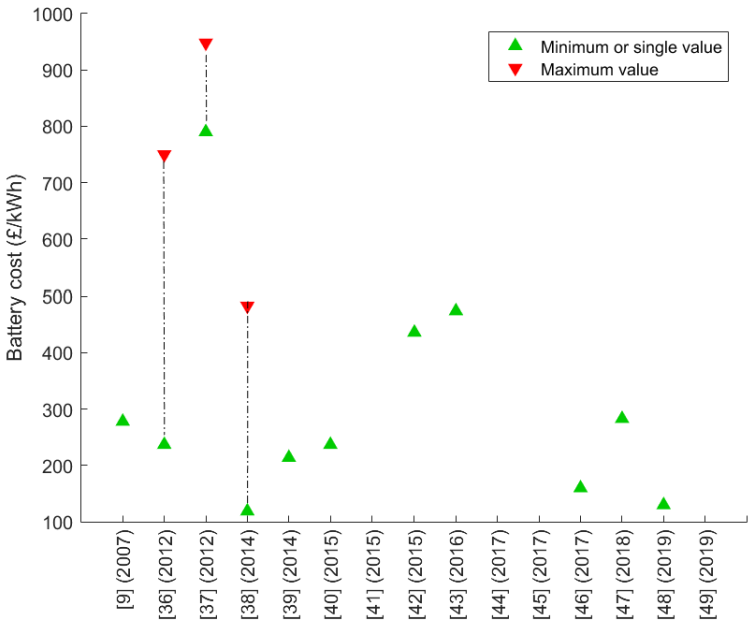

Figure 2.3-2 Battery investment costs considered in different studies in chronological order

In the above figure, a general decreasing trend is seen for the costs, in line with the data reported and forecasts shown in Figure 1.4-4 and Figure 1.4-5; in particular, the trend seems almost retrace that of Figure 1.4-5: the battery cost starts at nearly 1000 £/kWh in the yearly 2010's, going down to under 400-300 £/kWh at the end of the decade. This easy comparison further evidences the irregularly low battery degradation cost utilised in [9].

Figure 2.3-3 shows the service payments employed in [9], [34]-[49].

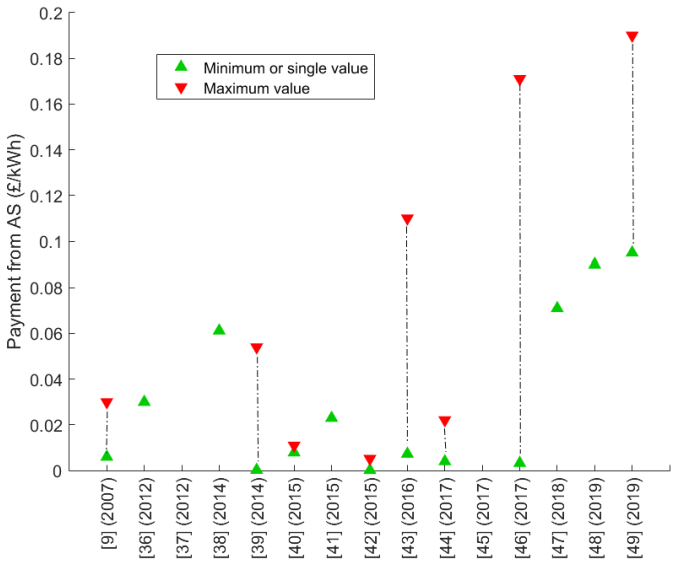

Figure 2.3-3 Service payments considered in research works in chronological order

It may seem from the figure above that there is an increase in the service payments, however, this is mainly due to the fact that the studies from 2017 either focused on other services (reserve, bill reduction, PV integration) or different countries (UK, Japan, Australia), or alternatively frequency regulation resulted not profitable. Due to the diversity of services, costs and model assumptions, [9], [34]-[49] were clustered to find similarities in their analysis according to the procedure outlined below:

- A total of 11 features were identified for the 15 studies ([9], [34]-[49]). All features are sequentially combined to determine a characteristic signature for each work.
- Each feature is normalised to the maximum value achieved by the research works along that feature. Therefore, the maximum value that a feature can achieve is 1.

- Reference [41] has been removed due to the its unnaturally high profits, which was due to the high energy and power committed. As it was an isolate case it has been removed.
- Year of publication starts at 0 for 2007, [9] to 1 for 2019.
- Countries are identified as [0.143,0.288,0.429,0.571,0.714,0.857,1] representing {China,Singapore,Japan,UK,Germany,Australia,USA} respectively.
- Services are identified as [0.333, 0.666 1] representing {Energy arbitrage,Demand provision,Ancillary services} respectively.
- Battery degradation consideration has been categorised as [0 0.333 0.666 1] representing studies that did not consider battery degradation, studies that considered a fixed number of charging/discharging cycles, models that considered one impacting parameter and models that considered more than one impacting parameters, respectively.
- EV availability consideration has been categorised as [0 0.5 1] representing studies that considered EVs as always available for V2G services, studies that considered a fixed availability pattern and finally studies that considered real-life patterns based on data.

Six clusters were chosen as a right trade-off between diversity and number of studies per cluster. The results are presented in Figure 2.3-4, where the lead author and the year of publication are reported for each study. The following discussion is structured based on four points:

- *Effect of time* – as technologies mature and reach mass production level, the associated costs decrease, making those technologies more profitable. This has been the case for battery degradation: in fact, all the clusters, with the exception of cluster 4 (blue curves) contain studies from a similar period of time and by comparing clusters 1, 2, 3, 4 and 6 a decreasing trend of battery degradation is seen. In addition, with time, as certain services become popular, the associated markets tend to saturate, leading to lower payments. That has been the case for frequency regulation in the USA; in fact, [44] compared to [9] reports a lower upper bound for the capacity payment.

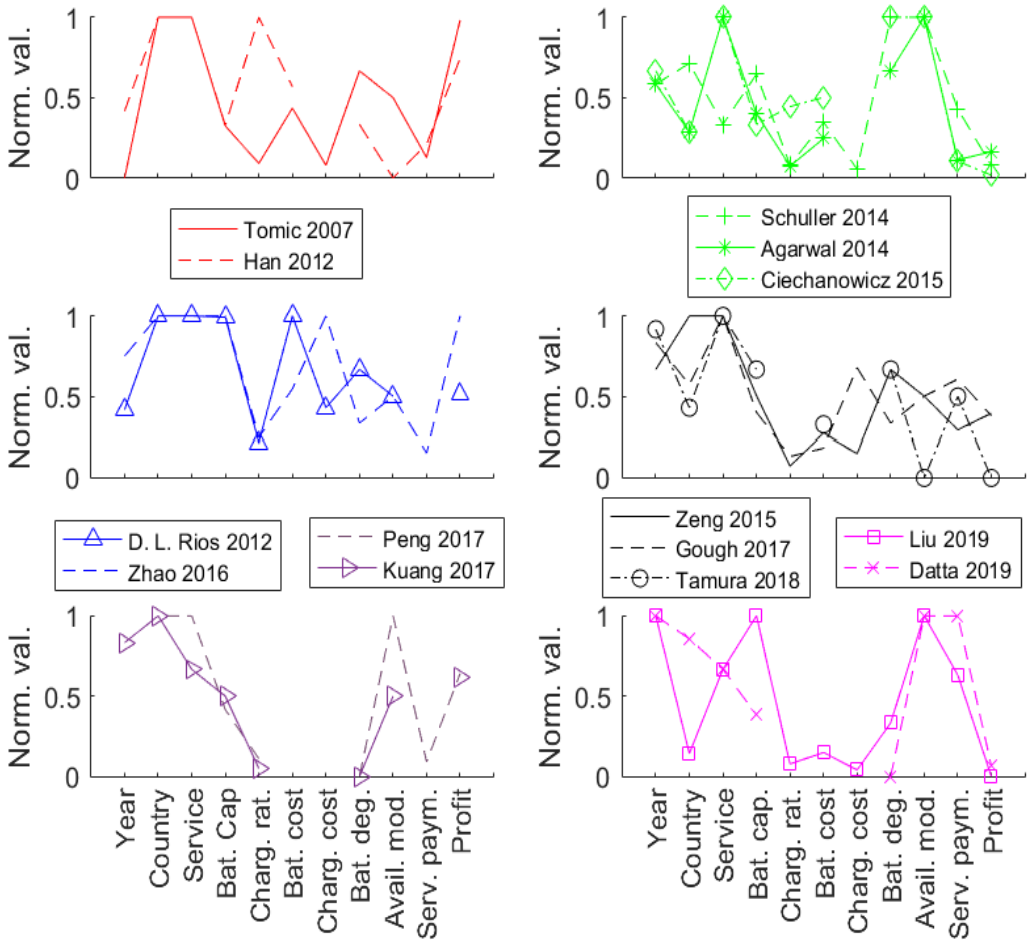

Figure 2.3-4 Clusters of the research works according to different parameters

- *Influence of the market* – the different market options in place, along with their regulations are crucial in promoting or discouraging the adoption of a certain technology. Again, that has been the case for requency regulation, which has been very popular in the USA and EVs were encouraged to participate. In fact, unsurprisingly most of the works that addressed frequency regulation dealt with the USA markets. However, as investigated in [43], various markets will provide different payments, and when the market is not made available, the service results unprofitable, as was the case for [47]. Another example is [46], which evaluated different ancillary services in the UK. Different services require different participation requirements: from few calls per year, i.e. reserve markets and capacity market, to several calls per day, i.e. frequency regulation. Participation

requirements, along with the level of payment provided for power (i.e. capacity) and energy will determine the feasibility of a service. In fact, in [46], energy arbitrage was not enough to provide a successful business model; capacity market or triad avoidance, both providing relatively high capacity (power) payment were necessary to improve the benefits.

- *Impact of battery degradation* – this is the main variable cost for V2G service provision. As already discussed, the cost of lithium-ion batteries has reduced over time, with current prices in the range of £/kWh 150-400. However, as demonstrated in current literature [38], [39], [42], [48], battery cycling inevitably leads to battery degradation. Any cost-benefit analysis aimed at assessing the feasibility of V2G services, needs to appropriately model and estimate prospective battery degradation incurring from service provision. To this end, some only [38] and [42] modelled battery degradation with two or more impacting parameters, i.e. DOD, SOC, charging rate, [37], [47] considered only one parameter, while the remaining works considered only the number of cycles as impacting factor or did not include battery degradation in their model. It can be seen that as accuracy of battery degradation increases, the corresponding profits decrease: compare for example [38] and [42] with [39], all in the same cluster (number 2, green curves in Figure 2.3-4). In fact, [39] and [42] provide the same service in the same country (Singapore), but the latter reported much lower profits due to a more accurate battery degradation estimation. Based on the results achieved in the available literature and depending on the magnitude of the impacting parameters mentioned above, we estimate a battery degradation cost in the range of £/kWh 0.075-0.3
- *Impact of EV availability model* – as storage operation is only a secondary function that EVs can serve, the impact of different transportation, consequently availability, models need to be considered in economic assessments of V2G services. However, very much like battery degradation, it was at times neglected [36], [47], or fixed availability was assumed [9], [37], [40], [43], [45], [46]. Only [38], [42], [44], [48] and [49] simulated the actual travelling pattern of EVs based on historical data. With the only exception of [44], which did not consider battery degradation, the remaining studies ([38], [42], [48] and [49])

reported low profits from V2G. Realistically, when considering the impact of all the factors highlighted in this review, V2G can bring £/vehicle/year 13-207.

2.4 Review of the impact of smart charging and V2G on distribution networks

Smart charging and V2G can help to mitigate the impact of bulk and uncontrolled EV charging, and consequently can help to accommodate a higher share of electric vehicles in the national vehicle fleet interacting with the electricity grid. More generally, smart and V2G charging from EVs could help to achieve an efficient utilization of the grid by addressing peak demands, integrating more intermittent renewable energy power and filling in the load curve in hours characterized by low power consumption. This can potentially lead to grid investment deferral. Following this idea, [50] evaluated the potential benefits for the DSO from investments in V2G services and compared them with the underlying grid investments. The authors inferred that there is a certain potential of peak electricity demand reduction resulting from a number of EVs providing peak shaving service. This in turn affects the duration curve of the network which depends on the electricity demand profiles. Ultimately, a balance is struck between the number of operational hours of storage, which determines battery degradation cost, and the avoided network investments. With 250 EVs, they showed that there was the potential of reducing the peak demand by 900 kW, by using 3.6 kW chargers. By considering a degradation cost of £/kWh 0.18 (resulting from a battery investment cost of £/kWh 267-623), they showed that below an annual energy throughput of 135 MWh/year, the avoided grid investments achieved by V2G were higher than the incurred battery degradation. However, they argued that with an average spot electricity price of euro/kWh 0.027-0.062 provided in North European countries, the economics of V2G did not make sense, as energy could have been bought from the wholesale market in order to satisfy the peak. However, as discussed in Section 2.3, the cost of lithium-ion batteries is currently in the range of £/kWh 150-300, and the associated battery degradation cost is £/kWh 0.075-0.3. Hence, peak power provision can become a profitable service in the near future. It should be

noted that [50] did not consider the travelling patterns of EVs, which would reduce the potential peak demand reduction with V2G, nor the cost of V2G chargers. Hence, an economic analysis of peak shaving, and the associated benefits that DSOs can reap, must be conducted. EVs can also be charged by imposing network constraints as was demonstrated in [51]. They tested the operation of a multi-agent system in a laboratory setup, where one EV was emulated by hardware in loop and 60 EVs were simulated. The emulated EV complied with network constraints.

[10], [52], [53], [54] and [55] further investigated the potential peak reduction capability of EV fleets equipped with V2G. In [10], the effect of smart charging on the electricity demand profile of a distribution network was analysed. The EVs were connected through a level 2 charging, either at home or in public areas, where renewable energy from PV and wind was available. 50,000 EVs performing smart charging enabled a peak demand reduction of 87 MW.

The location where information is stored, and hierarchy of computation can influence the potential achievable grid relief. In fact, measurements for an entire distribution network can be collected and utilised in a central server, or the decision-making privilege can be shared among multiple agents, distributed in the network. [10] and [55] evaluated the difference in these two strategies by exploiting intelligent EV charging to perform peak shaving and reduce the variability of the load profile in a local distribution grid. Local and global control strategies were performed and compared to a business-as-usual scenario with uncontrolled charging. Future scenarios with different PHEV penetration level were simulated and these are 15%, 45% and 75%. Given the nominal voltage level of 230±10%, uncontrolled charging led to more voltage deviation. Scenarios simulating a 10%, 30% and 60% of PHEV penetration rate were considered. The local control strategy let to improvements in peak demand in the order of 8-38% compared to the BAU case, while the global strategy achieved 8-42% of improvement. Both the local and global energy control strategies improved the flatness of the load profile, but the global energy control strategy resulted in the most optimal load profile. Although global control strategies provided the highest improvements in peak demand, it should be noted that the implementation cost of a centralised control strategy is

disproportionately higher than that of a decentralised system, due to the onerous communication infrastructure. The additional grid relief given by a centralised architecture must be compared against the incurring costs when choosing between the two strategies. It was further evidenced by [10] and [55] and confirmed by [54] and [56] that the penetration rate of EVs brings an additional dimension when evaluating grid benefits. The authors of [54] evaluated the provision of peak load support as well as voltage unbalance mitigation in a cluster of three feeders of a distribution network in Australia. They showed that above a rate of 40% EVs being available for those network services, there are beneficial effects in terms of voltage rise mitigation. In [56], for 25% and 50% EV penetration levels in a distribution network (corresponding to 31,250 and 62,500 EVs) it was shown that uncontrolled charging increased the peak demand by 36% and 74%, respectively. However, the benefits also scaled up proportionally as smart charging achieved peak levels that were 13% and 27% lower than those caused by uncontrolled charging.

As reported in [50], the category of the electricity demand profiles will have a substantial influence on the potential peak demand reduction achievable by EVs. For instance, if the load duration curve of a network exhibits a substantially high peak compared to its base demand, then EVs have to provide V2G support for a limited number of hours per year and targeted to critical moments. Conversely, if the load duration curve is flatter, than the EVs must be available for longer periods in order to achieve some peak demand reduction. This aspect was investigated by [53] where three case studies, namely high-rise residential buildings, office buildings and commercial buildings were analysed to quantify the benefits of peak shaving. 15 EVs achieved a peak demand reduction of 9.34-10.62%, 27.21% and 15.25%, respectively.

Few works evaluated the benefits of V2G for behind-the-meter services [57], [58]. In particular, in [57], the possibility of integrating EV charging with the energy generated by PV systems and a backup solution in case of emergency conditions were analysed. They applied their energy management strategy to a commercial building with 220 office-working stations, a 341.6 kWp PV installation, a 60kWh stationary storage and 48 EVs. The results showed that V2G can optimally integrate with PV by charging during periods of excessive generation

and supplying the evening demand. They also validated backup provision in emergency conditions. Similarly, in [58], a model for grid stabilisation with 250 EVs residential/commercial buildings in Brazil was developed. A three-level tariff was considered for the case of peak demand reduction, while the variability of the net power exchange was minimized to improve grid stability. However, they found that optimising grid stability does not lead to the maximum profit for users, which further emphasises the need for MOO strategies, as those implemented in this research.

2.5 Transportation compatibility for V2G implementation

From the works reviewed so far, it is clear that the economic potential of V2G depends on several factors, which have been discussed individually in Section 2.3. Crucially, the underlying influence of both driving requirements and EV charging behaviour impose strict constraints, as in order to be available to provide V2G services the EV needs to be both parked and plugged in. Due to the usage of the EV for transportation, and the associated charging or battery state of charge requirements, it is not always possible to provide grid supporting services. As already emerged from analysing the literature in Section 2.3, accurate prediction of EV travelling patterns is pivotal in accurately estimate V2G profitability and develop profitable business models. In fact, [38], [46] and [53] evaluated the availability of EVs for providing certain V2G services and found that some service provisions are limited by the characteristics of the users' driving pattern. To this end, the research works analysed thus far have addressed this requirement with different methods: by considering EVs parked for 24 h, by considering a fixed availability period or by simulating realistic travelling patterns from historical data.

Full availability. Studies such as [36], [47] and [50], assumed that EVs were always available for V2G services. While this can provide the maximum achievable profits/benefits, it is not an accurate representation of the results achievable in real-life conditions.

Fixed availability. Several studies, [9], [37], [40], [41], [43], [45], [46], [54] and [58] considered certain availability periods where all simulated EVs were made available for V2G

services. Although this model is better than the previous strategy, in real-life operation, unless contracted, not all EVs will comply with set availability period. In fact, there is always diversity in EV patterns, where different plug-in/plug-out times and energy requirements must be simulated.

Random availability. As discussed in Section 2.3, [38], [42], [44], [48] and [49] randomly generated diverse EV travelling patterns, with associated plugging-in/out times and charging requirements. In addition, [55] simulated EV availability based on random plug-in and out times normally distributed around 17:30 and 6:30 respectively with a standard deviation of 45 minutes. [52] adopted a forecasting model for the energy required by EVs based on US driving patterns. In particular, the work done in [53] was effective in modelling the impact of different driving patterns. For instance, EVs were not available at residential buildings during the office hours. For office buildings, the EV availability patterns were opposite to that of residential buildings. Differently from the previous two cases, in the case of commercial buildings, the travelling patterns can be considered known ahead as they depend on the tasks that need to be carried out, i.e. for postal delivery.

Five notable works accurately estimated EV availability patterns using probabilistic methods. In [59] the operation of different size of EV fleets was analysed in order to both satisfy the EV charging requirements and to provide frequency regulation. The distribution of the driving schedules was randomly sampled from real-life EV usage data and information n the daily driving routine. They estimated that the probability of having a high availability of EV battery capacity was high during the night, in the early morning and at late evening. These profiles were compared against the frequency regulation capacity requirements; as a result, the probability to meet a certain grid-facing bid requirement and to bid the optimal grantable capacity taken up and paid for by the grid were calculated. This represented an exemplary approach in considering EV availability for V2G purpose. Similarly, in [60] the potential EV power capacity to provide frequency regulation was estimated. Different factors including probability of EVs arriving at the parking spot at certain states of battery charge, in terms of initial SOC and required SOC, time of arrival and planned departure time, and a queuing system for different services were considered. EVs were assigned to the types of grid services

depending on their availability and the capacity available for that service was estimated. In [61], a Markov Chain Monte Carlo (MCMC) method was employed to extract the trip and idling time information from real-life vehicle driving data. This study found that EVs are driving, parked at home, parked at workplace and parked at other places 5.2%, 59.6% 33.6% and 1.6% of the time respectively. In [61], due to the high probability of the EV being parked at home or workplace, the authors considered these as charging locations. The simulated synthetic driving pattern then fed into a V2G scheduling, aimed at household peak shaving. An equally effective estimation model based on a queuing system was employed by [63]. The charging requirement of the vehicles was modelled with a queuing system based on a random probability distribution for each vehicle. Then the stochastic net demand for the parking lot was calculated from such probabilities. Random availability models allow an accurate estimation of the influence of EV travelling constraints on V2G benefits; in fact, as was shown in Section 2.3, and emphasised by [42], whenever randomised travelling patterns were considered, the associated benefits from V2G were reduced from excessively optimistic figures to realistic levels.

2.6 Optimisation strategies applied to charging scheduling

In the previous sections, a selection of notable literature addressing the topics of the benefits of V2G services and the influence of the transportation requirements as well as EV charging behaviours were reviewed. As evidenced by the results presented, the benefits and drawbacks of V2G can be expressed as a range of figures, depending on the setting, conditions and boundaries of the case study. The model adopted to depict the stochastic nature of EV utilisation has a strong influence on the results. This diversity in the available results in the literature indicates that this topic should be addressed by a mathematical optimisation problem, which attempts to model the real-life implementation as closely as possible.

Several studies have addressed optimal charging scheduling for single objectives and multiple objectives. The grid impact has been widely addressed as a critical objective. In [52] the power flow in a distribution network RES was optimally controlled by scheduling

EV charging. In [54] voltage deviation caused by excessive PV generation was successfully mitigated by discharging the batteries of EV fleets. In [57] the electricity demand of a residential building was satisfied with a combination of PV system and EVs. The availability of EVs and their capacity to provide demand peak shaving was investigated in [53]. In the framework proposed in [64], by making use of electricity demand and PV generations forecasts, an aggregator and several EV agents performed load levelling. A decentralised optimisation process for EV charging scheduling was proposed in [65]. Although their work did not consider RES, the proposed method effectively performed load levelling with a fleet of EVs. A decentralised approach was also proposed in [66] to optimally charge EVs in order to reduce demand peak and variance. Power imbalance reduction was addressed in an optimisation process performed in [67]. Their proposed method reduced the mismatch between PV generation and electricity demand. A number of studies also have aimed at minimizing the EV charging cost [38] as well as energy arbitrage [58]. In [68], EV charging/discharging was controlled to implement optimal energy management in a micro-grid with availability of wind generation. Their method reduced the energy cost of the building. Provision of frequency regulation was explored in [52]. However, a major lack of research on battery degradation minimization has been identified, as none of the aforementioned studies addressed this issue. Indeed, few research included battery degradation in their economic analysis but only as a constant parameter, based on estimated cycle life and unaffected by the charging schedule. Moreover, apart from [69] other studies did not minimise CO_2 emissions.

Only a number of studies in recent literature have applied MOO in the context of smart grids and EVs. In [70] grid load variance was minimised while providing voltage control by scheduling grid-connected EVs with a centralised approach. However, the objective functions were sequentially optimised and, since the results of the top layer fed the lower layer, the objectives did not conflict with each other. [71] optimally deployed EV charging infrastructure to minimise annual investment cost and maximise annual captured traffic flow (number of EVs charging at the EVSE), by performing a centralised decision plan. In [72], EV battery swapping stations were simulated in a distribution network in order to minimize

battery charging cost, power loss cost, to flatten the network voltage profile and release network capacity. [73] optimally scheduled energy storage systems by minimising both battery calendar degradation (as will be defined in chapter 4.3 this is time-dependent degradation) and energy costs. However, in their proposed methodology, the two objectives were linearly combined. In [69], a notable approach of scheduling EV charging to minimize cost and emission was proposed, but a comprehensive framework addressing all the relevant objectives was not proposed. In [74] an improved optimal power flow in a distribution network with EVs, wind energy and PV was implemented to address CO_2 emission and operational cost. The uncertainty regarding RES generation and EV availability considered with a Monte Carlo simulation and multi-objective genetic algorithm was implemented to address the two objectives. This study was able to highlight the trade-off between the two objectives; however, as the authors themselves point out, their centralised approach suffers from high computational expense, at the point that parallel computation was proposed as a solution to reduce this burden. Furthermore, battery degradation was not addressed in their work. Fuel consumption and battery degradation and were linearly combined for optimal drive-train energy management strategy in [75]. Although the approach proposed in the paper is effective in optimising the two objectives, the interaction with the grid was not investigated since no charging scheduling was implemented. Load variance and charging cost were minimised with a weighted sum method in [76] with a decentralised approach. Although some measures to reduce battery degradation were mentioned, i.e. reduce the maximum SOC level, it was not optimised as a separate objective. Similarly, no mention was made on the environmental footprint of the charging process, and the weighted sum method may not find Pareto solutions if the final objective function is not convex; in general, ε-constraint (an optimisation strategy which consists of setting multiple constraints related to the objectives in order to define the Pareto frontier) is superior as it overcomes such problem.

Game theory based approaches have also been implemented to energy management (see [77]), where different players with different strategies seek a Nash equilibrium. However, a framework and methods to adapt game-theoretical approaches to multi-objective optimisation have not been proposed yet.

2.7 Conclusions

This chapter presented the recent trends on V2G technologies in terms of their profitability and the most advanced optimisation techniques to integrate EVs and RES by achieving different objectives. Based on the analysis of the results from the presented studies and real-life demonstration projects a number of key conclusions can be drawn:

- Smart charging and V2G services provide benefits both from an economic and a grid operation point of view. Additionally, Smart charging and V2G reduce the impact of EV charging on the optimal grid operation.
- The availability of EVSE and their rating are other major influencing factors that decide the economic viability of V2G services.
- Aggregators will play a primary role as intermediary between V2G service providers at different scales and stakeholders that demand such services.
- EV batteries are the storage assets for V2G services and their capacity should be dimensioned adequately.
- To allow V2G profitability, EV batteries must become more economically competitive and they should currently be exploited as power sources, i.e. high powers and low energies actually provided.

The main research gaps can be summarised as:

- Lack of a holistic solution to simultaneously optimize the critical objectives of energy cost, battery degradation, grid net exchange and CO_2 emissions. None of the studies has addressed the trade-off between these objectives. Indeed, only a subset of the aforementioned objectives has been optimised.
- There is an evident lack of studies addressing battery degradation minimisation as an optimisation process.
- CO_2 emission has been seldom addressed as an objective, and its conflict with other objectives has not been satisfactorily highlighted.

- The trade-off between ancillary service provision and other energy services has not been explicated in the literature.
- A decision making process tailored to key smart grid stakeholders, namely end electricity user, EV owner and electricity system operator has not been proposed in previous works.
- None of the reviewed studies proposes the concept of dynamic battery degradation model, and no mention to an adaptive algorithm is made in literature.
- Real-time charging scheduling is being explored as a key research objective however, this is not developed in a multi-objective framework.
- Game theoretical models do not take into account grid constraints and focus mainly on the payoff maximisation.

As stated in Chapter 1, the aim of this research is to fill the aforementioned gaps by:

- Optimising end-user electricity cost, EV battery degradation, grid net exchange and CO_2 emissions.
- Developing an adaptive dynamic battery model with three key stress-factors, which is used to minimize cycle degradation.
- Simulating ancillary service provision and highlighting the trade-off with other objectives.
- Developing a decision-making process in order to control EV charging, which involves the end electricity user, the EV owner and the system operator.
- Implementing real-time multi-objective optimisation based on dynamic programming, to control the charging/discharging process of a commercial battery in a laboratory setup.
- Proposing a game theoretical framework, that enables energy trading among prosumers and EV users while complying with grid constraint.

In this chapter, a literature review of research works that addressed EV charging scheduling to provide energy services was carried out. The next chapter focuses on the development of mathematical models that depict various utility functions representing the interests of the stakeholders involved in smart grids.

Chapter 3 Modelling of a synergetic EV-RES integration framework

3.1 Introduction

As stated in Chapter 1, the aim of this research is to develop strategies to optimally schedule EV charging in order to achieve technical, economic and environmental objectives. For this purpose, mathematical optimisation algorithms have been applied to control EV charging. Hence, the objectives to be achieved have to be described with mathematical models. It is worth noting that these objectives should be modelled based on the behaviour and interests of a number of stakeholders. Hereafter, the word "stakeholder" will be used to address those individuals or groups - which could be persons, organisations or institutions - that can obtain benefits by interacting with RES and EVs. As both RES and EVs are connected to the electricity system, we define as stakeholders those individuals or groups that interact with the electricity system. The latter is categorised into three main levels:

- Transmission system; characterised by high voltage (HV), 400kV-132kV;
- Distribution system; characterised by medium (MV) to low voltage (LV), 66kV- 0.4V;
- Behind the meter; it is primarily installed at low voltage and depending upon the power rating, could be single phase (230V) or three phase (400V).

As RES and EVs are mainly connected at medium voltage level, the distribution system will constitute a crucial field upon which a number of strategies proposed in this research are based. However, as the three levels are interconnected, actions undertaken at one level will

have effects at the other levels. For instance, frequency regulation services control the electrical frequency mainly at a transmission level, but their effect are felt all the other levels. From transmission level to behind the meter, the stakeholders include:

- Energy producers connected at HV;
- Transmission system operator (TSO);
- Distribution system operator (DSO);
- Energy producers connected at medium voltage;
- End-electricity-users connected at MV;
- End-electricity-users connected at LV;
- EV owners (which could also be at the same time the users).

Other stakeholders that cannot be categorised according to their physical interconnections but are more of business stakeholders are automotive OEMs, charging operators (companies that buy and dispatch energy for charging EVs in streets and car parks), EV charger dealers (can be different from operators, they sell charging equipment), EV battery manufacturers, the electricity wholesale market and ancillary service market regulator, utility companies in charge of the distribution of electricity to the end-users, local authorities and policy makers.

Figure 3.1-1 describes the physical connections and business relationships among the aforementioned stakeholders.

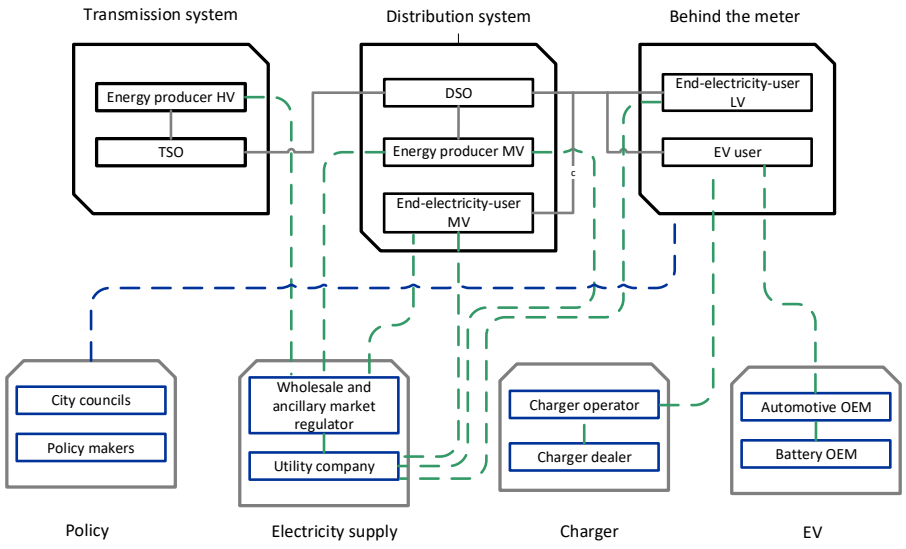

Figure 3.1-1 Stakeholders involved in the electricity system with physical connection (grey), business (green dashed) and policy (blue dashed) relationships

Following from the discussion above, the stakeholders involved in the electricity system have been first categorised in two layers, namely the physical layer and the business & policy layer. In the first layer a further allocation has been made according to the voltage level of the electricity connection, from the transmission level to behind the meter; only stakeholders that are physically connected to the electricity system are included in this layer. In the business and policy layer, the stakeholders have been differentiated in four categories according to the economic/policy area that they operate within. Stakeholders that engage with the electricity networks are electricity retailers/utility companies and market regulators. EV manufacturers (OEM) and battery manufacturers are involved from the automotive industry. The providers of EV charging equipment and the operators also cover important roles for optimal EV integration. Finally, policy makers and practicing organisations set the regulation with which the other stakeholders should interact and influence the implementation of the EV technology. The stakeholders on the second layer establish business and policy relationships with the stakeholders at the physical layer. In particular, the interaction with the stakeholders from the policy area are based on regulation that supports (or potentially hinders) the integration of EVs and RES. In this chapter, a framework modelling the interaction of a subset of these stakeholders will be developed, with a focus on the distribution system. Therefore, the structure of Figure 3.1-1 will be modified as in Figure 3.1-2.

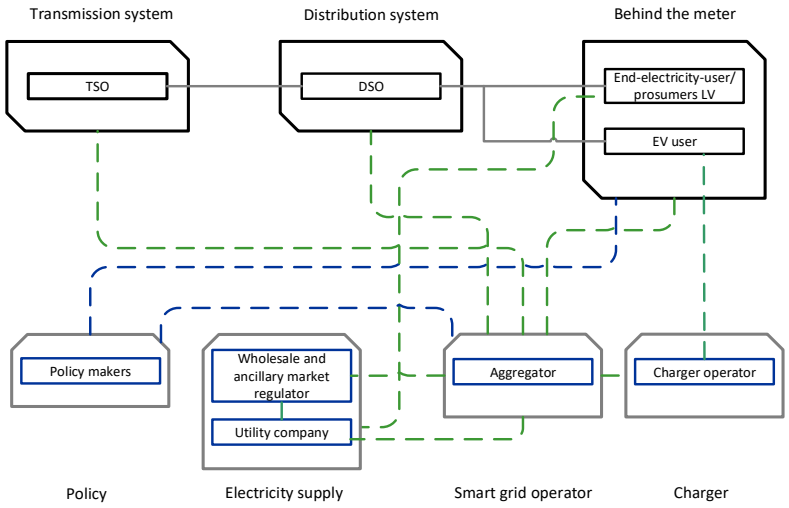

Figure 3.1-2 Stakeholders involved in the framework of multi-objective optimisation of EV charging

Stakeholders involved in the manufacturing industry, i.e. EV and battery OEMs, are not considered within the boundary of this research since at the current market status there is limited scope for their involvement. Although, there have been efforts to involve more OEMs from the point of view of new services (charging schemes, insurances) and interoperability, more business focused strategies should be modelled which are beyond the scope of this research. Similarly, the energy producers from conventional sources (coal, gas, hydro and nuclear) are not modelled and only their environmental impact is considered in the CO_2 emission calculation. In fact, in this research, only energy produced from PV systems connected to the LV network will be modelled; the reason for such preference lies in the distributional dimension of such systems and their flexibility. This is in line with a global interest in promoting small-scale distributed generation as a way forward towards a smart grid. For this reason, utility scale PV systems will not be modelled, although the methods proposed in this work can also be extended to this category. The most evident difference from the more generalised structure presented in

Figure 3.1-1, is perhaps the idea of a new stakeholder which plays a crucial role in modern electricity systems; an aggregator. The aggregator is an agent who manages EVs in order to provide charging services to the EV users [78] and energy services to other stakeholders (i.e. electricity system operators). In this work, an aggregator is defined as a rational agent, which controls a group of generation and storage assets, to provide energy services to grid users/operators with the aim of improving societal benefits. As can be seen in

Figure 3.1-2, the importance of the aggregator is immediately noticeable from the fact that it interacts with all the stakeholder groups. In this sense, the aggregator is seen as a player, which links together the key stakeholders involved in the smart grid at transmission and distribution level.

In this chapter, different parts of a smart grid will be modelled along with the behaviours of the aforementioned stakeholders, to ultimately develop an optimisation framework for effective integration of EVs and RES. The architecture of this framework is presented in Figure 3.1-3.

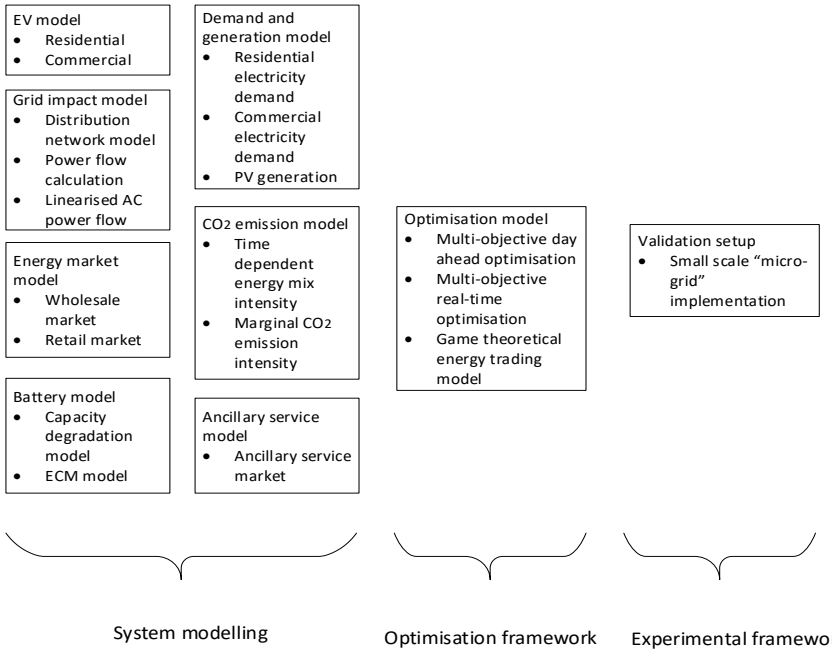

Figure 3.1-3 Multi-objective EV-RES integration model

In order to implement optimal EV charging, the main elements of the system such as EVs, PV generation, distribution network, electricity and ancillary markets are modelled in this chapter. A more detailed and dedicated modelling approach is implemented in Chapter 4 to describe li-ion battery degradation, as it is the main storage asset utilised for the energy services. Multi-objective optimisation methods are developed to control EVs and stationary energy storage systems to improve societal benefits and fulfil the interests of the involved stakeholders. Real-time optimal control strategies are then developed and implemented in a laboratory experimental setup. It should be noticed, that the present research proposed a number of MOO frameworks, based on the considered scale. In fact, the scale or boundaries of the implementation setup will decide the involved users/players/stakeholders, the underlying power network and the data and communication network. When decentralised optimisation is implemented (see Section 6.2), virtual agents process measurement data locally and no information is shared with any entity outside their boundaries. On the other hand, when a hybrid optimisation is implemented, as in Section 6.3, at least the actions of all the involved players and the grid status must be known. This is because the more extended boundary now includes the whole micro-grid and a mix of local and global information feed the optimisation process. However, as large-scale validation was not possible, a scaled-down

residential “micro-grid” setup was tested and the results are presented in Chapter 7; again, since the interactions with other players could not be generated, a decentralised real-time optimisation algorithm was tested.

3.2 Modelling EV utilisation pattern

In this research, a framework for the utilisation of EVs as a short-time storage for various energy services is proposed. However, the main function of an EV is transportation. When EVs are travelling, they cannot serve as storage as there is no electrical connection with the grid. Inductive charging is beyond the scope of this work. Therefore, EV transportation patterns and requirements should be taken as a constraint for energy optimisation purposes. This means that the energy required by the EV user for transportation is always supplied with the maximum priority. In fact, the methods proposed in this work can be implemented in a consensus based scheme, where the EV users authorizes third parties, i.e. aggregators, to manage the charging/discharging process of their vehicles for a short period of time, with the guarantee that sufficient energy will be supplied on time before the next departure. Although research works addressing travelling behavioure changes due to smart charging/V2G services are available, this aspect is not within the scope of this research. This is because, as shown in Chapter 1, the EVs are only being deployed from 2010, and there are several barriers related to range anxiety, and because EVs require uses to be more invested in the planning of the journeys, as public charging infrastructure are only currently being scaled up. Since the technology has not reached a level of penetration that is sufficient to propose models that ask users to sacrifice on their travel, these approaches are not proposed in this research. To this end, the travelling requirements of the user will always be given the highest priority and some capacity margin will always be left in the EV in case of emergency. In order to quantify the EV charging requirement in an average scenario, the distribution of daily driven miles is considered. The UK government conducts National Travel Survey (NTS) on a yearly basis, which provides valuable data that supports modelling the behaviour of the average EV user [79]. These statistics refer to the national car fleet, which mainly comprises ICE vehicles, however, as EVs are increasingly adopted, they will be used under the same travelling

patterns as ICE vehicles. Therefore, it can be assumed that this model applies to EVs. Figure 3.2-1 shows the distribution of daily driven mileage and the cumulative distribution for different ranges, which is taken from the NTS data.

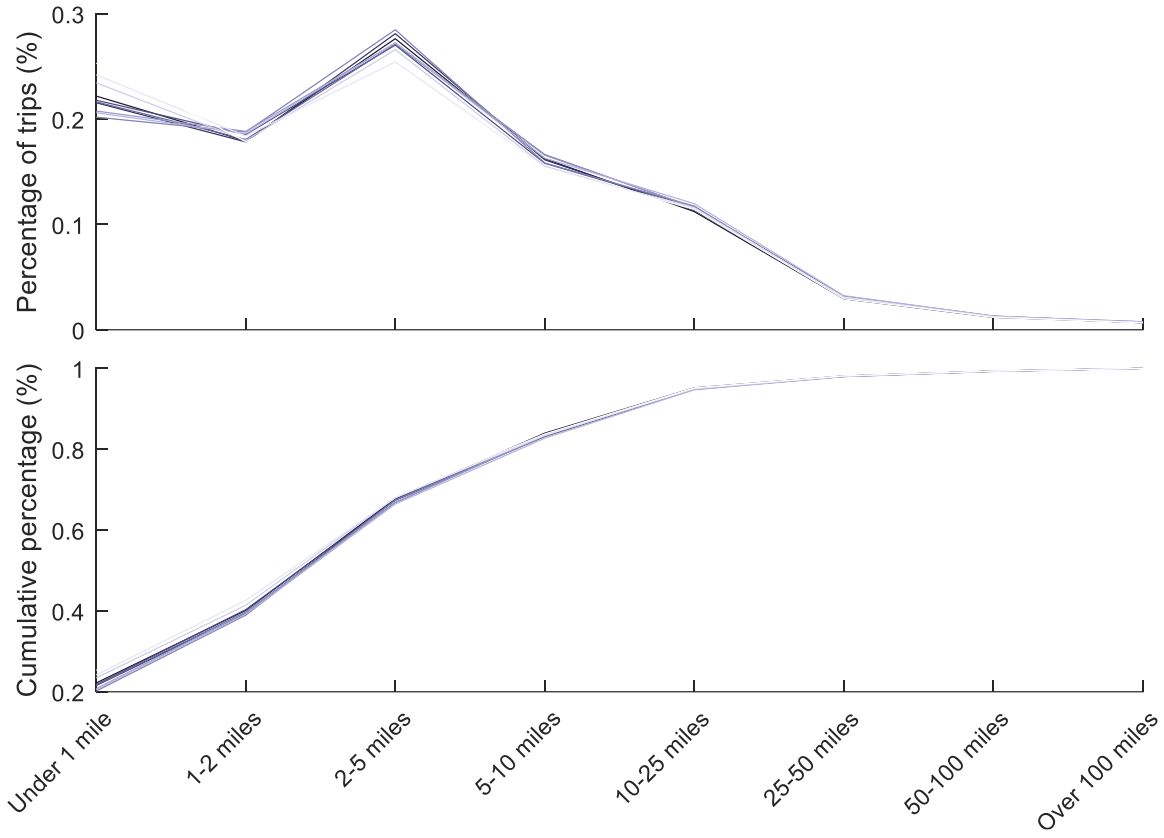

Figure 3.2-1 Distribution of daily driven mileage for ten years 2009-2018 (light to dark) [79]

As can be seen, the behaviour in the past ten years stayed practically unchanged. Furthermore, the average EV in the UK travels for short distances on a daily basis, as the cumulative probability for mileages below 20 miles is 90%. With the current average EV ranges being well above 100 mi, this indicates that the rest of the EV capacity is potentially available for energy services. Another important parameter, which determines the availability of EVs for energy services, is the start times of trips. To this end, Figure 3.2-2 presents the

distribution of daily trip start times for weekdays and weekend days as an average of the past five years.

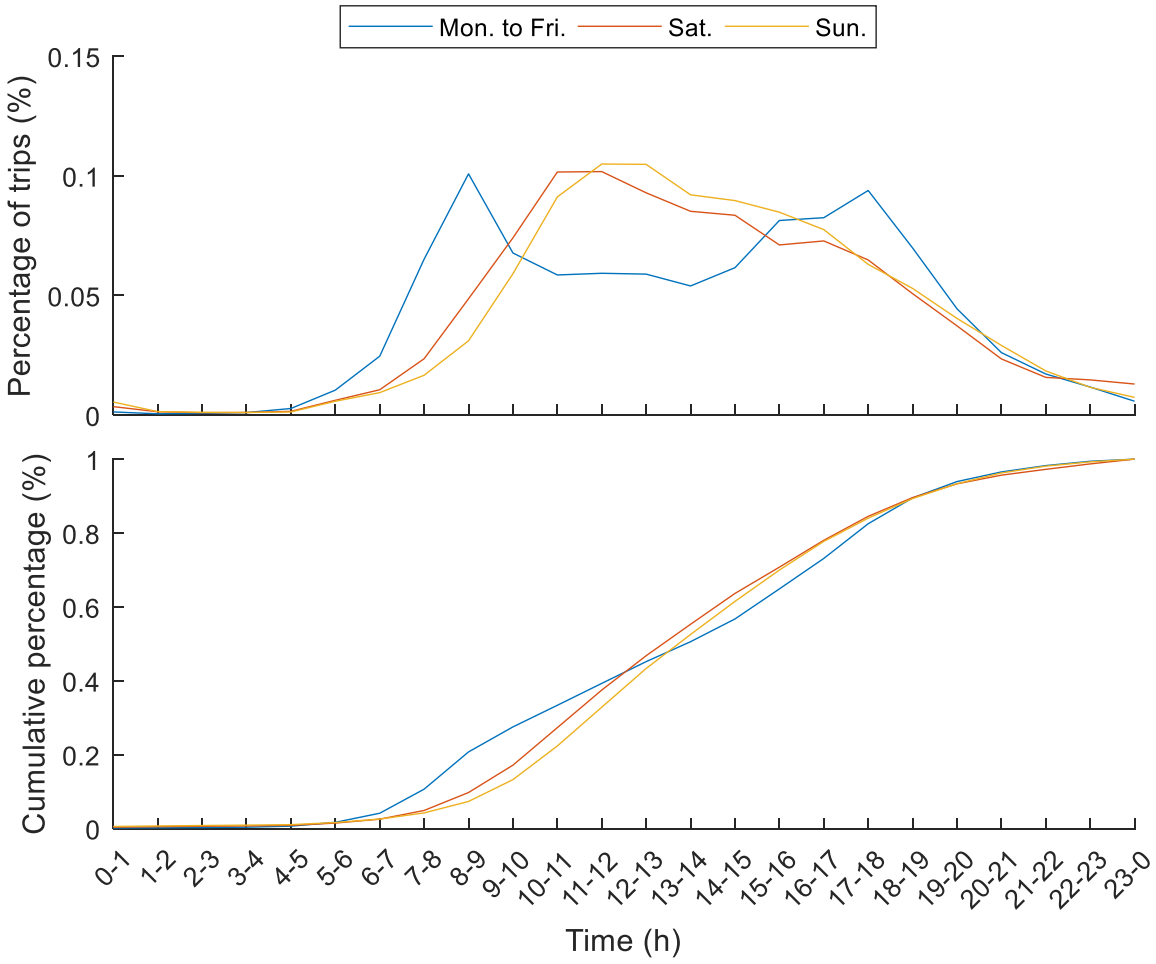

Figure 3.2-2 Distribution of trip start time throughout an average week from 2014-2018 in the UK [79]

A clear difference between the pattern in the weekdays and those in the weekend days is evident. In fact, the weekend profile shows to peaks corresponding to the business hours, 9am to 5pm. On the other hand, the weekend profiles show one surge of trips located in the middle of the day, as drivers use their cars for other activities than professional jobs. This is further confirmed by a classification of the trip start times according to different purposes, as shown in Figure 3.2-3.

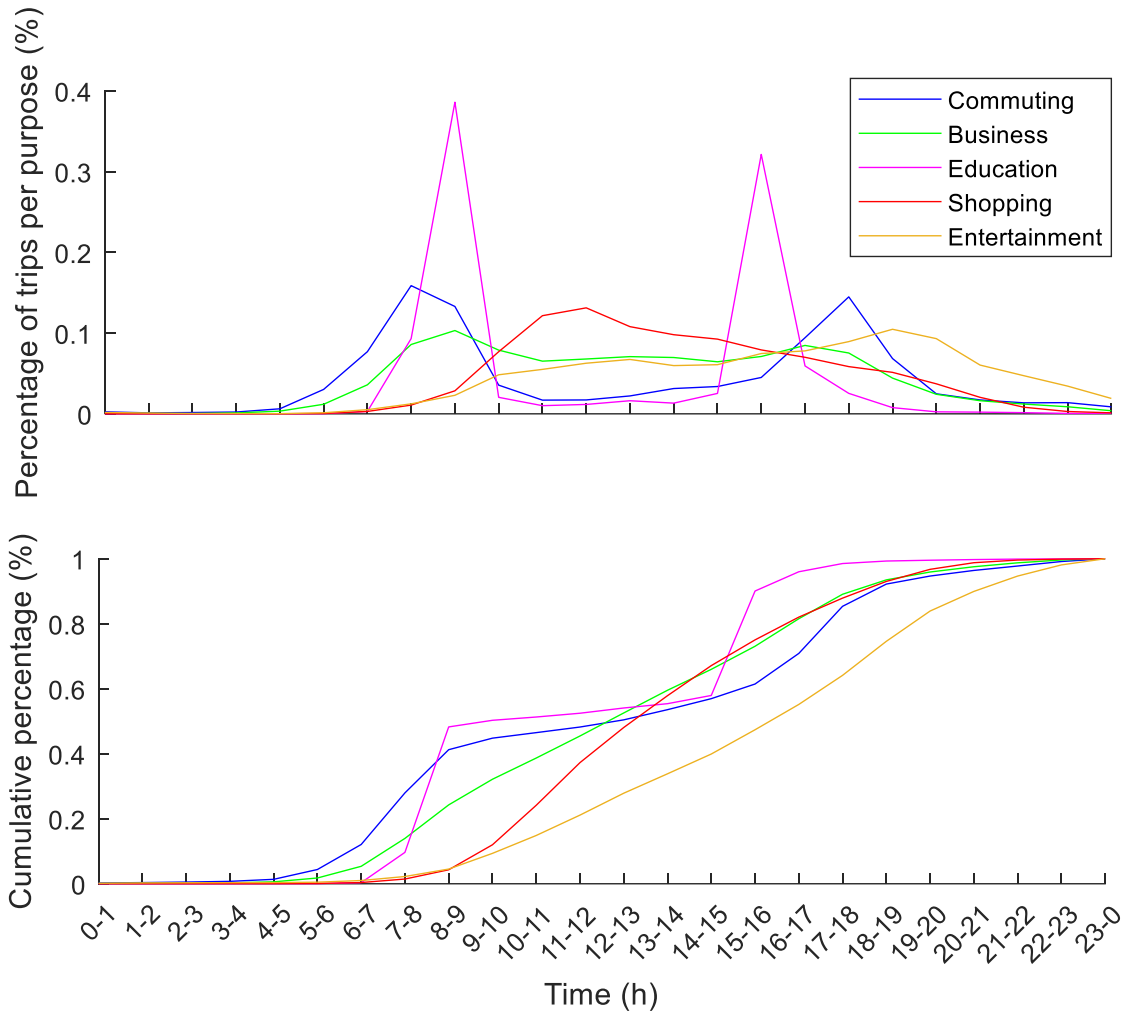

Figure 3.2-3 Distribution of trip start time for an average week for 2014-2018 for different purposes in the UK [79]

The distributions for the five different purposes are radically different; travelling patterns for education (school/university drop off), commuting and business show the typical double peaks located before and after the business hours. In contrast, trips for activities such as shopping and other entertainments are mainly focused on the daily hours, with the highest probability in the middle of the day. By comparing Figure 3.2-3 with Figure 3.2-2, it is clear that during the weekdays, the activities are mainly dominated by professional and education purposes with a comparably smaller extent of shopping and entertainment. In contrast, weekend days are mainly devoted to shopping and entertainment. In accordance with the findings presented this far, the probability distribution of charging initiation times,

categorised according to different locations, match the travelling patterns of EVs as shown in Figure 3.2-4.

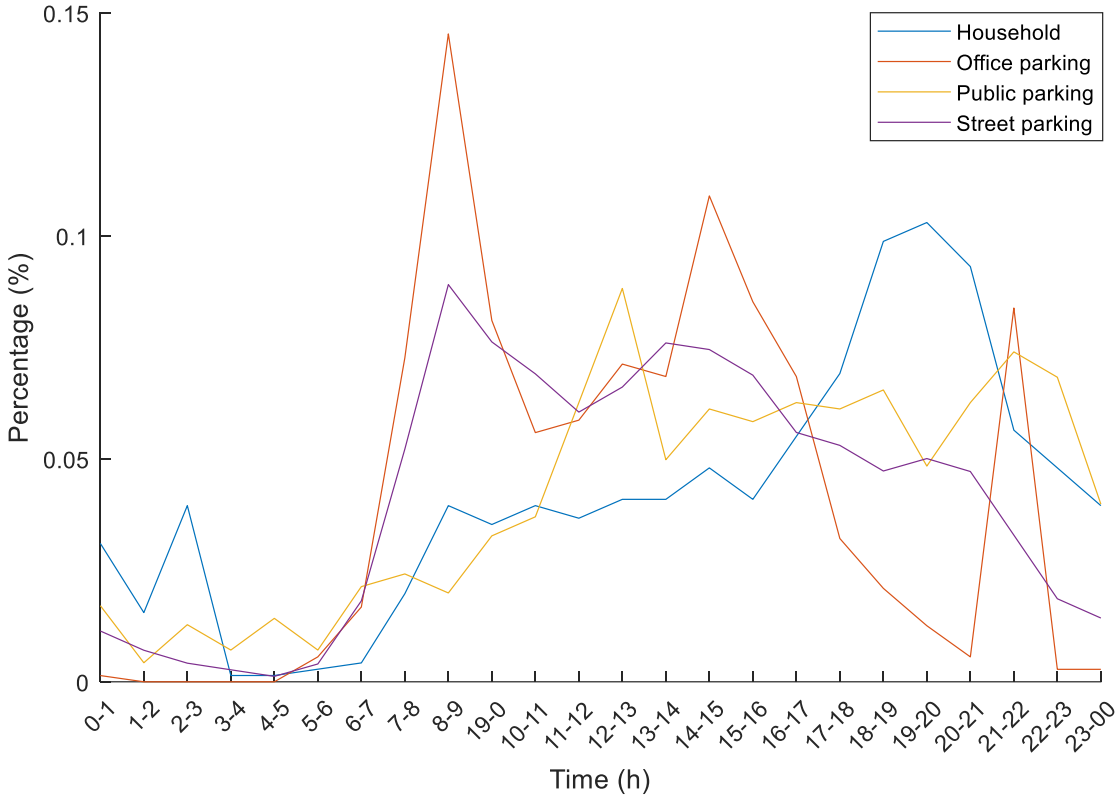

Figure 3.2-4 Distribution of charge start time for different locations in European cities [80]

High probability of charging initiation in households is observed around the evening peak time, i.e. 6 – 9pm, while office parking matches the business hours. An unusually high probability of office charging is noticed at around 22:00 hrs which may be due to utility vehicles that plug-in for the night. A more regular pattern is found in public and street parking, with lower probability during the night compared with the daily hours. It should be noted that this data was collected for EVs in several European cities with the exception of the UK; therefore, the pattern observed in the continent may not necessarily apply to the island. However, this data is only used as a verification of the behaviour of the EV users who initiate charging events as soon as a destination is reached. A further convention adopted hereafter is that departures and arrivals always refer to the households as main idling location; when

relevant, other locations will be explicitly named in the text. Figure 3.2-5 presents the probability distribution of measured SOCs upon plugging-in for EVs in European cities.

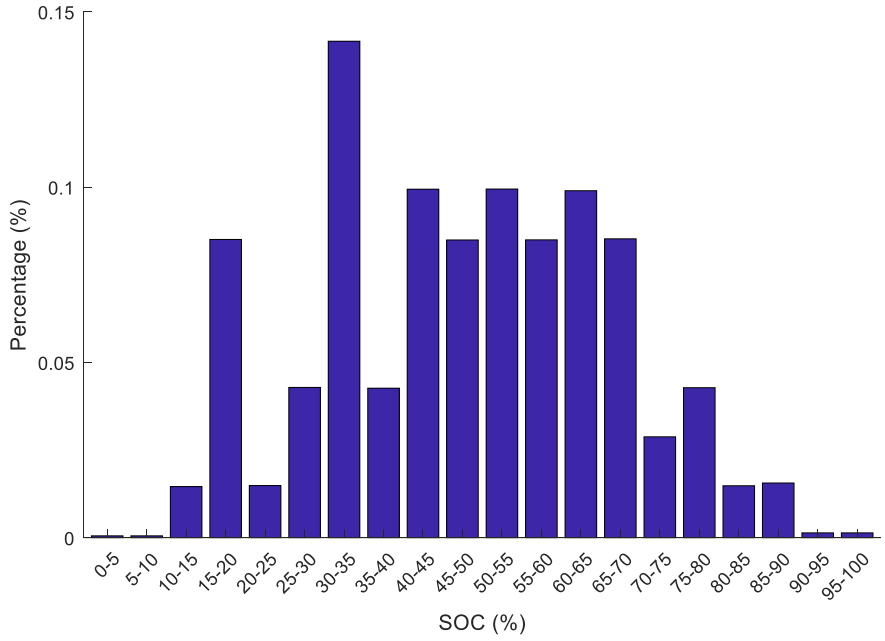

Figure 3.2-5 Distribution of SOC upon plugging-in for European cities [81]

It can be observed that the mid SOC range is particularly prevalent, confirming the relatively short distance travelled which leaves nearly half of the battery capacity intact. It implies that not all EVs will be charged on a daily basis, with only those plugging-in at low SOC requiring a charge.

In this research, the EV transportation model is defined by three parameters:

1) Daily departure and arrival times for trips
2) Daily driven miles
3) Initial SOC upon plugging-in.

It should be noted that when an EV drives more than once per day, the driven mileage has been spread for each trip proportionately to the travelling time (times when the EV is unavailable at home). Further, in this work, a framework where the EV users themselves input this information for the optimisation is proposed. However in absence of such an

interface, it is essential to model the probability distributions of these variables. To this end, in [61], a model that determined the probability distributions of EVs being in various states, i.e. parked and plugged-in, driving, etc. for weekdays and weekends based on data extracted TOU surveys was proposed. Their results match with the data presented above where the probability of being plugged-in at home is low during the day than the evening hours, with the probability being higher in weekend days. The different probabilities of plugging-in/out and daily travelling miles are now fitted to probability distributions. The data is taken from [79] and [80] while the expressions are basic tools of statistical analysis. The probability distributions of these parameters are captured with statistical distribution functions, i.e. normal or Gaussian [82] and Weibull distributions [83], which mathematical representations are provided by the following equations:

$$f(x|\mu,\sigma^2) = \frac{1}{\sqrt{2\pi\sigma^2}} e^{-\frac{(x-\mu)^2}{2\sigma^2}} \tag{3.1}$$

$$f(x|\lambda,k) = \begin{cases} \frac{k}{\lambda}\left(\frac{x}{\lambda}\right)^{k-1} e^{-\left(\frac{x}{\lambda}\right)^k}, if\ x \geq 0 \\ 0 \qquad\qquad\qquad\quad , if\ x \leq 0 \end{cases} \tag{3.2}$$

where the two parameters depicting the trend of a normal distribution are the average value μ and the standard deviation σ. A Weibul distribution is also represented by two parameters; namely the shape parameter k and the scale parameter λ.

In particular, the departure and arrival times from trips, based on the data presented in Figure 3.2-2 are described by:

$$\underset{\mu_d,\sigma_d,\mu_a,\sigma_a,\kappa_d,\kappa_a}{\text{argmin}} \sum_{t=0}^{23} \left[y(t) - \frac{\kappa_d}{\sqrt{2\pi{\sigma_d}^2}} e^{-\frac{(t-\mu_d)^2}{2{\sigma_d}^2}} - \frac{\kappa_a}{\sqrt{2\pi{\sigma_a}^2}} e^{-\frac{(t-\mu_a)^2}{2{\sigma_a}^2}} \right]^2 \tag{3.3}$$

where, argmin stands for the mathematical process of finding the arguments, namely $\mu_d, \sigma_d, \mu_a, \sigma_a, \kappa_d$ and κ_a that minimise the function in brackets. More details regarding mathematical optimisation is provided in Chapter 5. Here, a parameter fitting process is utilised where the sum of the squared error between the actual probability data, $y(t)$ and the parametrised statistical model is minimised. Two normal distributions are used to model the

probabilities of the different plug-in SOCs from the data depicted in Figure 3.2-5 and expressed as:

$$\underset{\lambda_s,k_s,\mu_s,\sigma_s,\kappa_s}{\operatorname{argmin}} \sum_{SOC=0}^{100}\left[y(SOC)-\frac{\kappa_{s1}}{\sqrt{2\pi{\sigma_{s1}}^2}}e^{-\frac{(t-\mu_{s1})^2}{2{\sigma_{s1}}^2}}-\frac{\kappa_{s2}}{\sqrt{2\pi{\sigma_{s2}}^2}}e^{-\frac{(t-\mu_{s2})^2}{2{\sigma_{s2}}^2}}\right]^2 \tag{3.4}$$

As the daily driven mileage probability presents one unique peak around 2 – 5 miles, one normal distribution is used to model the probability of daily mileages, as described by

$$\underset{\mu_p,\sigma_p,\kappa_p}{\operatorname{argmin}} \sum_{mi=0}^{100}\left[y(mi)-\frac{\kappa_p}{\sqrt{2\pi{\sigma_p}^2}}e^{-\frac{(mi-\mu_p)^2}{2\sigma p^2}}\right]^2 \tag{3.5}$$

The results of the parameter fitting process are presented in Table 3.2-1.

Table 3.2-1 Results of probability distribution parameter fitting

Parameter		Statistical distribution parameters	Fitting error
Departure and arrival times	Week-day	$\begin{cases}\mu_d = 7.9, \sigma_d = 1.54, \kappa_d = 0.32\\ \mu_a = 15.8\,, \sigma_a = 3.31, \kappa_a = 0.7\end{cases}$	$e^{fit} = 1.7 \times 10^{-3}$
	Saturday	$\begin{cases}\mu_a = 13.3\,, \sigma_a = 5.41, \kappa_a = 0.54\\ \mu_a = 13.3\,, \sigma_a = 5.41, \kappa_a = 0.54\end{cases}$	$e^{fit} = 7.5 \times 10^{-3}$
	Sunday	$\begin{cases}\mu_a = 13.3\,, \sigma_a = 5.41, \kappa_a = 0.54\\ \mu_a = 13.3\,, \sigma_a = 5.41, \kappa_a = 0.54\end{cases}$	$e^{fit} = 7.5 \times 10^{-3}$
Plug-in SOC		$\begin{cases}\mu_{s1} = 47.5\,, \sigma_{s1} = 18.7, \kappa_{s1} = 8.18\\ \mu_{s2} = 0.47\,, \sigma_{s2} = 5.16, \kappa_{s2} = 2\end{cases}$	$e^{fit} = 11 \times 10^{-3}$
Daily driven mileage		$\mu_p = 1.8\,, \sigma_p = 2.41, \kappa_p = 1.45$	$e^{fit} = 6.9 \times 10^{-3}$

It should be pointed out that in this research, the level of charge in EVs is always kept above 20% of the full capacity as a precaution against unexpected trips. Furthermore, as will be discussed in Chapter 4, keeping SOCs near the lower extreme can damage the health of the battery. Hence, although Figure 3.2-5 shows a high probability in the range 15-20% of SOC, the operational SOC range considered in the current work is 20-90%. It can be seen that the distribution of trip initiation times matches well with that shown in Figure 3.2-3 for education and commuting purposes, with the peak of departures being located at 8:00 hrs and arrivals at nearly 16:00 hrs. Figure 3.2-6 provides a graphical example of the fitted probability

distribution of arrival and departure against the real travel data, as for Figure 3.2-2, for weekdays, Saturdays and Sundays. It can be seen that two the two distributions manage to replicate the real data on weekdays, while both on Saturday and Sunday, departure and arrival have the same probability distribution spread across the whole day. For the latter two, the fitting error is undoubtedly higher than that of weekdays, but still below 1%. By randomly generating arrival and departure times from these distributions, it will be ensured that arrivals always occur after departures.

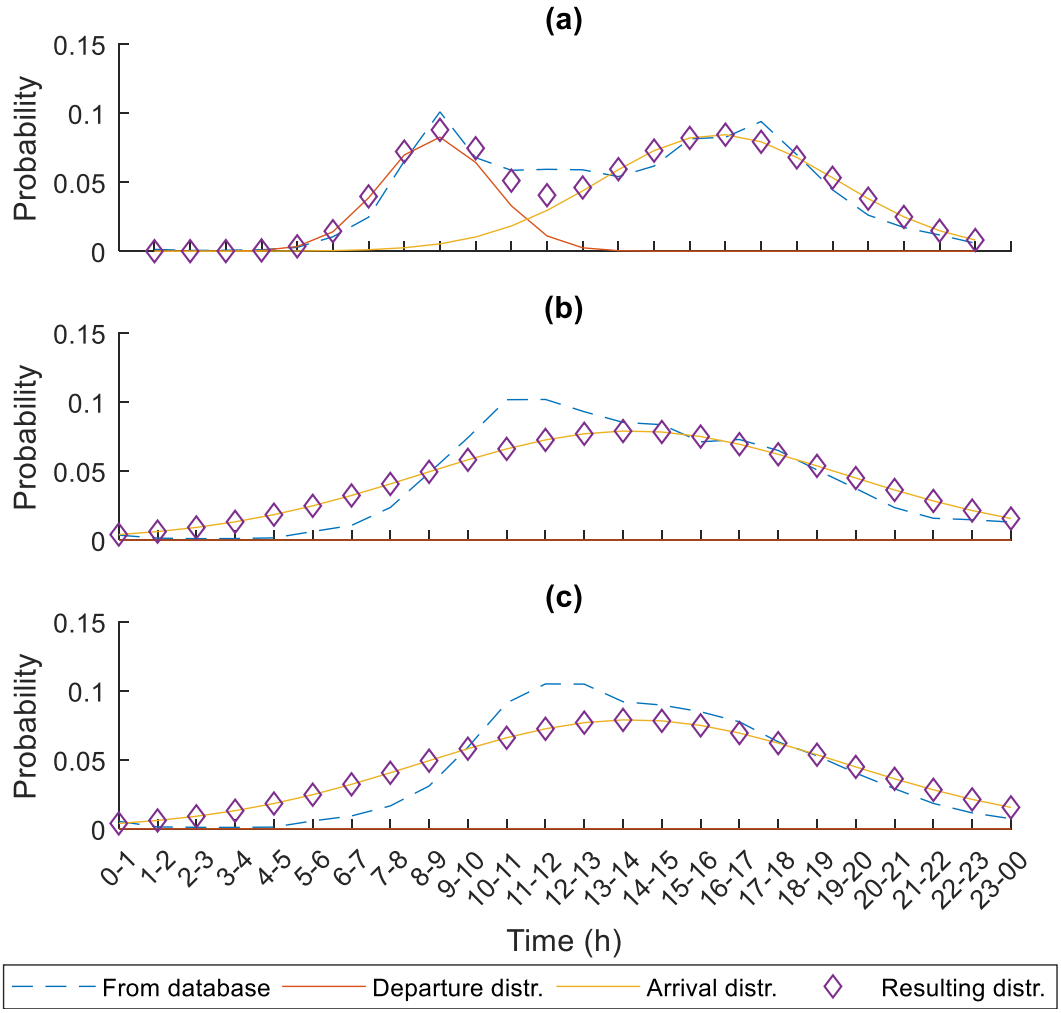

Figure 3.2-6 Parameter fitting of departure and arrival probabilities for (a) weekdays, (b) Saturday and (c) Sunday

Figure 3.2-7 the fitting results for the distribution of daily travelled miles.

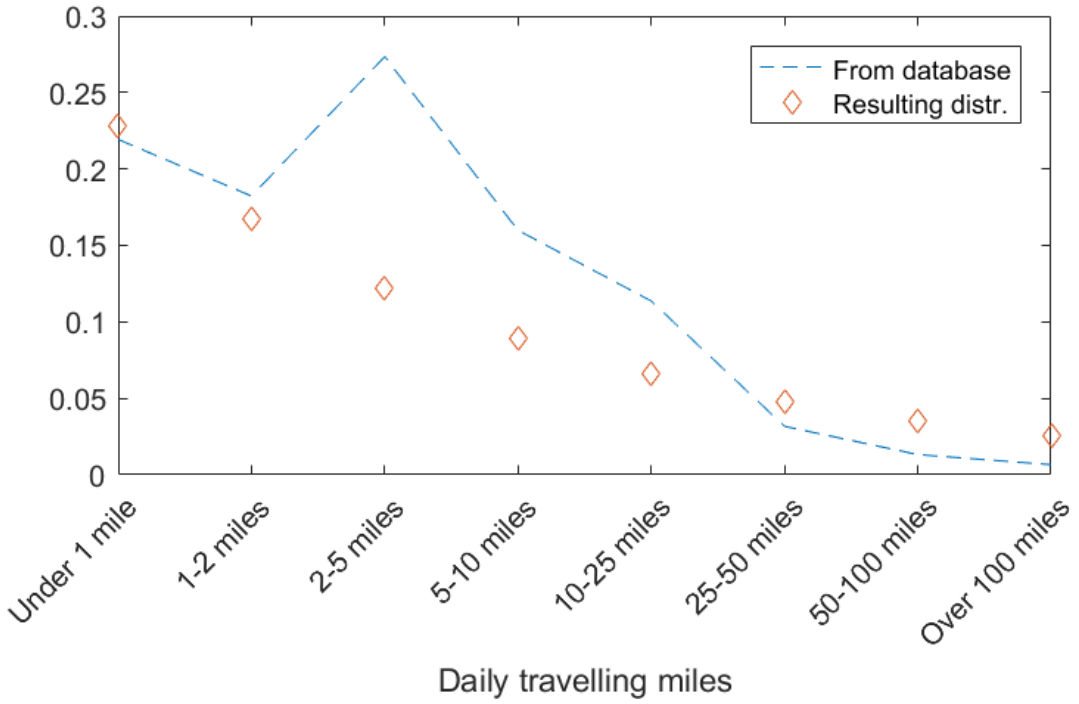

Figure 3.2-7 Parameter fitting for daily travelled miles

3.3 Modelling electricity demand and PV generation

EVs are seen as a suitable solution to minimise the mismatch between electricity demand and local renewable generation, bringing more economic and environmental benefits. This is because both these dimensions are variable, with renewables being also intermittent. Hence, understanding and modelling this uncertain behaviour is a key task in order to ensure a seamless integration of EVs and renewables. In this research, the only form of renewable that will be considered and modelled will be small-scale residential rooftop PV systems. This choice is motivated by the advantage that small scales can bring in terms of a more local generation. Ideally, PV systems could be fitted on any household roof without major building work required. Similarly, only domestic electricity demand will be modelled, although some comparisons with commercial demand profiles will help in identifying different utilisation patterns.

3.3.1 Modelling of electricity demand

Electricity demand in households originates from daily necessities, hence in order to estimate the probability of certain demand levels, i.e. peak demand or low demand, the probabilities that certain activities are initiated should be studied. It follows that, potentially each household will have its own pattern, which will be dictated by the habits of the inhabitants. Modelling the behaviour of electricity users is beyond the scope of this research, as a dedicated investigation is required to accurately model the probability of occurrence of electricity demand, especially at such a small scale. It should be noted that at a higher scale, i.e. neighbourhood, district or city level, the demand profile is much smoother; hence more suitable to forecasts [84]. However, if that profile is to be adopted, the information of the individual will be lost, and the optimisation should be applied to the aggregation of households rather than a single archetype. Figure 3.3-1 shows typical electricity demand profiles for the four seasons, from winter to autumn, weekdays and weekends extracted from the data made available by Ofgem [85]. These profiles have been averaged across several user profiles, hence the smooth behaviour. It can be seen that, especially the winter season is characterised by high demand, with weekdays, Saturdays and Sundays having the highest evening peaks from 18:00 to 19:00 hrs. The winter weekday profile shows two peaks, one located in the morning at 8 and the other at 18:00 to 19:00 hrs evening, while electricity consumption decreases in the middle of the day. After winter, autumn is the season with the highest evening peak, followed by spring and summer. Furthermore, Sundays show high electricity consumption during the day hours, especially between 12:00 to 14:00 hrs. Although these profiles are useful to understand the seasonal effects on the electricity demand, since they are averaged over a large number of users, an overall smoothing effect is obtained. Hence, these profiles do not represent the behaviour of a single conventional residential demand.

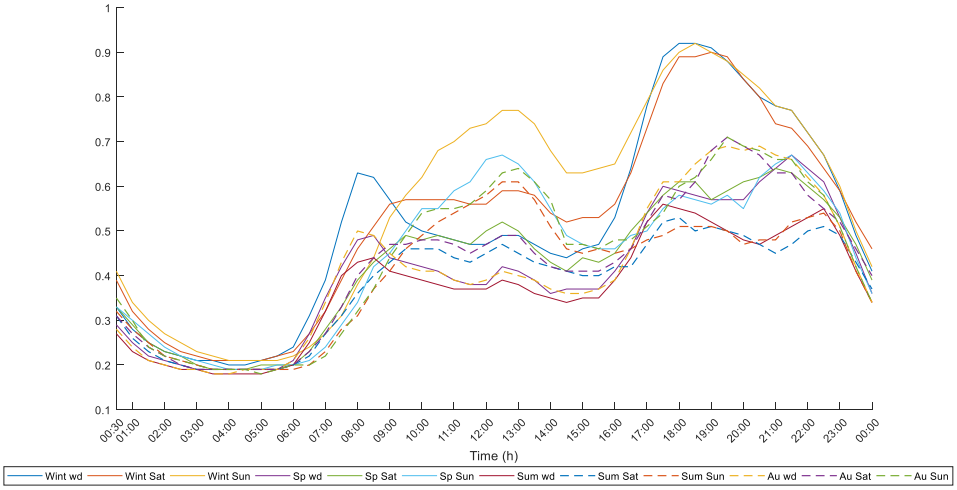

Figure 3.3-1 Average UK electricity demand profiles for four seasons, weekdays and weekends [85]

Year-long data from one of the SEEV4-City project pilots was available, which can be used to study the electricity demand of a typical household.

Figure 3.3-2 shows a typical electricity demand profile; as can be seen, when analysing the behaviour with high-resolution data (5min period) there are several peaks, caused by the starting of household appliances, such as kettle and electric shower.

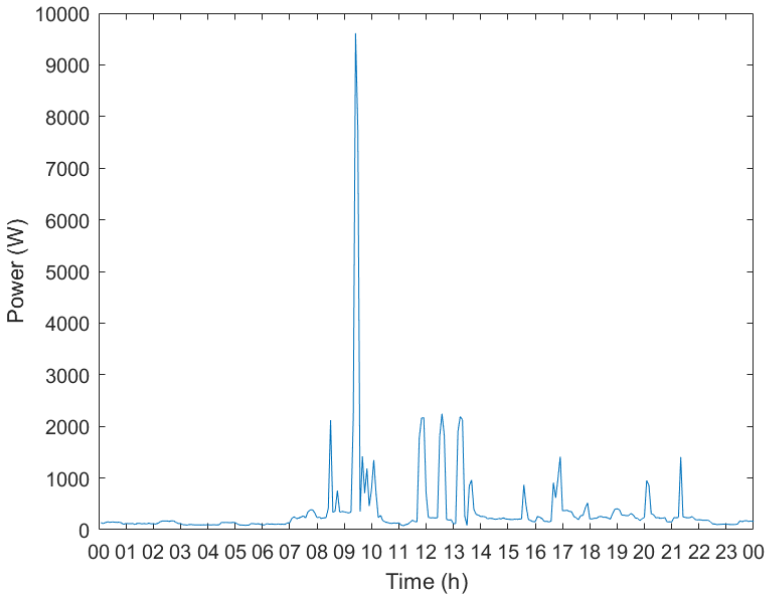

Figure 3.3-2 Typical single household electricity demand profile

Validated electricity demand models for single households are available in literature [86] and these will be used when suitable. Here, a basic approach for predicting future electricity demands of a single household is presented. A variety of methods can be utilised to predict electricity demand in a household, the main ones being:

1) Regression
2) Artificial Neural Network
3) Clustering

However, due to the high randomeness of the electricity demand at single household scale, which is dominated by the householders behaviours, the clustering method is the most sensible approach, and it has been used in this research. This is because, historical electricity demand data is categorised in clusers and future demands can be associated to a certain cluster, rather than, for instance, trying to find the relationship between demand and weather parameters.

3.3.2 Partitioning of electricity demand data using k-means clustering

Following above remark, in this work, clustering methods have been implemented to partition the electricity demand data in few typical characteristic profiles that along with their occurrence probability can provide a sufficiently comprehensive demand model.

The k-means clustering algorithm [90] aims at categorising a set of m measurement data in n partitions $\boldsymbol{P} = \{P_1, P_2, \dots, P_n\}$ in order to minimise the variance in each partition. The following equation

$$\underset{\boldsymbol{P}}{\operatorname{argmin}} \sum_{i=1}^{n} \sum_{x \in P_i} \|x - \mu_i\|^2 \tag{3.6}$$

formalises this concept, where the variance in each partition is minimised for a range of partitions. It presents the sum of dissimilarities/variance in all the partitions for an increasing number of partitions; as can be seen in Figure 3.3-3, quite evidently the variance will tend to zero with increasing number of partitions, but concurrently, the number of profiles in each

cluster will also reduce, making the whole clustering process meaningless. The aim is to find a right trade-off between homogeneity and crowding in each partition.

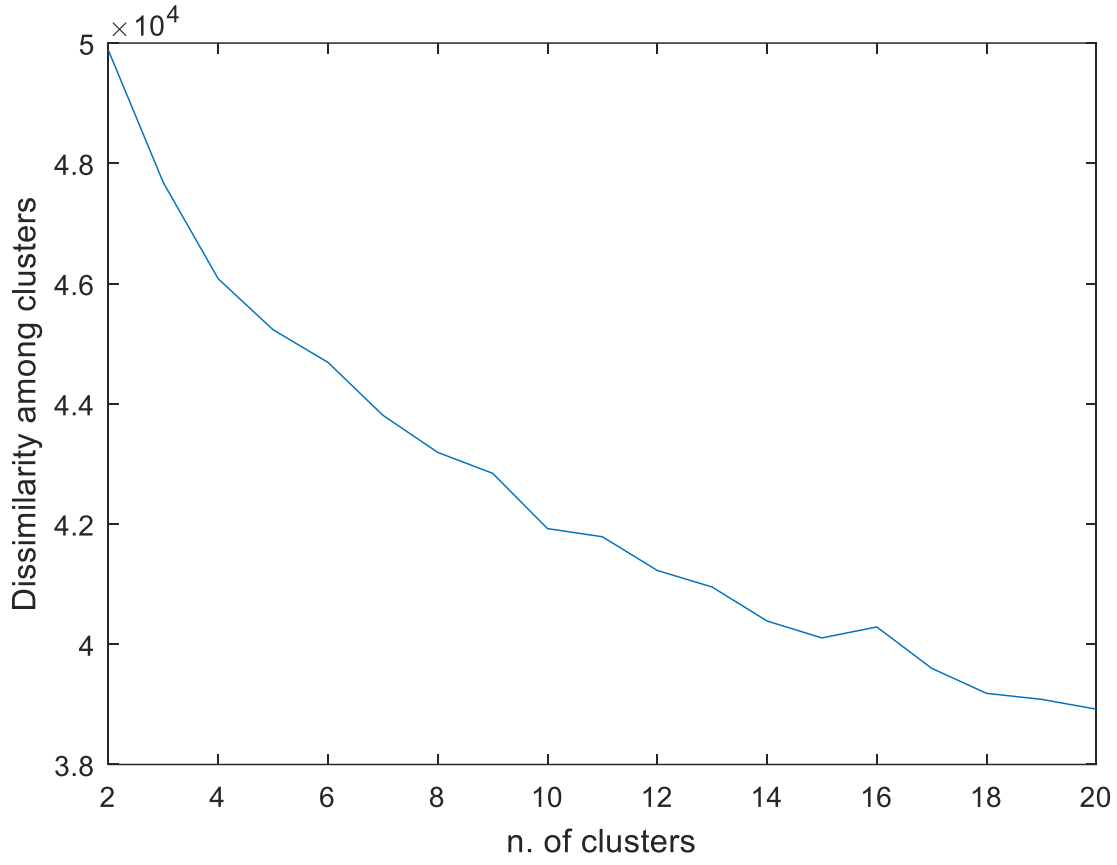

Figure 3.3-3 Average variation within clusters for increasing number of clusters

It has been observed after several tentatives that 10 partitions sufficiently satisfy the above reasoning. Figure 3.3-4 presents the classification of the daily electricity demand profiles in ten clusters.

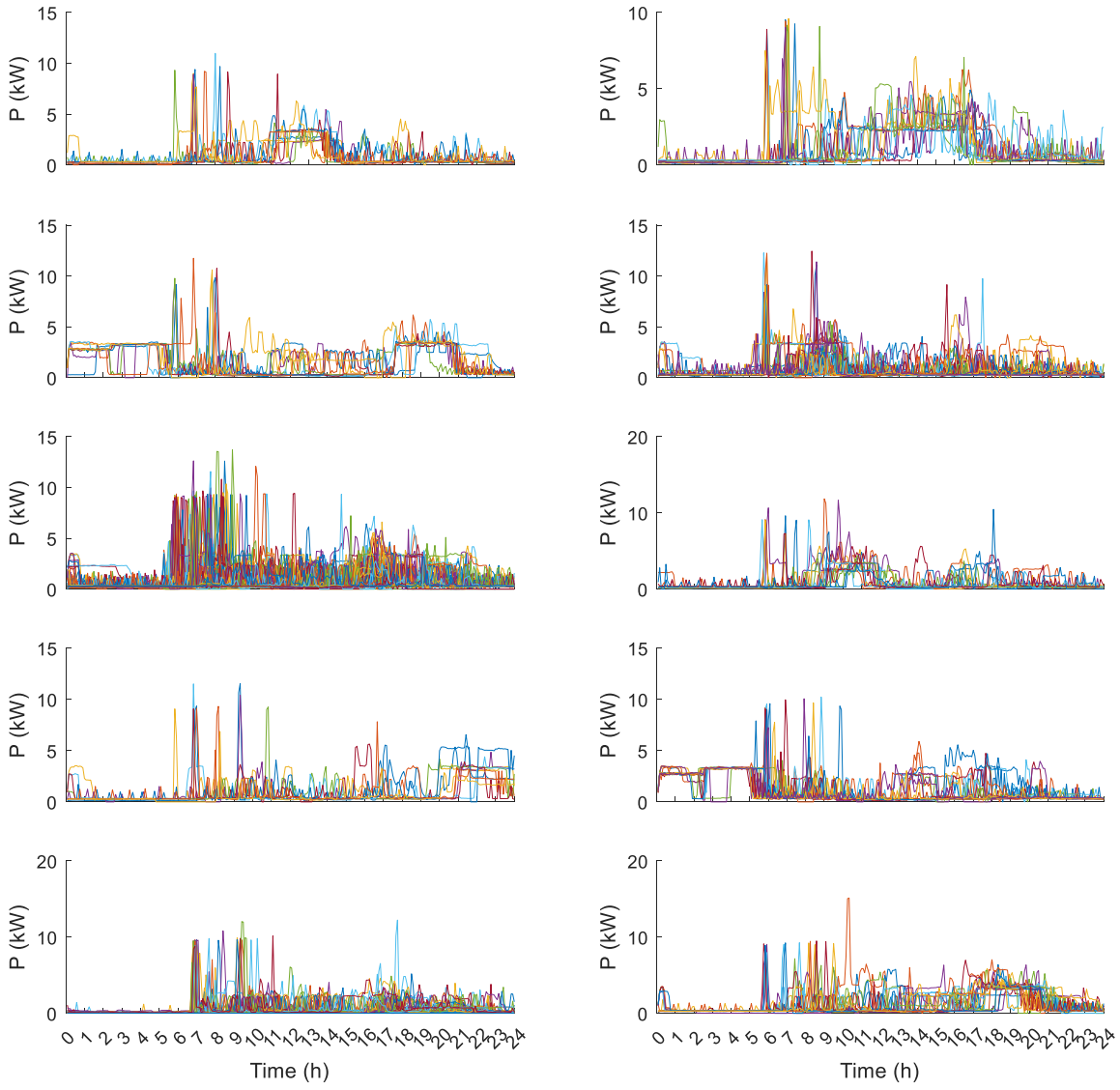

Figure 3.3-4 Partition of daily electricity demand in ten clusters

As can be seen, the ten clusters are sufficiently populated and there is a degree of similarity among the profiles in one cluster. For instance, comparing the profiles in cluster four, an evident high consumption in early morning is noticeable, which is not present in cluster nine. It should be pointed out that this approach will have to be applied to each house under consideration, since from the analysis presented thus far, it is clear that the individual

behaviour and preference of the inhabitants will ultimately decide the electricity demand of each household. With the ongoing installation and progressive operation of smart meters, residential users will become accustomed to this process and demand models tailored to each user profile will become increasingly established.

3.3.3 Modelling of PV generation

Capitalising from the previous Section, some of the approaches adopted for modelling electricity demand can also be suitably applied for PV generation forecast. For the purpose of this research, a suitable PV prediction model should:

a) Take weather information for a future time period as input;
b) Provide a prediction of the power generated for the future time period.

Data driven methods have been widely adopted in predicting future PV generation as they are effective in considering multiple parameters and provide a unique prediction as an output. They represent black-box models that rely on data and are not limited by physics based relationships [91], the latter coming with inherent approximations. Therefore, in this research, a data driven approach is adopted, where historical information is utilised to train an ANN and predict future PV power output; as will be shown in the next section, this method provided accurate forecasting of PV generated power.

3.3.4 Prediction of PV power output using ANN

The input data utilised for training the algorithm is listed in Table 3.3-1; this data format has provided the best accuracy after a number of tentatives.

Table 3.3-1 Input data for ANN training [92]

Parameter	**Resolution**
Global horizontal irradiation	Hourly
Air temperature	Hourly
Seasonal effect function $f^{seas} = \sin\left(d \times \frac{2\pi}{365} - \frac{\pi}{2}\right) + 1$	Single value
Output	Generated power [kW]

The final configuration of the ANN was a feed-forward network, with 2 layers and 12 neurons, which was trained with the backpropagation algorithm. The training performance is displayed in

Figure 3.3-5. The algorithm finds good correlation between the input data and the measured output and with minimal error (the correlation coefficient, [93] defined as the ratio of the covariance between inputs and outputs and the product of their standard deviations resulted $R = 0.96$). The weather data used to train the network is collected by weather stations located all over the UK and is itself a result of some forecasting. The disadvantage of this approach is the reliance on datasets that are indispensable for training the network. Naturally, any error in the original dataset will inevitably translate in prediction errors. Furthermore, datasets regarding specific locations may not be available. This major issue will need to be addressed in a world that is becoming increasingly reliant on data.

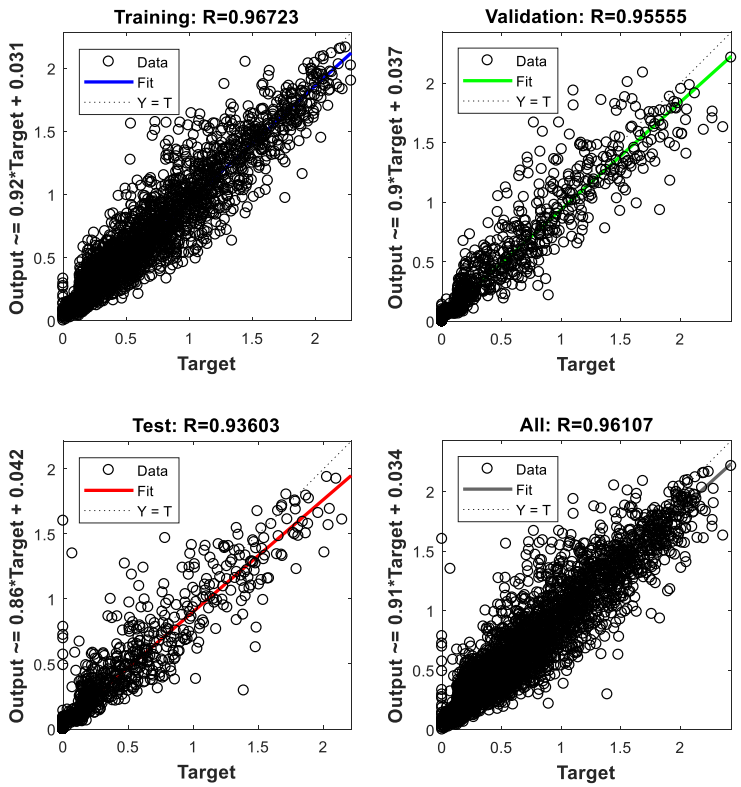

Figure 3.3-5 Training results of an ANN for PV generation forecast

3.4 Modelling of grid impact in distribution networks

The electricity network is the foundation of a smart grid and its efficient operation provides societal benefits to all the users and therefore should be the major objective for any optimal energy control strategy. The electricity network is mainly divided in transmission and distribution network (DN), with the latter providing both medium and low voltage users. Since RES and EVs are almost only connected to the DN, in this Section, we model DNs and the impact of PV and EVs on the operation of the grid. Figure 3.4-1 represents a typical electricity system, comprising of the transmission and distribution system, along with its components.

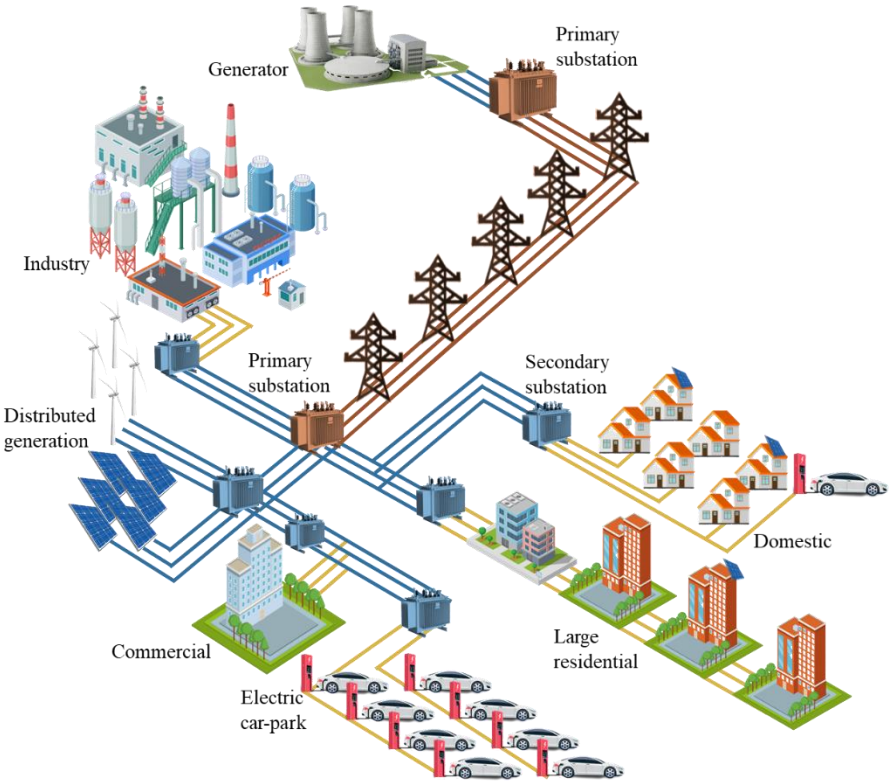

Figure 3.4-1 Illustration of a typical electricity system

The key elements of an electricity system are generation, demand sources and the network connecting them. Electricity can be generated by conventional power plants (coal, nuclear, hydro) and distributed sources, i.e PV and wind. Electricity demand is characterised by

different user profiles, such as industrial, commercial and residential. As EVs are increasingly deployed, they also demand electric power and domestic electricity consumers can become prosumers by installing rooftop PV systems. As aforementioned, the electricity network is divided in transmission and distribution, which are represented in Figure 3.4-1 with red and blue colors respectively. Furthermore, as DN covers both medium and low voltage, the latter is represented by the yellow connections. As can be seen from the figure above, transformers, buses and feeders/lines are the main constituent elements of any electricity network, connecting the electricity generation and consumption elements. In this work, the DN will be abstracted as a black-box where h generation buses and $n - h$ load (or demand) buses are connected. This block will contain the models of all the other elements, such as feeders, transformers and active components, such as any capacitor bank. This is done because changes/upgrades of the network are carried out by the system (network) operators and aggregators and users cannot unilaterally influence their decision (often, users do not have information on the network, only local measurements are available). On the other hand, users can change the way they interface with the electricity network in order to optimise its operation. For the purpose of this study, one bus in the electricity network is allocated to a single domestic user and the power injected or demanded from the bus is that of the associated user. Figure 3.4-2 provides a conceptual representation of the proposed block network model.

Scholars have modelled the electricity network with the bus admittance matrix [94], $\overline{\boldsymbol{Y}}$, which depends on the topology of a DN. The bus admittance matrix assigns admittances to each component of the DN and allows calculating the powers flowing in the network. The necessary definitions for modelling distribution networks and the power flow calculation methodology is provided in appendix A1. The methods presented in this Section have been used to develop [P6].

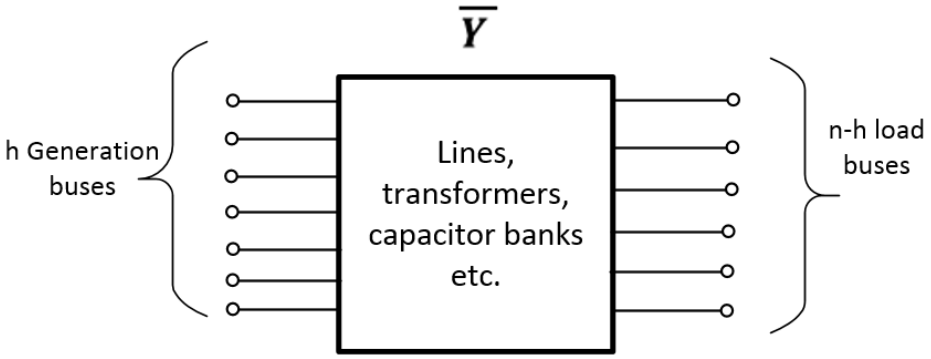

Figure 3.4-2 Block model of the distribution network with generation and load buses

In this research, the Newton-Raphson method has been implemented to determine the impact of EV energy management strategies on DNs. However, as the impact of multi-objective EV charging strategies on the DN will be directly considered in the optimisation process in Chapter 6.2, the power flow equations [95] presented in equations equations A.6.a and A.6.b are reintroduced here to better suit the optimisation process in equations 3.8.a and 3.8.b. Let L be the set of all feeders in the DN, S the set of all buses that are located at the beginning of the feeders and E the set of all buses that are located at the end of the feeders.

$$P_l^{ij} = {E^2}_{s,i}\, G_l^{ii} + E_{s,i}\, E_{e,j}\left(G_l^{ij}\cos\delta_l + B_l^{ij}\sin\delta_l\right), \forall l \in \mathrm{L}, \forall i \in \mathrm{S}, \forall j \in \mathrm{E} \quad (3.7.a)$$

$$Q_l^{ij} = -{E^2}_{s,i}\, B_l^{ii} - E_{s,i}\, E_{e,j}\left(B_l^{ij}\cos\delta_l - G_l^{ij}\sin\delta_l\right), \ \forall l \in \mathrm{L}, \forall i \in \mathrm{S}, \forall j \in \mathrm{E} \quad (3.7.b)$$

Where P_l^{ij} and Q_l^{ij} are the active and reactive powers flowing in the feeder l from bus i to bus j, $E_{s,i}$ and $E_{e,j}$ are the voltages of bus i and bus j respectively, G_l^{ii} and B_l^{ii} are the self-conductance and self-susceptance (defined in appendix A1) of bus i and finally G_l^{ij} and B_l^{ij} are the mutual-conductance and mutual-susceptance between bus i and bus j. The latter parameters can be determined by the bus-admittance matrix. $\delta_l = \theta_l^i - \theta_l^j$ is the phase difference along the feeder l between the phase angle of voltage at bus i and at bus j. It should be noted that power flows from bus j to bus i are also considered and defined as P_l^{ji} and Q_l^{ji}.

Finally, the active power losses in the DN can be expressed as

$$E_t^{loss} = \sum_{l\in \mathrm{L},\, i\in \mathrm{S},\, j\in \mathrm{E}} \left(P_l^{ij} + P_l^{ji}\right) \tag{3.8}$$

The relationship between powers at the buses and powers in the feeders is explicated by the Kirchhoff law for currents (in this case for powers) expressed as

$$P_i^d - P_i^g = P_l^{ij} - P_l^{ji},\ \forall l \in \mathrm{L}, \forall i \in \mathrm{S}, \forall j \in \mathrm{E} \tag{3.9.a}$$

$$Q_i^d - Q_i^g = Q_l^{ij} - Q_l^{ji},\ \forall l \in \mathrm{L}, \forall i \in \mathrm{S}, \forall j \in \mathrm{E} \tag{3.9.a}$$

Where P_i^d and Q_i^d are the active and reactive powers demanded at bus i and P_i^g and Q_i^g are the active and reactive powers generated at bus i. P_l^{ij} is the active power flowing in the feeder l that starts in bus i and ends in bus j and P_l^{ji} the power flowing in the feeder l in the opposite direction. While optimising the energy exchanged in a DN and the power flows, the following constraints on the voltage magnitude and phase angles respectively should always be respected, as detailed in the following equations

$$\underline{E} \leq E_i \leq \overline{E},\ \forall \mathrm{i} \tag{3.10}$$

$$\underline{\theta} \leq \theta_i \leq \overline{\theta},\ \forall \mathrm{I} \tag{3.11}$$

where $\underline{E}, \overline{E}$ are the minimum and maximum statutory limit for voltage magnitudes and $\underline{\theta}$, $\overline{\theta}$ are the minimum and maximum limits for the voltage phase angles for every bus i.

3.5 Modelling CO_2 emissions

Arguably, the main driver for promoting EVs as the prime solution for clean transportation must lie on their comparatively low carbon footprint. In fact, EVs do not cause tail-pipe emissions, which limits CO_2 emissions and slashes particulate. The overall carbon footprint of EVs, including manufacturing, usage, maintenance and decommissioning, is lower than the average ICE vehicle and this Section aims to formulate a methodology to calculate and optimise CO_2 emissions of EVs and households. To allow a fair saving calculation, the whole

lifecycle for both ICE vehicles and EVs should be taken into account; however, the operation of the vehicle is the only controllable part within the scope of this research. This is because, emissions during manufacturing, maintenance and decommissioning are dictated by current and future industrial processes and technological advancement, which are beyond the scope of the present work. Therefore, in this work, CO_2 emissions are calculated from the emissions during usage and emissions during manufacturing, maintenance and decommissioning are not considered.

The CO_2 emissions due to the EV utilisation will depend on the national energy mix, which changes during the day, week and season. Therefore, there are periods of low gCO_2/kWh, which usually happen in off-peak periods (when low-carbon power plants are operated), as opposed to periods with high gCO_2/kWh, which usually happen in peak times (when CO_2 intensive power plants are deployed). An example of this is given in Figure 3.5-1, which shows the UK energy mix based CO_2 emission for 09/11/2017 (winter day). These figures have been obtained considering the lifetime CO_2 emission values for the various generation types listed in Table 3.5-1. This demonstrate that the equivalent CO_2 emission per kWh imported from the grid varies significantly.

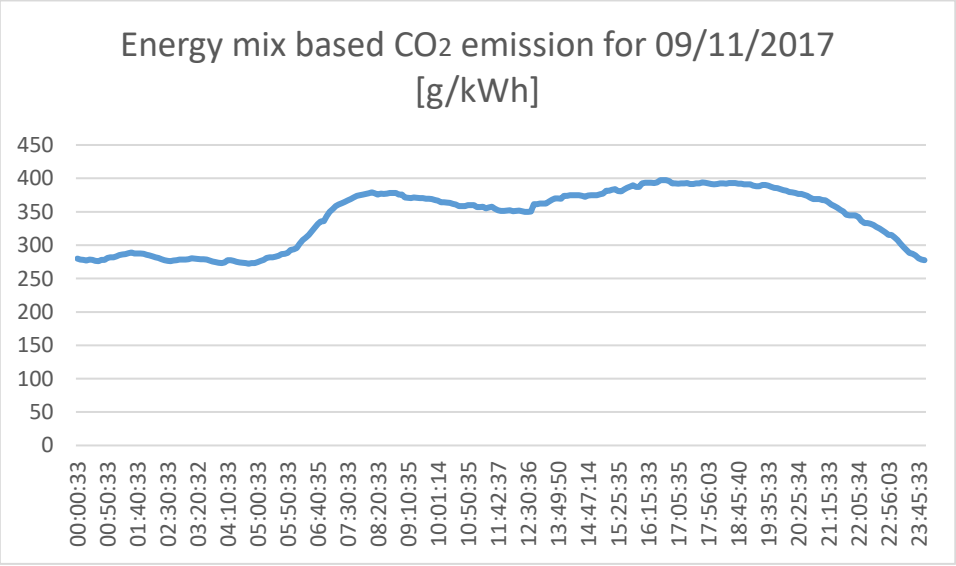

Figure 3.5-1 CO_2 emission caused by the UK national energy mix [99]

Table 3.5-1 Average CO_2 emission for different generation types [99]

Generation type	Lifetime CO_2 emission [g/kWh]
Wind	11
Nuclear	16
Hydro	20
PV	40
CCGT	487
OCGT	487
Oil	650
Coal	870

Therefore, CO_2 emission caused by EV operation can be reduced by implementing smart energy management and charging of EVs. Scheduling BEV charging to occur during off-peak low-carbon periods and peak local PV generation will reduce overall CO_2 emissions, maximize the energy autonomy and at the same time smooth the overall grid demand profile. The CO_2 emitted for satisfying the electricity demand of a household or charging an EV can be defined as

$$\mathbb{E}^{CO2} = \sum_{t=1}^{T} e_t^{CO2} \, P_t^{arch+} \, \Delta t \tag{3.12}$$

Where $t = 1, \dots, T$ is the time-period in consideration for the analysis (hour, day, week etc.), e_t^{CO2} is the CO_2 emission factor at time t and Δt is the length of the simulation time-step. In the equation above, P_t^{arch+} is the power absorbed by the archetype (household or EV) and the + sign indicates that only power consumption contributes towards CO_2 emissions. In fact, although an archetype may also inject power to the grid, especially during PV generation periods, and this may be consumed locally by other users resulting ultimately in CO2 savings, negative CO_2 emissions are not considered in this work. Carbon savings are considered only as reduction of positive CO_2 emissions.

The emission factor e_t^{CO2} considered in (3.13) can be modelled differently according to the assumptions adopted. To this end, both average CO_2 emissions and marginal CO_2 emissions may be considered. The former considers the specific CO_2 emission in $kgCO_2/kWh$ at

different hours in a day, by assuming that the national energy mix is largely unaffected by the local energy management. As such, the CO_2 intensities of the different generations sources are weighted according to their outputs as proportion of the national demand. The following equation is employed for this purpose:

$$\langle e_t^{CO2} \rangle = \frac{ef^{Coal} P_t^{Coal,g} + \ldots + ef^{Wind} P_t^{Wind,g}}{P_t^{nat,d}} \quad (3.13)$$

where, $\langle e_t^{CO2} \rangle$ is the average CO_2 emission factor, $P_t^{nat,d}$ is the national electricity demand at time t, $P_t^{Coal,g}, \ldots, P_t^{Wind,g}$ are the power generated by the different generation sources at time t and $ef^{Coal}, \ldots, ef^{Wind}$ are the CO_2 intensities of the generations sources as presented in Table 3.5-1.

The concept of marginal CO_2 emission factor considers a national energy mix that responds to variation caused by the local energy management. Marginal CO_2 emission factors consider the incremental amount of CO_2 emitted for providing one additional kWh. For this purpose, the merit order considered in the optimal economic dispatch of the different power plants is profoundly relevant. In fact, generation volumes from different types of power plants are dispatched according to their variable (marginal) costs, which itself is not within the scope of this research. However, it should be considered that if one additional kWh was consumed, this would be provided by different types of power plants, according to the consumption hour, as the merit order will decide which plants provide the spare capacity to satisfy the unforeseen demand. Decisions regarding the merit order are entirely dependent upon the wholesale market rules, and therefore cannot be known in advance. However, by studying the variation of the output of the different generation sources, an idea of the daily/seasonal merit order can be made. Figure 3.5-2 shows the output variation of different generation sources in correspondence to the national electricity demand for January 2019.

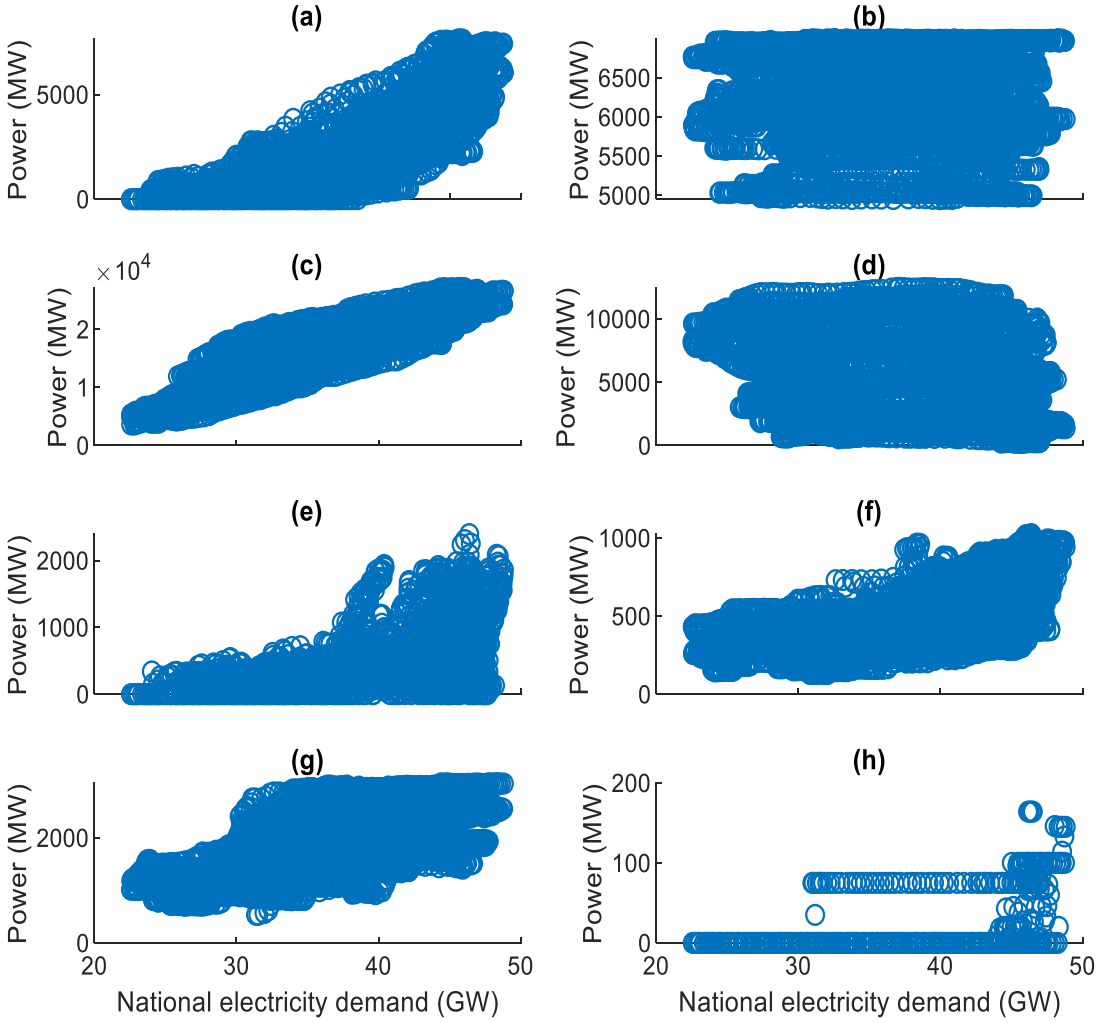

Figure 3.5-2 Power generation variation for (a) Coal, (b) Nuclear, (c) CCGT, (d) Wind, (e) Pumped-hydro, (f) Hydro, (g) Biomass and (h) OCGT [99]

It can be seen that Combined Cycle Gas Turbines (CCGT), coal, nuclear and wind provide most of the UK national electricity demand, with the latter being inflexible due to variable wind speed. Moreover, RES such as PV and wind are given a prioritised injection to the network in order to meet environmental targets. On the other hand, nuclear production is quite stable, whereas it is CCGT that ramps up covering the full range of electricity demand and supplies up to half of the overall consumption (more than 27 GW out of a peak demand

of 48.8 GW). Pumped-hydro, hydro, biomass and Open Cycle Gas Turbines (OCGT) have limited capacity, with the former ramping up only in correspondence of peak demand and the latter being seldom activated.

Following from the above considerations, a marginal generation analysis can be conducted: for each period in consideration (ideally every month), the ramping rate of each generation sources can be estimated for each demand cluster:

- Divide the whole electricity demand range in n clusteters $\{\Delta D_1, \dots, \Delta D_n\}$;
- For each cluster n, quantify $\frac{\partial P(\mathrm{G})}{\partial D_n} \approx \frac{\Delta P(\mathrm{G})}{\Delta D_n}$ $\forall$G; where G is a generation source;
- Calculate the marginal CO_2 emission $me^{\Delta D_n} = \langle \frac{\Delta P(\mathrm{G})}{\Delta D_n} \, ef^{\mathrm{G}} \rangle$ as the contribution of the different sources weighted according to their emission factor ef^{G} to the overall marginal emission factor, for every demand cluster.
- For every hour, measure the national electricity demand, which will be categorised in one of the predefined demand clusters and correspondingly will be assigned a certain marginal emission factor me_t.

Although this methodology rigorously models savings in CO_2 emissions, (it quantifies the emission for an additional kWh or one kWh less), as currently electro mobility is far from being prominent, it could be argued that variations of EV charging demand will not cause measurable variations in the overall national emission factor. Hence, under this assumption, the average CO_2 emission factor will be employed in the remainder of this research. However, it should be pointed out that the methodology developed in this research can be generalised to include marginal emission factors (as will be seen, only the hourly based emission factor will change in the objective function), which will be particularly relevant at future EV penetration rates.

3.6 Modelling ancillary service provision

Ancillary services are “Those services necessary to support the transmission of electric power from seller to purchaser, given the obligations of control areas and transmitting utilities within those control areas, to maintain reliable operations of the interconnected transmission system.” [32]. The aforementioned services include, load following, frequency regulation, reactive power regulation, reserve among others. These services vary in technical requirement and economic remuneration, therefore the profitability for each of them ought to be evaluated case-by-case. A stack of multiple services can also be provided by the same asset if these services are not mutually conflicting. Among these, frequency regulation (FR) has been widely considered as one of the most viable ancillary services for EV fleets [9], [36]-[48]. Such service requires provision/absorption of power in correspondence to frequency deviations. Electricity demand can also be controlled to respond to frequency. Hence, in this work, FR will be modelled and analysed in terms of the prospective revenues, technical constraints and overall feasibility.

However, due to the country specific regulation and the dynamic national regulatory landscape, other services than FR should also be at least referenced. Therefore, in the next paragraphs, we elaborate upon the range of ancillary services that can be provided by EV fleets, and focus on modelling of frequency regulation provision by EVs and how this can be implemented in coordination with other objectives.

Reserve services consist of provision of additional power, or demand reduction, in response to unforeseen increases in demand or unavailability of generation units. Depending on the minimum capacity and response requirements, reserve services can provide different options to EV fleets as suitable revenue streams; the types of reserve service are detailed in Table 3.6-1.

Table 3.6-1 Range of available reserve services in the UK [100]

Type of Reserve	Capacity Requirement	Response time	Payment
Fast Reserve	50 MW	Minimum service time of 15 minutes	Availability fee (£/h) Nomination fee (£/h) Utilisation fee (£/MWh)
Short Time Operating Reserve (STOR)	3 MW	240 minutes, for 2 hours	Availability fee (£/h) Utilisation fee (£/MWh)
Demand turn-up	1 MW	In terms of hours	Availability fee (£/h) Utilisation fee (£/MWh)
Black start	Accept instantaneous loading or demand blocks of 35-50 MW	Ability to provide at least three sequential black starts	Availability fee (£/h) Exercise price (£/MWh)

As can be seen, services such as Fast reserve and Black start require significant capacity, which may take up to thousand vehicles to be available in order to be qualified for service provision. On the other hand, STOR and Demand turn-up are more manageable as with minimum capacity requirements set as 3 and 1 MW respectively, these services can be provided with less than hundred EVs.

Along with reserve services, reactive power provision is a fundamental service that ensures an efficient grid operation. Voltage levels in the electric power grid are influenced by reactive power flows. If the right amount of reactive power is provided, then the network voltage can be controlled. In the UK, the National Grid procures Obligatory and Enhanced reactive power services where the former is mandatory for large generators whose output exceeds 50 MW, and the latter can be provided by any other generator. It should be noted that in order to

control voltages through the provision of reactive power, the provider should be connected to the transmission network due to the relatively low resistance. Therefore, reactive power provision is not considered in this research.

Finally, the different types of FR services are presented in Table 3.6-2.

Table 3.6-2 Frequency regulation services in the UK [100]

Type of Frequency Regulation service	**Capacity requirement**	**Service time**	**Payment**
Mandatory frequency Response (MFR)	10-100 MW	Continuous	Holding payment (£/h) Response energy payment (£/MWh)
Firm Frequency Response (FFR)	1 MW	Static or continuous	Availability fee (£/h) Utilisation fee (£/MWh)

It should be noted that, as the name suggests, MFR could be provided by only those generators that exceed certain capacity thresholds, while FFR is procured through tenders. Moreover, given also the relatively low minimum capacity requirement (this can be satisfied with up to 25 EVs); FFR is a more suitable service for EV fleets. Concluding this brief survey on the ancillary services available in the UK, the prospective payments for 2018/2019 of the most promising services are shown in Figure 3.6-1.

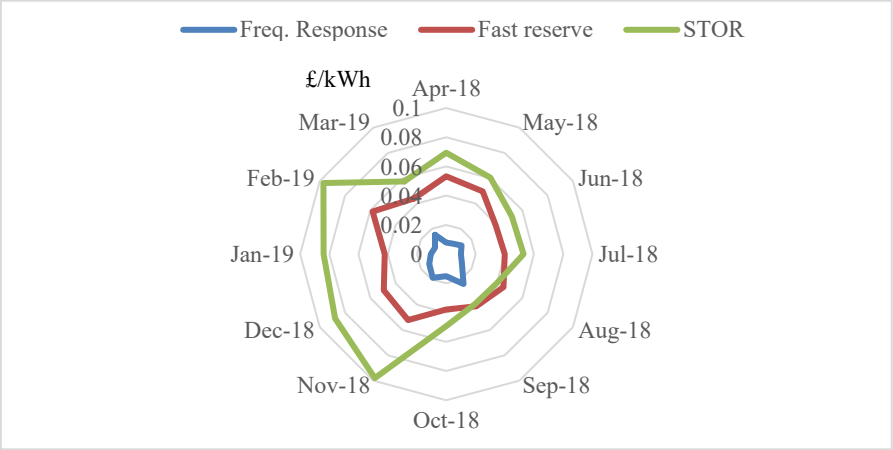

Figure 3.6-1 Average payment for UK ancillary services in 2018/2019 [100]

Although FFR shows the lowest payment, due to the favourable operating conditions (little energy exchange and overall energy neutral as inferred in [9]) and due its requirement throughout a year (STOR is procured around certain periods) it is still the preferable option. In the following paragraphs, FFR provision is modelled as an additional scenario in the optimisation framework.

Ancillary services such as FFR require the regulation of the output of the generation/demand asset according to the frequency deviation from the nominal value of 50Hz. Frequency regulation can be categorized in dynamic and static response. The former implies the automatic change of the active power output of the provider in response to a frequency change. This service is categorised in Primary Response, Secondary Response and High Frequency Response. In order to provide Primary Response , extra active power has to be supplied or the demand has to be reduced 10 s after requested and for a further 20 s. The Secondary Response needs the active power in 30 s and for a further 30 minutes whereas the High Frequency Response needs the provision in 10 s and for indefinite time. For static frequency regulation, a constant response, in terms of increased generation or reduced demand, must be provided after the frequency exceeds certain thresholds. Dynamic FR is carried out with the droop control approach, which determines the regulation power provided in correspondence of a certain frequency deviation.

When providing this service, EVs will have to follow the regulation signal, as defined by the following equations:

$$reg^t = -k^d f \qquad if\ \underline{f} \le f \le \overline{f} \tag{3.14}$$

$$reg^t = -\overline{P^{EV}} \qquad if\ f \le \underline{f} \tag{3.15}$$

$$reg^t = \overline{P^{EV}} \qquad f \ge \overline{f} \tag{3.16}$$

Where $k^d = \frac{\overline{P^{EV}}}{(\overline{f} - \underline{f})}$ is the droop coefficient of the frequency controller, f is the electrical frequency, $\overline{f}$ and $\underline{f}$ are the upper and lower frequency limits of the droop-controller. Figure 3.6-2 represents the relationship between the electrical frequency and the response of a droop controller for a maximum frequency deviation of ±0.2 Hz, ±0.5 Hz and ±0.8 Hz.

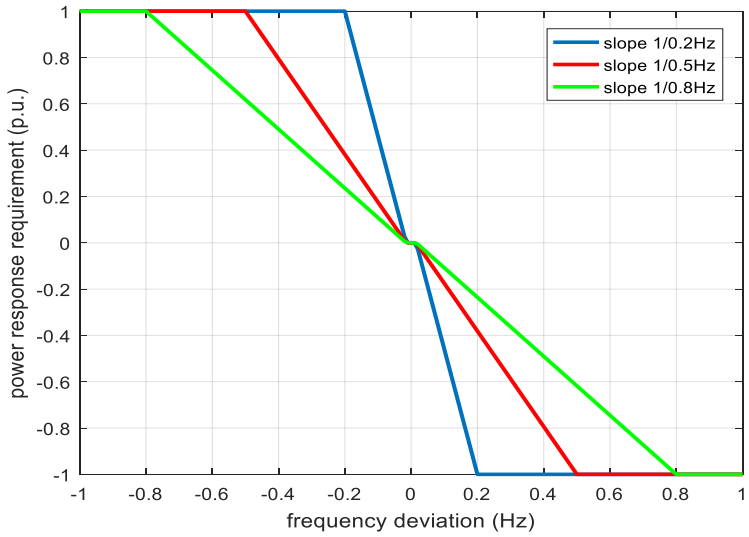

Figure 3.6-2 Droop control for different frequency deviation ranges

We assume the EV provides FFR from 23:00 to 7:00, which is the period that is deemed the most profitable for the UK National Grid ESO [101]. This means in that period the EV is not available for other energy services, such as peak shaving or energy arbitrage. It is implied that availability for FFR should be compatible with the driving pattern of the EVs. According to [9], frequency regulation does not lead to net change in battery charge. Therefore, we assume that the SOC of an EV at the end of the FFR provision window is the same as the

SOC at the beginning of that window. However, participation to FFR schemes implies battery utilisation, which leads to degradation. On the other hand, this service provides a remuneration. The interaction between this service provision and other optimisation strategies are modelled based on the principles outlined as follows:

- The UK National Grid procures FFR for 8 hours on a daily basis. Providers can decide to provide or not to provide such service; to this end this decision is binary;
- The provision period is fixed and cannot be optimally distributed throughout the day according to a mathematical computation;

As a result of the above assumptions, the trade-off between FFR provision and other optimisation strategies is brought to a binary decision variable ($FFR \in [0,1]_{\mathbb{N}}$) which governs the FFR provision, and limits the time steps available for other optimisation algorithms. Hence, we analyse two scenarios, with and without ancillary service provision.

On the other hand, if static regulation services was provided, the full committed power must be provided when requested. The regulation signal can be therefore expressed by

$$reg^t = \overline{P^{EV}} \qquad if\ f \geq \overline{f_s} \tag{3.17}$$

$$reg^t = -\overline{P^{EV}} \qquad if\ f \leq \underline{f_s} \tag{3.18}$$

$$reg^t = 0 \qquad if\ \underline{f_s} \leq f \leq \overline{f_s} \tag{3.19}$$

where $\overline{f_s}$ and $\underline{f_s}$ are the upper and lower frequency limits for the static response.

Arguably, frequency regulation can be provided also with unidirectional controllable chargers, i.e. smart charging. This would minimise the underlying battery degradation as the EVs are only charged for their transportation and not discharged, which reduces their cycling. However there can be instances where smart charging would not be as effective as bidirectional charging and we motivate this assertion in the rest of this subsection. For sake of example, let us consider the situation depicted in Figure 3.6-3.

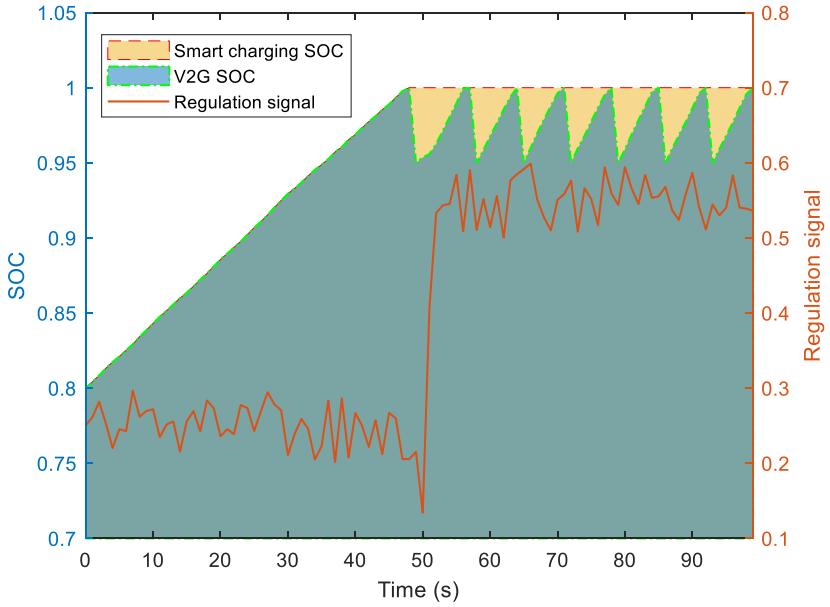

Figure 3.6-3 Example of frequency regulation provision with smart charging and bidirectional charging

The figure above depicts a potential regulation signal provided by the TSO and the evolution of the SOCs of a fleet of EVs under smart charging and with bidirectional charging. It should be noted that in this case the regulation signal is entirely positive, which implies that regulation down (charging) is requested. It can be seen that when regulation is carried out with smart charging, the EVs are charged until their batteries are full (SOC=1) and further regulation is not carried out. On the other hand, when bidirectional charging is available, the EVs are discharged and then charged again by following the regulation signal. It is evident that smart charging does not allow the same flexibility of bidirectional charging because it is limited by the maximum battery capacity of the EVs. Therefore, if only smart charging was available, after the EV batteries are fully charged, they cannot continue providing regulation services. Nevertheless, as discussed above smart charging causes little battery wear, hence it can be bring considerable value. For these reasons, in this research regulation will only be provided with bidirectional charging.

3.7 Conclusions

In this chapter, mathematical models of the core elements of a multi-objective EV charging optimisation framework have been developed. As will be seen in Chapter 6, these models along with key objectives, will contribute in defining the stakeholders involved in a smart grid. The typical household has been selected as the main environment for this research due to the long EV availability and decentralisation of renewable generation. In this context, the first and the central stakeholder modelled in this work is the EV owner whose behaviour has been studied in terms of daily travelled distance, home-parking times and available SOC upon plugging-in. It has been shown that their behaviour can be represented with probability distributions, from which diverse but coherent EV utilisation profiles will be generated to feed the optimisation process. Next, residential electricity demand and PV generation have been modelled: the former is largely dependent on the user's behaviour while the latter is weather reliant. Due to the highly sporadic nature of small-scale electricity consumption, clustering of historical data and a probabilistic approach are the most suitable methods, while the rest are unable to capture demand peaks. However, ANN showed a good performance in depicting PV generation as the dependence on weather is more evident. Distribution networks have been modelled by means of bus-admittance matrices. Furthermore, the principles for including network parameters in the optimisation process, through the AC power flow equations and suitable constraints, have also been briefly outlined; further details will be provided in Chapter 6 when this method will be applied in an energy trading system for EV owners and prosumers. The environmental impact of electricity consumption, both household and EV charging demand, has been modelled with the average CO_2 emission factor. Although marginal emission factor is perhaps a more accurate depiction of the carbon footprint, it is only relevant to larger EV penetration rates where EV charging management can have implications on the marginal generation plant. After presenting the most promising ancillary services available in the UK, FFR has been modelled and chosen as the most suitable for EV fleets, in terms of the prospective payment and more importantly, the operating conditions that will cause less battery degradation as will be seen in the next chapter.

Chapter 4 Modelling Degradation in Lithium-Ion batteries

4.1 Introduction

Lithium-Ion batteries are currently the leading battery technology due to their large application in electronics and the automotive industry. Electric energy is stored through the movement of lithium ions backwards between low and high potential energy states, which happens because of a number of electrochemical reactions, [102]. When lithium ions are in the positive electrode (cathode), their energy state is low whereas they have the highest energy when they are in the negative electrode (anode). An external voltage difference (over-potential) forces lithium ions to move from the cathode to the anode, where they intercalate, a process denoted as charging, during which an external current flows inside the battery. In this process, the ions absorb electrons from the charge collector (made of copper). While discharging, ions naturally move (decalate) from the anode to the cathode, giving up their electrons and supplying a useful current outside the battery. A pictorial representation of the charging/discharging process is provided in Figure 4.1-1. The cathode and anode have a porous meshed structure that enables intercalation and decalation. Metal conductors attached to the anode and cathode allow the electron absorption and release to provide current flow to a load. An organic electrolyte is placed between the two electrodes to allow movement of ions. It is kept apart by a porous separator to prevent a short circuit of the electrodes. The electrolyte employed is typically a combination of lithium salts, such as $LiPF_6$, $LiBF_4$, or $LiClO_4$, in an organic solvent.

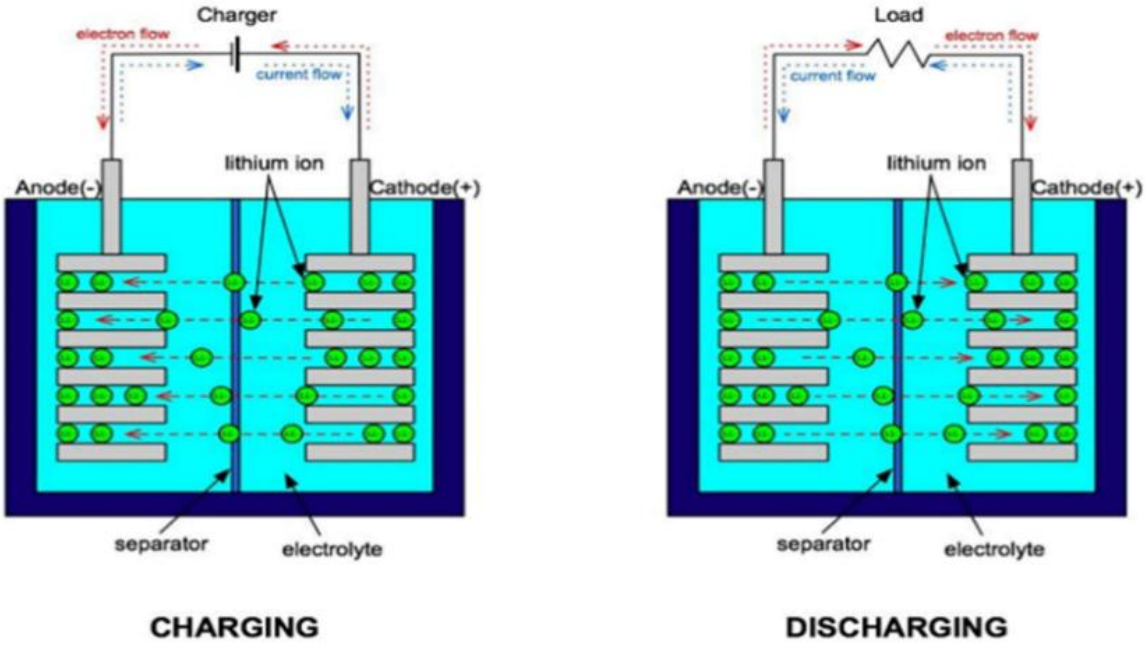

Figure 4.1-1 Lithium-ion charging/discharging process [103]

Lithium has the highest electrode potential per unit mass of any metal, so a lithium ion cell theoretically has the highest specific energy of any configuration. When fully lithiated, the maximum theoretical capacity per gram of active lithium is 372 mAh g-1

In recent years, lithium-ion batteries have been widely adopted in many applications, ranging from mobiles phones to electric vehicles and aerospace applications. The anode is commonly made of graphite, while the cathode can be made of lithium cobalt oxide $LiCoO_2$ (LCO), lithium iron phosphate $LiFePO_4$ (LFP), lithium manganese oxide $LiMn_2O_4$ (LMO), lithium nickel manganese cobalt oxide $LiNiMnCoO_2$ (NMC), lithium nickel cobalt aluminium oxide $LiNiCoAlO_2$ (NCA) and lithium titanate $Li_4Ti_5O1_2$ (LTO) [13]. The main features of lithium-ion batteries are their high energy and power density, compared to other types of batteries of similar size, and their low self-discharge rate. However, they do have some shortcomings such as their high cost, poor performance in low temperature and propensity to degradation. In this chapter, battery degradation is mathematically modelled based on experimental results and such models are later utilised as part of an optimisation process, which will control the factors that cause battery degradation. For the customary utilisation of and EV, the battery is

charged using chargers, and then discharged during driving. Both of these processes cause degradation. As the focus of this research is on optimising the charging process of EVs, the degradation caused by driving will not be modelled although the model developed in the current work can be (and is) applied to real-life driving profiles to quantify the overall degradation. Any battery degradation caused by charging is modelled.

In this context, as the battery is utilised, the phenomenon known as degradation, affects the performance of the battery, both by reducing its useful capacity and increasing its internal resistance. To this end, state of health (SOH) of the battery is a crucial parameter to be monitored, which can be adapted to both capacity fade and resistance increase according to the following equation

$$SOH = min\left(\frac{C_t}{C_0}, \frac{R_0^i}{R_t^i}\right) \tag{4.1}$$

where C_t is the battery capacity at time t, C_0 is the initial capacity of the battery when it is new, R_t^i is the internal resistance of the battery at time t and R_0^i is the internal resistance when the battery was new. In equation 4.1, the minimum symbol indicates that SOH is the minimum between the two parameters, as these two phenomena happen in different timeframes throughout the life of the battery and in a way that is dictated by the battery chemistry. The two terms presented in equation 4.1 are often denoted as capacity fade and power fade respectively. Both contribute to a reduction in the performance of the battery. The occurrence of these two phenomena are associated to chemical reactions that happen inside the battery. To this end, a useful classification is determined by the battery state: if the battery is charged or discharged, it is said to be cycling, whilst when no charging/discharging event happens the battery is considered idle or in storage conditions.

The most critical reactions along with the trigging parameters that cause degradation are listed in Figure 4.1-2, from red to blue indicating the severity of their influence. It should be noted that the order adopted in this study cannot be generalised to all lithium-ion chemistries, as different types will exhibit different dependencies.

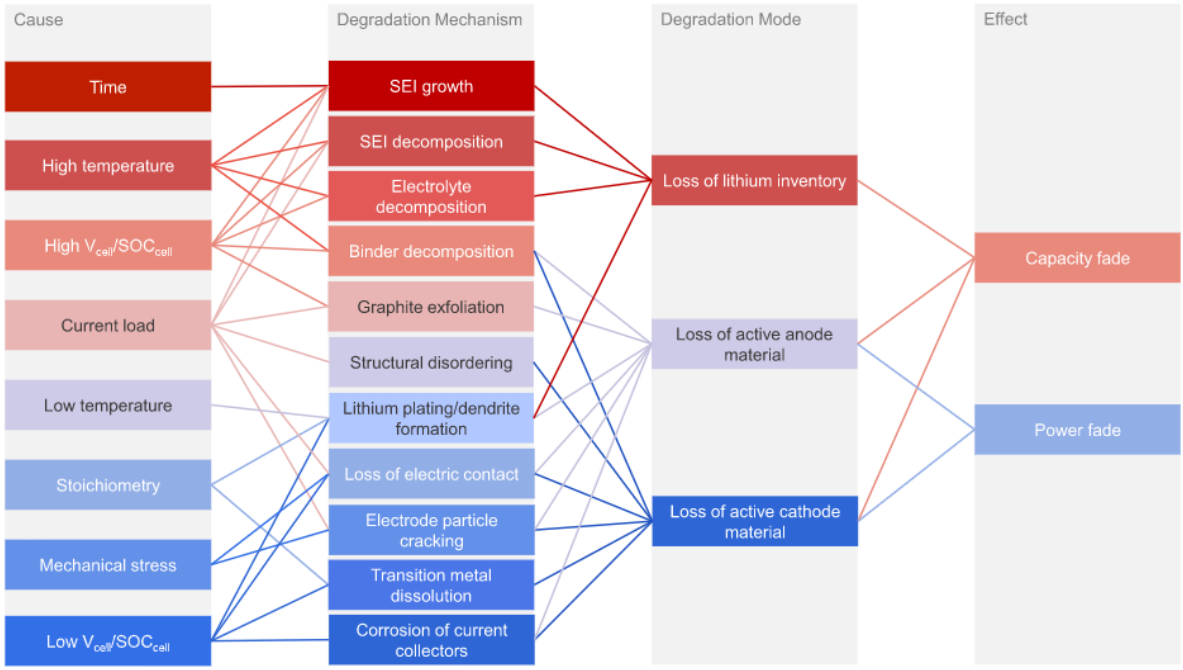

Figure 4.1-2 Lithium-ion battery degradation reactions [104]

However, according to the current literature [105]-[109] the main reactions that have the highest impact on battery degradation are:

- Lithium deposition
- Solid electrolyte formation (SEI)
- Crack propagation
- Loss of active material

The reasons for the occurrence of capacity and power degradation are for the resistance increase: SEI formation, electrolyte degradation, isolation or fracture of active material, reduction in the number of electrical conduction paths in the electrode, while isolation, chemical degradation, fracture of active material and loss of cyclable active material are the reasons given for capacity loss [105].

As can be seen from Figure 4.1-2, a number of physical parameters will activate and/or accelerate these reactions leading to an increased degradation. It is widely recognised in the current state of the art [14], [105]-[111], [109] that the main impacting parameters are:

- *Battery cell temperature*, which is also dependent on the ambient temperature. It is suggested that a cell is operated around a temperature of about 20 °C to attain the minimum degradation [112], [113]. Operation at higher cell temperatures than 20 °C tends to reduce battery lifetime due to unwanted side reactions damaging the cell [114]. Very low temperatures reduce performance and lifetime due to an increase in the internal cell resistance [115]. Temperature accelerates all chemical reactions, including those that are unwanted and lead to degradation, and increases stress. The dependence of battery degradation upon cell temperature is modelled with the Arrhenius law, which models an exponential behaviour.
- *State of Charge* (SOC); literature suggest that low average SOC, help in lowering battery degradation [116]. High SOC increases degradation with a linear or even exponential dependence [105]. Average SOC changes with cycling schedule. If a certain amount of charge is to be applied to the battery within a 24-hour period, then the time and duration of charging can be altered to change the average SOC. For example, leaving the EV battery at a low SOC with subsequent delayed recharging can yield a lower average SOC over a 24-hour period than early charging with the battery then remaining at a high SOC for some hours.
- *Depth of Discharge* (DOD)/*amount of charge transferred*; the more charge transferred during cycling i.e. the greater the DOD per cycle and the greater the number of cycles, the greater the degradation [117]. High DOD causes continuous stripping and depositing of solid electrodes. Some studies infer that DOD can have a higher impact than SOC [105], while others do not find a clear dependence upon DOD [118].
- *Current rate (C-rate)*; C-rate is defined as the charging power as a percentage of the battery's maximum capacity. Therefore, for a battery with a maximum capacity of 24 kWh, a charger rated 24 kW achieves 1C charging. Increased charge rates accelerate degradation, with a factor that is linear at rates under 1C [119]. Domestic chargers provide power at either 3 kW or 7 kW (i.e. under 1C for passenger EVs). Faster discharge due to high driving speeds and/or hard acceleration has similar effects on degradation due to an increased battery discharge rate. High C-rates are known to

increase internal resistance [105], with the effect being amplified when combined with the other parameters.

Scholars worldwide have put a considerable effort, in order to capture the behaviour of battery degradation with mathematical models. The battery models present in current literature can be categorized in two major groups [105]:

- physics or electrochemistry based [106]-[109]
- Empirical [14], [110] [111].

Although other classifications are also possible, for the scope of this research this differentiation is sufficient in highlighting the advantages and drawbacks of the two approaches and choosing the one that is more suitable for the current work. When referring to electrochemistry based models, we mean models that represent electrochemical processes but validated with experiments, and we ignore other models i.e. single particle models etc. This is because, as will be seen in the next paragraphs, there is a constant trade-off between accuracy of such models and practical implementability, and the models referred to in the current work can be fitted with experimental data.

In [109] an electrochemical degradation model that captured the impact of loss of active material and side reactions, such as SEI formation and lithium plating, at different C-rates and temperatures was proposed. They fit the parameters of such models with cycling data on 2.6 Ah 18650 NCA batteries, cycled two different discharge rates, namely 2C and 4C, and at 45 °C. They observe that high ambient temperature led to accelerated SEI formation but on the other hand, low temperatures caused lithium plating. High currents caused loss of active material, which is the dominant phenomena at high C-rates. However, the authors did not model the effect of the combination of these two parameters and no mention to SOC was made.

In [108] an electrochemical model that accounted for lithium-ion diffusion and kinetics, fitted using experimental data was developed. The main drawback of the approach adopted by the authors lies in the fact that the model consisted of non-trivial partial differential equations,

which are unsuitable for being included in a mathematical optimisation process; in fact, the authors themselves comment on the computational burden for implementing such model and propose utilising external servers. Another shortcoming is the absence of any relationship with external physical parameters, i.e. temperature or C-rate.

An electrochemical model to represent SEI formation at the anode and iron dissolution in lithium iron phosphate batteries was proposed in [107]. Here, a distinction between storage and cycling conditions is made: storage SOC and temperature are the most impacting parameters in storage conditions and C-rate, temperature and overall energy throughput influence capacity fade during cycling. An ordinary differential equation based model is constructed and fitted using experimental results with commercial LFP batteries at different temperatures (20, 40 and 60 °C), SOCs (10, 50 and 100%) and discharging rates (0.1, 0.5, 1 and 2C). The results showed that temperature is a major impacting factor influencing both storage and cycling. Batteries stored at high SOCs exhibited higher degradation than those at low SOCs and the magnitude of the discharging current showed a clear impact on the capacity fade during cycling. Although this work succeeds in capturing the impact of three major impacting parameters on capacity fade, the proposed model is complex (we believe it is unsuitable for state of the art optimisation methods) and does not represent the combination of such parameters.

In [106], a mechanistic model that depicted different degradation mechanisms, namely, loss of lithium inventory, loss of active material and ohmic resistance increase was developed. With a more empirical approach then the works discussed above, the authors have performed cycling tests on three types of battery, LFP, LMO and NMC, at 1/3C charging and 1.5C discharging at two different temperatures, namely 5 and 45 °C to depict the summer and winter variation. The results showed that the three batteries exhibit different propensity to the aforementioned reactions: resistance increase and loss of lithium inventory happened in all three batteries while loss of active material was not noticed in the LFP battery. They continue by defining a mathematical model based on the Arrhenius equation to link the effect of C-rate and temperature. Their model was successful in simulating the behaviour of real batteries when tested under dynamic conditions, but no mention to SOC was made.

A similar approach was adopted in [110] in modelling loss of active lithium and SEI layer formation based on accelerated degradation testing performed at different discharging rates (0.2, 0.5, 1 and 2C). Despite an exponential model linked the impact of C-rate and temperature, the authors assumed constant temperature, hence this dimension is not developed in their work.

Rather different from the previous literature, two notable research works, [14] and [111], employed empirical modelling to depict the influence of the impacting parameters on capacity fade and resistance increase. Both studies tested commercial NCA batteries, by separating storage and cycling conditions and seemingly reached completely opposite conclusions. While the authors of [111] argued that under certain conditions V2G could in fact improve battery life (by discharging the battery to keep it at low SOC), the work conducted in [14] deemed V2G an unavoidable cause of battery wear. Aside from their conclusions however, their approach in modelling battery degradation is to our best understading the simplest yet effective as the impact of each parameter and their interactions are quantified based on testing results, without focusing on chemical reactions. This method is in our view the best as the only manageable parameters are the external physical ones and the measured results are both capacity fade and resistance increase, which are the inputs and outputs of the latter two studies.

More specifically, in [14], storage testing at three temperatures (-27, 20 and 55 °C) and SOCs (0, 50 and 100%) was performed and a double quadratic model was used to depict the interaction between these two parameters. As for cycling tests, different utilisation patterns were tested by combining driving cycles, charging and discharging sessions. Similarly, in [111], storage testing at 10, 25 and 45 °C and 20, 50 and 90% SOC was performed and the Arrhenius law was employed to depict calendar degradation. Two different discharge rates, namely 0.4 and 1.2C were utilised for the cycling tests and quite unexpectedly and in disagreement with the above literature the results showed that capacity fade was independent from the discharging rate and more influenced by the overall energy throughput.

Thus far, the major research gaps identified in the current literature can be summarised as:

- The majority of the research works consider a subset of the impacting parameters; some of them are neglected with assumptions on the working conditions;
- The combinations of these parameters are often neglected;
- In no case, more than two impact parameters have been considered together.
- A lack of studies on non-accelerated analysis has been noticed because most of the time a constant current profile is adopted instead on realistic load profiles;
- The available models have been developed based on tests conducted on specific battery chemistries and no mention to an adaptive battery degradation model is made. An adaptive battery model is defined as a mathematical representation of the degradation of the battery that is updated in order to improve its accuracy with measurements as they become available during the life of the battery.

Following these considerations, the present work develops an adaptive behavioural and capacity fade model that brings the following contributions to knowledge:

- Development of a comprehensive degradation model that captures the impact of the main physical parameters which can be manipulated by optimisation algorithms;
- Modelling the interaction between such parameters which has been often overlooked in current literature;
- Dynamic modelling, to simulate the impact of real-life operating conditions;
- Adaptive modelling to accurately fit the degradation behaviour of diverse battery types.

Thus, the proposed adaptive battery model is depicted in Figure 4.1-3.

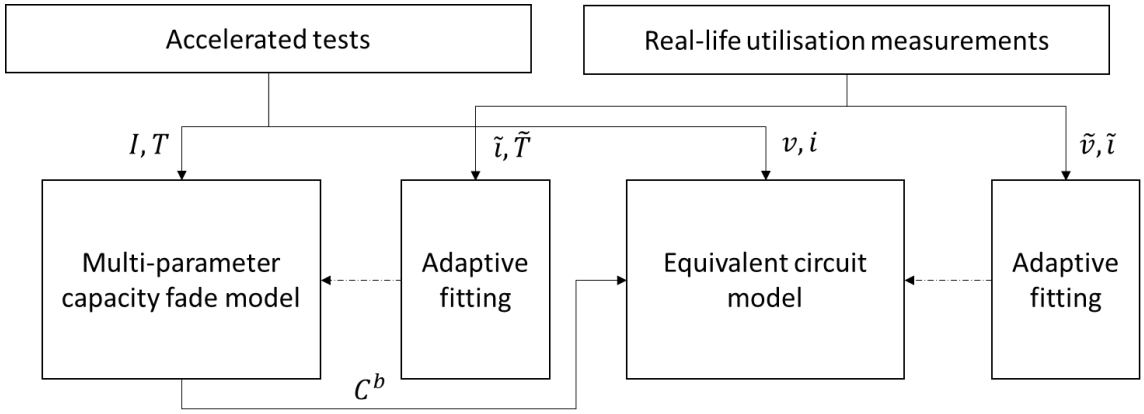

Figure 4.1-3 Adaptive battery degradation model functional diagram

At first dynamic capacity, fade and equivalent circuit models are developed based on measurements collected from accelerated tests. The capacity fade model adjust the maximum battery capacity C^b as an input to the equivalent circuit model. Then, using real-life utilisation patterns, i.e. diverse voltage, currents and temperature profiles, namely $\tilde{v}, \tilde{\imath}$ and $\tilde{T}$, the models are validated and recurrently fitted to adapt the model to the specific battery.

The remainder of this chapter is organised as follows: in Section 4.2, the concept of equivalent circuit model is discussed and a predictive model is developed. Section 4.3 models the impact of the main influencing parameters on battery degradation and develops an adaptive degradation model that addresses the diverse behaviour of different lithium-ion battery types.

4.2 Development of an equivalent circuit model

In order to operate a lithium-ion battery within an optimisation framework, a number of parameters need to be modelled before addressing the degradation process. This is because lithium-ion batteries are characterised by a non-linear behaviour, hence a suitable model that depicts their dynamics. To this end, the equivalent circuit model (ECM) is a simple yet effective method for representing the internal reactions on lithium-ion batteries. This modelling approach has been developed in [P5]. The main components of and ECM are shown in Figure 4.2-1.

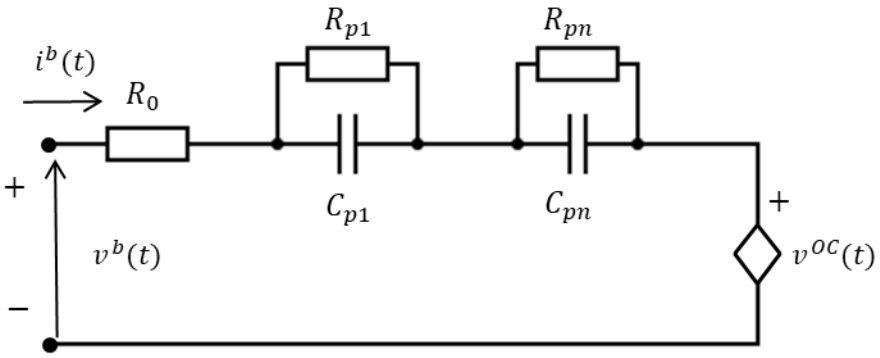

Figure 4.2-1 ECM of Lithium-ion battery

The main components of the ECM model are the DC internal resistance R_0 representing the polarisation of the battery, a controlled voltage source $v^{OC}(t)$, representing the open circuit voltage (OCV) and various RC pairs, which provide time constants representing different internal reactions, such as charge transfer and diffusion among others [111]. $v^b(t)$ and $i^b(t)$ are the voltage and current of the battery and these are the only parameters that are measurable from outside (an overall impedance can be measured but the in order to separate the different impedance components, complex measurement systems must be employed, i.e. electrochemical impedance spectroscopy). The OCV is dependent on the state of charge (SOC) of the battery; the relationship between OCV and SOC can be modelled by a function; more details will be provided in the next paragraphs. The number of RC pairs should be conveniently chosen based on the trade-off between the accuracy required by the design experiment and the computational complexity. A right balance between accuracy and computation effort is given by the one-time constant model, shown in Figure 4.2-2, which will be referred to hereafter.

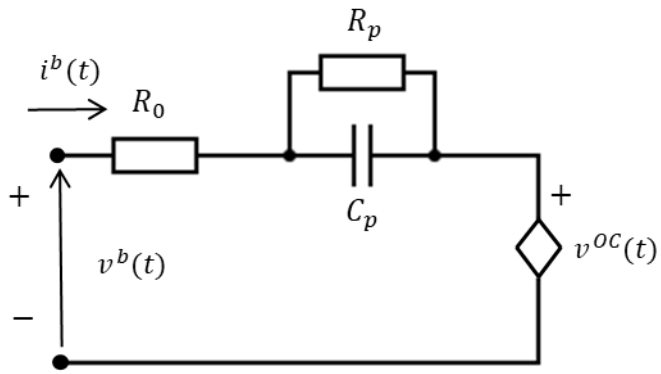

Figure 4.2-2 One-time constant ECM model

According to industrial standards, the charging/discharging process of lithium-ion batteries is governed by the so-called constant-current and constant-voltage charging process (CC-CV). Figure 4.2-3 shows the behaviour of the battery voltage and current during the CC-CV process.

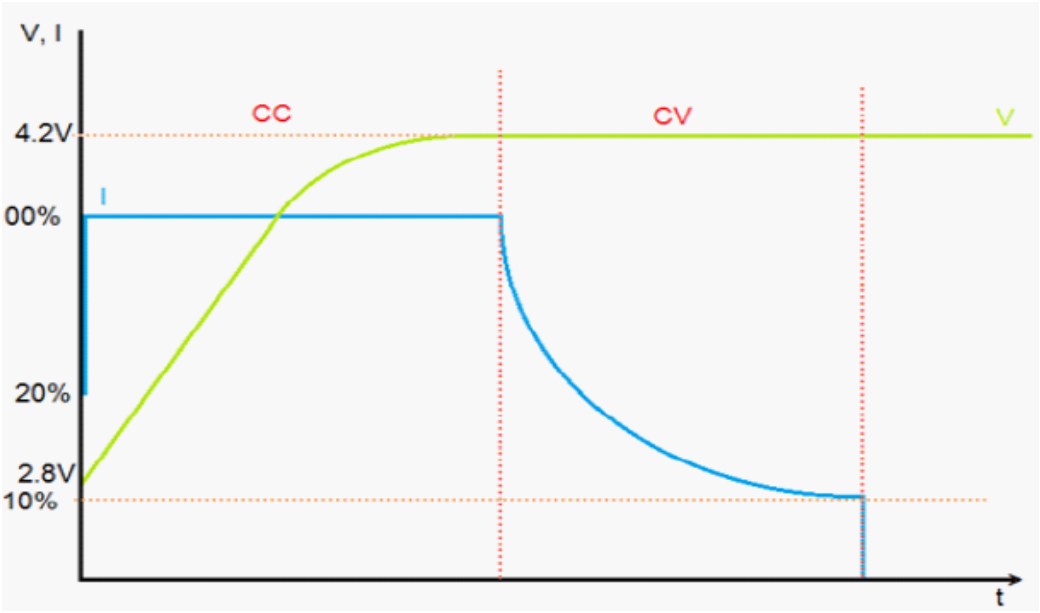

Figure 4.2-3 CC-CV charging process

Under CC mode as the name suggests, the battery is charged with a constant current while the battery voltage increases from the minimum limit (if the battery was fully discharged) to the

maximum limit. When the battery voltage reaches the maximum value, the supplied current decreases exponentially, while the voltage is kept constant; the CV phase ends when the supplied current is reduced below a certain cut-off current. Since when the battery reaches the maximum voltage the first time, the battery does not reach full SOC, further charging is carried out in the CV phase. As current is progressively reduced, the CV phase takes longer than the CC charging process and requires less power.

Next, referring to the single RC pair model in Figure 4.2-2, the dynamic behaviour of the battery charging process is modelled. First, CC process is modelled, where the battery is supplied with a constant current I^{b0}, as depicted by

$$\dot{v}^{cp}(t) = -\frac{1}{R_p C_p} v^{cp}(t) + \frac{1}{C_p} I^{b0} \tag{4.2}$$

$$v^{b}(t) = v^{OC}(t) + v^{cp}(t) + R_0 I^{b0} \tag{4.3}$$

where $\dot{v}^{cp}$ is the derivative of the voltage at the capacitor's terminals and the battery voltage v^b is provided by Kirchoff law for voltages in an electrical circuit. Lower case letters are used to represent dynamic variables that change with respect to time.

In literature, the relationship between the open-circuit voltage v^{OC} and the SOC of the battery has been modelled with a linear relationship [120], as shown below

$$v^{OC}(t) = m\, SOC(t) + b \tag{4.4}$$

Figure 4.2-4 shows the relationship between OCV and battery capacity (or SOC). A 3.2 Ah li-ion battery was charged for 20 steps of 10 minutes and was allowed to rest for 60 minutes in between. The rest period allowed eliminating any capacitive effect and provided the true OCV. In Figure 4.2-4, the data points related to the charging process have been removed and only those associated with the rest time have been shown. The linear fit provided $m = 0.8$ and $m = 3.32$.

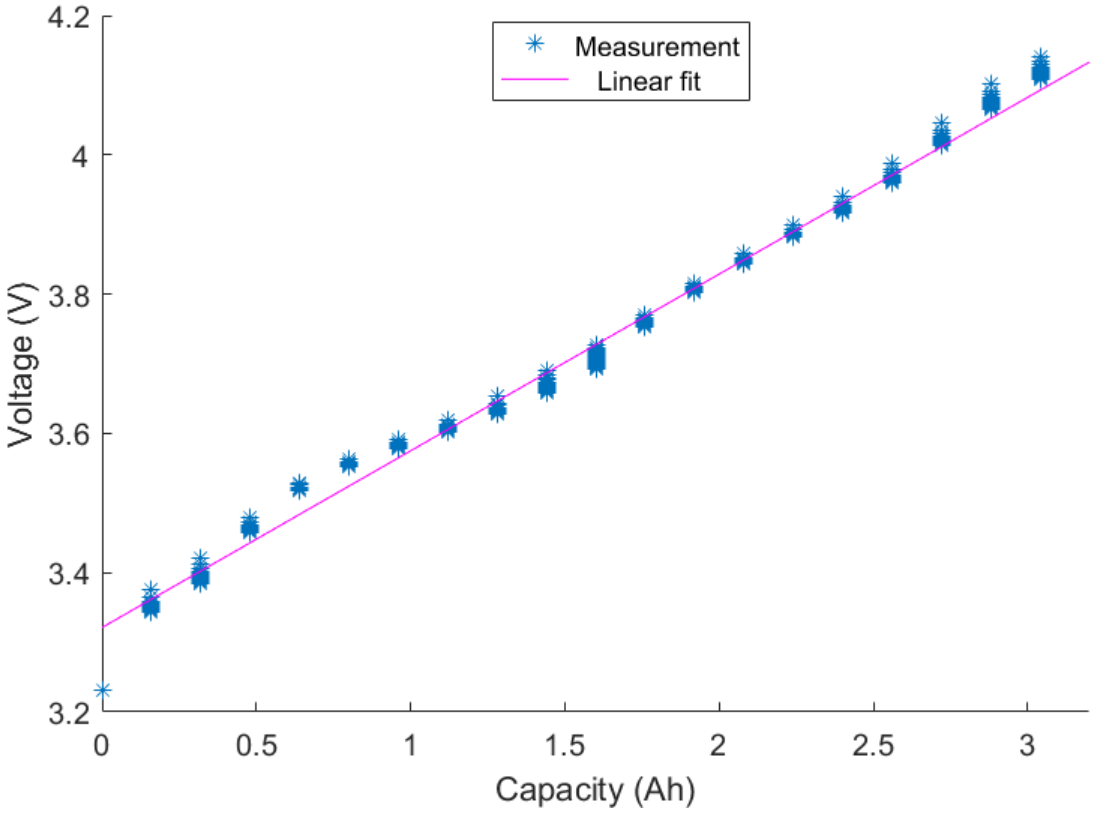

Figure 4.2-4 Variation of open-circuit voltage with respect to battery capacity

The solution of the first-order differential equation in 4.2 provides the behaviour of the voltage across the capacitor as

$$v^{cp}(t) = R_p I^{b0} - e^{\frac{-t+K_1}{R_p C_p}} \tag{4.5}$$

where, since the capacitor is initially discharged ($v^{cp}(0) = 0$), the integration constant K_1 can be determined with simple steps.

$$v^{cp}(0) = 0 = R_p I^{b0} - e^{\frac{K_1}{R_p C_p}} \tag{4.6.a}$$

$$\ln\left(R_p I^{b0}\right) = \frac{K_1}{R_p C_p} \tag{4.6.b}$$

$$K_1 = R_p C_p \ln\left(R_p I^{b0}\right) \tag{4.6.c}$$

$$v^{cp}(t) = R_p I^{b0} - e^{\frac{-t}{\tau_1}} e^{\frac{K_1}{\tau_1}} = R_p I^{b0} - e^{-\frac{t}{\tau_1}} \quad e^{\frac{\tau_1 \ln\left(R_p I^{b0}\right)}{\tau_1}} \tag{4.6.d}$$

$$= R_p I^{b0}\left(1 - e^{-\frac{t}{\tau_1}}\right)$$

Therefore, inputting (4.4) and (4.6.d) in (4.3), the overall battery voltage can be represented as:

$$v^b(t) = k\,SOC(t) + b + R_p I^{b0}\left(1 - e^{-\frac{t}{\tau_1}}\right) + R_0\, I^{b0} \tag{4.7}$$

where $\tau_1 = R_p C_p$ is the time constant associated with the RC pair. Since battries connected to the grid are controlled in terms of the power consumed/supplied, the expression of the power absorbed during CC mode is given by

$$p^b(t) = v^b(t)\, I_{b0} = m\, SOC(t)\, I_{b0} + b\, I_{b0} + R_p I^{b0^2}\left(1 - e^{-\frac{t}{\tau_1}}\right) + R_0\, I^{b0^2} \tag{4.8}$$

As can be seen from the expression above, given a constant current supplied to the battery, the actual power exchanged is not constant, as the battery voltage increases. Furthermore, as evidenced by 4.7, the components of the ECM will also determine the magnitude and dynamic of the power exchanged with the battery. Consequently, any variation of the ECM components will also affect the overall power exchanged. Given that as the battery is utilised, the resistive components increase, this will ultimately result in a reduction of the power performance of the battery, otherwise known as power fade.

Under CV mode, the battery is subject to a constant external voltage V^{b0}, and the current is progressively decreased. The overall dynamics of the battery under CV mode can be represented as

$$\dot{v}^{cp}(t) = -v^{cp}(t)\left(\frac{1}{R_p C_p} + \frac{1}{R_0 C_p}\right) + \frac{1}{R_0 C_p}\left(V^{b0} - v^{OC}(t)\right) \tag{4.9}$$

$$i^b(t) = \frac{1}{R_0}\left(V^{b0} - v^{cp}(t) - v^{OC}(t)\right) \tag{4.10}$$

The solution of the first order differential equation in (4.9) along with (4.10) provides the behaviour of the current in the battery during the CV charging process

$$v^{cp}(t) = \frac{K_2\, e^{-\frac{(R_0+R_p)t}{\tau_1\tau_2}}}{R_0+R_p} + \frac{\tau_1\left(V^{b0}-v^{OC}(t)\right)}{R_0+R_p} \tag{4.11}$$

where $\tau_2 = R_0 C_p$. Since after the CC phase, $v^{cp}(t^s) = R_p I^{b0}$, where t^s is the time when the switch between CC and CV happens. Hence:

$$K_2 = \left(R_0 + R_p\right)v^{cp}(t^s) - \tau_1\left(V^{b0} - R_p I^{b0}\right) \tag{4.12.a}$$

$$v^{cp}(t) = \frac{\left((R_0+R_p)R_p I^{b0} - \tau_1\left(V^{b0}-R_p I^{b0}\right)\right) e^{-\frac{(R_0+R_p)t}{\tau_1\tau_2}}}{R_0+R_p} + \frac{\tau_1\left(V^{b0}-v^{OC}(t)\right)}{R_0+R_p} \tag{4.12.b}$$

$$i^b(t) = \frac{1}{R_0}\left(V^{b0} - \frac{\left((R_0+R_p)R_p I^{b0} - \tau_1\left(V^{b0}-R_p I^{b0}\right)\right) e^{-\frac{(R_0+R_p)t}{\tau_1\tau_2}}}{R_0+R_p} + \frac{\tau_1\left(V^{b0}-v^{OC}(t)\right)}{R_0+R_p} - v^{OC}(t) \right) \tag{4.12.c}$$

From the above expression, the power exchanged with the battery during the CV mode can be determined by

$$p^b(t) = V^{b0} i^b(t) = \frac{1}{R_0}\left({V^{b0}}^2 - \frac{V^{b0}\left((R_0+R_p)R_p I^{b0} - \tau_1\left(V^{b0}-R_p I^{b0}\right)\right) e^{-\frac{(R_0+R_p)t}{\tau_1\tau_2}}}{R_0+R_p} + \frac{V^{b0}\,\tau_1\left(V^{b0}-v^{OC}(t)\right)}{R_0+R_p} - V^{b0} v^{OC}(t) \right) \tag{4.13}$$

From the mathematical formulation presented thus far, it can be concluded that the overall power exchanged with the battery can be modelled as a expressed hereby:

$$p^b(t) = \begin{cases} expression\ (4.8)\ if\ v^b(t) < \bar{V}^b \\ expression\ (4.13)\ if\ v^b(t) = \bar{V}^b \end{cases} \tag{4.14}$$

The output of the model is presented in Figure 4.2-5, where the behaviours of the battery voltage, current and SOC are depicted. One charging session, including CC at 1.3A and CV phases, is presented.

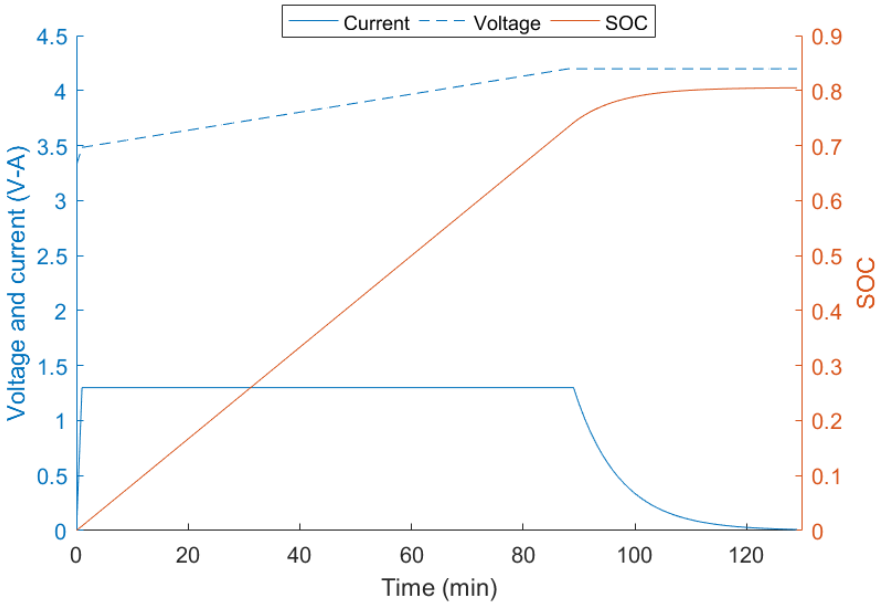

Figure 4.2-5 Output of the ECM model

It can be seen from Figure 4.2-5, that the battery is not fully charged at the end of the CV mode, as the SOC reaches only 80%. This is because, since the current is exponentially reduced, significant time will be required to fully charge the battery. Hence, a cut-off current of 0.01 A is utilised to end the CV phase.

4.2.1 Development of a self-adaptive ECM model

Based on the analysis carried out in this Section, a self-adaptive ECM model is developed, which will track any variation of the battery internal parameters due to degradation. Figure 4.2-6 presents the measurement of internal resistance for a battery with 2.6 Ah, that was cycled at 0.5C (i.e. 1.3 A) and 80% depth of discharge (DOD) at a constant ambient temperature of 25 °C (by means of an environmental chamber). This data was received from previous experiments [P7].The battery was cycled for 890 cycles, comprising of charging and discharging and the measurement is automatically carried out by the Arbin battery charger (which has 16 channels with a maximum current output of ±10A).

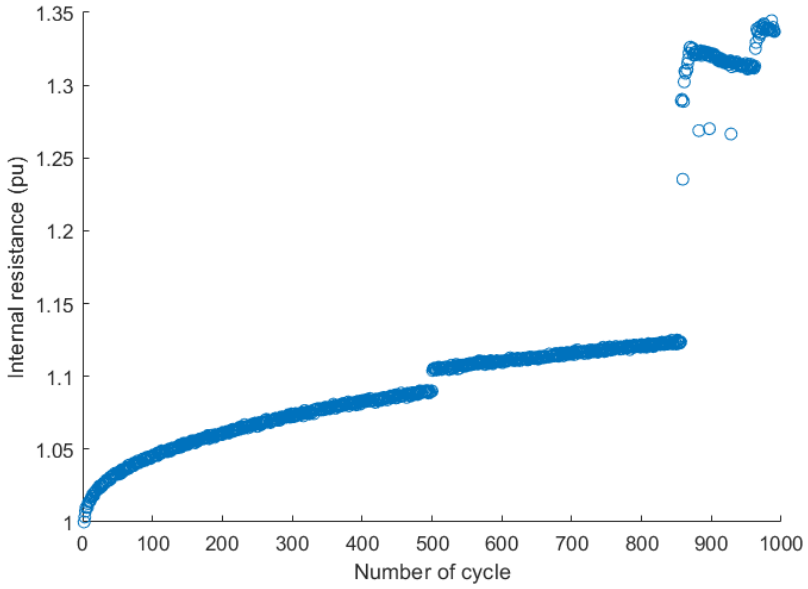

Figure 4.2-6 Internal resistance increase due to battery cycling

It can be seen from Figure 4.3-7, that the internal resistance increases by a 20% compared to its initial value, and right before reaching 900 cycles, a sudden increase is noticed. These kind of variations are common in li-ion batteries, which are particularly susceptible to environmental conditions. Furthermore, due to the long testing duration, sometimes the charging equipment and the environmental chamber may need to be stopped for maintenance. When battery cycling was reinitiated, a variation of the impedance and capacity was noticed. However, the overall behaviour throughout the life of the battery shows an increasing trend, which should be captured for an accurate ECM model.

Motivated by this phenomenon, a self-adaptive ECM model is proposed where the values of the components are adjusted based on the real measurements. As the only parameters that can be measured externally are the battery voltage and current, only these are inputted in the ECM model, and the error between the real measurement and the output of the model is minimised by adjusting the ECM parameters. For this purpose, only the CC phase is sufficient. A functional diagram of the proposed approach is presented in Figure 4.2-7, where v^b and i^b are the measurements of the battery voltage and current respectively, v^{b*} is the output of the model and R_0^*, R_p^* and C_p^* are the adjusted ECM parameters.

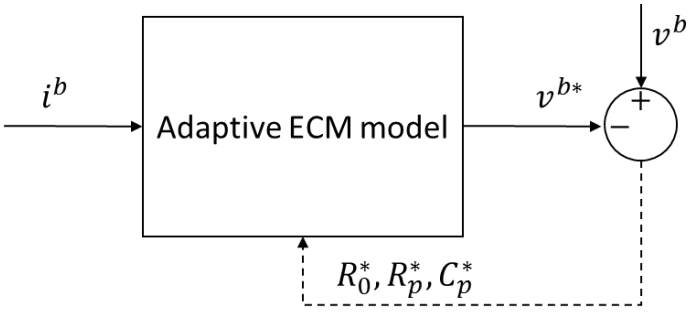

Figure 4.2-7 Functional diagram for the self-adaptive ECM model

The ECM parameters are adjusted by minimising the error between the output of the model and the measured battery voltage as

$$\underset{R_0^*,R_p^*,C_p^*}{\operatorname{argmin}} \sum_{t=1}^{T^{CC}} \left[v_t^b - \left(k\, SOC_t + b+, R_p^* i_t^b \left(1 - e^{-\frac{t}{R_p^* C_p^*}} \right) + R_0^*\, i_t^b \right) \right]^2 \tag{4.15}$$

where, v_t^b and i_t^b are the battery voltage and current measured at time step t and T^{CC} is the number of time steps that determine the duration of the CC phase. It should be noted that, as the battery degrades T^{CC} will reduce since due to the resistance increase, the voltage of the battery reaches its maximum value sooner than when the battery is new. Figure 4.2-8 shows a comparison between the output of the adaptive model and the real voltage measurement for one period of CC charging, and Table 4.2-1 provides the fitted ECM parameters with the associated fitting error. This method was implemented for all the cycles in the life of the battery presented in Figure 4.2-6, and the results are shown in Figure 4.2-9. It can be seen from the results that the resistive factors, namely R_0 and R_p, increase as the battery is utilised, in line with the measurements presented in Figure 4.2-6. The value of the capacitance C_p however, seems unchanged with the utilisation of the battery. This implies that, as the battery is utilised, for the same current i^b, the voltage drops $R_0\, i^b$ and $R_p\, i^b$ will increase, reducing the duration of the CC phase since the maximum voltage is reached earlier. Consequently, the CV phase will last longer, but as concurrently, the battery capacity is also fading (as will be shown in the next Section), the overall performance of the battery is reduced. Similarly, by referring to equation 4.7, for the same power provided to the overall battery, as R_0 and R_p

increase, the actual power that increment the SOC, namely $(m\,SOC(t)+b)\,i^b$, decreases, because the two loss terms, i.e. $R_0\,i^{b^2}$ and $R_p\,i^{b^2}$ increase.

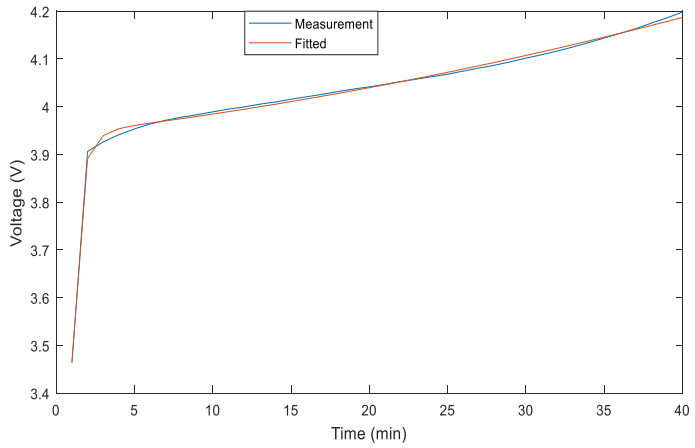

Figure 4.2-8 Adaptive ECM model output against real voltage measurement

Table 4.2-1 ECM parameters for one period of CC charging

R_0	R_p	C_p	Error
60 mΩ	59 mΩ	0.196 F	0.133%

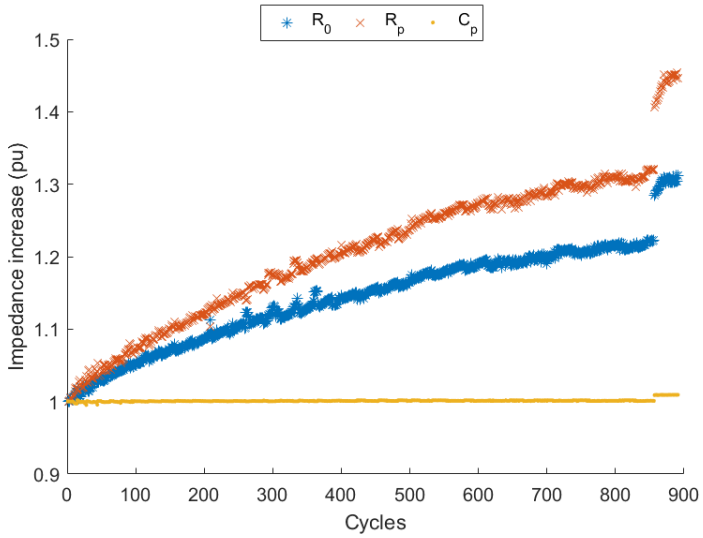

Figure 4.2-9 Fitted ECM parameter increase throughout the life of a battery

4.3 Development of a dynamic empirical capacity fade model for Lithium-Ion batteries

In this Section, a dynamic capacity fade model is developed from cycling tests performed on LFP and and other lithium-ion batteries. As discussed in the introduction, this approach has been adopted by the likes of [111] and [14], and their research groups which are among the most prominent scholars in this field. The reason for the selection of this method must lie in the flexibility of this modelling approach, that is not limited by the nature of the chemical reactions, which may or may not manifest in the battery under testing (see Ouyang *et al.* [106]), but connects with the external parameters that are always measurable in any charging/discharging cycle. Furthermore, the inherent constitutional diversity among different lithium-ion chemistries is addressed with an adaptive fitting approach, which makes use of real-life utilisation measurements to fine-tune the model. The present research builds upon and extends the work carried out in [121] as it provided a suitable base for the development of a dynamic battery degradation model. The contribution of presented in this thesis are:

- improvements of the cycling degradation model by adding average SOC as an impacting parameter and additional testing on automotive batteries;
- validation of the model based on historical data;
- development of an adaptive degradation model using operational data.

In [121], both calendar and cycling tests were conducted on a variety of lithium-ion batteries including LFP and lithium polymer. In agreement with the current literature, they found that:

- Under storage conditions, temperature and storage SOC influence calendar degradation; the interaction of these two parameters are multiplicative in the sense that they augment each other.
- Under cycling conditions, C-rate, temperature and average SOC have the most impact; the authors did not find any clear dependence upon DOD.

In a similar direction, the present work proposes a calendar-cycling model based on the following assumptions, which follow from the knowledge of current literature and experimental tests:

- Under storage conditions (i.e. $|i| = 0$), calendar degradation occurs, and ambient temperature and storage SOC are the impacting factors. This type of capacity degradation is quantified in the unit of time, i.e. s, min or h.
- When cycling (i.e. $|i| \neq 0$), C-rate, cell temperature and average cycling SOC are the impacting factor. Cycling degradation is quantified in the units of energy throughput, i.e. Wh or kWh. Time related degradation, i.e. calendar effect, still occurs but the cycling effect is dominant and overshadows the calendar effect. This assumption is reasonable and in line with previous works [14] [111] considering that the two forms of degradation manifest at different scales, i.e. calendar ageing in time and cycling ageing in throughput, and that calendar ageing occurs across long time-scales, e.g. weeks, months or years, while cycling is performed at least on a daily basis.
- Optimisation processed cannot influence ambient temperature (discussed below). average SOC is changed and its impact is considered in the cycling degradation model.
- A thermal model that represents the impact of a charging/discharging current on the cell temperature is not considered, as below 1C current, the temperature increase is negligible.

In accordance with [121], which shows that for slow charging rates the increase in temperature is negligible, a simple thermal model is considered in equation

$$Q = R\, I^2 = C^H\, \Delta T \rightarrow\ \Delta T = \frac{R\, I^2}{C^H} \tag{4.16}$$

where Q is the heat exchange, R is the battery internal resistance, I is the charging/discharging current, C^H is the heat capacity of the cell and ΔT is the temperature variation caused by the current. The internal resistance of a Nissan Leaf cell has been measured as 6 mΩ. As it has been shown in Section 4.2, this resistance increases as the

battery degrades, hence the impact of the current will increase. However, the measured resistance increase is only 20%, therefore the conclusions reached here are still applicable when the battery reaches end of life. The specific heat capacity of the cell is considered as $795\ \frac{J}{kg\ K}$ [122] and the mass of a cell is 0.914 kg [123]. The corresponding heat capacity of a cell results $727\ \frac{J}{K}$. By supplying the battery with a 3 kW charger, the 360 V battery pack is subject to 8.3 A, while the cell takes 4.16 A.

$$\Delta T = \frac{6\times10^{-3}\ 4.16^2\ 3600}{727} = 0.51\ \frac{^{\circ}\mathrm{C}}{h} \tag{4.17}$$

Based on the above assumptions, the capacity fade model is developed. As calendar effects due manifest across long time, these tests are often time consuming. Considering that these will not affect the optimisation process, the proposed model is fitted with the information provided in [14]. In agreement with [105], [111], [121] and [14] calendar degradation has been defined in the following equations

$$C(t) = C_o - \alpha^s t^{0.5} \tag{4.18}$$

$$\alpha^s = f(T^{amb}, SOC^s) = \left(\zeta_1 e^{(\theta_2\, T^{amb})} + \zeta_2\, e^{(-\theta_4\, T^{amb})}\right)(\zeta_3\, SOC^s + \zeta_4) \tag{4.19}$$

where $C(t)$ is the battery capacity at any time $t > 0$, α^s is the storage degradation coefficient and the relationship with time is defined with an exponent 0.5 [14] [111]. From the considerations above, the storage degradation coefficient depends on the ambient temperature T^{amb} and the storage SOC, SOC^s; here a similar relationship as the Arrhenius law has been used with two exponentials, aimed at capturing the impact of both high and low storage temperatures. The multiplication between the two terms ensures that the combinations of temperature and SOC causes degradation. It follows that, with one parameter kept constant, increase along the other parameter will inevitably lead to higher degradation. In addition, the highest degradation can be seen at both high storage temperature and SOC. These considerations can be ascertained in Figure 4.3-1, where at constant T^{amb}, calendar degradation increases linearly with SOC^s, while at constant SOC, the exponential term is noticeable.

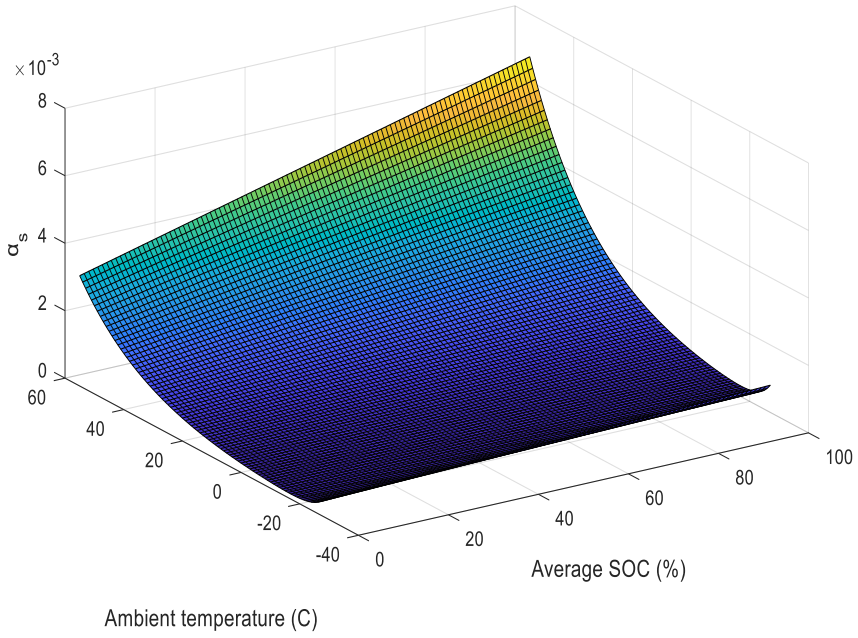

Figure 4.3-1 Storage degradation coefficient as a function of temperature and SOC

The square root of the battery calendar age is used because it has been observed that when the battery is new, depending on the storage conditions, the battery degrades faster and after some time, this effect is less pronounced.

As evidenced by the survey of the available literature on battery degradation modelling, a dynamic model that accounts for a distribution of the impacting factor is seldom considered. In the majority of the cases, accelerated testing serve to fit the model but the authors do not elaborate on the necessary steps to extend the model to an equivalent dynamic one. In the present work, the above a dynamic battery model is developed with a simple memory based multi-path (MMP) approach. A simple example is provided here to clarify this approach.

Let us consider three possible battery storage states S^{s} as below

$$\mathrm{S}_n^s = \begin{pmatrix} T_n^{amb} \\ SOC_n^s \end{pmatrix} = \left\{ \begin{pmatrix} 22 \\ 0.49 \end{pmatrix}, \begin{pmatrix} 16 \\ 0.01 \end{pmatrix}, \begin{pmatrix} 16 \\ 0.19 \end{pmatrix} \right\} \tag{4.20}$$

As depicted by Figure 4.3-2, at each of these storage conditions, corresponds an equivalent accelerated degradation curve of the type specified by 4.18.

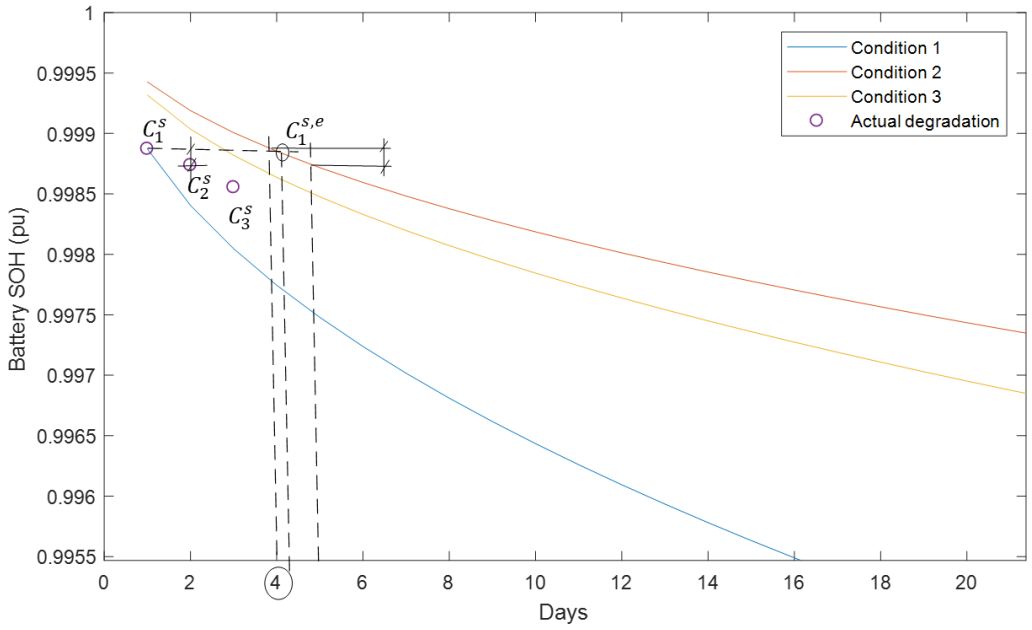

Figure 4.3-2 Equivalent accelerated battery degradation curves for different storage states

Each of these curves indicate capacity fade due to storage and the severity of degradation is decided by the storage coefficient, which in turn depends on three battery states. Assuming that the battery is stored at these three different states in the three consecutive days (one day is chosen as an adequate unit of time for calendar degradation, which manifests over weeks, months and years) then equivalently, the degradation *path* will be sequentially defined by the blue curve, than red and finally yellow. The battery will be one day at the blue curve (at state 1) and will be subject to certain degradation dictated by the associated curve, where C_1^s is the capacity of the battery after day 1 (stored in the memory). After the first day, the storage state has changed, and now the capacity point is projected onto the red curve which is the relevant one for the day and an equivalent point $C_1^{s,e}$ is obtained; the battery will then be on the red curve for one day and will degrade according to that curve; fromC_1^s, the next capacity point will be C_2^s (stored in the memory) and the process will continue for the next storage stages.

The method proposed in this research is aligned with what was discussed in [124]. The simple pseudo-code for the MMP approach is presented hereby.

MMP dynamic algorithm

Input: Battery initial capacity C_0^s and the set of daily storage states $\mathrm{S}^s = \{\mathrm{S}_1^s, \mathrm{S}_2^s, \dots, \mathrm{S}_n^s\}$

1: **for** $i \leftarrow 1$ **to** (n) **do**

2: Calculate daily capacity from (4.18) and (4.19) with $C_o = C_{i-1}^s$, $t = i$ and S_i^s

3: Update memory with current capacity C_i^s

4: **end for**

Under the present work, cycling degradation can be controlled with optimisation techniques, and an accurate model can ensure improvements in battery life from V2G services. Following from the assumptions outlined at the beginning of the current Section, when the battery is utilised, cycling degradation is dominant, with calendar degradation being prominent otherwise as shown in , Figure 4.3-3, which shows a typical EV battery utilisation pattern.

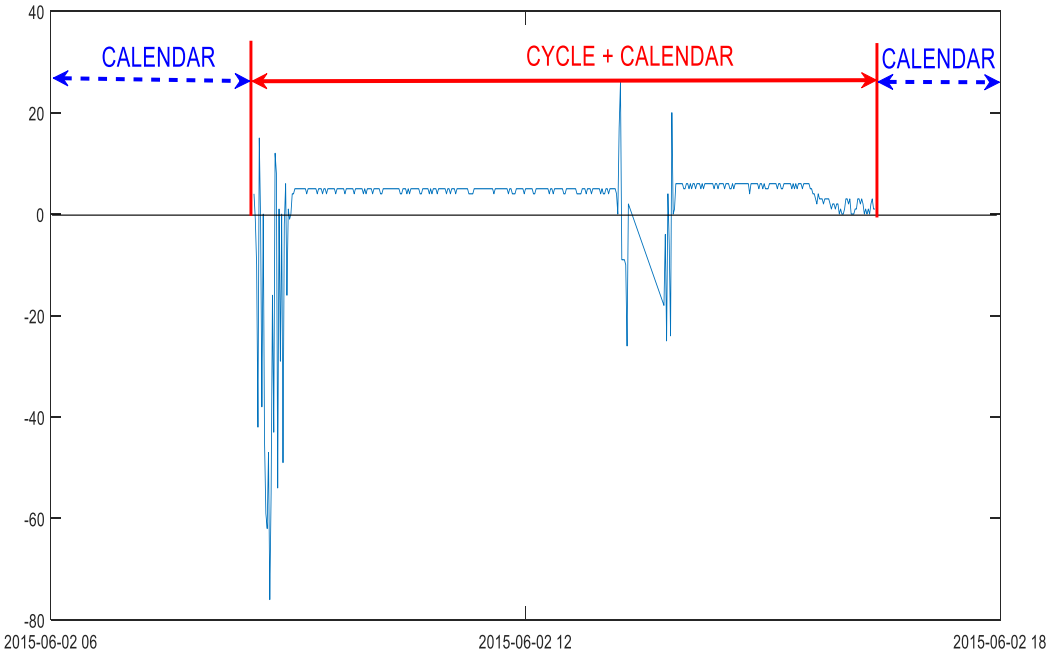

Figure 4.3-3 Example of a daily EV battery utilisation pattern

In agreement with current literature [105], [111], [118], capacity fade due to cycling degradation can be represented as

$$C(Wh) = C_o - \alpha^c Wh \tag{4.21}$$

$$\alpha^c = f(T^b, \langle SOC \rangle, C^r) = \gamma_1 \left(\gamma_2 {T^b}^3 + \gamma_3 {T^b}^2 + \gamma_4 T^b + \gamma_5 \right) \times \tag{4.22}$$

$$\times \ (\gamma_6 \langle SOC \rangle + \gamma_7) \times (\gamma_8 C^r + \gamma_9)$$

where, Wh is the energy throughput, α^c is the cycling degradation coefficient which depends on the battery temperature T^b, average SOC $\langle SOC \rangle$, and the charging/discharging rate C^r. Few points to be noted are that the effect of charging and discharging has been considered the same, as in [110] and DOD has not been considered as an impacting factor as evidenced by [121], thus all the cells have been cycled at the same DOD. A series of cycling tests have been conducted on two different batteries as detailed in Table 4.3-1.

Table 4.3-1 Battery type and specifications

Cell Type	**Chemistry**	**Specifications**
Type A	Commercial Panasonic 18650B Lithium-ion	Maximum voltage: 4.2 V
		Minimum voltage: 3 V
		Capacity: 3.2 Ah
Type B	Automotive LFP	Maximum voltage: 4.2 V
		Minimum voltage: 3.2 V
		Capacity: 33 Ah
	Other equipment	
Battery charger 1	Arbin, 16 channels, maximum ±10 A, maximum voltage 10 V	
Battery charger 2	Neware, 2 channels, maximum ±300 A, maximum voltage 10 V	
Temperature chamber	CM, testing temperature 25℃	

The testing conditions for the two battery types are presented in Table 4.3-2.

Table 4.3-2 Battery testing conditions

Cell Type	Battery temperature	Average SOC	C-rate
Type A	25 °C	0.3	0.3C
	40 °C	0.7	1.2C
Type B	25 °C	0.5	0.1C
			0.3C
			1C

It should be noted that the information regarding the chemistry of battery A was not available. The test setting has been set taking into account a number of factors:

1) Limited availability of automotive cells, which were physically inseparable from one another. This implies that they were always subject to the same environmental conditions, i.e. temperature.
2) Limited number of 18650 cells, which limited the number of test that could be performed, also to account for the diverse performance among the cells in a batch.
3) Failure of some cells, which again limited the number of available cells (hence tests) and lengthened the testing period.

The testing equipment is shown in Figure 4.3-4, where the software, the two types of batteries and two battery charger and the environmental chamber are shown.

The results from the cycling tests for type A cells are shown in Figure 4.3-5. The data on the experiments on cell A and B is the result of extensive testing carried out throughout this research. To ensure good readability of the results a specific colour, line-type and marker scheme has been used:

- The difference in temperature is indicated by the solid (25 °C) and dashed (40 °C) lines;
- The difference in average SOC is indicated by the circle (35%) and asterisk (70%) markers;
- The difference in C-rate is indicated by the black (0.3C) and red (1.2C) colours.

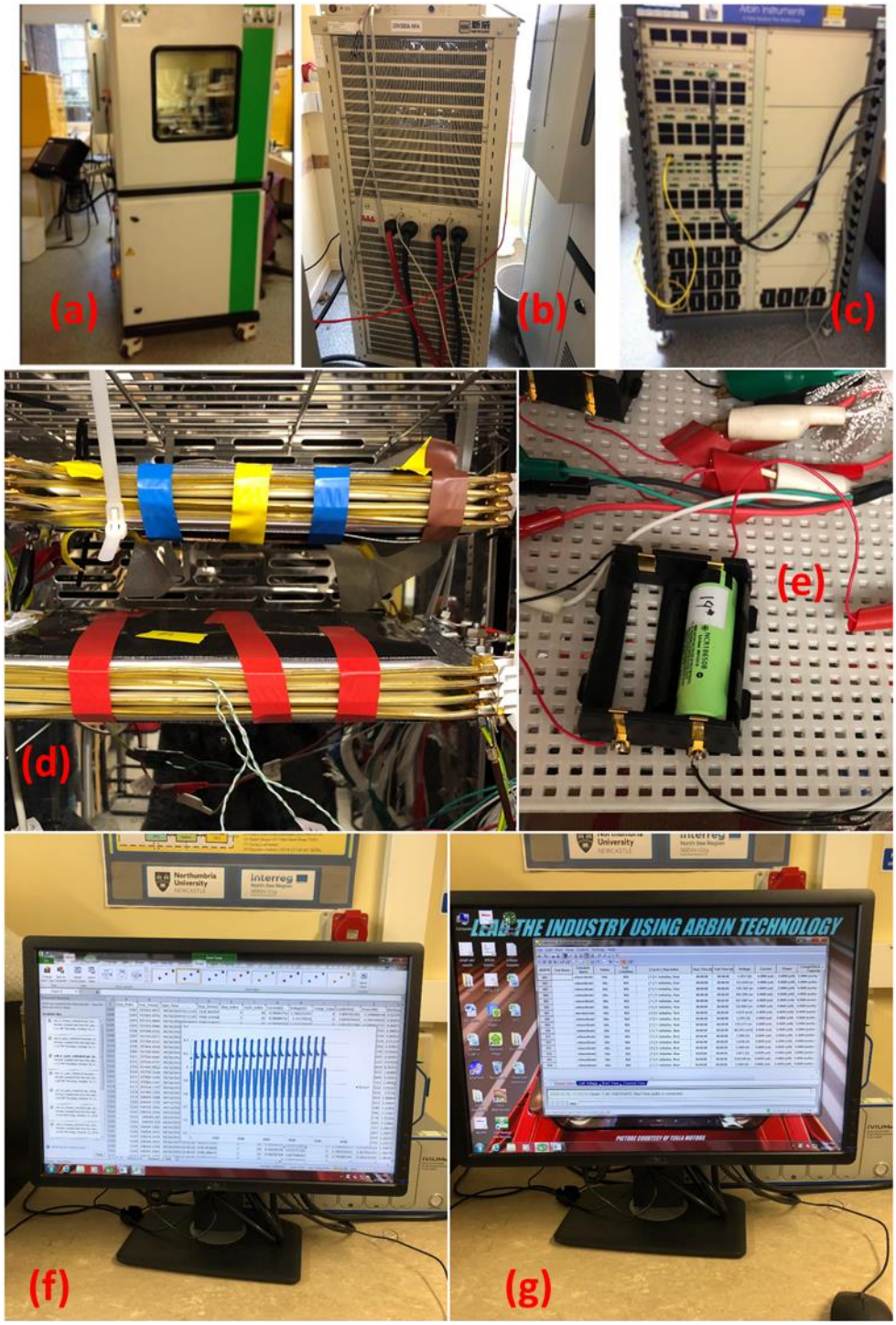

Figure 4.3-4 Experimental setup for battery testing: (a) environmental chamber, (b) Neware charger, (c) Arbin charger, (d) battery typed B, (e) battery type A, (f) sample of cycling data and (g) testing software

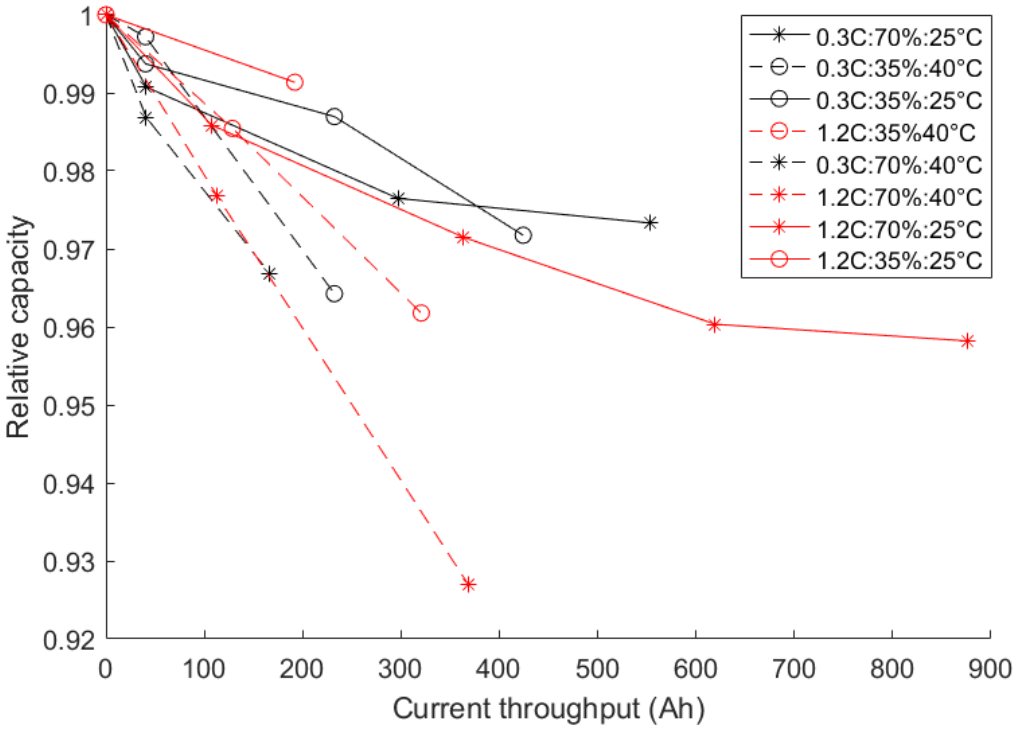

Figure 4.3-5 Cycling degradation tests for type A cells

The results exhibit the following trends:

- By comparing the solid lines with the dashed ones, the effect of the temperature can be seen; in all the four cases, the relative capacity given by the dashed line, representing the tests performed at 40 °C, are for the majority of the time lower than their solid counterparts, representing the corresponding tests performed at 25 °C. This indicates that increased temperatures negatively affect battery cycle life.
- By comparing the two solid black lines and two solid red lines in pairs, the impact of average SOC can be seen; for these pairs, the only variant is the average SOC, and the first pair does not exhibit significant difference, whereas the difference in battery life is evident in the second pair. This is because, the impact of average SOC on battery life is augmented by the combination with the other parameters; in fact, in the second pair, the C-rate is 1.2C, which increases the negative impact of average SOC. This is further evidenced by the corresponding dashed lines, which indicate a higher temperature of 40

°C. In fact, the difference between the two red dashed lines and the two black ones is evident: the circle markers are always above the corresponding asterisk markers. Again, this is due to the amplification effect that the temperature has on the negative impact of average SOC.

- The impact of charging rate is not significant in the type B cells as when the black lines are compared with the corresponding red lines, their difference does not follow any pattern.

Figure 4.3-6 shows the results of the tests performed on type B batteries for different charging rates.

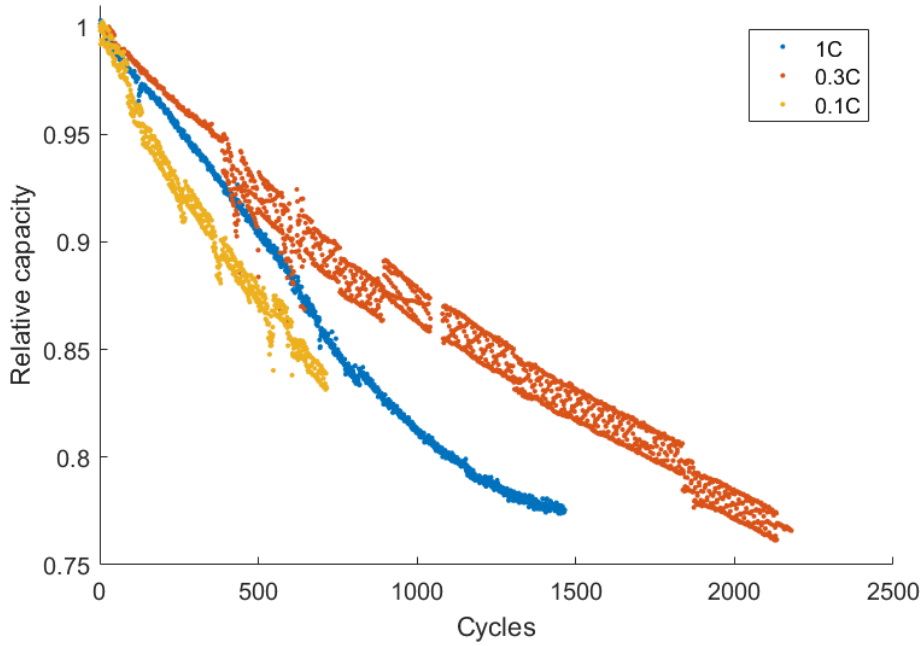

Figure 4.3-6 Cycling degradation tests for type B cells at different charging rates

In this second case, there is a significant difference between the cell cycled at 0.3C and the one at 1C, however, an abnormal behaviour is shown by the cell cycled at 0.1C. In fact, this particular cell degraded faster than even the cell cycled at 1C. The reason for this must lie on the initial conditions of these cells. The automotive cells have higher capacity compared to the 18650 cells, hence they require high current. Due to the number of channels of the

Neware high current cycling machine being limited to two, only the first and the second cells (1C and 0.3C) were cycled with that machine. Cell three was cycled with an Arbin machine with a lower rating but the results were not satisfactory. Hence, once the first cell (at 1C) reached end of life, the spare channel was then assigned to the third cell. Meanwhile since the third cell could not be separated from the rest, it was subject to some calendar degradation. Therefore, when the tests were finally restarted, the performance of the cell degraded. Evidence of this can be seen in Figure 4.3-7, where the internal resistance of the three cells are presented.

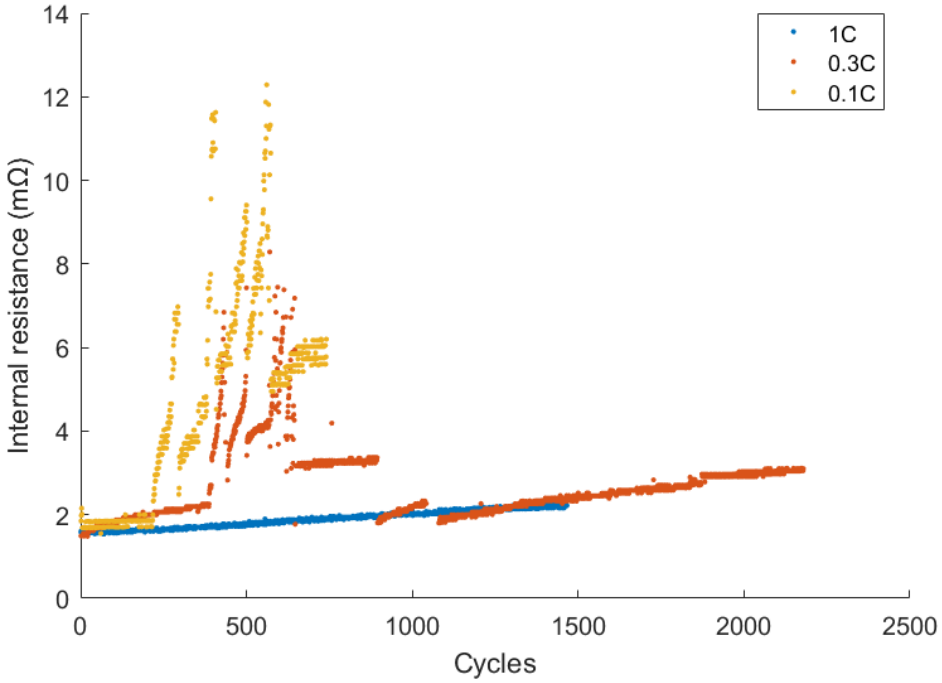

Figure 4.3-7 Internal resistance for the three type B cells

As can be seen from above, the internal resistance of cell three is consistently higher than all the other cells and an abnormal trend is seen. A plausible explanation is provided: the automotive cells come in a module of four cells sticked together. The cells were not separated, to avoid accidental damage. Hence, all the cells were subject to the same temperature. In addition, cell 3 was cycled with an Arbin machine with limited current output per channel (max 10 A), which was not able to handle such large cells; hence several

channels broke down, leading to erratic cycling results. In order to be able to cycle cell 3 properly, we waited until cell 1 reached end of life and only then cycled cell 3 with the Neware (more powerful) machine. However, during this period cell 3 stayed at 25 °C, because they could not be separated from the other cells, and have suffered calendar degradation. This may give a plausible explanation of the erratic data. Hence, the results for these tests cannot be considered reliable and we only use the results of the first two cells. Due to the limited time available and the long time required for a full testing period required by such large cells, further tests could not be conducted.

Figure 4.3-8 presents the behaviour of the cycling degradation coefficient α^c defined in equation. The black surface represents the degradation coefficient when the batteries are cycled at 0.3C while the red surface provides the degradation at 1.2C.

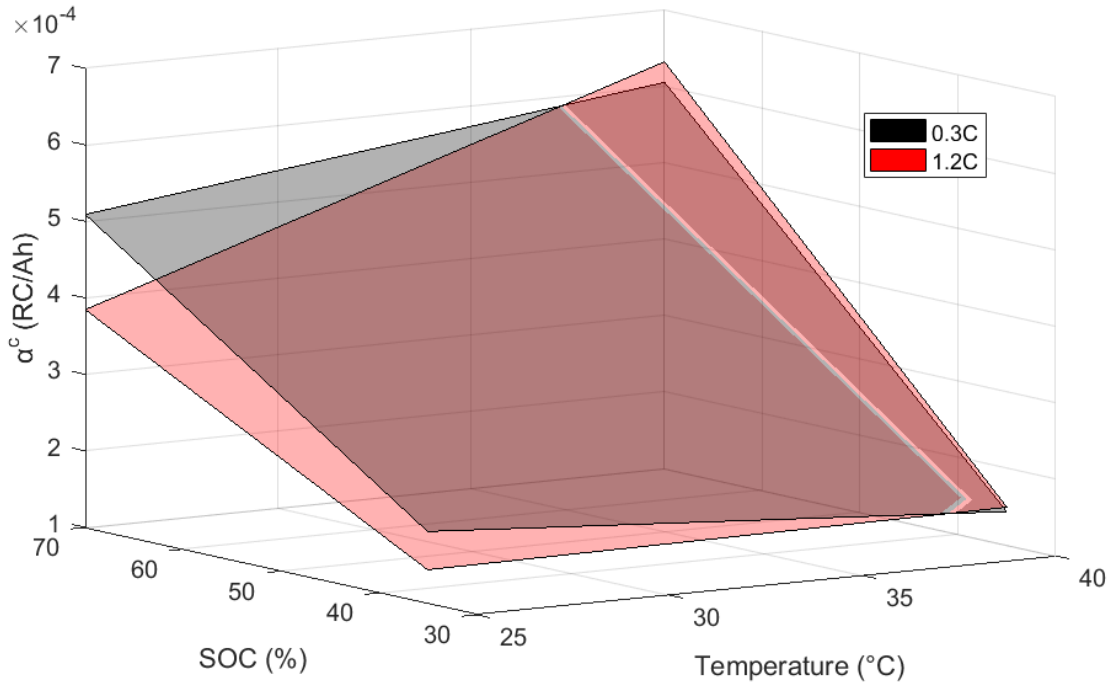

Figure 4.3-8 Behaviour of cycling degradation coefficient with respect to the impacting parameters

As discussed, from the figure above, the impact of temperature and average SOC is evident and how it is the combination of different parameters that influence degradation, while the cells seem unaffected by high charging rates.

The parameters of a modified version of the model in equation 4.22 has been fitted using a particle swarm optimisation (PSO) approach; more details regarding the algorithm will be given in the next chapter. The modified model incorporates only a linear relationship of the degradation with respect to the parameter temperature, to truly reflect the actual setting of the experiment, which did not test more than two temperature conditions.

Hence, the results of the fitting of the modified model, expressed in the following equation, are presented in Table 4.3-3.

$$\alpha^c = f(T^b, \langle SOC \rangle, C^r) = \gamma_1(\gamma_2 T^b + \gamma_3)\,(\gamma_4 \langle SOC \rangle + \gamma_5)(\gamma_6 C^r + \gamma_7) \tag{4.23}$$

Table 4.3-3 Fitted parameters for the type A battery degradation model

γ_1	γ_2	γ_3	γ_4	γ_5	γ_6	γ_7
$-2.54\ 10^{-8}$	4.98	-94.33	42.02	39.26	0.27	-3.52

As discussed before, the impact of charging rate is negligible compared to the other parameters (at least one order). The results of the tests performed on type B batteries have been fitted: as only the impact of charging rate was investigated, only the last term of equation 4.22 was used. The resulting model is shown in the equation below

$$\alpha^c = f(C^r) = (\,13 \times\ C^r + 6.1) \times 10^{-5} \tag{4.24}$$

As for the type B batteries other parameters were not tested, a model including the impact of SOC and temperature can still be attained, by scaling 4.24. As the only common charging rate that was tested for the two battery types is 0.3C, equation 4.24 must be scaled in a way that its output is unitary when the charging rate is 0.3C. Consequently, for any charging rate above 0.3C, the effect of this term will be that of an amplification of the effect (compared with the effect of 0.3C) of the other parameters, whereas if the charging rate is below 0.3C, the impact of the other parameters will be attenuated (compared with the effect of 0.3C).

Therefore, to obtain the battery degradation model for type B batteries, 4.22 and 4.23 are modified as

$$\alpha^c = -2.54\ 10^{-8} \times (4.98\ T^b - 94.33) \times (42.02\ \overline{SOC} + 39.26) \times (1.29\ C^r + 0.61) \qquad (4.25)$$

It should be noted that the underlying working assumption is that the automotive battery will behave as same as the 18650 cell with respect to temperatures and SOC, which should be ensured with more tests. However, due to both time and hardware limitations, this constitutes a future work.

The cycling degradation model differs from the calendar degradation model in the sense that, under the assumptions stated at the beginning of this chapter, cycling degradation is directly influenced by the operation of the battery, while calendar degradation is not. Hence, an economic value must be attributed to cycling degradation, as it must be compared against the incurred benefits from providing energy services with said battery. To this end, an approach similar to [9] is proposed, where the cost incurred by exchanging 1 kWh with the battery is expressed as

$$c^d = \frac{c^B}{E^L} \qquad (4.26)$$

where c^d is the cost associated with the exchange of 1 kWh of energy, c^B is the investment cost of the battery per kWh and E^L is the prospective lifetime energy throughput under certain charging condition. The lifetime of an EV battery is often measured as the number of complete charging/discharging cycles before the capacity of the battery falls below 80% of its original value. Consequently, the lifetime energy throughput is the energy that the battery exchanged until it reaches end of life, as shown in Figure 4.3-9.

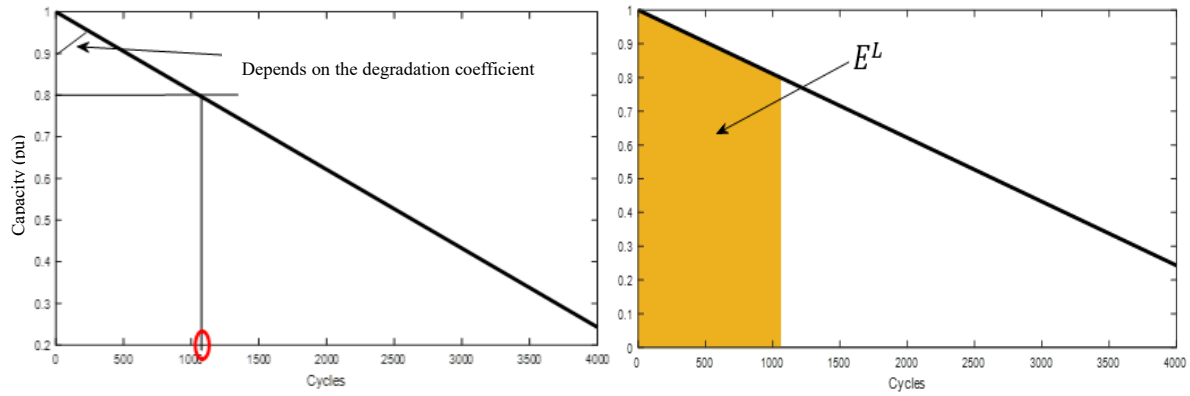

Figure 4.3-9 Graphical representation of lifetime energy throughput

As can be seen above, a certain number of equivalent cycles can be attained before the battery reaches end of life (red circled), deciding the lifetime energy throughput, which is the area underneath the capacity degradation curve (in yellow). The lifetime energy throughput can be defined accordingly as

$$E^L = 2 \times n^{EOL} \overline{E^{EV}} DOD \tag{4.27}$$

where n^{EOL} is the number of full cycles before the battery reaches the End of automotive life (EOL), $\overline{E^{EV}}$ is the maximum energy of the EV battery, DOD is the depth of discharge adopted in the tests (90%), and a cycle is defined as an equivalent charging-discharging sequence [hence the 2 is employed in (4.27)]. n^{EOL} can be defined as

$$n^{EOL} = \frac{0.2}{\alpha^c} \tag{4.28}$$

where α^c is the cycling degradation coefficient provided by the battery degradation model.

Finally, the overall battery degradation model was validated using real-life EV battery utilisation data, including temperatures, SOC and current. The associated SOH has been obtained as the ratio $\frac{\Delta SOC}{Ah}$, which is the current throughput to change the battery SOC of 1%. This can be considered as an indication of SOH since when the battery degrades, less current will be required to change the SOC. The daily average temperatures and SOCs of the EV under monitoring is shown for the period May 2015-May 2016 in Figure 4.3-10. It should be

pointed out that the daily average battery temperature (measured by internal sensors) is represented, as ambient temperature measurements were not available.

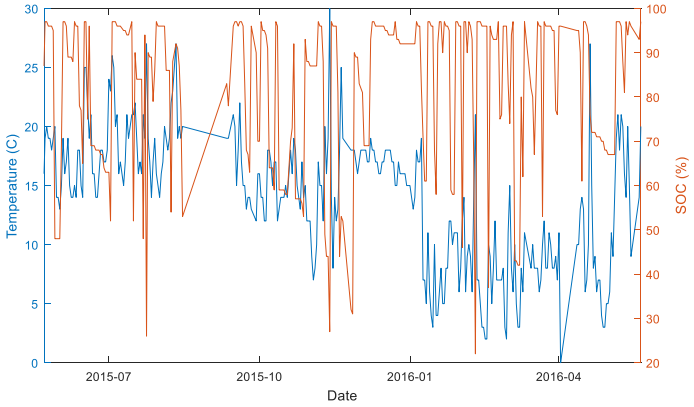

Figure 4.3-10 Average daily temperature and SOC

Figure 4.3-11 presents the exchanged currents for the same period and minute based temperatures and SOC, for the calculation of cycling degradation. The reason for averaging temperatures and SOCs on a daily basis for calendar degradation calculation, and taking higher resolution data for cycling degradation lies again in the different timeframes in which these two phenomena manifest. Calendar degradation is a tedious process hence the chosen time unit is a day, while cycling degradation happens for every cycle.

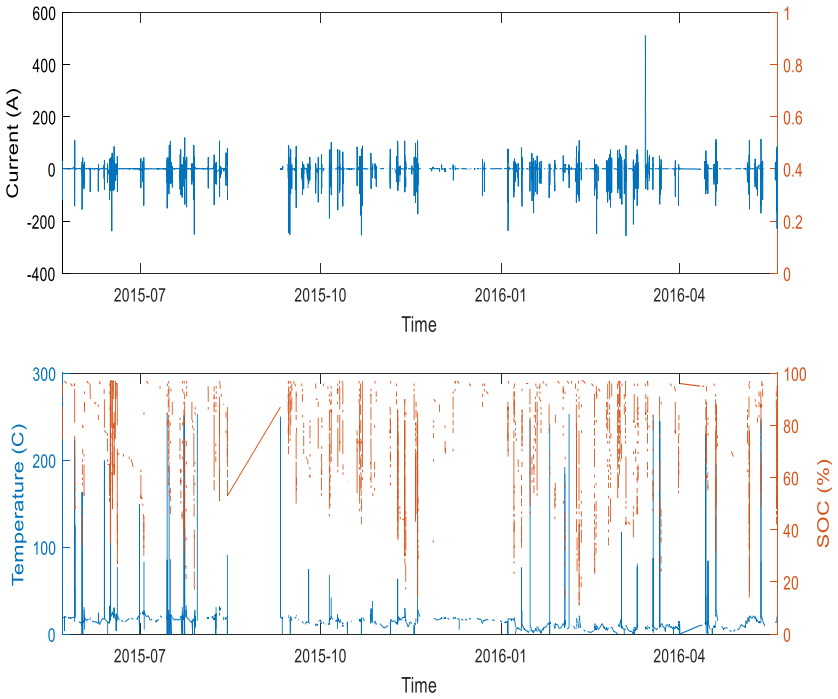

Figure 4.3-11 Minute based current, temperatures and SOCs

The incurred variation of SOH as a result of calendar degradation is shown in

Figure 4.3-12 and the capacity degradation due to cycling degradation is shown in Figure 4.3-13.

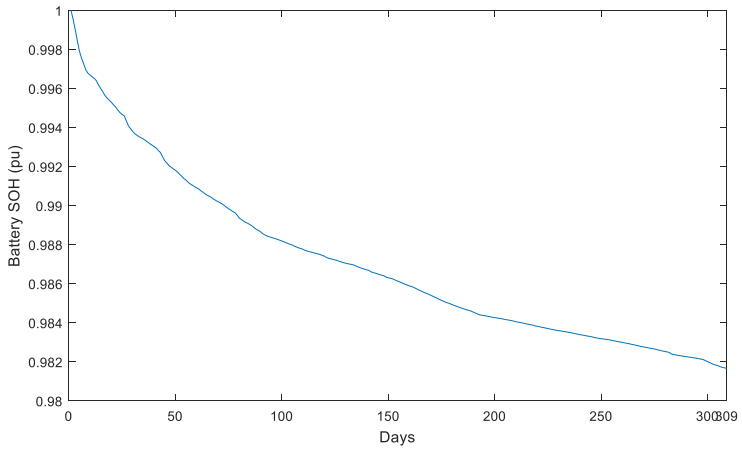

Figure 4.3-12 Calendar degradation model output

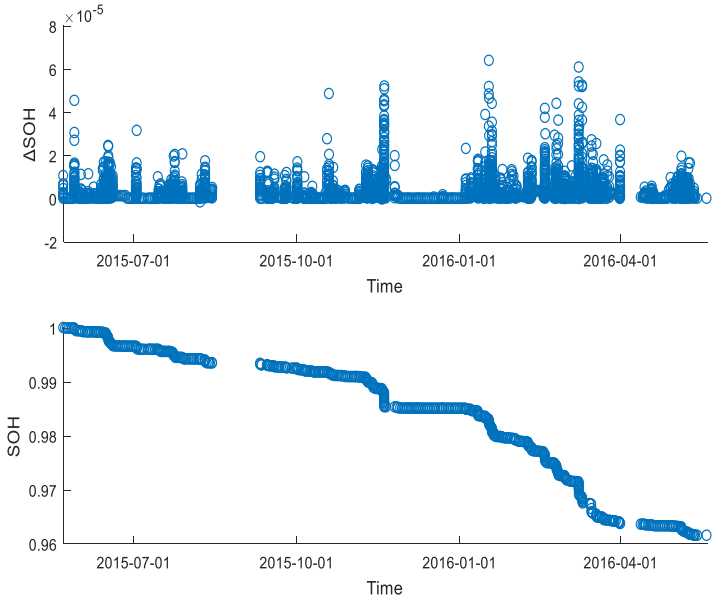

Figure 4.3-13 Cycling degradation model output

It could be seen that calendar degradation follows the behaviour dictated by the square root of time, while cycling degradation is linearly dependent to the utilisation. In fact, as in the period January – April 2016 the EV was used more (see the current in Figure 4.3-11), the battery degraded faster. Finally, Figure 4.3-14 compares the model output against SOH measurements from $\frac{\Delta SOC}{Ah}$ variations.

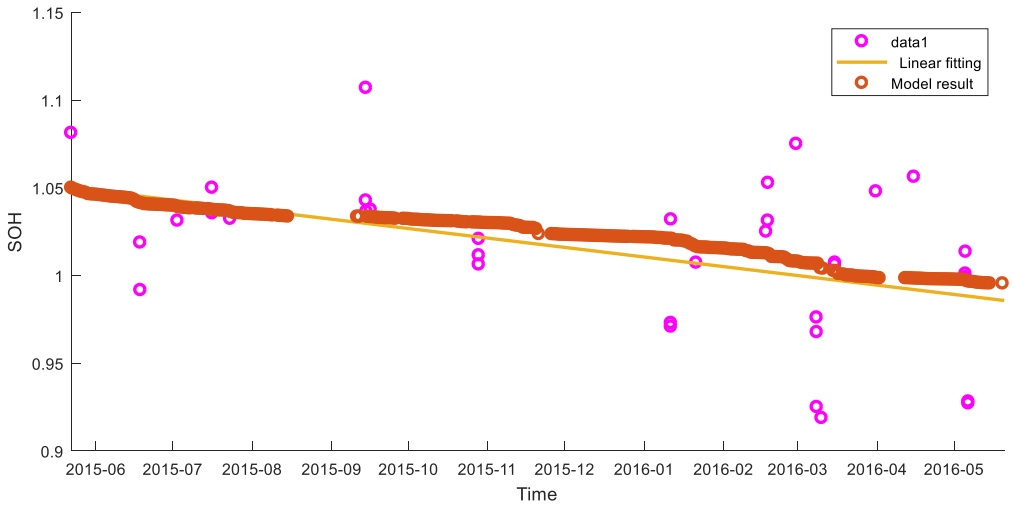

Figure 4.3-14 Comparison between measured SOH and model output

It could be seen that a significant variation is seen in the measured data, as the measurement will depend on the operating conditions at that time (temperature affects the cyclable capacity), but the overall trend shows a decrease. In addition, the best linear fit indicated that the beginning capacity was 5% higher than the nominal; hence the model output has been shifted upwards. A good agreement between the model output and the measured data is seen, especially in the period until September 2015 and from March to May 2016.

4.3.1 Extension to a self-adaptive capacity fade model

As discussed in the introduction of this chapter, the empirical battery degradation models available in current literature are primarily based on accelerated testing and seldom support dynamic operation of the battery. Furthermore, they are based on a few chemistries of lithium-ion batteries. This aspect is especially limiting since as it has been shown in the previous Section, different chemistries exhibit radically different behaviours (note that in the research, type A batteries did not show any dependency on the charging rate while in type B batteries, this effect was self-evident). To overcome such limitation, an ad-hoc battery model should be developed for each individual battery, as the chemistry, manufacturer (hence processes), batches and even transportation conditions are different, all influencing the batteries' behaviour. It is clear that an accelerated testing framework accommodating such diversity is prohibitive in time and cost dimensions hence another way must be found. Fortunately, the EV on-board measurement systems are constantly being improved and concurrently, communication protocols, such as the open charge point protocol (OCPP) and open smart charging protocol (OSCP) are advancing at high pace [125]. These technologies enable real-time measurement and control ultimately improving the management of the valuable battery data. This operational data can be used to optimise the utilisation of the battery. Similarly to Section 4.2.1, an adaptive fitting model is proposed to customise the battery model proposed in Chapter 4.3 for any type of EV battery. The operating principles for a self-adaptive battery degradation model is hereby described.

- The proposed model makes use of temperature, current and capacity measurements $\mathbf{M}_i = \{\boldsymbol{T}_i^b, \boldsymbol{I}_i, SOH_i\}$ to fit a capacity fade model in an automated manner (note: the bold

letters indicate that these are measurement vectors; average SOC can be measured from the current).

- As capacity measurements require one full charge-discharge cycle of the battery, and this cannot be performed daily (the EV will be charged fully only when the user needs to travel; as per chapter 3.2 daily driven mileage in the UK can be satisfied by a fraction of the total EV battery capacity, hence the EV will not be fully charged on a daily basis), a periodic *adjustment cycle* (to adjust the model), is programmed.
- After each adjustment cycle, the model is fitted with the whole set of measurements available at the time.
- The previous model parameters are taken as initial values to fit the model by minimising the error expressed in the following equation

$$\underset{\gamma_1,\dots,\gamma_7}{\operatorname{argmin}} \sum_{i=1}^{n} \left[SOH_i - \left[\gamma_1 \left(\gamma_2 \boldsymbol{T}_i^b + \gamma_3 \right) \left(\gamma_4 \langle \boldsymbol{SOC} \rangle_i + \gamma_5 \right) \left(\gamma_6 \boldsymbol{I}_i + \gamma_7 \right) \right] \right]^2 \tag{4.29}$$

The algorithm for a self-adaptive capacity model is hereby presented, where a PSO optimisation algorithm has been used to minimise the fitting error.

Self-adaptive capacity fade model

Input: Set of measurements $\mathbf{M}_{1,n}$ until current adjustment cycle n, current model $\boldsymbol{\gamma}_{n-1} = \{\gamma_1, \dots, \gamma_7\}$

1: **for** $i \leftarrow 1$ **to** (n) **do**

2: Fit the model by minimising 4.26 with initial values $\boldsymbol{\gamma}_{n-1}$

3: **end for**

The model has been tested with the real-life utilisation data for the period May 2015 – May 2016: a full year has been divided in 18 Sections, each including one adjustment cycle (it means that the SOH is known only in these 18 time points). Once the model was fitted in a certain adjustment cycle, it was then used to predict the capacity fade for the rest of the year and the error is presented in Figure 4.3-15.

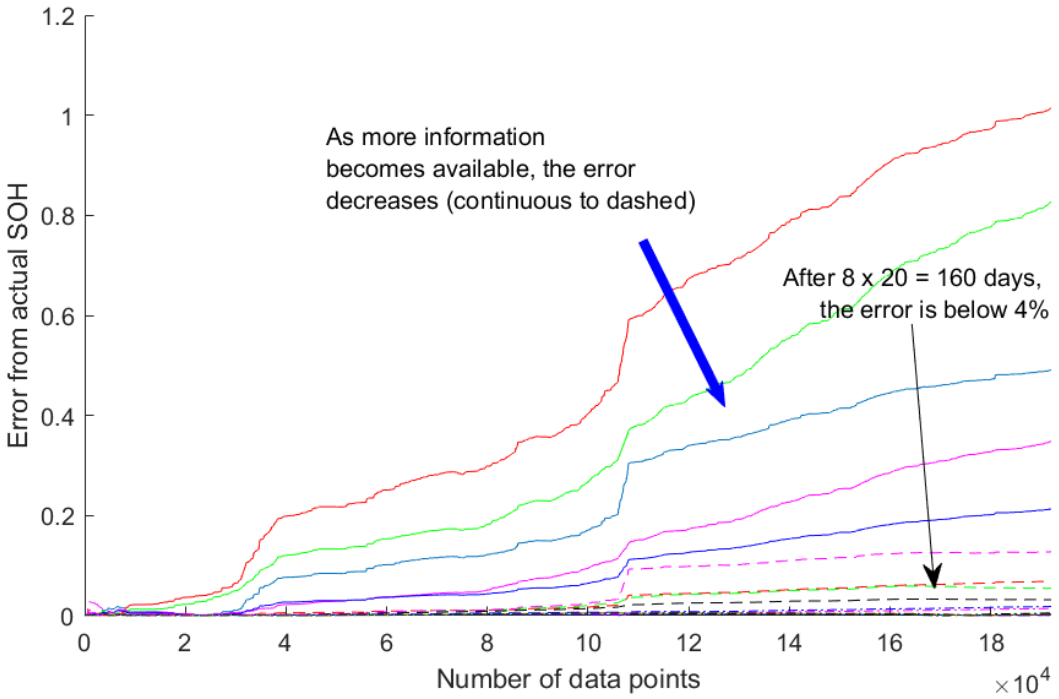

Figure 4.3-15 Prediction error of the self-adaptive capacity fade model

4.4 Conclusions

In this chapter, a framework for modelling EV battery degradation has been presented. There are several chemical processes that cause battery degradation and the most rigorous approach is to model these reactions. However, as it has been discussed, such approach is not suitable for models that will have to be considered in an optimisation process. The main reason is that these models only predict battery degradation, but the latter is not linked to the operational parameters, such as voltage, currents and temperature. Hence, empirical models are more suitable for developing an optimisation-friendly degradation model. First, a one-time-constant ECM model has been developed, in order to control the power exchanged with the battery. The model has been extended in its adaptive form, by utilising operational data. Then, an empirical capacity fade model has been developed based on accelerated degradation tests. Two types of batteries, automotive and commercial 18650, have been tested and they have shown different behaviour with respect to the impacting parameters. In particular, the

18650 batteries were insensitive to different charging rates while the automotive cells showed some dependency. Once the models were adjusted, they have been validated using real-life EV battery utilisation data and the model showed good agreement with measurements. As in real-life a large range of batteries will be employed for transportation, an adaptive capacity fade model, based on periodic fitting, was proposed, and it is seen that after 160 days the model can predict battery degradation efficiently. This is due to the dynamic nature of EV utilisation and variable seasonal conditions, where for instance, some temperatures may not be reached at some time of the year, hence the model will not know how the battery could behave in those situations. Overall, lithium-ion battery degradation is a complex process that is highly dependent on a multitude of factors, i.e. battery type, manufacturing method, operating conditions etc. and it is non-linear. As it will be seen in the next chapter, this will decide the algorithms that can be employed for a multi-objective optimisation framework that also accounts for battery degradation.

Chapter 5 Development of an optimisation framework for smart EV charging scheduling

5.1 Introduction

In this chapter, the main principle for mathematical/numerical optimisation are provided. The past two chapters have been dedicated to the development of mathematical models that describe physical systems. The adopted formulation allows an automatic controller/decision maker to govern the physical system by controlling the variables that have been defined. For instance, one of the most widely implemented optimisation is that of the energy cost of an archetype (household, commercial building etc.), which can be controlled by manipulating the power/energy exchanges between the said archetype and the local electricity grid based on a price function. As will be shown in this chapter, the aim is to find the values of the governing variables that minimise or maximise certain functions. Set as the main aim of this research, multi-objective optimisation will deal with the simultaneous minimisation/maximisation of a set of functions, which will result, in some cases, in conflicts. The key contribution of this work is to propose an optimisation framework that deals with multiple objectives, highlights their inherent conflictual interrelationships and introduces a Pareto based approach to provide a range of optimal solutions. Subsequently, a decisional framework is proposed, based on MCDM rules, where the involved decision makers are engaged in showing their preference. As will be discussed, multi-objective-optimisation (MOO) applied to EV charging scheduling is still an emerging research area and rules for the real-life implementation of such framework are yet to be defined. Therefore, we believe the contribution to knowledge that this work brings is to pave the way for future

implementation of MOO for EV charging. In this chapter, a generic optimisation framework for single objective is first defined along with basic definitions regarding mathematical optimisation. Then MOO is formally introduced along with suitable MCDM rules.

5.2 Single-objective optimisation

In this section, basic definitions required for mathematical/numerical optimisation are provided, along with algorithms for non-linear optimisation. The reason for such classification is simple: the majority of the mathematical models defined in Chapter 3 and 4 are non-linear. As will be shown, this decision adds considerable complexity in the optimisation algorithms adopted in this research, which is directly translated into computational time. If linear programming approaches could be adopted, the computational effort may be drastically reduced. Another aspect afflicting non-linear optimisation is the scale issue: due to the complexity associated with non-linearity, the available algorithms are sensitive to the scale of the problem in terms of number of variables and constraints. These types of problems do not scale well with increasing number of decision makers/agents as computational time is at the very least directly proportional (as will be seen in MOO quadratic) to this number. Therefore, whenever possible, linearization techniques should be adopted to simplify the nature of the problem. However, as the aim of this research is to provide an operational optimisation framework, linearization techniques are beyond the set scope, hence they constitute a relevant but future work. In addition, the work conducted in this research is on deterministic optimisation, hence stochastic processes and robust optimisation are not within the scope of this research. The definition of a mathematical optimisation problem can be found in appendix A2.

5.2.1 Solution of a mathematical optimisation problem

Given a generic non-linear optimisation problem

$$\min_{x \in \mathbb{R}^n} f(x) \quad \text{s.t.} \tag{5.1.a}$$

$$h_k(x) = 0, k = 1,2, \dots, p \quad (5.1.b)$$

$$g_j(x) \geq b_j, j = p+1, \dots, m \quad (5.1.c)$$

where 5.1.b and 5.1.c are the equality and inequality constraints, respectively. The above optimisation problem can also be transformed in standard form by considering slack variables: $g_j(x) - s_j \geq b_j$ and $s_j \geq 0$ (now the vector x will also include the s_j).

$$\min_{x \in \mathbb{R}^n} f(x) \text{ s.t.} \quad (5.2.a)$$

$$c_i(x) = b_i, i = 1,2, \dots, m \quad (5.2.b)$$

$$x \geq 0 \quad (5.2.c)$$

In this research, the interior point algorithm (IP) is implemented for the non-linear convex optimisation problems as it is an efficient and widely adopted method [127]. Under this approach, a class of penalty function methods are then used which transform the constrained convex optimisation problem in a sequence of unconstrained minimisation problems. There are two classes: exterior point penalty and interior point penalty. The former calculates iteratively a series of infeasible points and reaches an end when it generates a feasible point. The latter, generates a series of feasible points, which are then converted in optimal descent points. As an example, let us consider

$$c_i(x) = 0 \quad (5.2.d)$$

If a solution $x_1 \in \mathbb{R}^n$ is infeasible, that is $c_i(x_1) \neq 0$ at least for one i, then there is the incurrence of a penalty in the form $\mu_i {c_i}^2(x_1)$, where $\mu_i \geq 0$.

There are other more suitable penalty functions that can be utilised, normally called barrier functions of the following form:

i) Inverse barrier function

$$\beta_i = -\frac{1}{c_i(x)} \quad (5.3)$$

ii) Logarithmic barrier function

$$\beta_i = \log[c_i(x)] \tag{5.4}$$

Consequently, the minimisation problem defined in (5.2) is transformed in a new augmented version defined in (5.5). The aim is to obtain the optimal solution as the penalty terms become nil: $\rightarrow 0 \Rightarrow x_k^* \rightarrow x^*$, where k is the number of iterations.

$$\min_{x \in \mathbb{R}^n} f(x) + \sum_{i=1}^{m} \mu_i \beta_i \tag{5.5}$$

The above optimisation problem is solved by defining a Lagrangian function and a system of equations that satisfies the Karush-Kuhn Tucker (KKT) optimality conditions [128] as defined by the following equations.

$$c_i(\boldsymbol{x}^*) - b_i = 0\ , \forall i \tag{5.6}$$

$$\nabla \boldsymbol{f}(\boldsymbol{x}^*) - \sum_{i=1}^{m} \lambda_i^* \nabla c_i(\boldsymbol{x}^*) - \mu_i \sum_{i=1}^{m} \frac{1}{x_i} = 0 \tag{5.7}$$

$$\lambda_i^* (c_i(\boldsymbol{x}^*) - b_i) = 0, \forall i \tag{5.8}$$

$$\lambda_i^* \geq 0, \forall i \tag{5.9}$$

Where (5.6) is the feasibility condition, (5.7) is the optimality condition, (5.8) represents the complementarity slackness (only if there are inequality constraints) consideration:= and (5.9) impose positive Lagrange multipliers.

The method for solving the system of non-linear equations may be the Newton-Raphson method presented in Chapter 3, which is not repeated here. The algorithm for IP is outlined in the Appendix A3 Algorithms for mathematical optimisation

The above single-objective optimisation method was applied in [P2] for an optimal stationary energy storage and EV charging scheduling, with the latter including battery degradation. As it was previously hinted, the computational burden of such solution algorithm lies in the iterative process. This is because, the optimal solution is iteratively approximated since the system of equations is non-linear.

As some objective functions may be not convex (concave), for them, the IP algorithm will only find local minima (maxima). In the recent decades a class of algorithms has overcome

this limitation, as they do not require any gradient calculations, hence are not trapped in local minima.

5.2.1.1 Metaheuristic algorithms - particle swarm optimisation

Metaheuristic algorithms make use of population behaviour to search the global optimum point in the feasible region. Among metaheuristic algorithms evolutionary algorithms and swarm-based algorithms are among the most popular and have been adopted in a wide variety of applications, including MOO. Evolutionary algorithms are inspired by the Darwin's theory of survival of the fittest, where only the strongest genes in a population can reproduce. On the other hand, swarm based methods make use of a population that moves in the feasible space searching for the optimum point and the direction of the swarm members is updated according to the best candidate solution. Due to the intuitivity and flexibility of the latter, particle swarm optimisation (PSO) has been adopted in this research for the minimisation (maximisation) of convex (concave) functions [129]. Given the optimisation problem:

$$\min_{x\in\mathbb{R}^n} f(x) \text{ s.t.} \tag{5.10.a}$$

$$h_k(x) = 0, k = 1,2,\dots,p \tag{5.10.b}$$

$$g_j(x) \geq b_j, j = p+1,\dots,m \tag{5.10.c}$$

where The PSO algorithm is generally based upon few iterative steps as listed below:

- Generation of a random population of candidate solutions, within the feasible region, $\mathrm{P}_p = \{x \in \mathbb{R}^n | h(x) = 0 \cap g(x) \geq 0\}$, where p is the number of particles.
- Evaluation of a fitness (objective) function on the population $f(\mathrm{P}_p)$
- Find the best member (solution) for the swarm $g_{d,k}$ and the personal best position for each particle in all the iterations thus far, $p_{i,d,k}$, where i is the index of the particle, d indicates the dimension and k is the iteration step.
- Define velocities of the members based on the following equation

$$v_{i,d,k+1} = \omega\, v_{i,d,k} + \varphi_{p,k}\, \xi_p\left(p_{i,d,k} - x_{i,d,k}\right) + \varphi_{g,k}\, \xi_g\left(g_{d,k} - x_{i,d,k}\right) \quad (5.11)$$

where, $\varphi_{p,k}$ and $\varphi_{g,k}$ are the damping coefficients for the personal best and global best directions, respectively, and ξ_p and ξ_g are randomly generated numbers, with $\xi_p, \xi_g \sim U(0,1)$.

– Update the positions of the members as defined by the expression below

$$x_{i,d,k+1} = x_{i,d,k} + v_{i,d,k+1} \quad (5.12)$$

– Check convergence criteria; if met, finish, otherwise repeat from the second step.

It should be noted that the above description accounts for the constraints only at the first step, while in the latter computations, only optimality is checked. To this end, the original objective function can be updated with the already discussed barrier functions that penalise violations of the constraints and ensures convergence to an optimal and feasible point. Based on the above description, the steps for implementing PSO is presented in Appendix A3 Algorithms for mathematical optimisation.

5.3 Multi-objective optimisation

The previous section was dedicated to the solution of single objective optimisation problems, where a decision variable is controlled in order to minimise (maximise) one objective function. However, societies of individuals in real-life, i.e. electricity user, EV user, DSO etc., generally pursue several objectives at the same time. When these objectives are equivalent, or in other terms, optimisation of one objective provides also the optimum point of the other objectives, then a single-objective optimisation is sufficient. On the other hand, when conflicts arise from two or more objectives, then MOO is the only rigorous method to find the *multiple* optimum solutions of the problem. We illustrate the conflict between two objectives with the aid of Figure 5.3-1.

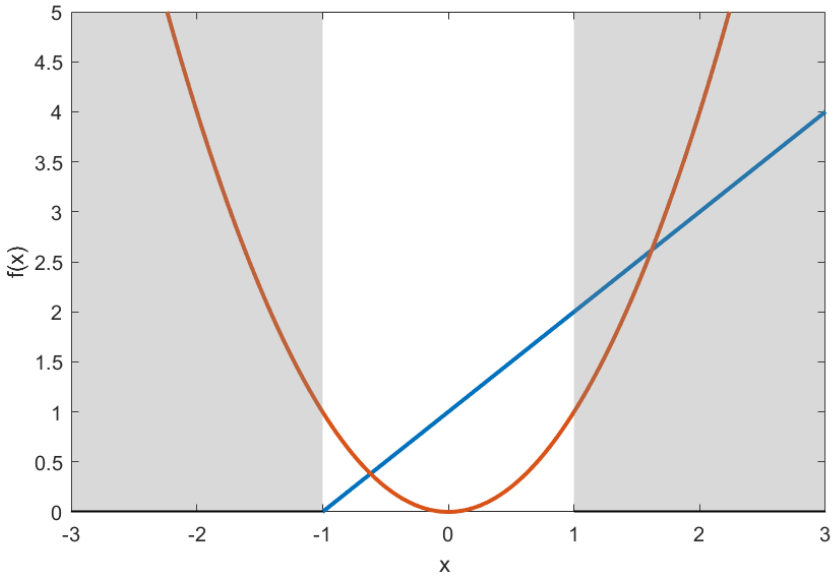

Figure 5.3-1 Conflicts between two objective functions

In the figure above, two objective functions are represented, namely:

$$f_1(x) = x + 1,\ x \in [-1,1] \tag{5.13}$$

$$f_2(x) = x^2,\ x \in [-1,1] \tag{5.14}$$

The feasible region is limited by the shaded area. As can be seen, the two functions attain their minimum values for two different values of x:

$$\underset{x\in[-1,1]}{\operatorname{argmin}} f_1(x) = -1 \tag{5.15}$$

$$\underset{x\in[-1,1]}{\operatorname{argmin}} f_2(x) = 0 \tag{5.16}$$

In fact, if $x = -1$, f_1 finds its minimum value in the feasible region, but f_2 is at its maximum value. Conversely, if $x = 0$, f_2 achieves its minimum value while f_1 does not (but it is not at its maximum value). A *trade-off* between these two conflicting objective functions is seen: improvements along one objective lead inevitably to a worse performance along the other objective. This trade-off is often represented by a *Pareto frontier*, named after the economist

Vilfredo Pareto who first proposed it. An example of the convex Pareto frontier for the above two functions is shown in Figure 5.3-2.

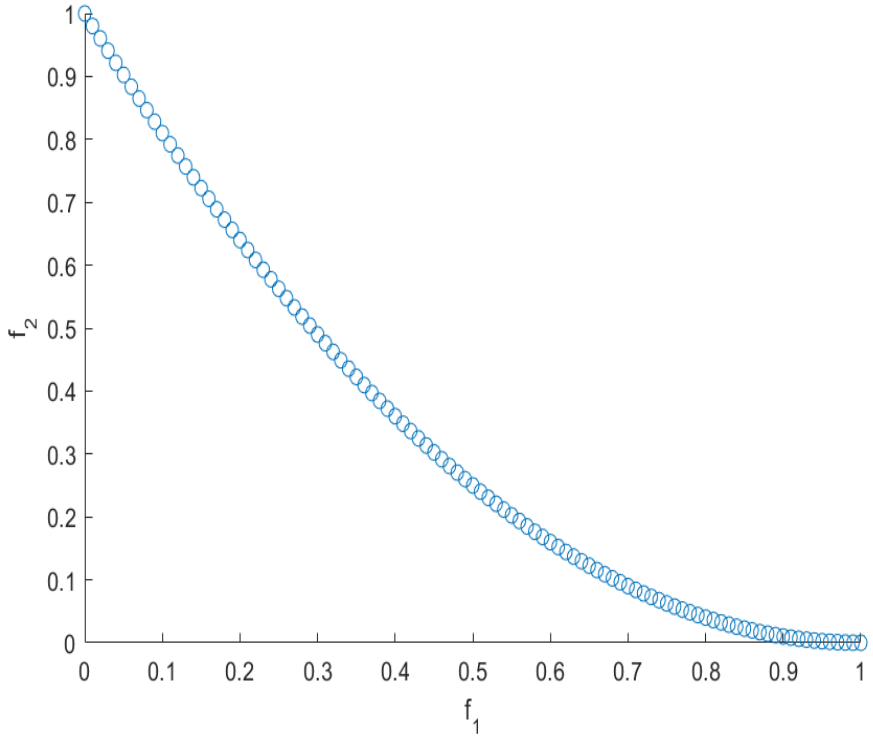

Figure 5.3-2 Convex Pareto frontier for two objectives

As already discussed, as f_1 tends to zero, f_2 tends to 1, its maximum value. Note how there are multiple optima and not a single one as each of these solutions is not better than the rest: one solution may have a lower performance along one objective but it will perform better along the other. To this end, the concept of Pareto dominance, as will be now introduces is of considerable relevance. Some definitions are presented hereby to facilitate the formulation of the MOO problem [130].

Definition 9. Given a MOO problem expressed as follows:

$$\min \boldsymbol{F}(\boldsymbol{x}): X \to \mathbb{R}^k = \tag{5.17}$$

$$k \geq 2$$

$$\begin{cases} f_1(\boldsymbol{x}): X \to \mathbb{R} \\ \quad \ldots \\ f_k(\boldsymbol{x}): X \to \mathbb{R} \end{cases}$$

where $X \subset \mathbb{R}^n$ is the feasible region, defined by the imposed constraints and $f_1, \ldots, f_k$ is the set of objectives

- *A solution $\boldsymbol{x}'$ is said to Pareto dominate another solution $\boldsymbol{x}$ and is indicated as $\boldsymbol{x} \prec \boldsymbol{x}'$ if*

$$f_i(\boldsymbol{x}') \leq f_i(\boldsymbol{x}) \qquad \forall i = 1, \ldots, k \tag{5.18}$$

$$f_j(\boldsymbol{x}') < f_j(\boldsymbol{x}) \qquad or\ at\ least\ one\ j = 1, \ldots, k$$

- *A solution $\boldsymbol{x}'$ is Pareto optimal/efficient/non-dominated if there is no other solution dominates it. The Pareto front is the set of all the Pareto optimal solutions.*

In other words, Pareto optimal solutions are those that cannot be improved along one objectives without deteriorating the performance along another objective. The aim is to produce all the Pareto optimal solutions in order to enable decision-making.

Among strategies aimed at obtaining the full Pareto front, the augmented ε-constraint method is widely implemented [69], [131], [132], [133], for fast and reliable MOO. With this approach, one objective is optimised while the others are converted into constraints. By varying the strictness of such constraints, a subset of the Pareto front can be obtained. It should be noted that the constrained single-objective optimisations can be performed with any of the two methods presented in Section 5.2.2, depending on the objective functions. At the beginning of this algorithm, lexicographic ordering is applied to define the range of the objective values, from their maxima to the minima. Under lexicographic ordering, the objectives are given priorities and are sequentially optimised; the values from the optimisations at higher priorities are used as constraints for the optimisations at lower levels. We subsequently apply non-dominated sorting to ensure that all the solutions are Pareto efficient. Non-dominated sorting compares all the solutions obtained from the Augmented ε-Constraint (ANEC) Algorithm. against each other, and only keeps those that are non-dominated.

5.3.1.1 The ANEC algorithm

The following pseudo-code outlines the augmented non-dominated ε-constraint method

Augmented non-dominated ε-constraint method

Input: MOO problem with $\boldsymbol{F^m}$ set of m objectives, $\boldsymbol{\Gamma}$ defined by p constraints and n^{max} divisions of the solution space

Initialisation: Lexicographic ordering

for k ← 1 **to** (m) **do**

  $\boldsymbol{\zeta^{lex}_{m\times m}} \leftarrow \boldsymbol{lex}\min_{\boldsymbol{x},f^k} \boldsymbol{F^m}$ (21)

end for

Define Nadir point $\boldsymbol{\Psi}_{m\times 1} = \max(\boldsymbol{\zeta^{lex}})$ and optimal point $\boldsymbol{\psi}_{m\times 1} = \min(\boldsymbol{\zeta^{lex}})$

Arbitrarily select objective f^i to be optimised

for j ← 1 **to** $(n^{max}+1)$ **do**

  for l ← 1 **to** $(n^{max}+1)$ **do**

    $\mathbf{q}_{m\times 1} = [\boldsymbol{j}, \boldsymbol{l}, \dots]$

    $\boldsymbol{\varepsilon}_{m\times 1} \leftarrow \boldsymbol{\Psi} - \boldsymbol{q} \times \frac{(\boldsymbol{\Psi}-\boldsymbol{\psi})}{n^{max}}$

    $\boldsymbol{\sigma} \leftarrow \underset{\boldsymbol{x}\in\boldsymbol{\Gamma},\boldsymbol{F}\setminus\{f_i\}=\boldsymbol{\varepsilon}+\boldsymbol{S}}{\operatorname{argmin}} (f_i(\boldsymbol{x})) - \gamma \sum \boldsymbol{S}$

    if infeasible

      Exit current for loop and continue the loop above

    end if

  end for

end for

for o ← 1 **to** $(size(\boldsymbol{\sigma}))$ **do**

  for p ← 1 **to** $(size(\boldsymbol{\sigma}))$ **do**

    Check $\boldsymbol{\phi}_o \prec \boldsymbol{\phi}_o$

  end for

end for

where f^k is the prioritised objective during Lexicographic ordering, $\boldsymbol{q}$ is the index vector for the nested for loops, $\boldsymbol{\varepsilon}$ is a vector representing the constraints for the objective functions that are not minimised. There will be as many nested for loops as $n^{for} = m - 1$. $\boldsymbol{S} =$

$[s_1, \dots, s_{m-1}]$ are the slack-variables adopted for the augmented-ε constraint and γ is an arbitrary constant value. As the Pareto optimal solutions are progressively calculated, the values of $\boldsymbol{\varepsilon}$ vary from the maxima of the single objective functions to the minima. $\boldsymbol{\phi}_o$ and $\boldsymbol{\phi}_p$ are solutions of the ε-constraint method. It should be noted that n^{max} is the number of divisions of the range of each objective values. As the ε constraint for one objective is varied within the for loop, the constraints of the other objectives are kept constant. In the for loops at higher levels, the ε constraints of the other objectives are varied. It is evident, that a number of computations will be infeasible; this is because as the objectives are conflicting and the objective values are constrained from their maxima to the minima, two conflicting objectives cannot simultaneously reach their minimum values. To avoid unnecessary computations, once an infeasible computation is found, the current for loop is ended and the loop at the higher level is continued.

5.3.2 Multi-criteria-decision-making with analytical hierarchy process

Once the full Pareto front is obtained, a decision needs to be taken to choose the preferred solution. If no preference is shown, the Pareto front represents the set of solutions that are equally optimal and therefore equivalent. MCDM techniques can help on choosing one solution from the Pareto front. In this research, the Analytical Hierarchy Process (AHP) [134] is employed.

AHP evaluates the performance of n alternative solutions along a set of m objectives. The decision maker prioritizes the different objectives with a relative comparison matrix $\boldsymbol{A}_{m\times m}$. The priority of each objective is quantified with relations a_{ij}. $a_{ii} = 1, \forall i$ as an objective has the same priority as itself. The relative comparison of two different objectives is outlined as follows: if i is more important than j, then:

$$\begin{cases} a_{ij} = k, \\ a_{ji} = \frac{1}{k} \end{cases}$$

where $k \in [1,9]$ determines the relative priority of j compared to i; $a_{ij} = 1$ indicates that i and j have the same importance while $a_{ij} = 9$ indicates that j is extremely important compared to i. An example of a pair-wise comparison matrix is shown hereby.

	$\boldsymbol{Ob_1}$	$\boldsymbol{Ob_2}$	$\boldsymbol{Ob_3}$
$\boldsymbol{Ob_1}$	1	5	9
$\boldsymbol{Ob_2}$	$\frac{1}{5}$	1	2
$\boldsymbol{Ob_3}$	$\frac{1}{9}$	$\frac{1}{2}$	1

With the pairwise comparison matrix with m objectives, where i denotes the columns, j denotes the rows and $a_{i,j}$ is the pairwise comparison weight between the objectives i and j, a normalised form is obtained as expressed by the following equation:

$$a_{i,j}^{n} = \frac{a_{i,j}}{\sum_j a_{i,j}}, i = 1, \dots, m \tag{5.19}$$

where $a_{i,j}^{n}$ is the normalised pairwise comparison weight between the objectives i and j, obtained by dividing $a_{i,j}$ by the sum of the weights in the respective column i. Next, an Eigenvector (or priority vector), which define the relative priorities between each criterion/objective, is calculated by averaging the rows of the normalised pairwise comparison matrix as defined hereby:

$$w_j = \frac{\sum_i a_{i,j}^{n}}{m}, j = 1, \dots, m \tag{5.20}$$

where w_j is the relative weight of the objective j compared to the overall benefit, the elements of the eigenvector all add up to one.

To ensure consistency of the decision making process a further check should be performed. For instance, if any stakeholders declares that financial benefits are more important than technical ones and the latter are more important than the environmental ones, an

inconsistency would arise if it were affirmed that environmental objectives are more important than the financial ones. The method consists of calculating the maximum eigenvalue λ^{max} as showed in the following equation

$$\lambda^{max} = W' A_j = \sum_j w_j \left(\sum_j a_{i,j}\right) \tag{5.21}$$

where W' is the eigenvector (transposed in a row) and A_j contains the sum of the columns of the original pairwise comparison matrix. The consistency index is defined as in the expression below

$$CI = \frac{\lambda^{max} - m}{m-1} \tag{5.22}$$

To ensure consistency, the ratio between CI and a random consistency index, RI, must be checked, as shown in the following equation

$$CR = \frac{CR}{RI} \tag{5.23}$$

where CR is called consistency rate and for the decision making process to be consistent it must be lower than 0.1. The random consistency index depends on the number of objectives as shown in Table 5.3-1.

Table 5.3-1 Random consistency index for different number of criteria

m	**1**	**2**	**3**	**4**	**5**	**6**	**7**	**8**	**9**	**10**
RI	0	0	0.58	0.9	1.12	1.24	1.32	1.41	1.45	1.49

Once the Pareto solutions are determined, they are multiplied by the elements of the eigenvector (there may be different eigenvectors if there are multiple stakeholders that hold different opinions) and an overall score is obtained for all the Pareto solutions. The solution having the highest score shall be chosen as the preferred solution.

5.4 Conclusions

In this chapter, the principles of mathematical optimisation have been defined with a focus on non-linear optimisation. Under single-objective optimisation, if the objective function is convex (concave) within the feasible space, then a classic algorithm such as the interior point method can be implemented, since the existence of a global minimum (maximum) is guaranteed. If the function is not convex (concave) in the feasible region, then there are multiple local minima (maxima) and the algorithm can be trapped in one of those. In that case, metaheuristic methods, such as evolutionary algorithms or swarm-based methods can find a global minimum (maximum). PSO is presented as an intuitive yet powerful algorithm to find a global minimum (maximum) efficiently. Once the optimisation problem starts considering more than one objective, some conflicts may arise, as it has been shown with two standard objective functions. Under such circumstances, Pareto analysis is of significant relevance as it highlights the trade-off among different conflicting objectives and fully inform the decision makers with the range of optimal solutions. The ANEC method is an efficient way of calculating a Pareto front. The AHP method has been used in order to take a decision by taking into account the priorities of the involved decision makers. The consistency of the decision making process must always be ensured. The chapter presented analytical tools to solve single-objective and multi-objective optimisation problems, which will be implemented in the case studies presented in the next chapter.

Chapter 6 Application of Multi-objective optimisation to electric vehicles in distribution networks

6.1 Introduction

In this chapter, a comprehensive multi-objective optimisation framework for controlling the charging/discharging process of EVs in distribution networks is proposed and tested. The modelling principles presented in Chapters 3 and 4 have been utilised to depict diverse households and EVs in a distribution network. The optimisation processes introduced in Chapter 5 have been implemented to manage EV charging in an efficient manner. This chapter is divided in two main Sections. In the first case study, a decentralised MOO framework is tested where individual EVs optimise their charging/discharging behaviour in order to attain certain objectives. As different stakeholders are involved in a distribution network, these charging schedule have consequences on the interests of all stakeholders. It is shown how the optimal solution for one stakeholder may not necessarily correspond to the preferred solution of other stakeholders, in fact some conflicts often arise. MOO and MCDM techniques are applied to solve these conflicts and it is shown how the involved stakeholders should share their benefits in order to reach a mutual consensus.

Secondly, a game-theoretical energy trading system is developed where different stakeholders/players engage in a local market in order to obtain the maximum benefits. As will be shown, all the players are price makers, hence the economic setup in the local market

depends on several factors, among which the availability of PV generation and network losses are the most important ones. It is shown how the decisions/strategies of the different players must reach an equilibrium. The conclusions then reflect upon the learnings and challenges encountered from the implementation of these two different, yet aligned frameworks.

6.2 Decentralised Multi-Objective optimisation

Nomenclature

Sets and indices

t	Current time step
Δt	Time interval, 15 min.
N^s	Total number of simulated time steps
N^a	Total number of steps from arrival to departure

Constants

η	Efficiency of the EV charger
$\overline{E^{EV}}$	EV Battery capacity (kWh)
$\underline{E^{EV}}$	Minimum EV battery capacity limit (kWh)
$\overline{f}$	Upper frequency limit of droop-controller (Hz)
$\underline{f}$	Lower frequency limit of the droop-controller (Hz)
$\overline{P^{EV}}$	Maximum charging/discharging rate of the EV charger (kW)

Parameters

π_t	Real-time price signal at time t (£/kWh)
P_t^d	Electricity demand at time t (kW)
P_t^{PV}	PV generation at time t (kW)
e_t^{kWh}	Specific CO_2 emission ($kgCO_2$/kWh)
C^B	Cost of the battery (£/kWh)
T^B	Temperature of the battery (°)
$\beta_{1\to8}$	Fitting parameters of the battery

	degradation model
reg^t	Regulation signal for FFR (kW)
f	Electrical frequency (Hz)
k^d	Droop coefficient (kW/Hz)
t^a	Arrival time of the EV
t^d	Departure time of the EV
A_t^{EV}	Availability of the EV at time t
$E^{EV,a}$	Energy of the EV upon arrival (kWh)
E^{trip}	Energy required for the next trip (kWh)
Functions	
$\mathbb{C}^e$	Energy cost of a H-MG (£/kWh)
$\mathbb{C}^d$	Battery degradation cost (£/kWh)
$\mathbb{P}^G$	Grid net exchange (kWh)
$\mathbb{E}^{CO2}$	CO_2 emissions of the H-MG ($kgCO_2$)
E_t^{EV}	Energy of the EV at time t (kWh)
E_t^L	Lifetime energy throughput under a certain charging condition (kWh)
n^{EOL}	Number of cycles before battery EOL
α^c	Battery degradation coefficient
Decision variables	
P_t^{EV+}, P_t^{EV-}	Charging/discharging of EV (kW)

The implementation of smart grids brings together several stakeholders at different scales. From the consumer-facing level to higher ones the relevant stakeholders are the EV owner, the end electricity user (also owning the PV system and the household electricity appliances), aggregators, distribution system operator (DSO), transmission system operator (TSO) and regulatory bodies - the latter enforcing environmental targets. Consequently, a variety of stakeholders, which otherwise would not collaborate, are brought together and each of them have their own aims/objectives. Some of these are equivalent while in some cases the objectives from the different stakeholders involved may be in conflict.

In this section, we propose a decentralised optimisation framework for day-ahead EV charging/discharging scheduling, where the information is gathered locally and processed by the individual agents that are in charge of the single home micro grids (H-MG). This choice is motivated by the onerous communication network, data privacy and safety issues entailed by a centralised approach [135]. Furthermore, the proposed approach facilitates the scalability of the optimisation algorithm with high EV penetration, where the computational burden is shared and not concentrated as in centralised management frameworks.

We define EV charging/discharging strategies and services, to benefit a variety of stakeholders including smart charging, V2X (vehicle to archetype), smart grid services, such as energy arbitrage and ancillary services (e.g. frequency response). The services that we consider ranging from the transmission level, to services behind the meter are ancillary services (involving the TSO), peak shaving, (involving the DSO), energy bill reduction and energy-autonomy maximisation, both involving the end-electricity user and the policy-maker (since increased energy autonomy achieves emission reduction).

As EV batteries are costly, utilizing them for the aforementioned services may cause additional battery wear. We safeguard the EV owner by minimizing battery degradation with the dynamic empirical model developed in Chapter 4. The aforementioned services are provided by considering transportation as the main purpose for EVs; therefore, this is taken as a constraint in the EV model. The proposed framework prioritises the inviolable EV travelling requirements, hence the charging scheduling are always compatible with the EV owner's need. From the end user to the DSO, the objectives modelled in this work are:

- Obj_1 is the energy cost of the dwelling, which is modelled based on a real-time price and taking into account the local PV generation.

- Obj_2 is the battery degradation incurred for EV charging/discharging for both transportation requirement and energy services (EVs are charged both for energy services and to have sufficient energy for transportation, whereas they are discharged for energy services. Discharge during driving has not been modelled as per Chapter 4.3).

- Obj_3 is the grid net exchange, which account for the interaction of the power absorbed/injected by the dwelling from/to the grid.
- Obj_4 is the CO_2 emission caused by absorbing energy from the grid.

Another critical stakeholder is the TSO, who procures ancillary services to ensure stable operation of the transmission network. As transmission and distribution networks are connected, the TSO is also considered here as a stakeholder. Therefore, ancillary service provision is modelled in the current work as an additional scenario, based on Section 6 in Chapter 3.

We then propose a multi-objective techno-economic-environmental optimisation (MOTEEO) framework and apply it to three case studies with two scenarios to provide the stakeholders with a comprehensive assessment of the prospective benefits. This framework has been presented in [P1]. Table 6.2-1 outlines the case studies and the scenarios simulated in the current Section.

Table 6.2-1 case study and scenarios for MOTEEO

	Scenario *i)* without ancillary service	**Scenario *ii)* with ancillary service**
Case study 1: home-micro-grid (H-MG)	Bidirectional home charging	Bidirectional home charging
Case study 2: distribution grid	a) Uncontrolled charging b) Smart charging c) Bidirectional home charging d) Bidirectional home and work charging	e) Bidirectional home charging
Case 3: utility function in home-micro-grid	Bidirectional home charging	

In the first case study, we highlight the conflicts among the objectives of the stakeholders (and ancillary service), and implement MOTEEO to a single dwelling with one EV. We evaluate two scenarios, aiming to show the additional benefits of ancillary service provision.

To quantify the benefits on a higher level, i.e. for the DSO, we then apply MOTEEO to an electricity distribution system with multiple dwellings and EVs. Smart charging and bidirectional charging strategies are applied in home and workplaces. In the case 2d, the EV can be charged at the workplace where we assume a PV system is present. Finally, we consider case study 3, where the utility function can be applied to combine the energy cost, battery degradation and peak demand in one objective to show the trade-off between these three objectives. We do this to highlight the importance of a joint-decision making process where benefits must be shared to satisfy all involved stakeholders.

The framework of MOTEEO for case study 1, a H-MG is presented in Figure 6.2-1. Different stakeholders have business relationships (dashed link) with various participants of a smart grid (i.e. the EV owner, EV-O, owns the EVs and pays the DSO, who is in charge of the distribution system for the use of the grid, the policy maker P-M enforces environmental targets etc.). It should be noted that the proposed framework is a general one, with a view to the future where car leasing and sharing will become mainstream; in that context, the EV-O will not be the householder, as is the case nowadays, but will still charge the EV at home. The components of the smart grid are modelled based on Chapter 3 and 4, and these models are integrated within MOTEEO. In particular, EVs communicate their charging requirements, arrival and next departure times; these set the constraint of the optimisation. Within MOTEEO, a range of services/objectives is modelled according the necessities of the involved stakeholders. The decision variables that optimize the objectives are the EV charging scheduling. MOO is applied to provide the full range of available solutions. The stakeholders then participate in MCDM and the EV charging/discharging scheduling are decided.

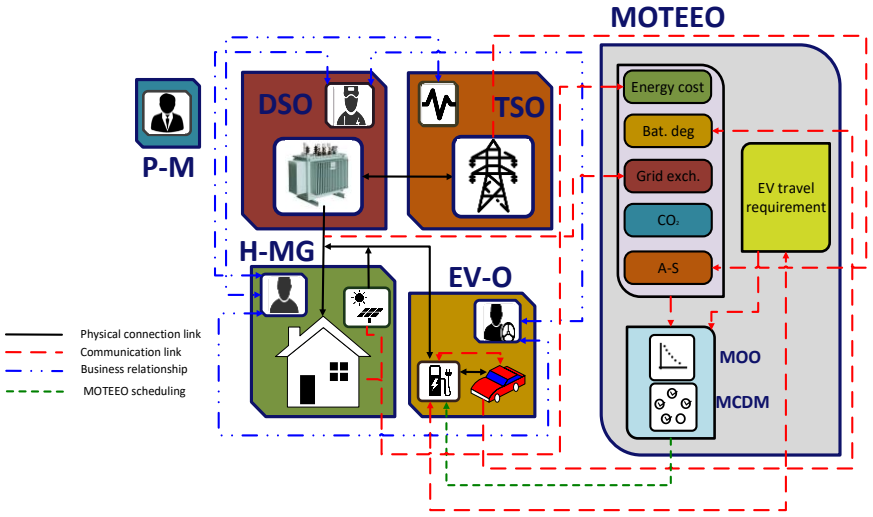

Figure 6.2-1 MOTEEO framework for single H-MG

The decentralised MOTEEO proposed in this research is then applied to multiple EVs and dwellings in a real distribution network as depicted in Figure 6.2-2. The business relationship links have not been depicted in favour of a clear illustration. Each EV applies MOTEEO, considering the objectives of the aforementioned stakeholders and the overall benefits are quantified. This case study is useful for the stakeholders at a higher level, i.e. DSO and policy maker, who can then quantify the prospective benefits at a higher scale than the single H-MG. These benefits are the reduction in the overall grid-peak demand and total CO_2 emissions. Finally, in case study 3, a utility function combining energy cost, battery degradation and grid net exchange is defined and optimised. This approach highlights the trade-off between the objectives and establishes the necessity of collaborative decision-making. It is worth pointing out that the proposed MOTEEO framework is a consensus-based approach where EV users authorise the use of their EV batteries for energy services for a specific period and within certain energy levels; the algorithm ensures that the energy required by the EV user for the next trip is made available at the next departure.

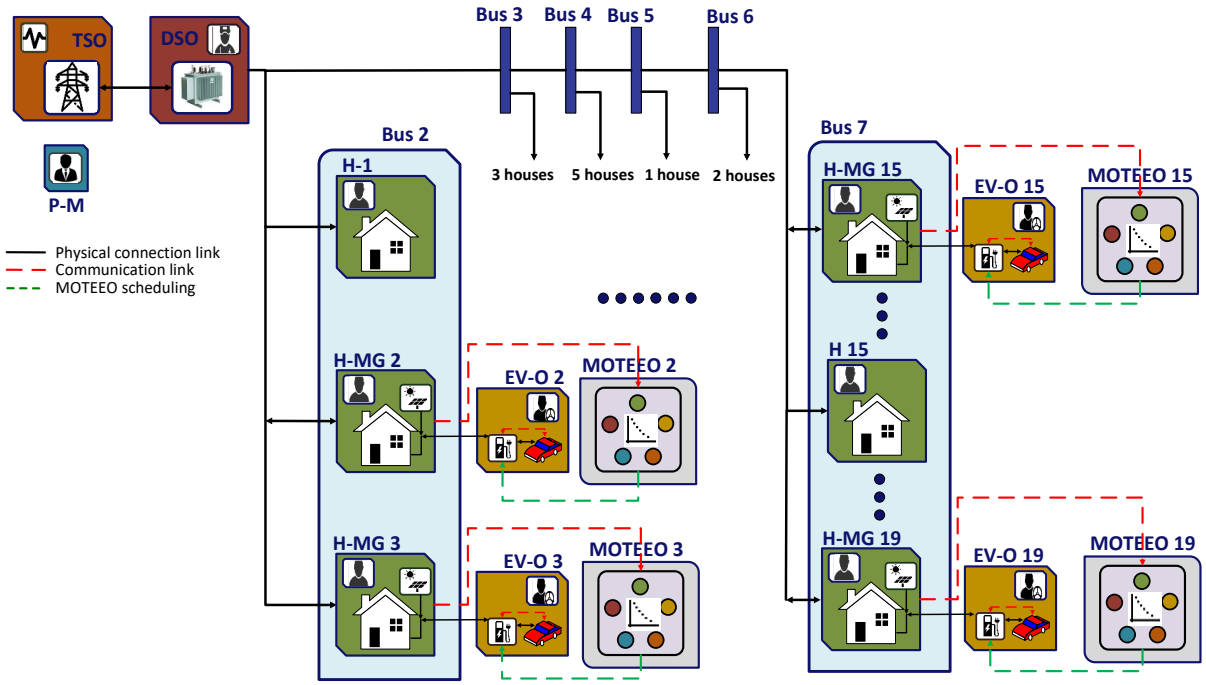

Figure 6.2-2 MOTEEO framework for a distribution network

6.2.1 Assumptions for the mathematical model

For the purpose of this research, a number of assumptions have been made while defining the mathematical mode. These apply to all the cases and scenarios.

- EVs have the same driving patterns as conventional internal combustion engine (ICE) vehicles.
- EV driving requirements are taken as constraints, and plug-in and plug-off times are approximated to the nearest quarter of an hour.
- The real-time electricity price provided to the consumer follows the same behaviour of the wholesale market price with distribution and transmission charges. This is not altered by EV charging.
- Upon arrival at home, the SOC of the EV battery, departure time for the next trip and the required energy (distance to drive) are known.

- The daily dwelling electricity demand and PV generation profiles are known. It is assumed that prediction techniques can provide such information to the deterministic optimisation performed in this study.
- The utility company or an aggregator is responsible for providing electricity supply to the final customers, and provides real-time pricing.
- An aggregator is responsible for the procurement of sufficient assets to meet the minimum requirement of EVs for frequency regulation. It is assumed that the aggregator is the DSO, so the revenue stream is directly passed from the DSO to the frequency regulation service providers.
- Under smart charging and bidirectional charging, EV chargers can regulate the output power continuously.
- Houses are symmetrically distributed across the three phases of a 400 V feeder, therefore we analyse one phase.
- All charging events follow a constant current profile (refer to Figure 4.2-5). Although real-life charging profiles also include constant-voltage charging (refer to chapter 4.2, in particular Figure 4.2-3 for more details), this simplification does not diminish the quality of the modelled results as during constant-voltage charging less energy is exchanged compared to constant-current charging.

The above assumptions are aligned with the current market structures and state of the art; in fact, short-term forecasting techniques achieve reasonable accuracy [136], hence demand profiles can be known day-ahead, although not at individual house level. Therefore, clusteting techniques, as implemented in section 3.3.2 can be used. There are examples of utility companies providing V2G services, where the EV user specifies the departure time and the required level of charge [137]. Companies with a portfolio of distributed energy providers are being developed with Nuvve being one of the major players [139]; they aggregate EV fleets to provide energy services and remunerate the EV owners. A DSO in the UK [140], is involved in major V2G projects with the aim of reducing grid reinforcement costs. This

highlights the interest of the system operators procuring V2G services by managing EV fleets.

6.2.2 Analytical formulation

The involved stakeholders pursue their objectives, which can be economic, technical/operational and environmental. Figure 6.2-3 presents the flowchart for the proposed MOTEEO framework. In the present work, three different case studies, representing different scales and operating conditions are implemented. The four objectives, and one scenario introduced earlier, are mathematically formulated from Sections 6.2.3 to 6.2.6. The EV energy constraints, travelling requirements and limitations of the charging equipment are modelled in Section 6.2.7. and the ANEC method is applied along with AHP to quantify multiple optimal EV charging scheduling.

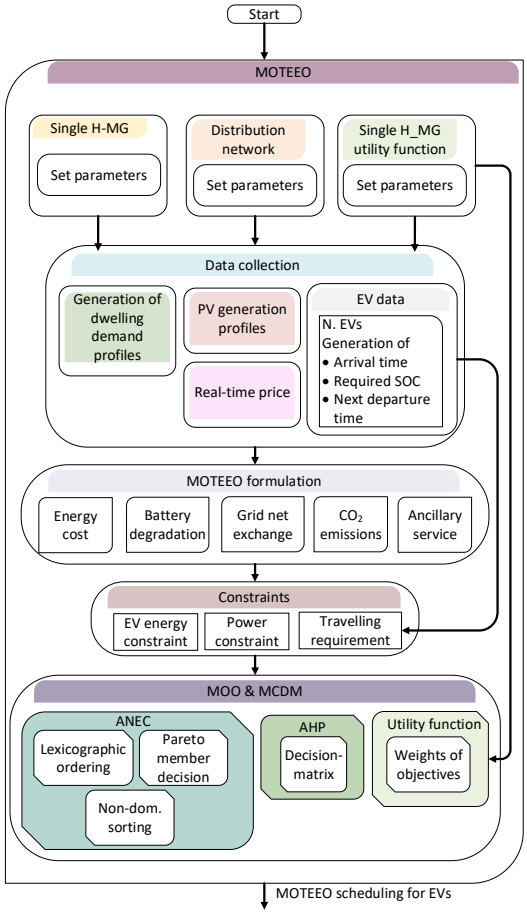

Figure 6.2-3 Flowchart of the proposed MOTEEO framework

6.2.3 Energy cost minimisation

From the point of view of the end electricity user, the operational cost of the archetype represents a fundamental objective that has to be minimised in order to receive a return from the assets. Investments in energy efficiency and RES are made with the main aim of minimizing operational costs. For this study, a function representing the energy cost of the H-MG, $\mathbb{C}^e$, is expressed by the following equation:

$$\underset{P_t^{EV+},P_t^{EV-}}{argmin}\ \mathbb{C}^e = \sum_{t=1}^{N^s}\left[\left(P_t^d - P_t^{PV} + P_t^{EV+} - P_t^{EV-}\right)\Delta t\ \pi_t\right] \tag{6.1}$$

where π_t is the price signal, P_t^d is the electricity demand at time t, P_t^{PV} is the PV generation at time t, P_t^{EV+} is the power charged to the EV at time t and P_t^{EV-} is the power discharged from the EV at time t. Δt takes into account the energy exchanged in the time-step and T^s is the total number of time steps considered in the scheduling. Here the decision variables are P_t^{EV+} and P_t^{EV-}: by iteratively manipulating their values, a minimum of the cost function for each time step can be reached.

6.2.4 Battery degradation minimisation

Battery degradation in EV batteries has been modelled in Chapter 4. The developed model presented in (4.21) to (4.28), are used here as an objective in the ANEC method.

6.2.5 Grid net exchange minimisation

Storage solutions can minimize the time mismatch between RES generation and electricity demand, by charging in periods of RES excess and discharging in periods of high demand. In this way, the net power exchange profile with the grid is flattened which allows an optimised generation dispatch and stable grid operation. It is therefore in the DSOs' interest to allow energy storage implementation, both stationary and mobile (EV). The aim of the optimisation is to minimize the variation of the net power exchange with the grid. This is because both excessive electricity demand (represented as positive power) and generation (represented as

negative power) lead to currents (hence losses) and voltage deviation (from 1 pu), which are adverse for the reliable operation of the grid. If any variation from nil power exchange can be minimised, losses and voltage deviations will also be minimised. The objective function representing the grid net exchange $\mathbb{P}^G$, can be described as follows:

$$\underset{P_t^{EV+},P_t^{EV-}}{argmin}\ \mathbb{P}^G = \sqrt{\sum_{t=1}^{N^s}\left(P_t^d - P_t^{PV} + P_t^{EV+} - P_t^{EV-}\right)^2} \tag{6.2}$$

where P_t^d, P_t^{PV}, P_t^{EV+} and P_t^{EV-} assume the same meaning as in Equation 1. This objective function is calculated as the variation of the net power exchanged with the grid. In fact, both positive and negative net powers are penalised and the root-square use used to have the same units as the powers (not kW^2).

6.2.6 CO_2 emission minimisation

EVs are seen as a major solution to reduce global CO_2 emissions from the transportation sector. However, the environmental benefits of EVs depend on the carbon intensity of the national/local energy mix. This is because the energy mix that is used to charge the storage, and hence the CO_2 emitted for energy provision, changes during the day, week and season. Therefore, there are periods of low specific $kgCO_2/kWh$ (off-peak), as opposed to periods with high specific $kgCO_2/kWh$ (peak). In this work, the emissions avoided by ICE substitution are not considered, because these cannot be controlled with intelligent charging strategies, which are the scope of this research.

Therefore, the objective function that aims to maximise environmental benefits can be defined as follows:

$$\underset{P_t^{EV+},P_t^{EV-}}{argmin}\ \mathbb{E}^{CO2} = \sum_{t=1}^{N^s}\left[\frac{\left(P_t^d - P_t^{PV} + P_t^{EV+} - P_t^{EV-}\right) + \left(\sqrt{\left(P_t^d - P_t^{PV} + P_t^{EV+} - P_t^{EV-}\right)^2}\right)}{2}\,\Delta t\; e_t^{kWh}\right] \tag{6.3}$$

where e_t^{kWh} is the time series of the average specific CO_2 emission for each kWh absorbed from the grid, as proposed in Chapter 3.5. Equation 6.3 considers only the CO_2 emissions

caused by electricity consumption (consumed power is deemed positive) and does not account for CO_2 emissions saved by the power injected in the grid (supplied power is deemed negative). This is because the user does not have control on the power once this is injected in the grid, which could also be curtailed. To explain the formulation of equation 6.3, let us consider the generic set of mathematical functions depicted in Figure 6.2-4. The function $f(t)$ (point marker in the figure) is the sine function, which has both positive and negative values in its domain. The function $\sqrt{f(t)^2}$ (o marker in the figure) takes the absolute value of $f(t)$. By adding these two functions and halving the total (x marker in the figure), only positive values of $f(t)$ are kept. Therefore, equation 6.3 considers only positive values of $\left(P_t^d - P_t^{PV} + P_t^{EV+} - P_t^{EV-}\right)$ which is the net power exchange with the grid.

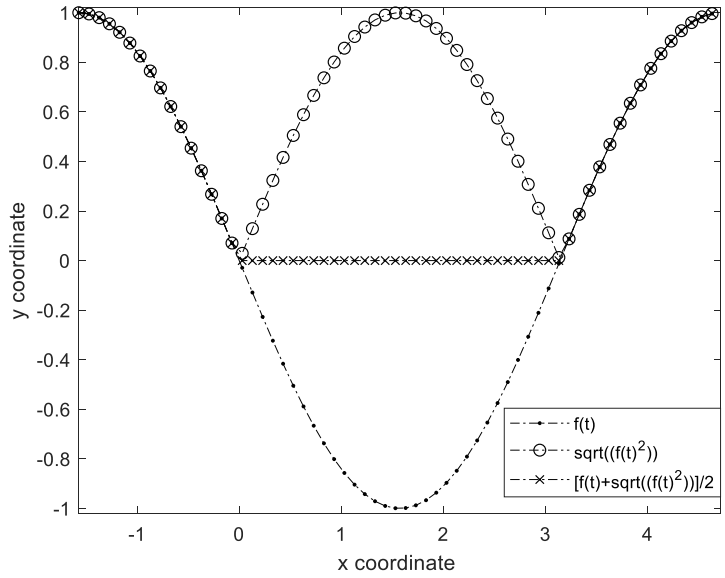

Figure 6.2-4 Generic mathematical functions

At present, these CO_2 saving mechanisms are not adopted in the electricity industry, but with the increasing concern on greenhouse gas emissions, this method represents a suitable approach for the future.

6.2.7 Constraints of the optimisation – EV model

The constraints for the various objectives presented so far that define the boundaries of the feasible region are presented. These are defined based on technical restrictions, usage behaviour as well as practical approach. The aim of the optimisation is to define power exchange profiles of EVs for different objectives, subject to constraints. The following set of equations link the power exchange of an EV with the energy stored:

$$E_t^{EV} = E^{EV,a} \qquad if\ t = t^a \tag{6.4}$$

$$E_t^{EV} = E_{t-1}^{EV} \qquad \text{if } A_t^{EV} = 0 \tag{6.5}$$

$$E_t^{EV} = E_{t-1}^{EV} - E^{trip} \qquad if\ t = t^d + 1 \tag{6.6}$$

$$E_t^{EV} = E_{t-1}^{EV} + \left(\eta\, P_t^{EV+} - \frac{P_t^{EV-}}{\eta}\right) \Delta t \qquad if\ A_t^{EV} = 1 \tag{6.7}$$

In (6.4), upon arrival of the EV, the energy stored in the battery is measured. In (6.5), if the EV is not available ($A_t^{EV} \in [0,1]_{\mathbb{N}}$ is a Boolean variable indicating the availability of the EV), then charging events cannot be initiated; hence, the energy state of the EV is unaltered. (6.6) takes into consideration the transportation constraint; in fact, at the departure time, the energy required for the next trip is deducted from the available capacity. If the EV is available, then in (6.7) the energy stored is modified by adding the energy charged and deducting the energy discharged by taking into consideration the efficiency of the EV charger η.

The physical constraints in terms of storage size and power ratings as well as EV travelling requirement are presented in the set of equations below

$$0 \le P_t^{EV+}, P_t^{EV-} \le \overline{P^{EV}} \qquad \forall t \tag{6.8}$$

$$\underline{E^{EV}} \le E_t^{EV} \le \overline{E^{EV}} \qquad \forall t \tag{6.9}$$

$$E_t^{EV} \ge E^{trip} + \underline{E^{EV}} \qquad if\ t = t_{dep,n} \tag{6.10}$$

$$P_t^{EV+} \times P_t^{EV-} = 0 \qquad \forall t \tag{6.11}$$

(6.8) and (6.9) are used to limit the power exchanged by the EV and the energy stored within the respective bounds. Here, a minimum limit of EV capacity of $\underline{E^{EV}} = 0.2\,\overline{E^{EV}}$ has been set provide for unforeseen journeys. (6.10) is used to ensure that the energy stored in the EV meets the need of the user for the next trip. Finally, Equation 6.11 ensure that charging and discharging do not happen at the same time.

6.2.8 Results and discussion

The proposed MOTEEO framework is initially applied at a household level to demonstrate the effectiveness of proposed method to model and maximize the interests of the five stakeholders. Subsequently, the strategy is applied to a typical distribution network with realistic penetration level of PV systems and EVs. Three EV charging strategies are adopted: uncontrolled, smart and bidirectional charging. The three decision makers (DMs) who are involved in the decision-making process are the end electricity user, the EV owner and the DSO. Finally, an alternative utility function based MOTEEO is applied for a single-household to show the importance of collaborative decisions where benefits are shared.

Case study setting

As introduced in Figure 6.2-1, a single-dwelling comprising of a 4 kW PV installation and a 30 kWh EV is considered for case study 1 and 3 and the associated parameters are detailed in Table 6.2-2.

Table 6.2-2 Setting for the case study 1

Parameters	
Electricity demand	Detached single-house, single-phase
RES type	Roof-top photovoltaic
RES system rating	4kW
$\boldsymbol{C^B}$	150 £/kWh
EV charger type	Type 2 conventional/Smart/Bidirectional/ single-phase
$\overline{\boldsymbol{P^{EV}}}$	3kW
$\boldsymbol{\eta}$	90 (90) %

Δt	15 min
Pricing strategy	Real-time pricing
Optimisation strategy	Day-ahead
T^B	18 C
t^a	17:00
t^d	10:00
$\overline{E^{EV}}$	30 kWh

The optimisation is performed one day-ahead, with a real-time price derived from the wholesale spot price by adding network charges and taxes [141]. The chosen demand, PV generation and price profiles are those of a typical winter day. From the modelling implemented in Section 3.5, two scenarios, with and without ancillary service provision, are simulated. Figure 6.2-5 depicts the evolution of the real-time price, and EV availability for case study 1optimisation. It can be demonstrated that when PV generation is available, minimizing grid net exchange corresponds to minimize CO_2 emissions. A practical demonstration is provided in the appendix, A.4. Consequently, we minimize Objective 1 – Energy cost, Objective 2 – EV battery degradation and Objective 3 – Grid net exchange. The mathematical optimisation process for case study 1 is hereby detailed.

A) $\zeta_{m\times m}^{lex} = lex\min_{x, f^k} F^m$ k = 1, 2, 3 and m=3, where f^k has the highest priority.

B) We define:

$\Psi_i = \max(\zeta_i^{lex})$ Nadir point and $\psi_i = \min(\zeta_i^{lex})$ for i = 1, 2, 3. Where ζ_i^{lex} are the results for objective i from the Lexicographic ordering.

C) **for** $o = 1, \dots, n^{max} + 1$ and $p = 1, \dots, n^{max} + 1$ We minimise:

D) $$\underset{P_t^{EV+}, P_t^{EV-}, s_2, s_3}{argmin} \quad \mathbb{C}^e = \sum_{t=1}^{N^s}\left[\left(P_t^d - P_t^{PV} + P_t^{EV+} - P_t^{EV-}\right)\Delta t\, \pi_t\right] - \gamma\,(s_2 + s_3)$$

E) Subject to (12) to (19) and

F) $\mathbb{C}^d = \varepsilon_2 + s_2$

G) $\mathbb{P}^G = \varepsilon_3 + s_3$

where

H) $\varepsilon_2 = o \times \frac{\Psi_2 - \psi_2}{n^{max}}$, $\varepsilon_3 = p \times \frac{\Psi_3 - \psi_3}{n^{max}}$ with $n^{max} = 6$, s_2 and s_3 are slack variables

and γ is an arbitrary constant

I) If FFR is provided, $A_t^{EV} = 0$ from 23 to 7.

J) **end for**

For case study 2, we apply the setting for case study 1 to all the EVs involved, in compliance with the associated electricity demand profiles (different for each house), PV generation and EV transportation requirements (generated randomly from National Time use Survey data).

For case study 3, we adopt the same setting outlined in Table 6.2-2 but with the implementation of a utility function; we present hereby the mathematical process.

A) $\underset{P_t^{EV+}, P_t^{EV-}}{argmin}\ \lambda_1 \mathbb{C}^e + \lambda_2 \mathbb{C}^d + \lambda_3\ \mathbb{P}^G$

B) Subject to (12) to (19)

Where $\lambda_1 = 1$, $\lambda_2 = C^B = 150$ and λ_3 depends on the grid utilisation fee set by the DSO

All the simulations have been carried out on a computer with an Intel Core i7-6500U CPU 2.5GHz processor and 16GB RAM. Time resolution for the optimisation in all case studies is 15 min. Sequential quadratic programming algorithm in Matlab 2017a has been employed for the non-linear optimizations.

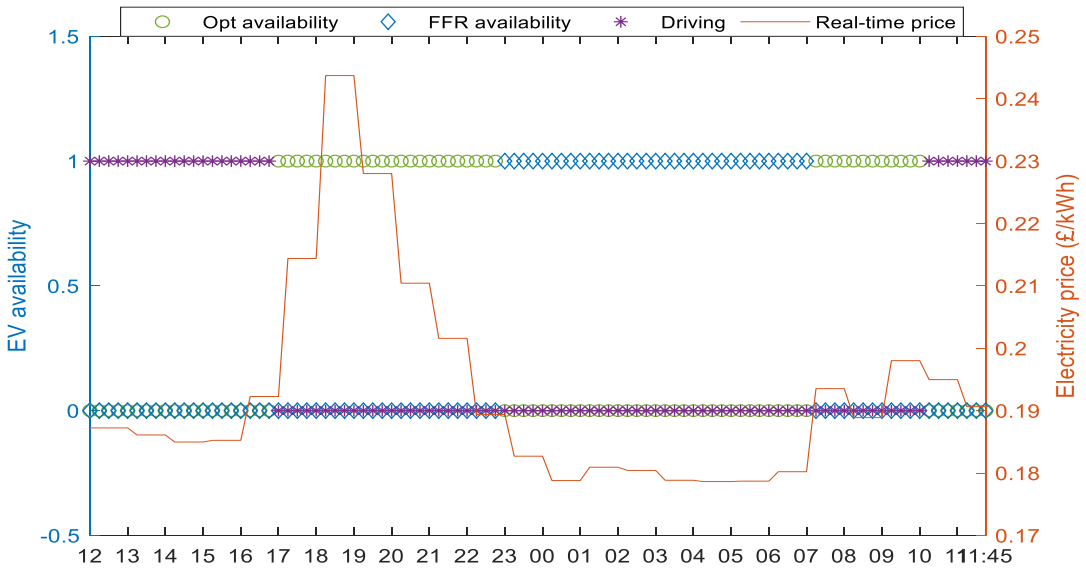

Figure 6.2-5 EV availability and real-time price

As depicted in Figure 6.2-2, a typical UK distribution network (DN) [142], comprising a 400V feeder, which provides electricity to 57 houses, is considered for case study 2. One phase of the 400V feeder is simulated assuming balanced three-phase load distribution therefore, 19 houses are individually simulated.

To quantify the unbalance in a three-phase distribution system, the three phases should be individually simulated and the conclusions, which are rather network and location dependent, should be evaluated on a case-by-case basis.

Eight days from four seasons, considering weekday and weekend, have been investigated. Different PV generation profiles, depicting the seasonal variations and different EV availability patterns have been considered in line with [61], and these are shown in appendix A.4. For case study 2, all the electricity demand profiles have been generated from the Centre for renewable energy systems technology (CREST) model [86].

The configuration of the typical DN is based on the PV and EV penetrations levels predicted for 2040 [15]. This year represents a crucial landmark because of the ban of ICE vehicles announced by the UK government [29]. By considering the current penetration of domestic PV systems [143], [144] and using the prediction of the UK National Grid Future energy scenario [15], a penetration rate of 50% is projected. This implies that in one phase of the LV feeder, 10 houses will be equipped with a PV system. Since the UK average PV system size is 3.35 kW, a normal distribution around a mean value of 3 kW is assumed; PV installation sizes will be randomly sampled from this distribution. An EV penetration rate of 50% is expected for 2040 [15], among those that have access to at least one car [79] hence, 10 EVs are simulated.

Table 6.2-3 lists the parameters adopted to produce the EV transportation model and other key assumptions for case study 2.

Table 6.2-3 Parameters of the case study 2

Parameter	Value
EV and PV penetration rate	50% [15], [143]
Average daily mileage	9 miles, [79]
Average daily energy consumption	1.74 kWh [79]
Arrival and departure times for trips randomly selected from National Time use Survey data	
Average PV size	3.35 kWp, [143]
$\overline{E^{EV}}$/ $\overline{P^{EV}}$	30 kWh/3 kW
EV charger type	Type 2 conventional/Smart/Bidirectional/ single-phase
Frequency regulation prices	From UK National Grid post-tender reports

Results of case study 1 for single H-MG

To demonstrate the effectiveness of MOTEEO, highlighting the conflict of the different objectives, we apply the proposed methodology to a single dwelling with one EV.

Single objective optimisation algorithm

With reference to the cost signal in Figure 6.2-5, it can be seen that under objective 1 the EV is charged at the minimum price available. Furthermore, the transportation constraints are

satisfied, as the EV is charged before the next departure (at 10 the vehicle departs and for instance under battery degradation minimisation, represented by the green stems in Figure 6.2-5, the vehicle is charged until then). It should be noted that one stem represents a constant power for the next 15 minutes, i.e. one stem at 9:45 represents a charge/discharge at constant power from 9:45:01 until 9:59:59.

Figure 6.2-6 shows EV charging scheduling for objectives 1, 2 and 3, scheduled separately, without FFR provision.

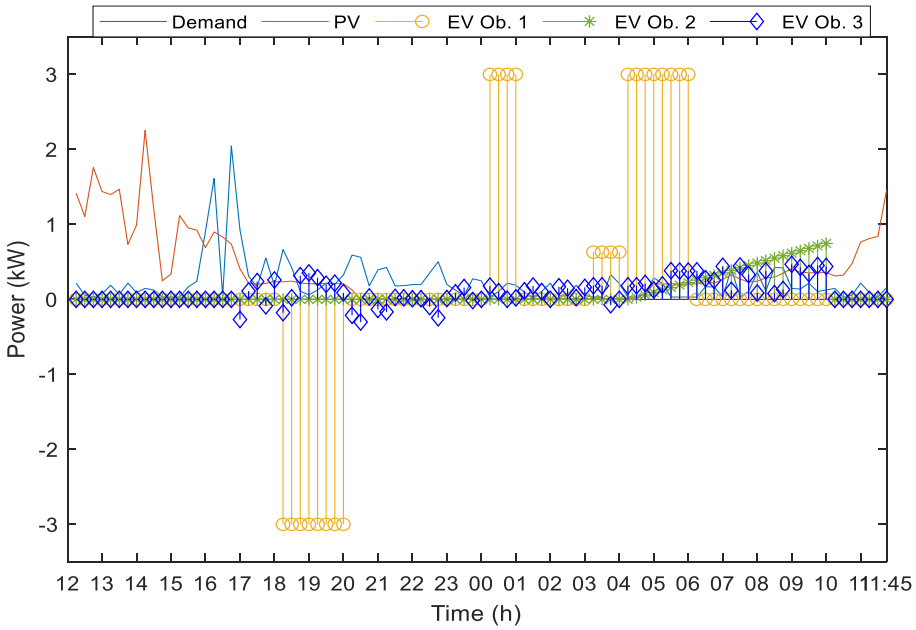

Figure 6.2-6 EV scheduling for single-objective optimisations without FFR

When the EV is charged to minimize battery degradation under Objective 2, the charging happens only close to the next departure to minimize average SOC. In addition, the charging rate is gradually increased to minimize degradation. This is because from (4.22), the combination of high charging rate and high average SOC causes high degradation; charging the battery at a lower constant charging rate would have increased charging duration leading to a higher average SOC and therefore degradation. At the same time, the full charging rate (3 kW) is not employed, as it would increase degradation; an optimum solution, which underlines a balance between the charging rate and the average SOC [their product is considered in (4.22)], is found. Under objective 3 EV is used to minimize the grid net

exchange. As during the PV excess hours the EV is mostly absent, PV energy autonomy is not fully maximised. However, upon arrival, the EV exploits as much PV energy as possible and the peaks of electricity demands are also provided by discharging the EV. Here, the conflict between the different objectives are unveiled. In fact, the EV is charged with radically different scheduling under the three objectives and the scheduling according to one objective inevitably worsen the performance along the others.

Figure 6.2-7 depicts EV charging scheduling for objectives 1, 2 and 3 with FFR provision. It should be noted that the EV does not initiate any charging event from midnight to 7:00 hrs and from 23:00 hrs to midnight, in accordance with FFR commitment.

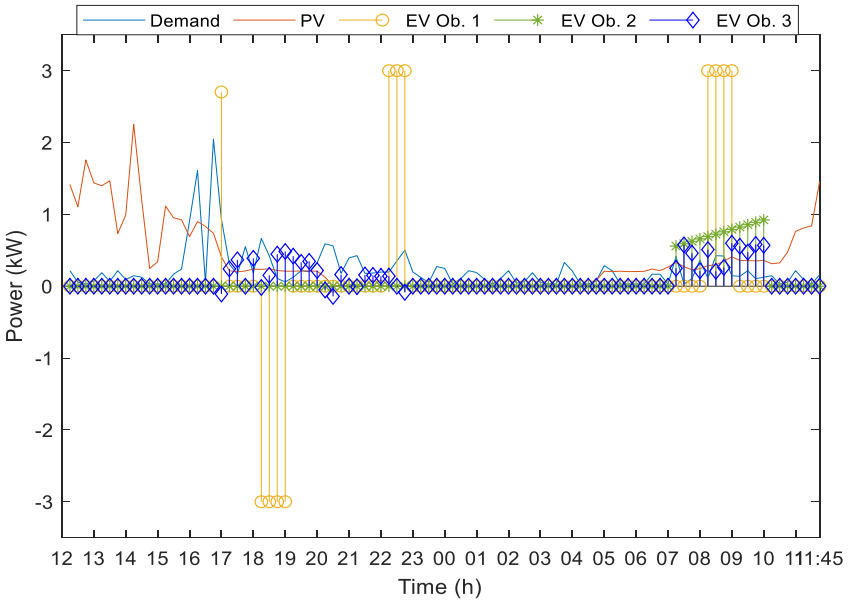

Figure 6.2-7 EV scheduling for single-objective optimisation with FFR

As shown in Figure 6.2-7, under objective 1, the EV charging happens right before the FFR window starts (from Figure 6.2-5 between 22-23, which along with 17-17:15 provides the lowest prices in the available window). As for objective 2, since the availability window is reduced, the EV cannor be charged from 3 to 9:45 with an increasing charging rate as from 23:00 to 7:00 is providing FFR. Consequently, the EV is charged from 7:00 to 9:45 at a higher rate (to meet the energy requirement), which leads to higher degradation. Under all objectives, the EV is charged before the FFR window, which keeps the EV at a higher SOC,

leading to a higher battery degradation compared to scenario i). In addition, the performance under objective 3 is worse as there is less availability of the EV to service/meet the electricity demand. Table 6.2-4 presents the results of the three single optimizations with and without FFR provision.

Table 6.2-4 Results of the single-objective optimisations

	Scenario *i)* (without FFR provision)			
	Energy cost (£)	Battery degradation (£)	Grid net exchange (kWh)	Emissions ($kgCO_2$)
min Obj_1	-0.2360	-0.0768	27.0978	4.5169
min Obj_2	-0.3971	-0.0247	13.2361	2.5341
min Obj_3	-0.4089	-0.0265	13.0176	2.4577
	Scenario *ii)* (with FFR provision)			
	Energy cost (£)	Battery degradation (£)	Grid net exchange (kWh)	Emissions ($kgCO_2$)
min Obj_1	0.2667	0.1422	20.1150	3.7907
min Obj_2	0.2275	0.1149	13.7651	2.6395
min Obj_3	0.1513	0.1172	13.5437	2.7107

Throughout this section, costs have been designated with negative sign while revenues assume positive sign. When FFR is provided, the energy cost is further reduced by the FFR profits (£0.637) and battery degradation increased (£0.0902), resulting in an overall profitable service. As for the fourth objective, the limitation of the available optimisation window due to FFR provision increases the CO_2 emissions slightly. Once the conflict between the objectives have been highlighted MOO and MCDM techniques are applied to find the optimal solutions for all the three objectives.

MOTEEO optimisation algorithm

Figure 6.2-8 and Figure 6.2-9 depict the Pareto fronts obtained from the ANEC method for scenarios i) and ii). The performance along the three objectives have been normalised to their maximum values expressed in Table 6.2-4 to allow comparative analysis. n^{max}, the number of divisions, was set to 6, which leads to a maximum of 49 Pareto efficient solutions. However, as discussed in Chapter 5.3, due to the conflict among objectives, a number of

computations were infeasible, and this led to 42 and 35 Pareto efficient solutions for scenarios i) and ii), respectively. Some of the solutions overlap at certain points; this could be avoided by dividing the solutions space with a higher resolution; however, this would increase the computational cost [defined as $O((n^{max}+1)^2]$. In this study, a rightful combination of both enough granularity of the Pareto front to informatively take decisions and computational cost has been achieved.

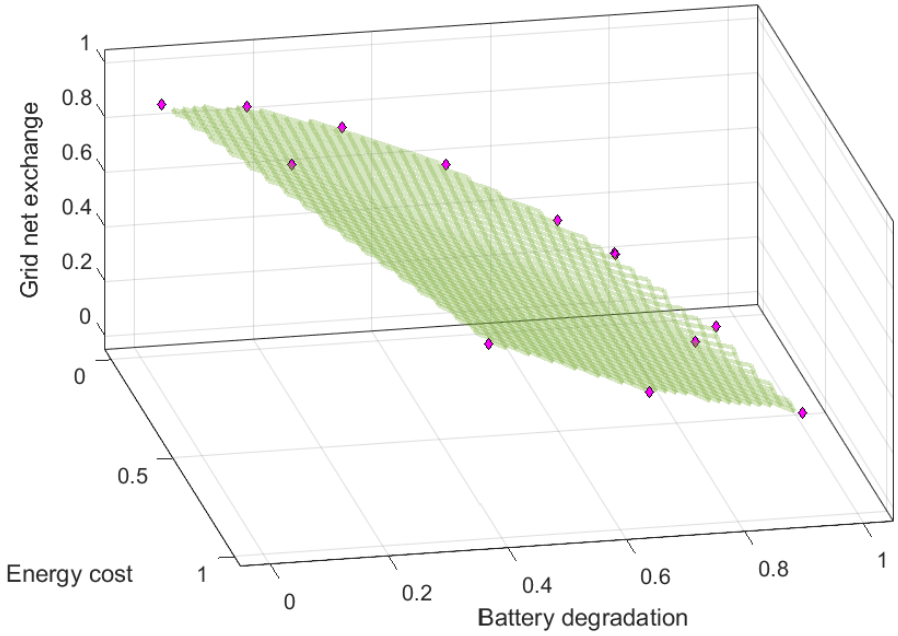

Figure 6.2-8 Pareto front with ANEC without FFR

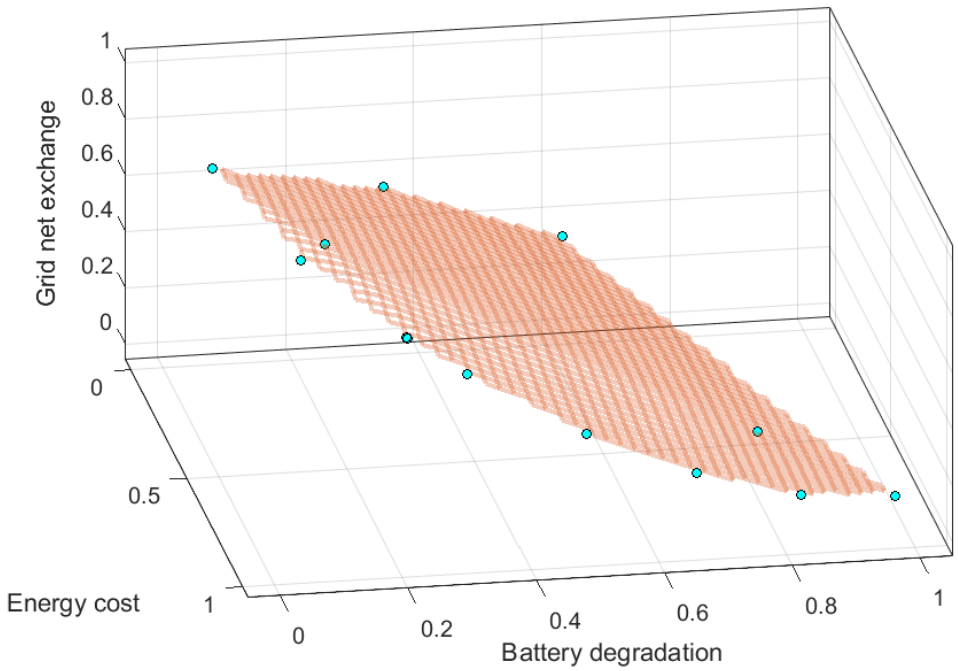

Figure 6.2-9 Pareto front with ANEC method with FFR

It could be observed in Figure 6.2-9 that in one part of the solutions space, minimising grid net exchange also leads to battery degradation minimisation. This is because when FFR is provided, in order to minimise energy cost, the algorithm schedules EV charging at 3kW during the minimum price period available (see Figure 6.2-7), which increases both battery degradation and grid net exchange (see Table 6.2-4). When battery degradation is forced to be reduced by the ε-constraint, the charging scheduling tends to the behaviour of EV Ob. 2 (green stems in Figure 6.2-6) which is closer to the behaviour of EV Ob. 3 (blue stems Figure 6.2-6), therefore reducing grid net exchange. However, when grid net exchange is forced to be reduced towards its minimum value, battery degradation is increased – this happens because in order to minimise grid net exchange, the EV must be charged when there is excessive PV generation and it has to be discharged when there is excessive electricity demand, both leading to battery degradation as the battery is cycled. AHP is applied to choose the optimal solutions among the Pareto members provided by the MOO, according to the different prioritisation of the stakeholders. Three stakeholders/decision makers (DM)

holding different priorities are considered. The decision matrix (following from Chapter 5.3.1) for the three DMs is shown in Table 6.2-5.

Table 6.2-5 Decision matrix for different DMs

	DM_1	DM_2	DM_3
Energy cost	0.7606	0.1577	0.0817
Battery degradation	0.1577	0.7606	0.1577
Grid net exchange	0.0817	0.0817	0.7606

DM_1 is the end-electricity user who wants to minimize the energy cost. DM_2 Is the EV owner who wants optimize the exploitation of the EV battery and DM_3 is represented by the DSO or the policy maker who wants to optimize grid utilisation and minimize CO_2 emissions. The consistency ratio found for the three pairwise decision matrices, related to the three DMs, is lower than 0.1 which verifies the consistency of the decisions. It should be pointed out that multi-objective optimisation applied to EV charging scheduling has only recently gained interest in t he research community. Hence, there is a lack of studies addressing the prioritisation adopted by the different stake-holders, especially the EV user, for the different objectives. Thus, the priorities have been set based on suitable prioritisation rules and could be verified by surveying a heterogeneous sample of potential stakeholders.

The results from the decision making process are shown in Table 6.2-6. It can be seen that MOO with MCDM finds the overall best option while still favouring the DM's choice. This is because once the full Pareto set is available, there is more freedom on choosing the option that achieve the best performance along the objectives while complying with the inherent prioritisation of the stakeholder.

Table 6.2-6 Results of the MOTEEO method with the application of AHP

	Scenario *i)* (without FFR provision)			
	Energy cost (£)	Battery degradation (£)	Grid net exchange (kWh)	Emissions ($kgCO_2$)
DM_1	-0.2360	-0.0768	27.0978	4.5169
DM_2	-0.3512	-0.0259	13.1984	2.3859
DM_3	-0.4015	-0.0262	13.0123	2.4458

	Scenario *ii)* (with FFR provision)			
	Energy cost (£)	Battery degradation (£)	Grid net exchange (kWh)	Emissions ($kgCO_2$)
DM_1	0.2475	0.1173	13.9531	2.6680
DM_2	0.2282	0.1149	13.7651	2.6395
DM_3	0.1548	0.1171	13.5437	2.7107

From the results, it can be seen that the stakeholders would choose the solution that naturally fits with their priorities, sacrificing the performance along other objectives. Comparing Table 6.2-6 with Table 6.2-4, some differences can be noticed. When providing FFR, DM_3 chose a solution that caused lower battery degradation and higher return for the end-user than with the single-objective optimisation. These differences compared to the single objective optimisation are due to fact that with MOTEEO the full Pareto front is considered when making the decision. In accordance with the weights presented in Table 6.2-5, the adopted solutions lead to higher overall benefits than the single objective optimisations. Consistent with the previous results, cost minimisation with FFR provision is particularly adverse for the battery as the combination of Vehicle-to-home (V2H), which implies that energy is echanged only between the EV and the household electricity network, and V2G leads to a higher utilisation. As previously mentioned a lower energy cost leads inevitably to a higher grid impact and vice versa, because the price signal is not dynamically updated by to grid operator to better reflect the grid status. In addition, under the optimal grid net exchange, CO_2 emissions are minimum. This effect will be particularly noticeable when the proposed methodology is applied to a real-life distribution system.

Results of case study 2 for a distribution network

MOTEEO optimisation algorithm

The application of MOTEEO for a typical UK DN allows the quantification grid peak power and overall CO_2 emissions at a higher scale compared to the single dwelling. Eight days have been simulated for the four seasons, including weekday and weekend. Four charging strategies, including uncontrolled charging (a), smart charging (b), bidirectional at home (c)

and work (d) are simulated with two scenarios related to the ancillary service provision. Under uncontrolled charging, upon arrival the EV is fully charged at the maximum power. Under smart charging, the EV charging is controlled but the EV is not discharged; hence, under this strategy FFR was not provided, as discussed at the end of chapter 3.6. Bidirectional charging enables EV discharging towards the H-MG or the grid. Figure 6.2-10 and Figure 6.2-11 depict the MOTEEO scheduling for scenario 2c) in the eight days. The preferred solution for the three decision makers, end-energy user, EV owner and DSO are shown. Other scenarios are not illustrated here for conciseness.

As can be seen in Figure 6.2-10 and Figure 6.2-11, diverse PV generation, due to seasonal effect, and EV availability, due to different travelling patterns on weekdays and weekends, have been simulated. As a general trend, EVs had higher availability for MOTEEO in the weekends. Higher availability and PV generation particularly benefitted grid net exchange minimisation under DM_3, as can be seen in spring and summer weekends. Under DM_2, to minimise battery degradation, the EVs are charged as close as possible to the respective departure times (it can be seen in Figure A.4- 6 and Figure A.4- 7, that EVs start leaving from 07:00), while under DM_1 price arbitrage is carried out.

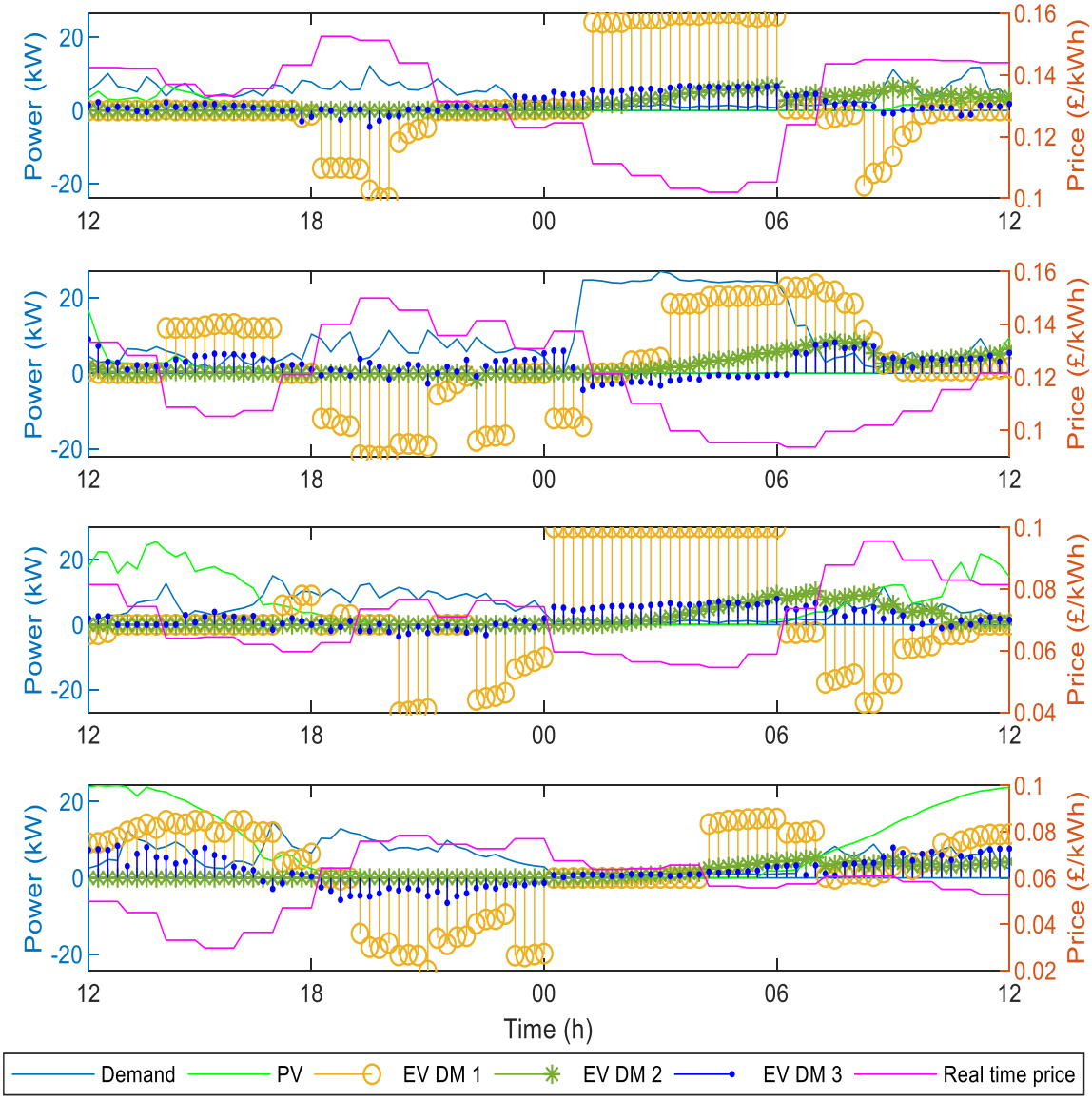

Figure 6.2-10 MOTEEO scheduling for scenario 2c) winter (weekday and weekend) and spring (weekday and weekend) from top to bottom

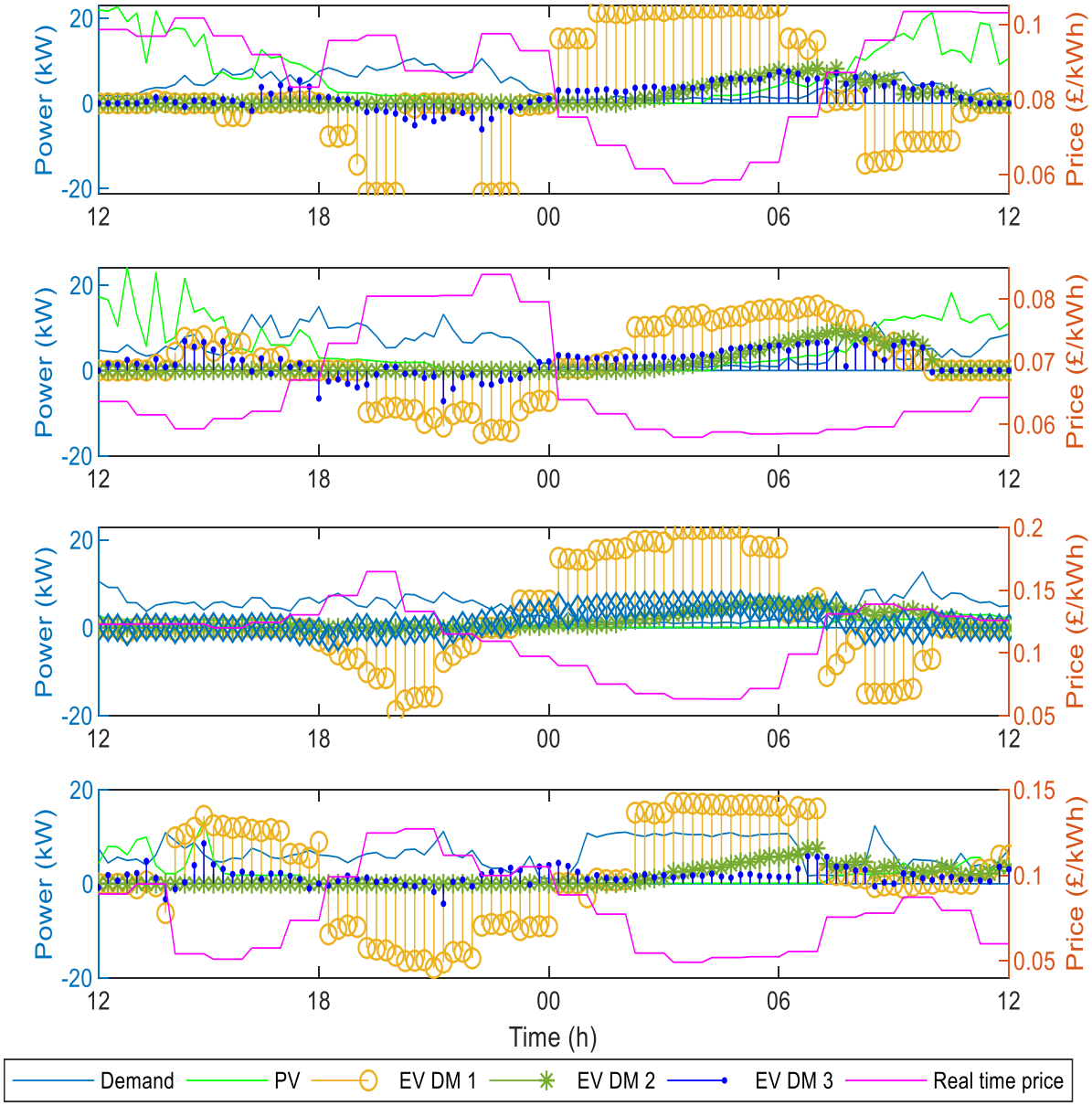

Figure 6.2-11 MOTEEO scheduling for scenario 2c) summer (weekday and weekend) and autumn (weekday and weekend) from top to bottom

Table 6.2-7 presents the results for case study 2. For all the scenarios, the MOTEEO framework calculated the Pareto fronts and the DMs chose the preferred solution based on the

MCDM criteria outlined in Chapter 5.3.2. The Pareto fronts for one day (summer weekend) are presented in the appendix A4, Decentralised MOO results.

Table 6.2-7 Results of the MOTEEO method for eight days

Case	DM	Energy cost (£)	Battery degradation (£)	Grid net exchange (kWh)	Emissions ($kgCO_2$)
Uncontrolled charging		-105.74	-28.55	1917	489.88
Smart charging	DM_1	-66.15	-9.97	178	334.48
	DM_2	-72.08	-9.42	176.74	333.96
	DM_3	-72.5	-10.2	170.53	322.30
Bidirectional charging at home – no FFR	DM_1	-52.79	-50.01	299	481.91
	DM_2	-71.40	-9.52	176.72	333.69
	DM_3	-72.80	-20.39	174.07	322.65
Bidirectional charging – home and work	DM_1	-52.73	-51.06	291.19	486.77
	DM_2	-71.26	-9.48	176.72	333.82
	DM_3	-72.57	-10.26	173.90	322.87
Bidirectional charging at home – with FFR	DM_1	-12.38	-26.74	276.1	392.50
	DM_2	-20.83	-13.59	176.32	342.03
	DM_3	-22.18	-17.5	171.26	334

Under uncontrolled charging, the EVs are charged at maximum power until 80% of SOC is reached. This produces the highest values for all the metrics in Table 6.2-7, indicating that it is the worst scenario under all the criteria. The three rows for each case shows the results of the solution chosen by the three DMs, namely, end-electricity user, EV owner and DSO (DM_1, DM_2 and DM_3 respectively). With smart charging the battery degradation is kept to a minimum and there is little difference between the three DMs along this dimension.

When bidirectional charging is employed, the improvements are higher; especially the energy cost can be further minimised as price arbitrage is performed. It should be pointed out that the performance along grid utilisation depends on the availability of PV generation (in colder

months the performance is worse than the warmer months) and EV availability pattern; the EVs may not be available or at high SOC, therefore it would be unable to charge from PV. The different interests of the stakeholders are again evident: with bidirectional charging at home without FFR, under the solution preferred by the DSO (DM_3), the total utilisation is reduced from 291.19 kWh to 173.9 kWh (-40.28%) when compared with the solution chosen by the end-electricity. Conversely, this solution increases battery degradation compared to the solution chosen by the EV owner (increases degradation by 7.6%). CO_2 emissions are always at their minimum under the scheduling preferred by DM_3 as it utilises more local PV generation. Depending on the electricity demand profile of the dwellings and EV travelling pattern, this may not necessarily lead to the best solution along the other directions; this is because the EV may be travelling when the peak demand (for that specific house, not necessarily the national peak demand) occurs.

When FFR is provided, it leads to an increase of all the metrics a part from the cost, because the optimisation window is reduced. However, FFR proves to be an overall profitable service as profits (£54.53) are higher than the incurred battery degradation cost (£3.53). Although an early replacement of the EV battery may cause distress for the EV owner, this is taken into account by the battery degradation cost, which is offset by the prospective profits by a large margin (more than four times). As discussed in the introduction chapter, the cost of lithium-ion batteries is expected to drop in future, providing a better economic case. The forecasts predict a range of scenarios, where the average trend shows a cost reduction of 33% compared to current values. Despite the uncertainty in the future battery cost, any cost reduction will proportionally reduce the cost of battery degradation (battery purchase cost is included in the model). The positive consequence is that, at the current state of the electricity market, the use of EV batteries for energy services will become more cost-effective, which will improve the profitability of V2X services for all the stakeholders.

A clear trade-off between the objectives is seen; the involved stakeholders must collaboratively take decisions and share benefits. It implies that all stakeholders must be sufficiently informed and capable of making informed decisions. Furthermore, a societal discussion will be required to see who can reap most of the benefits, and who must shoulder

the burdens. To this end, the DSO is particularly suitable to manage this as a considerable improvement in grid utilisation is achieved which will defer grid investments. Therefore, it is in the DSO's interest to share the profit with the electricity users (in the form of reduced electricity bills), who lose 27.34% under the case chosen by DM_3, and EV owners (subsidising part of their batteries), who lose 7.6%, to stimulate participation to the MOTEEO program. If the profit is not shared, than end users and EV owners will not participate to energy services and no peak reduction will be achieved; in the worst case, uncontrolled charging will cause negative impacts with increased EV penetration, and hence costs to the DSO.

6.2.9 Results of case study 3 for cross-case comparison

Smart incentives and intelligent tariff structures are critical for an effective implementation of MOTEEO. Among the possible solutions, the implementation of peak demand charges from the DSO, subsidy for the EV batteries and dynamic pricing are noteworthy. As an example of a smart tariff scheme, the case of commercial users in Flanders, Belgium is presented. Commercial users can purchase energy from the wholesale market but are charged transmission and distribution tariffs based on the peak demand [145] [146]. We adapted this tariff to case 1 scenario i) (without FFR) to highlight the importance of intelligent tariff schemes by applying the utility function [147] to combine the objectives with the value/cost they bring. The energy cost, the battery degradation cost and the peak demand charge have been combined in one function. Table 6.2-8 presents the result of case 3.

Table 6.2-8 Results of the MOTEEO method with a utility function

	Energy cost (£)	**Battery degradation (£)**	**Grid net exchange (kWh)**	**Emissions ($kgCO_2$)**
Case 3	0.14	-0.0121	10.26	1.55

By comparing Table 6.2-8 with the results of the single optimization in Table 6.2-4, a general improvement along all the dimensions can be seen. In fact, under this case, the peak demands are targeted, leading to a better performance along Obj_3 and Obj_4 but with a 28.1% reduction in battery degradation (£0.0121 instead of £0.0170) when compared to the single-objective

optimization of Obj_3. Therefore, the effectiveness of the utility function, which requires the cooperation of the three main stakeholders, has been demonstrated. Unfortunately, it is not always possible to assign a utility weight to all the objectives. Especially for Obj_3, the peak demand penalty should be decided by the DSO in relation to the incurred investments for grid reinforcement, which should be calculated on a case-by-case basis (as these are both network and location specific). In countries/regions where these types of tariffs are not available, a joint decision between the involved stakeholders is critical to satisfy all the criteria.

6.3 Game-theoretical Multi-Objective optimisation in a local energy market

Nomenclature

Sets	
I	Set of all prosumers
J	Set of all retailers
K	Set of all EV users
L	Set of all feeders
B	Set of all buses
Constants	
π_t^w	Wholesale market price at time t (£/kWh)
η_i	Charging/discharging efficiency of the storage in prosumer i
η_k	Charging/discharging efficiency of the EV k
$\bar{P}_i$	Maximum charging/discharging rating for ESS i
$\overline{E}_i, \underline{E}_i$	Maximum and minimum energy limit of the ESS of the prosumer i (kWh)
$\bar{P}_k$	Maximum charging/discharging rating for EV k
$\overline{E}_k, \underline{E}_k$	Maximum and minimum energy limit of the EV k (kWh)
R_l	Resistance of feeder l (Ω)

X_l	Reactance of feeder l (Ω)
G_l^{aa}, G_l^{ab}	Conductance elements related to buses a and b of the feeder l of the network bus-admittance matrix (S)
B_l^{aa}, B_l^{ab}	Susceptance elements related to buses a and b of the feeder l of the network bus-admittance matrix (S)
Δt	Duration of a time step (h)
$\alpha_1, \dots, \alpha_5$	Fitting parameters of the battery degradation model
T^s	Simulation period
T_k^{av}	Availability period of EV k
Parameters and functions	
κ	Energy price of the local market (£/kWh)
λ_1	Energy price in the LM at the current time step (£/kWh)
u, v	Coefficients of the LM price (£/kWh)
Λ	Specific network losses in the system ( )
L^{tot}	Total network losses in the system (kWh)
E^{tot}	Total energy traded in the market (kWh)
s_j	Market share of the retailer j ( )
P_l	Active power exchanged through feeder l (kW)
Q_l	Reactive power exchanged through feeder l (kVar)
v_l^S	Voltage of the bus at the start of feeder l (V)
v_l^E	Voltage of the bus at the end of feeder l (V)
θ_l	Phase difference in feeder l (°)
δ_l^S, δ_l^E	Phase angle at the buses at the beginning and at the end of feeder l (°)
$u(E_j)$	Profit function of retailer j (£)
$P_{l_1}^{b+}$	Active power flowing out of bus b, through feeder l_1
$P_{l_2}^{b-}$	Active power flowing in bus b, through feeder l_2
P_b^{gen}, P_b^{dem}	Active power generated and demanded in bus b

$E_{i,t}^{d}$	Electricity demand of prosumer i, at timestep t (kWh)
$E_{i,t}^{PV}$	PV generation of prosumer i, at timestep t (kWh)
$E_{i,t}^{ESS}$	Energy stored in the ESS of prosumer i, at timestep t (kWh)
$E_{k,t}^{d}$	Electricity demand in the archetype with an EV k, at timestep t (kWh)
$E_{k,t}^{PV}$	PV generation in the archetype with an EV k, at timestep t (kWh)
$SOC_{k,t}$	State of charge of the EV k at timestep t ( )
E_{1}^{ED}	Total energy exchanged in the energy district in the current time step (kWh)
E_{1}^{ED+}	Total energy demand of the EV (kWh)
$E_{j,1}^{-}$	Energy supplied by the retailer j at the current time step (kWh)
$s_{i,1}, s_{j,1}, s_{k,1}$	Market share of the prosumer i, retailer j or EV user k ( )
$A_{k,t}$	Availability of the EV k at timestep t
c_{k}^{deg}	Battery degradation cost of EV user k (£/kWh)
$LCOE_i, LCOE_k$	Levelised cost of energy for prosumer i or an archetype with an EV k (£/kWh)
Cost functions	
$\mathbb{C}_i$	Cost function of retailer j (£)
$\mathbb{C}_i$	Cost function of prosumer i (£)
$\mathbb{C}_k$	Cost function of prosumer k (£)
Decision variables	
E_i^{ch}, E_i^{dis}	Energy charged and discharged by the storage asset of prosumer i (kWh)
E_k^{ch}, E_k^{dis}	Energy charged and discharged by the EV k (kWh)

In this Section, a hybrid optimisation model based on a game-theoretical energy-trading framework is proposed in order to achieve economic, technical and environmental objectives of different stakeholders. The approach adopted in this case study is different from the Pareto analysis performed in 6.2 from the very core of the optimisation setting which is a hybrid framework. The motivation behind this study rose from perhaps the only shortcoming of a

decentralised approach, which is the limited knowledge on the overall system's status. In fact, under decentralised optimisation, each agent is responsible for their own archetype where measurements and information are exchanged only locally. If on one hand this approach prioritises data privacy and allows a distribution of the computational burden, as the system's status is dependent on the decisions of all the agents/stakeholders, each agent is not aware of the global variables. On the other hand, with the method proposed in this Section, each agent has the ability to influence the system variables, and is aware of that. The overall optimisation is formulated as a game among the involved players/agents/stakeholders while taking into account the system is operating conditions.

The framework of the energy-trading model is presented in Figure 6.3-1.

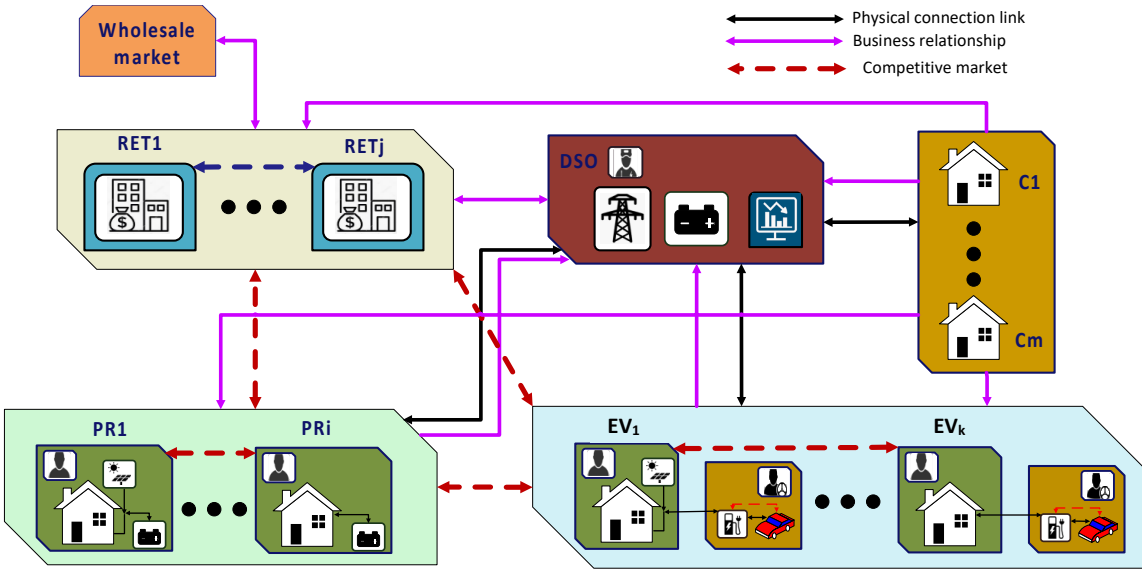

Figure 6.3-1 Hybrid framework for the game-theoretical energy trading model

In this study, different types of rational agents/players are modelled, each achieving different objectives and these are:

- Retailers (RET) purchase energy from the wholesale market and sell energy in the local market.

- Prosumers (PR) employ PV systems and energy storage to trade energy in the local market after satisfying their own electricity demand. In case of surplus, the additional energy is offered in the market at a certain price; when their electricity demand is higher than the local generation, prosumers assume the role of consumers. Their aim is to minimise their cost (maximise their revenue) by trading energy in the market. Their actions, as those of the EV users, will affect the price of the local energy market, and they aim to strike a balance between satisfying their electricity demand and low prices.
- EV users (EV) utilise EVs as storage to trade energy in the local market and satisfy electricity demand. As opposed to stationary storage, as is the case for PRs, EVs are not always available and must take into account the degradation of the battery caused by increased energy exchange.
- Consumers (C) aim at satisfying their electricity demand by purchasing electricity from the local market.
- Distribution system operator (DSO) is in charge of operating the local distribution network and balance the energy exchanged in the grid. This is done with a utility scale storage, which can be charged with excess energy that is not sold in the market, and then discharged to provide the outstanding demand. For simplicity, it is assumed that there is no power exchange with the transmission system.

These players are connected to an energy district (ED) and interact/trade in a local market (LM). However, it should be pointed out that although modelled, for simplicity, retailers have not been simulated.

6.3.1 Methodology

In this Section, the objectives of the players are mathematically modelled along with the associated constraints and the game framework is defined. It should be noted that the DSO assumes the role of a LM regulator, ensuring energy balance in the ED and efficient grid operation.

The objective function of the prosumers is presented in the following equation:

$$\underset{E_i^{ch},E_i^{dis}}{\operatorname{argmin}} \mathbb{C}_i = \sum_{t=1}^{T^S} -\kappa \left(E_{i,t}^{d} - E_{i,t}^{PV} + E_{i,t}^{ch} - E_{i,t}^{dis}\right) - LCOE_i \left(E_{i,t}^{d} - E_{i,t}^{PV} + E_{i,t}^{ch} - E_{i,t}^{dis}\right)^{-} + \pi_1^w \left|E_{i,1}^{d} - E_{i,1}^{PV} + E_{i,1}^{ch} - E_{i,1}^{dis}\right| \Lambda_i \ , \forall \mathrm{i} \in \mathrm{I} \tag{6.12}$$

where κ is the price of the energy in the LM, $E_{i,t}^{d}$ and $E_{i,t}^{PV}$ are the electricity demand and generation within the prosumer's household and $E_{i,t}^{ch}$, $E_{i,t}^{dis}$ are the charging and discharging schedules of the stationary energy storage, which are also the decision variables. $LCOE_i$ indicates the cost of energy for providing energy back to the grid, which is determined by the investment in the PV and storage system, as indicated by the equation below:

$$LCOE_i = \frac{c^{i,PV} + c^{i,ESS}}{\sum_{n=1}^{N} E_n^a} \tag{6.13}$$

where $c^{i,PV}$ and $c^{i,ESS}$ are the investment costs for the PV and energy storage system (ESS) respectively, E_n^a is the yearly PV generation at year n and N is the total number of years for the investment in renewable energy. The levelised cost of energy (LCOE) of a PV and ESS system will depend on the investment costs and annual irradiance, as well as national supporting policies. In equation 6.12, the $(\ \ )^{-}$ notation indicates the negative part of the overall energy as expressed in the expression below (energy consumption has been designated with positive sign while supplied energy is represented with a negative sign throughout this Section).

$$\left(E_{i,t}^{d} - E_{i,t}^{PV} + E_{i,t}^{ch} - E_{i,t}^{dis}\right)^{-} = \frac{\sqrt{\left(E_{i,t}^{d} - E_{i,t}^{PV} + E_{i,t}^{ch} - E_{i,t}^{dis}\right)^2} - \left(E_{i,t}^{d} - E_{i,t}^{PV} + E_{i,t}^{ch} - E_{i,t}^{dis}\right)}{2} \tag{6.14}$$

In (6.12), π_1^w is is the wholesale energy price at the current timestep and Λ_i is the specific energy losses. More detailes will be provided in the next paragraphs. Equation 6.12 is formulated as an energy cost minimisation, which is subject to the constraints expressed by the following equations

$$E_{i,t} = E_{i,t}^{d} - E_{i,t}^{PV} + E_{i,t}^{ch} - E_{i,t}^{dis}, \forall i, \forall t \tag{6.15}$$

$$0 \leq E_{i,t}^{ch}, E_{i,t}^{dis} \leq \bar{P}_i \, \Delta t, \forall i, \forall t \tag{6.16}$$

$$E_{i,t}^{ESS} = E_{i,t-1}^{ESS} + \eta_i \, E_{i,t}^{ch} - \frac{E_{i,t}^{dis}}{\eta_i}, \forall i, \forall t \tag{6.17}$$

$$\underline{E_i} \leq E_{i,t}^{ESS} \leq \overline{E}_i, \forall i, \forall t \tag{6.18}$$

$$E_{i,t}^{ch} \times E_{i,t}^{dis} = 0, \forall i, \forall t \tag{6.19}$$

(6.15) is employed as the energy balance equation in the household's energy system, (6.16) is used to limit the charged and discharged energies within the rating of the inverter and (6.17) is utilised to define the energy stored in the ESS for each time step with respect to the energy exchanged and the charging/discharging efficiency. The energy stored in the ESS is limited to its capacity limits from (6.18) and (6.19) is used to ensure that charging and discharging do not happen simultaneously.

Similarly, the objective function for the EV user is expressed hereby as

$$\underset{E_k^{ch}, E_k^{dis}}{\operatorname{argmin}} \mathbb{C}_k = \sum_{t=1}^{T_k^{av}} \kappa \left(E_{k,t}^{d} - E_{k,t}^{PV} + E_{k,t}^{ch} - E_{k,t}^{dis}\right) - LCOE_k \left(E_{k,t}^{d} - E_{k,t}^{PV} + E_{k,t}^{ch} - E_{k,t}^{dis}\right)^{-} + \pi_1^w \left|E_{k,1}^{d} - E_{k,1}^{PV} + E_{k,1}^{ch} - E_{k,1}^{dis}\right| \Lambda_k - c_k^{deg}, \forall k \in \mathrm{K} \tag{6.20}$$

where all the symbols retain the meaning as in (6.12) aside from T_k^{av} which is the availability period (as parked at home and plugged-in) of the EV k, and c_k^{deg} is the cost of battery degradation incurred by the EV k due to the charging/discharging schedule as expressed by the following equation:

$$c_k^{deg} = \sum_{t=1}^{T_k^{av}} \alpha_1 \times \left[\alpha_2 \left(E_{k,t}^{ch} + E_{k,t}^{dis}\right) + \alpha_3\right] \times \left[\alpha_4 SOC_{k,t} + \alpha_5\right] \tag{6.21}$$

The above equation is obtained from Chapter 4.3 and $SOC_{k,t}$ is defined in a matrix form in the equation below:

$$\boldsymbol{SOC}_{k,t} = \frac{\begin{bmatrix} 1 & 0 & \cdots & 0 \\ 1 & 1 & \cdots & 0 \\ \vdots & \vdots & \cdots & 0 \\ 1 & 1 & \cdots & 1 \end{bmatrix} \begin{bmatrix} E_{k,1}^{ch} \\ \vdots \\ E_{k,T^{av}}^{ch} \end{bmatrix} \eta_k - \begin{bmatrix} 1 & 0 & \cdots & 0 \\ 1 & 1 & \cdots & 0 \\ \vdots & \vdots & \cdots & 0 \\ 1 & 1 & \cdots & 1 \end{bmatrix} \begin{bmatrix} E_{k,1}^{dis} \\ \vdots \\ E_{k,T^{av}}^{dis} \end{bmatrix} \left(\frac{1}{\eta_k}\right)}{\overline{E}_k} \tag{6.22}$$

The constraints for the energy cost minimisation formulated in (6.20) are expressed in the following set of equaitons in a similar manner as for the ESS.

$$E_{k,t} = E_{k,t}^{d} - E_{k,t}^{PV} + E_{k,t}^{ch} - E_{k,t}^{dis}, \forall k, \forall t \tag{6.23}$$

$$0 \leq E_{k,t}^{ch}, E_{k,t}^{dis} \leq \bar{P}_k \, \Delta t, \forall k, \forall t \tag{6.24}$$

$$E_{k,t}^{ESS} = \begin{cases} E_{k,t-1}^{ESS} + \eta_k \, E_{k,t}^{ch} - \frac{E_{k,t}^{dis}}{\eta_k}, if \; A_{k,t} = 1 \\ E_{k,t-1}^{ESS}, \; otherwise \end{cases}, \forall k, \forall t \tag{6.25}$$

$$\underline{E}_k \leq \; E_{k,t}^{ESS} \leq \; \overline{E}_k, \forall k, \forall t \tag{6.26}$$

$$E_{k,t}^{ch} \times E_{k,t}^{dis} = 0, \forall k, \forall t \tag{6.27}$$

(6.25) is used to ensure that charging/discharging events are initiated only if the EV is available at the time step t.

Both in (6.12) and (6.20), the specific system losses have been utilised, which is now defined as follows:

$$\Lambda_k = \frac{L^{tot}}{E_1^{ED}} \tag{6.28}$$

where L^{tot} are the total active losses and E_1^{ED} is the total energy exchanged in the ED at the current timestep. It should be noted that in the objective functions of both the prosumers (equation 6.12) and the EV users [equation (6.20)], the specific losses are multiplied by the total energy exchanged by their respective archetypes, and the ratio of the latter with respect to the overall ED's energy exchange represents the share of the market held by the prosumer or EV user as shown in the equation below:

$$\left|E_{k,1}^{d} - E_{k,1}^{PV} + E_{k,1}^{ch} - E_{k,1}^{dis}\right| \Lambda_k = \left|E_{k,1}^{d} - E_{k,1}^{PV} + E_{k,1}^{ch} - E_{k,1}^{dis}\right| \frac{L^{tot}}{E_1^{ED}} = s_{k,1} L^{tot} \tag{6.29}$$

where $s_{k,1}$ is the share of the market held by the prosumer k at the current time step (this is also defined for EV users), which means that the prosumers and EV users pay a penalty that

is proportional to the overall losses and their market share. Hence, the only two ways to reduce this penalty is to either reduce their contribution to the losses or the market share.

To compute the overall losses, the AC power flow equations must be computed as previously expressed in Chapter 3, by (3.7.a) and (3.7.b), with the overall losses expressed by (3.8) (E_t^{loss} is denoted here as L^{tot}). Furthermore, the voltage magnitude and phase angle constraints expressed by (3.10) and (3.11) are enforced in the calculation of the power flows. With this framework, not only the players must comply with suitable grid constraints but also it is in their interests to minimise losses in order to improve their profit. Although for simplicity, retailers are not included in the energy trading system, the framework is generic enough to include them, and their objective function is expressed by the following equation:

$$\underset{E_{j,1}^{-}}{\operatorname{argmin}}\ \mathbb{C}_j = (\lambda_1 - \pi_1^w)\, E_{j,1}^{-} - \pi_1^w E_{j,1}^{-}\, \Lambda_k, \forall j \in J \tag{6.30}$$

where, $E_{j,1}^{-}$ is the energy supplied by the retailer at the current timestep and λ_1 is the current energy price on the LM. It should be noted that the retailers only deal with the energy traded at the current time step and do not consider future transactions in their objective function. This is because, retailers do not have constraints to be complied with (their only objective is to maximise their profit). For future implementation, additional constraints can be introduced, i.e. capacity limitations.

Finally, the energy price in the local market, κ, is modelled: in the proposed framework, κ is a vector containing T^s prices, with the first being λ_1, the LM price at the current timestep, and the rest is made by the wholesale market price for the future timesteps; in practice, the latter is known one day ahead. This is because, the market players, i.e. retailers, prosumers and EV users, can influence the market price at the current time step (they are price makers), whereas they do not have control on future prices. Indeed, prosumers and EV users consider future situations within their optimisation frameworks, but this is to make an optimal choice by taking into account their future states (availability of PV, energy required for driving). On the other hand, the LM price depends on the energy that is actually exchanged, which is only

realised in the current time step while for future time steps, the energy has not been exchanged yet. The following equation explicates the price structure.

$$\kappa = [\lambda_1, \pi_2^w, \dots, \pi_{Ts}^w] \tag{6.31}$$

Once the energy trades in the current time step have been agreed, the optimisation windows slides forward by one time step, a new LM price is then decided upon while the rest is made up by the wholesale market price, and this procedure is repeated iteratively. This method has been applied in [P3], and a visual representation of the above procedure is presented in Figure 6.3-2.

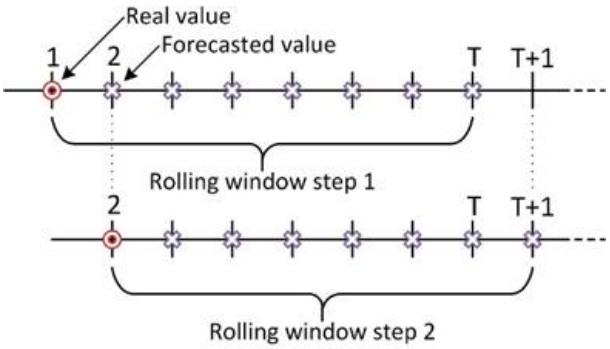

Figure 6.3-2 Depiction of the rolling window approach

The LM price has been set as an increasing monotonic function to promote competition between players as presented hereby:

$$\lambda_1 = u\, E_1^{ED+} + v \tag{6.32}$$

where u and v are positive constants and E_1^{ED+} is the total energy demand of the ED. According to (6.32), the higher is the electricity demand in the ED the higher will the price be in the current time step. Conversely, in those time steps when PV generation is abundant, the price will be at the minimum, allowing the players to perform arbitrage by looking ahead in time (they can refer to the future wholesale market price as in equation 6.31). However, if stimulated by a low price the players increase their consumption; this will lead to an increase of the LM price. The key is therefore to find an *equilibrium* between energy conservation (low prices) and energy exploitation (high prices), a concept that will be further elaborated in

the next Section. This Section is concluded by highlighting the key objectives and constraints that ultimately make the proposed framework a MOO problem:

- The objective functions of the PRs and EVs, aim at maximising their profit (economic), and by considering the battery degradation cost (refer to equation 6.20) also battery life is improved (battery); this is because the optimisation algorithm will weigh any charging/discharging action against the cause battery degradation cost, and will implement any action that offsets such cost. This implies that any action that does not provide enough revenue will not be undertaken, leading to less utilisation and therefore less battery degradation.
- The constraints on the network operation and the consideration of the total losses in the objective function ensures an effective grid operation (grid utilisation);
- The formulation of the energy price proposed in this work rewards the integration of PV generation (by lowering the market price) and achieves increased renewable energy integration (CO_2 minimisation).

6.3.2 Development of a non-cooperative game theoretical energy trading system

In this work, the trading between the three types of stakeholders namely, PR and EV is modelled as a competitive and non-cooperative game. Under this framework, when one player strategically acts in order to maximise its own profit, inevitably, the benefits of the other players are affected. This is opposite to cooperative games where different players can benefit by forming coalitions among them, as their objective functions are aligned.

In non-cooperative games, the idea of Nash equilibrium is of maximum importance. The following definitions help in formulating the game framework.

Definition 10. *Given the game* $\{N, (X_i)_{i\in N}, (\Phi_i)_{i\in N}\}$*, with* $\mathrm{N} = [1, \dots, n]$*,* $\boldsymbol{x}^* = [x_1^*, \dots, x_n^*]$ *is a Nash-equilibrium if* $\Phi_i(\boldsymbol{x}^*) \leq \Phi_i(x_i)\ \forall x_i \in (X_i)_{i\in N}$

where N indicates the number of players, X_i is the strategy set of the player i and Φ_i is the cost function of the player i. In other words, under Nash equilibrium, no player has incentive to change their strategy, given the strategy of the other players, because it would otherwise lead to a lower benefit. As the optimisation framework presented in the previous Section constrained the actions of the players, in particular with constraints (3.10) and (3.11) (network constraints), this game is a coupled constraints game and the implementation of a Nikaido-Isoda (NI) function is proposed in order to find the Nash equilibrium of this game [148], [149]. With this formulation, the equilibrium search problem is transformed into an optimisation problem as presented in the following expression:

$$\Psi(\boldsymbol{x}, \boldsymbol{y}) = \sum_{i=1}^{n} [\Phi(\boldsymbol{y_i}|\boldsymbol{x}) - \Phi(\boldsymbol{x})] \tag{6.33}$$

Under the notation adopted in (6.33), $\boldsymbol{y_i}|\boldsymbol{x}$ is a vector containing the strategies of all the players, where the ith agent plays y_i, while the remaining $1, \dots, i-1, i+1, \dots, n$ agents keep playing x_j. If it was not obvious before, here it is reiterated that the different x_j are also vectors containing the strategies of the player j (for instance the charging/discharging schedule for all the hours). The NI function is the summation of the improvement in payoff (reduction of cost) for the ith agent when they play y_i, while the remaining players are still playing x_j. As per the definition above, Nash equilibrium is reached when no player can unilaterally improve their payoff, which equivalently means when the NI function reaches a nil value, as also stated in the definition below.

Definition 11. *The optimum response of a game* $\{N, (X_i)_{i \in N}, (\Phi_i)_{i \in N}\}$ *where 6.33 holds is* $\underset{\boldsymbol{y} \in X}{\operatorname{argmax}} \Psi(\boldsymbol{x}, \boldsymbol{y})$

This is because, near Nash equilibrium, the NI function is non-positive and the maximum value is zero, which corresponds to Nast equilibrium. In this work, a relaxation algorithm (NIRA) is used to find Nash equilibrium through the NI function as previously proposed by [149]. The pseudocode for the NIRA algorithm is provided hereby.

Nikaid-Isoda relaxation algorithm

Input: Non-cooperative game structure $\{N, (X_i)_{i\in N}, (\Phi_i)_{i\in N}\}$, weight α^s and convergence threshold δ^c

1: **Initialisation:** Set initial strategies of the players as $\boldsymbol{x}_0 = \emptyset$

2: $s \leftarrow 0$

3: **while** $\Psi(\boldsymbol{x}, \boldsymbol{y}) > \delta^c$ **do**

4: Calculate optimum response $Z(\boldsymbol{x}) = \underset{\boldsymbol{y}\in X}{\operatorname{argmax}}\, \Psi(\boldsymbol{x}, \boldsymbol{y})$

5: Calculate strategies at next step as $\boldsymbol{x}_{s+1} = (1 - \alpha^s)\, \boldsymbol{x}_s + \alpha^s\ Z(\boldsymbol{x}_s)$

6: $s \leftarrow s + 1$

7: **end while**

In the above implementation, the optimum response for all the n players (the dimension of the action space can be different for each player) is obtained by maximising the NI function. The strategies are then updated using a weighted sum with weight α^s between the strategy at the current iteration and the optimum response. This process is iteratively implemented until the distance between the NI function value and zero is within the set threshold. It should be noted that while calculating the NI function, each player updates their own strategy assuming that the strategy of all the other players are kept unchanged. To this end, each player only knows his or her own feasible set (defined by the constraints) and the strategy of the other players. Hence, sensitive information regarding demand profiles and utilisation behaviours are not exchanged among players. This is the reason for calling such method a hybrid strategy: although decisions are taken locally, overall system variables are controlled. In the next Section, the proposed game framework is applied to realistic case study in an ED.

6.3.3 Results and discussion

Case study setting

In this section one full day of operation of a micro-grid has been simulated, implementing the proposed game-theoretical energy trading system. The simulated micro-grid is based on a real distribution network that is the same as the one adopted in Chapter 6.2. There are 19

households connected to one phase of the three-phase electricity network. The parameters of the case study are outlined in Table 6.3-1.

Table 6.3-1 Game-theoretical energy trading case study setting

Parameter	**Value**
Number of prosumers, i	2
Number of retailers, j	0
Number of EV users, k	5
Average daily mileage and arrival and departure times for trips	Randomly generated from National Time use Survey data
Average PV size	3.35 kWp, [143] (actual PV sizes are randomly generated considering this as mean)
$\overline{E}_i$ and $\bar{P}_i$	[2, 2] kWh and [1, 0.5] kW
$\overline{E}_k$ and $\bar{P}_k$	[30, 30, 60, 30, 30] kWh and [3, 3, 7, 7, 3] kW
EV charger type	Type 2, Bidirectional, single-phase
$LCOE_i$, $LCOE_k$	0.053 £/kWh
u, v	$1 \times 10^{-4}, 3 \times 10^{-3}$ £/kWh

As can be seen, a mix of slow and semi-fast charging points have been deployed (see Table 1.1-1), and there is one long range EV. The capacities of the stationary storage systems have been chosen based on common industrial standards. All the households, ESSs and EVs have been randomly deployed in the distribution network, among which, only the household with EV 2 (connected at bus 3 of the distribution network in Figure 6.2-2) is not provided with a PV system. This is to show the difference between the decentralised optimisation and one where a local market is in place and players can trade energy among themselves. In fact, in the decentralised case, when the EV user does not have its own PV system, only the

household electricity demand will be considered in the optimisation. On the other hand, when a local energy trading system is available, excess PV energy will be offered in the market and all the users that can control their energy exchange will be able to access that energy.

Figure 6.3-3 presents the charging and discharging schedule of the 5 ESS for 24 hours (96 steps of 15 minutes each), with a comparison between a self-optimisation (where the agents/players choose their charging schedule purely based on the information on their archetype), which is represented by the bar plot, and the energy trading system in a local market, represented by the blue stems.

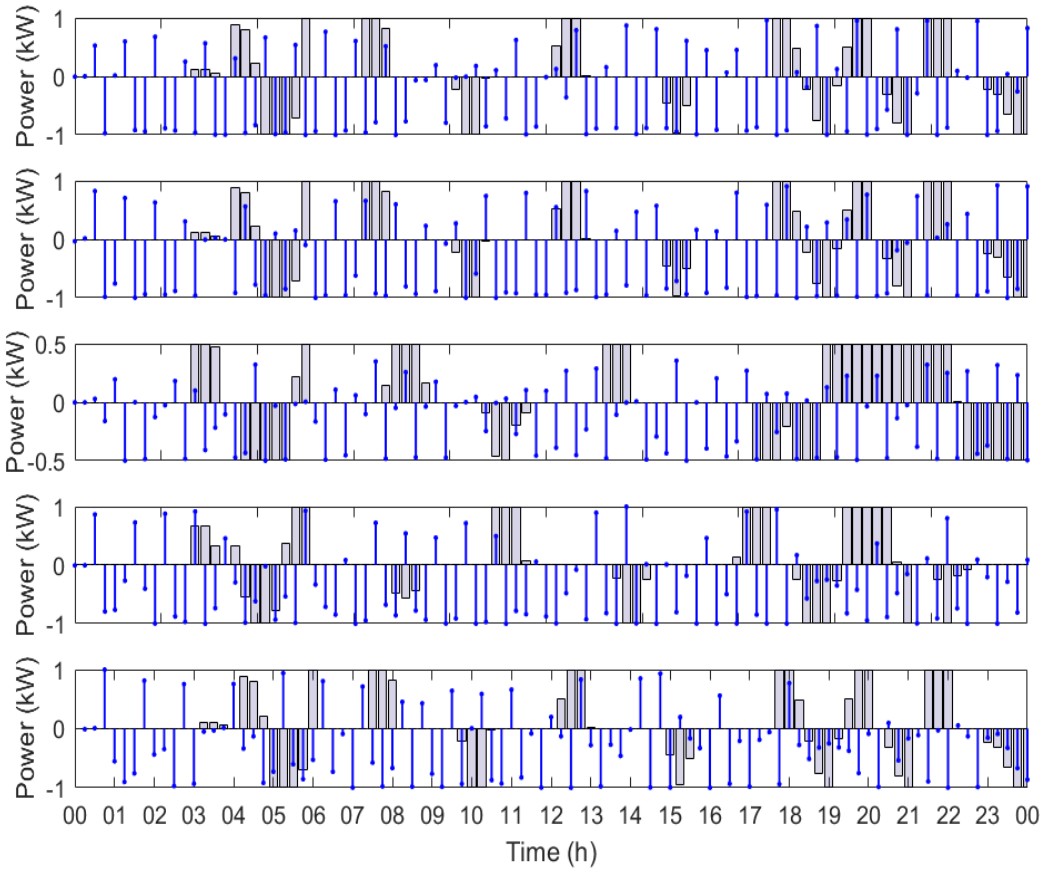

Figure 6.3-3 Charging and discharging schedules of the 5 ESSs

The difference between the two strategies that is immediately noticeable is that while looking at their own archetypes, the ESS are cycled only in selected periods (following the price

curve), whereas when a local market is in place, the utilisation of the ESSs is spread across the day, intervening when required in the overall system. Similarly, Figure 6.3-4 shows the schedules for the 5 EVs, with the bars representing a selfish optimisation process and stems showing their actions in the proposed energy trading system.

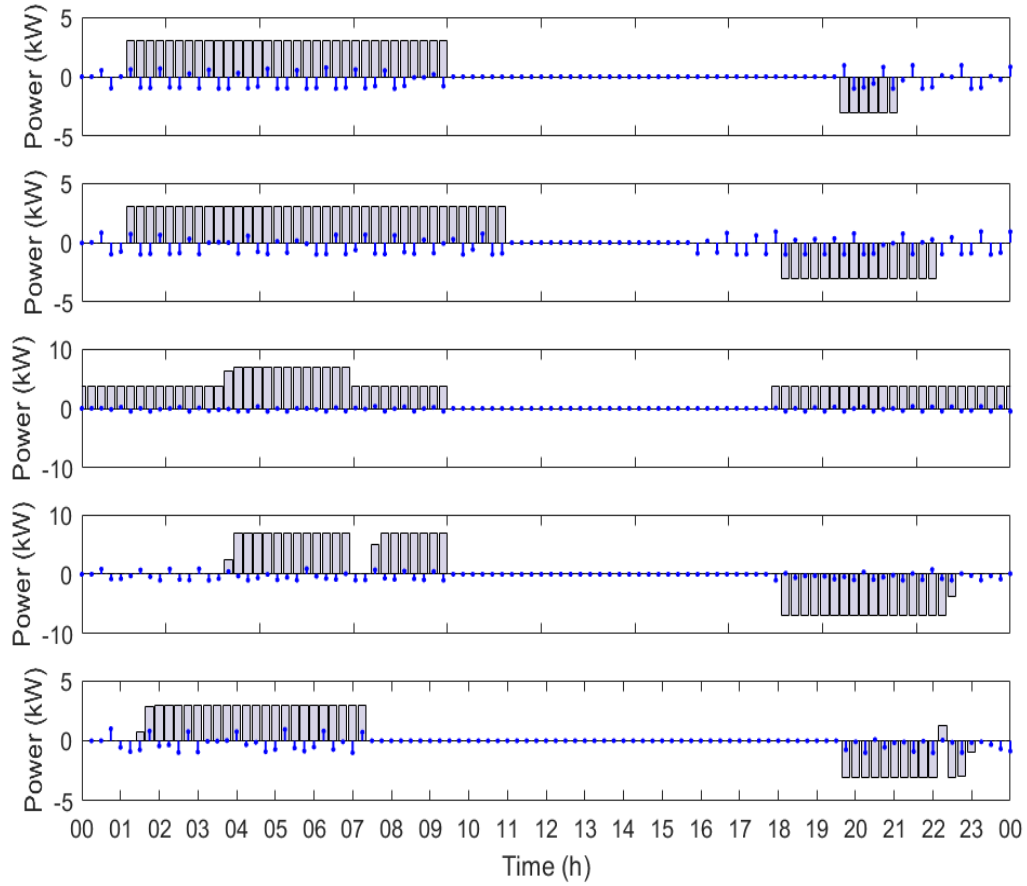

Figure 6.3-4 Charging and discharging schedules of the 5 EVs

It can be seen that contrary to the selfish optimisation process, charging and discharging powers of the EVs are reduced in the energy trading system. The reason for this is twofold: charging more power would increase the energy price in the local market (see figure Figure 6.3-5) negatively affecting the benefit of the player; high power exchange will increase network losses. As both these aspects are captured in the payoff functions of the players, their actions are more precautionary towards the grid status. Figure 6.3-5 depicts the difference

between the wholesale market price and the local market price; a part from 9:00 hrs and 17:00 hrs, the local market price is always below the wholesale market price, indicating an improved benefit for all the users (players and not players, the latter not having any form of storage, hence not able to change their demand).

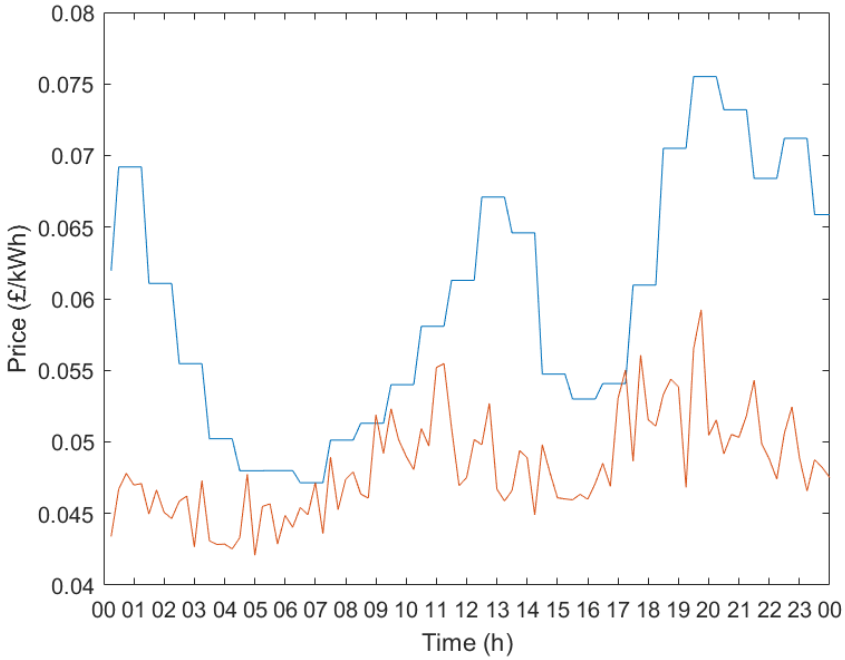

Figure 6.3-5 Wholesale market price (blue) and local market price (red) for one day of operation

To confirm the benefit of the energy trading system, Figure 6.3-6, shows the total power exchanged with the ED, in the selfish optimisation case and with the local market approach. Overall, the net power exchange is not only flatter, but also reduced with the local market approach. This is further confirmed by the reduction in the incurred losses as shown in Table 6.3-2, where a 38% reduction of the active power losses is achieved with the local market approach. Although this method has proved beneficial towards both the grid and the involved players, the downside lies in the computational efforts. Depending on the number of players and the simulated time steps, the optimisation process can require computational times that are larger than the simulated time steps. One solution to this issue is reducing the resolution of the optimisation process (one-hour time step instead of 15 minutes) and reducing the number of players. In addition, linearization of the objective function can also help. Finally,

evolutionary algorithms and swarm-based approaches can help in improving the performance of the optimisation process, as the calculation of the NI function is certainly non-convex.

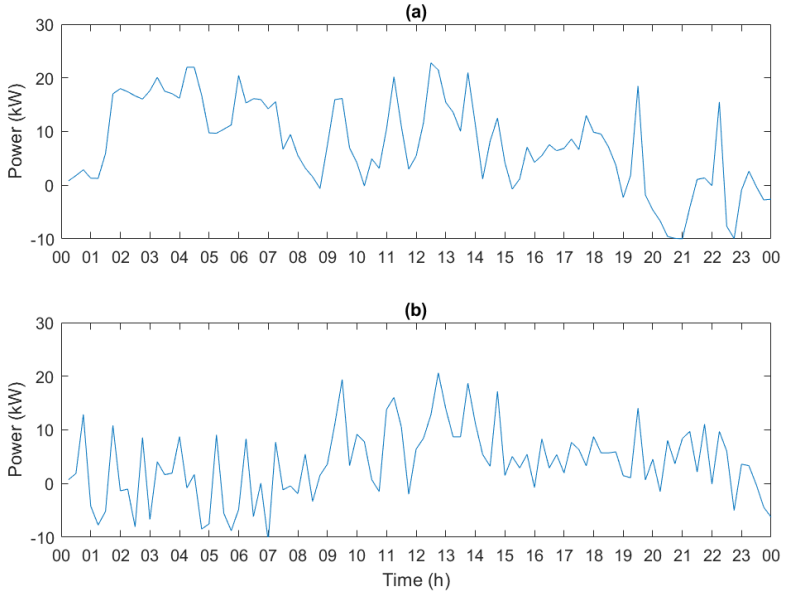

Figure 6.3-6 Total power exchange of the ED with selfish optimisation (a) and with the energy trading system (b)

Table 6.3-2 Normalised losses with selfish optimisation and with the energy trading system

	Initial schedule	Game theoretical energy trading
Normalised Losses (pu)	1	0.62

6.4 Assesment of economic feasibility of V2G services

In order to perform a sensitivity analysis, in this section, electricity self-consumption by V2G in a domestic setup will be investigated by varying key input parameter. The necessity of this assessment lies on the fact that the optimisation framework and its cost-benefit outputs are sensitive to the input parameters and serves and variation of the latter naturally lead to diverse results. Therefore, this analysis is carried out in order to demonstrate the coherence and robustness of the optimisation process. Ultimately, this section aims at answering a

fundamental research question that has motivated this research: *is V2G currently profitable?* For this purpose, a six V2G operation scenarios are modelled and compared with a business-as-usual (BAU) case where V2G is not performed and the EV is charged in an uncontrolled manner, as soon as it is connected. Under V2G the EV is used to minimise the electricity cost of the householder while minimising battery degradation. Hence, the objective function for the optimisation constructed by combining equations 6.1 and 4.19-4.25. The system configuration for the two cases is presented in Table 6.4-1.

Table 6.4-1 System components for two comparison cases

Case	Business-as-usual	V2G cases
Electricity demand	Domestic	
PV System (kWp)	3	
EV (kWh)	30	30
EV charger (kW)	3	3 (bidirectional)

The system components are the same in both cases, apart from the EV charger, which is bidirectional in the V2G case. As aforementioned, six V2G scenarios with different input parameters are simulated and their economic results are compared; the details of the scenarios are presented in Table 6.4-2.

Table 6.4-2 Assessment parameter categories for assessing economic feasibility of V2G (shaded parameters represent the base scenario)

Assessment parameter	S1	S2	S3	S4	S5	S6
Electricity tariff	Fixed	Economy 7	Fixed			
Battery cost (£/kWh)	150	150			+20%	-20%
Tariff multiplier (£/kWh)	Current	Current	+20%	-20%	Current	

As can be seen, the parameters that constitute the base scenario (S1) are shaded in grey, and any variation of one parameter represents a different scenario. For instance, un der S2 the electricity tariff is an Economy 7 tariff [150], the battery unit investment cost is 150 £/kWh and the tariff is scaled to the current situation. Similarly, the other scenarios are modelled

based on the variation of one parameter. The economic parameters adopted for the scenarios are listed in Table 6.4-3.

Table 6.4-3 Economic parameters for the scenario analysis [151][152][153]

Parameter	Value
Fixed electricity tariff (£/kWh)	0.13
Economy 7 (£/kWh)	0.14 (07:00 – 22:45) 0.6 (23:00 – 06:45)
Bidirectional charger cost (£)	6000
Bidirectional charger investment life (years)	10
Discount rate	4%

The different scenarios will be compared against their underlying net present value (NPV) of the investment of the bidirectional charger, as defined in the equation below.

$$NPV_i = \sum_{n=1}^{N} \frac{CF_{i,n}}{(1+d)^n} \tag{6.34}$$

Where, i is the index that represents one V2G scenario, n is the year within the investment's lifetime, N is the number of years in the lifetime of the investment, $CF_{i,n}$ is the annual cash-flow for the year n under scenario i and d is the discount rate.

Figure 6.4-1 shows one day of scheduling out of a whole year simulation for the BAU case and the V2G case, for all scenarios.

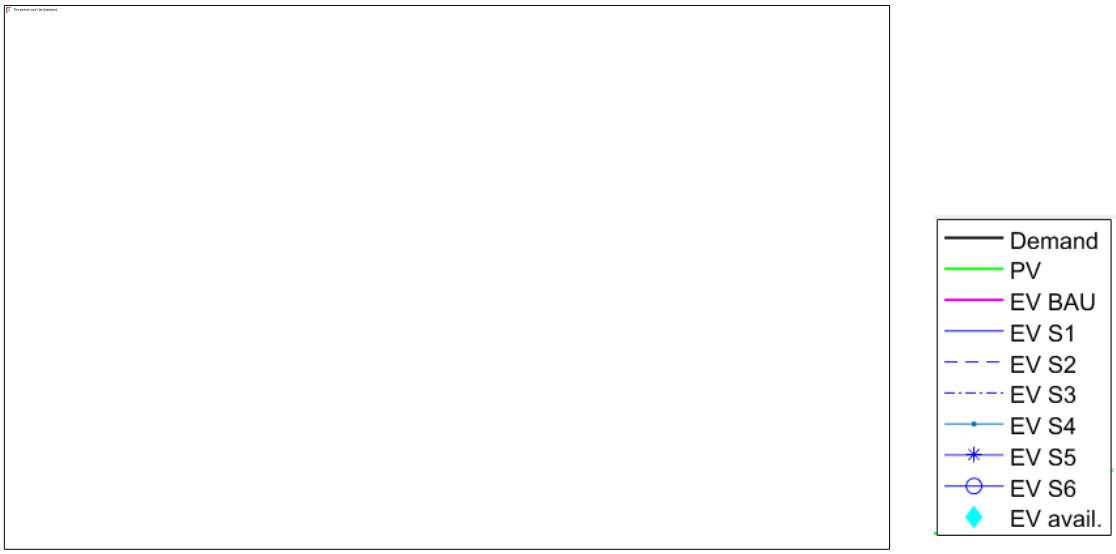

Figure 6.4-1 Sample of one day of scheduling under BAU and V2G case for all scenarios

It can be seen that with the BAU approach, the EV is charged upon arriving at home (at 13:00) at the highest rate (3kW), which manages to capture some of the excess PV generation. However under the V2G scenarios, the charging rate is adjusted in otder to match the excessive PV generation. Furthermore, under Economy 7 tariff (S2), the EV is scheduled to provide all the electricity demand peaks before 23:00 (note that after 23:00 there are other demand peaks where however the EV is not discharged under S2). Conversely, when battery cost is increased from the current value, less charging/discharging is carried out. This is due to a proportionally greater battery degradation caused for the same scheduling. Figure 6.4-2 presents a comparison of the annual costs under BAU and V2G cases for the six scenarios, by dissecting in electricity and battery degradation costs.

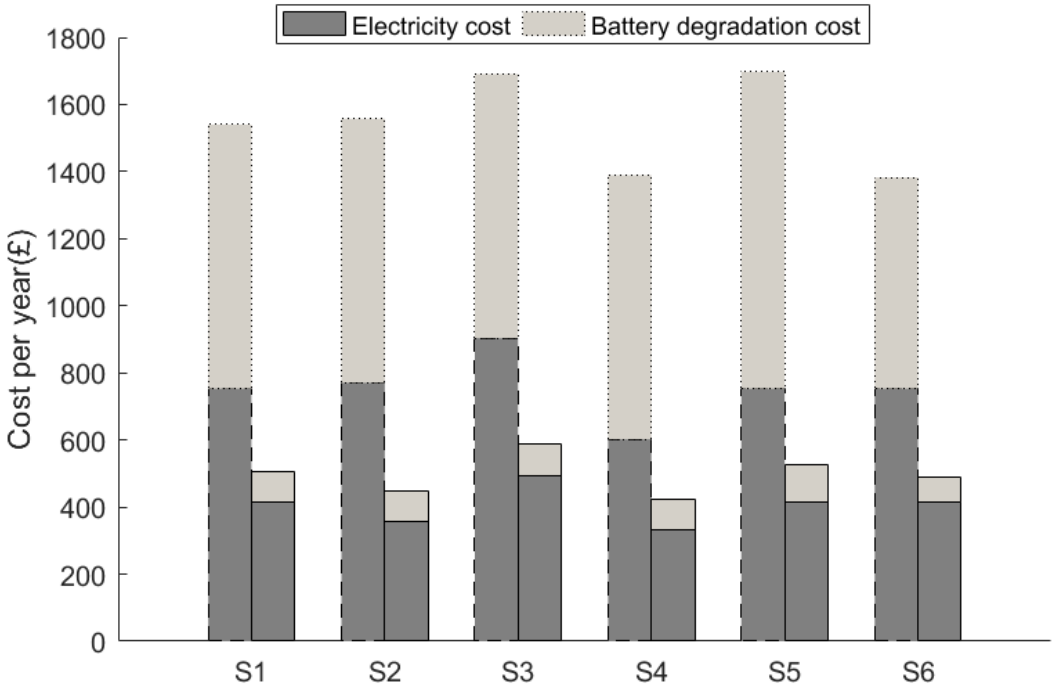

Figure 6.4-2 Cost comparison between BAU (bars with dashed lines) and V2G cases (bars with continuous lines)

Table 6.4-4 provides a breakdown of the annual costs for the six V2G scenarios. It should be noted that the difference between the costs incurred under the BAU case and the costs provided in Table 6.4-4 represents the annual cash-flow $CF_{i,n}$ in equation 6.34.

Table 6.4-4 Cost breakdown for six V2G scenarios

Cost element	S1	S2	S3	S4	S5	S6
Electricity cost (£)	414.24	358.70	493.19	332.36	416.15	414.52
Battery degradation cost (£)	92.90	90.84	93.61	90.22	108.64	75.11

It can be seen that although the electricity price profile is changed between scenarios S1-S4, the incurred battery degradation does not vary significantly. This is because the objective function accounts for the proscpective battery degradation caused by the charging/discharging process and minimises it, while providing the service. One important

point to be noted is that Economy 7 tariff brought both low expense in terms of electricity cost and low battery degradation. In fact, both costs are lower only under scenario S4, where the electricity tariff is 20% lower compared to the current situation. Of course, when battery investment cost is lowered, the underlying degradation cost decreases proportionally, whereas, electricity cost is nearly the same as the base scenario; overall this results in lower annual costs. Table 6.4-5 presents the NPV in 10 years for the six V2G scenarios.

Table 6.4-5 NPV for six V2G scenarios

	S1	S2	S3	S4	S5	S6
NPV (£)	2,378	2,983	2,956	1,838	3,508	1,246
NPV (only electricity cost) (£)	-3,252	-2,662	-2,671	-3,810	-3,268	-3,255

In the first row, the NPV considering the difference between the costs incurred under BAU case and V2G case is presented, while in the second row, only the difference in electricity cost is considered. As can be seen, without considering the benefit obtained by improving the utilisation of the battery (which is done in the approach presented in this research), the investment in a bidirectional charger is not profitable. On the other hand, when the benefit on reduced battery degradation is considered, V2G is overwhelmingly profitable across all the scenarios. In particular, the higher is the electricity cost or battery investment cost, the higher the NPV. This is because, if the electricity tariff or battery investment cost is high, then the negative impact of an uncontrolled charging/discharging process (as it is the case of the BAU case) is particularly severe. Furthermore, Economy 7 tariff also improves the NPV and it is particularly suitable for V2G (notice that it has the highest NPV among S1-S4) as end-electricity-users can choose to defer consumption in off-peak hours and reduce consumption during peak hours. Overall, the optimisation process exhibits stable results, as the difference in NPV is proportional to the variation of the input parameters.

6.5 Conclusions

In the present work, the MOTEEO and the NIRA approaches are proposed and applied in three case studies and for different charging strategies in order to find the synergy of several

objectives. Mathematical models of the objectives and scenario are constructed to represent the interests of the associated stakeholders. The conflicting objectives of stakeholders are resolved by multi-objective optimization with multi-criteria-decision-making technique, and game theory. By implementing the proposed methodology to the case studies considered in this work, some noteworthy conclusions were drawn and are summarised as follows.

Under MOTEEO, the end-electricity users can increase their benefits by 81% (compare 2e with 2b) by providing frequency regulations service and the DSO can improve the grid utilisation by 41.78%. However, these are the maximum achievable benefits along one objective and there needs to be cooperation between the stakeholders to increase the overall social benefits. This suggests that a larger (or new) regulatory role must be played to ensure that overall social benefits are obtained. The DSO must share the benefits achieved from improved grid utilisation (investment cost deferral) by ensuring a revenue to the end-electricity user and the EV owner. The quantification of such revenue is case-dependent and each distribution network should be studied individually. Therefore, a collaborative decision process has been proposed. The implementation of a smart utility function under MOTEEO targets the peak demand by combining the objectives of the end-electricity user and the DSO achieving optimal grid operation while minimizing the damage to the battery (28.1% of reduction in battery degradation compared to the case without MOTEEO).

The NIRA algorithm applied to the case of an energy trading system in a local market has been proved beneficial for both the grid and the users. In fact, the proposed method reduced the network losses by 38%, and improved the financial benefits of the involved players by providing them with a lower energy price. An overall flatter net power profile also ensures grid investment deferral as current peaks are reduced. However, as in MOTEEO, the computational effort of the NIRA algorithm depends on the required accuracy (in MOTEEO, the accuracy of the Pareto frontier and in NIRA the number of players and time resolution). Therefore, when possible, the optimisation problems should be simplified with linearization techniques or with evolutionary and swarm based algorithms. A sensitivity analysis has been performed by varying electricity tariff and battery investment costs and the results from six V2G scenarios have been compared against the business as usual approach of uncontrolled

charging. It has been shown that V2G can reduce battery degradation compared to uncontrolled charging and when this benefit is considered in the economic calculation, V2G scenarios provide positive return for the investment in a bidirectional charger. As the cost of V2G chargers and lithium-ion batteries decrease, V2G will be increasingly profitable.

Chapter 7 Implementation of real-time multi-objective optimisation in a micro-grid

7.1 Introduction

In this research, strategies for optimal management of EV charging have been proposed at two levels, decentralised and centralised. This is motivated by the inherent trade-off between the advantages and drawbacks of the aforementioned strategies. It has been shown that at a decentralised level, the information is collected and processed locally, which distributes the computational burden among the different agents. Furthermore, with this approach, the privacy of the user is ensured as limited information is exchanged with third parties. However, as this strategy performs a local management, the status of the overall system, especially at a higher level, may be sub-optimal. This is because information is not exchanged among agents; hence, if a contingency event happens outside the boundary of an agent, this would not be taken into account while scheduling EV charging. Conversely, centralised management enables an optimal operation of the overall system since a central operator monitors the system's status. This however comes at the expense of a higher computational burden and reduced privacy, as the central manager has access to local measurements. In addition, with this strategy, the risk of a system breakdown increases as there is a single control point, and the measurement and communication system is more onerous [135]. Hence, we proposed a hybrid management scheme, where the agents at the lower level and the central system operator interact in a market, managed by a market regulator.

In this chapter, multi-objective optimisation techniques are implemented in a practical setup. The aim is to control charging and discharging of storage assets in a micro-grid. This is done by developing an agent/controller that receives measurements from the elements of the micro-grid, and based on the status of the micro-grid, controls the storage. Since this framework was implemented in a laboratory setup without any commercial electric vehicles, stationary battery storage modules were used, and will be designated as EV hereafter. As the objective is to control hardware in a lab experiment, real-time or online, control algorithms will be developed. This approach differs from that of Chapter 6 where day-ahead scheduling was implemented. The approach was deterministic, where all the information was known ahead to time. In this new context, only measurements of the status of the system are available and future status unknown. Therefore, the forecasting techniques developed in Chapter 3 will provide additional information that will estimate the future state of the system. In addition, decisions on the optimal scheduling will have to be implemented within a fixed period as the optimisation window is discretised in fixed steps. A schematic illustration of the scheduling flow is provided in Figure 7.1-1.

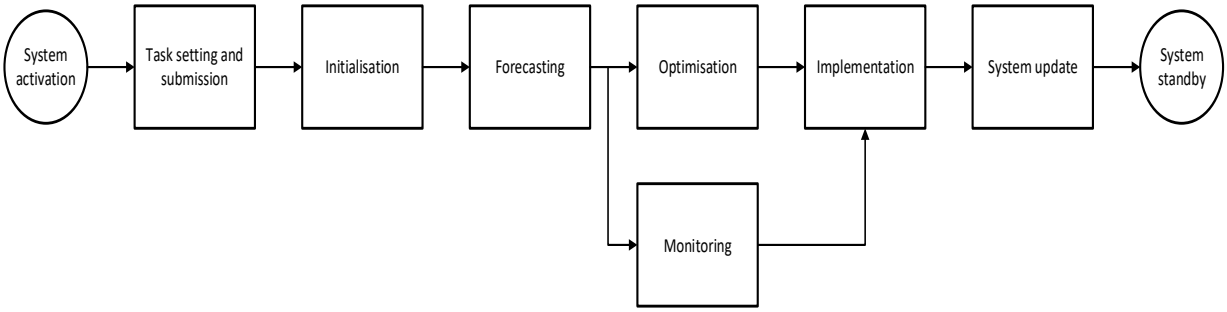

Figure 7.1-1 Flow diagram for real-time scheduling of a micro-grid

The real-time smart control system is initiated by the user as the proposed method is based on the consensus of the EV user. This is aligned with the approaches available in real-life [137], where upon arrival, the EV user plugs the car in the charger. Then they communicate the time for the next departure and the minimum level of energy they require. In this research this information is provided through a graphical user interface (GUI) developed with the

MATLAB 2018a software. The EV user also specifies their priorities for three objectives, namely, energy cost, battery degradation and grid impact. Based on the demands of the EV user a charging task is built and submitted to the system. The system is then initialised by measuring its initial status, which is made by the following information:

- Battery minimum voltage
- Battery maximum voltage
- Battery initial voltage
- Time at initiation
- Wholesale electricity price (known one day ahead)
- Electricity demand (forecasted with the method in chapter 3.3.2).

The PV generation is then forecasted for the rest of the day based on an ANN, as described in Section 3.3. The charging task and the associated predicted parameters are submitted to a real-time optimisation process aimed at controlling EV charging by calculating the trade-off between cost, degradation and grid impact and applying a prioritisation rule based on the decision made by the user; more details are provided in the next Section. The optimal charging schedule is communicated to the charging infrastructure, which then executes the charging task. Voltage, current, power and energy exchanged with the battery are constantly monitored throughout the whole task, and data is continuously logged to allow post processing. Once the charging deadline has been reached, the system goes in standby. A functional diagram describing the elements of the micro-grid, the information flow is presented in Figure 7.1-2.

The experimental setup contains a number of hardware that together emulate a “micro-grid” (MG). An Arduino UNO board is used to communicate the optimal charging schedule to the battery charger, which then implements the charging/discharging command. Table 7.1-1 provides a summary of the main specifications of the components in the experiment setup.

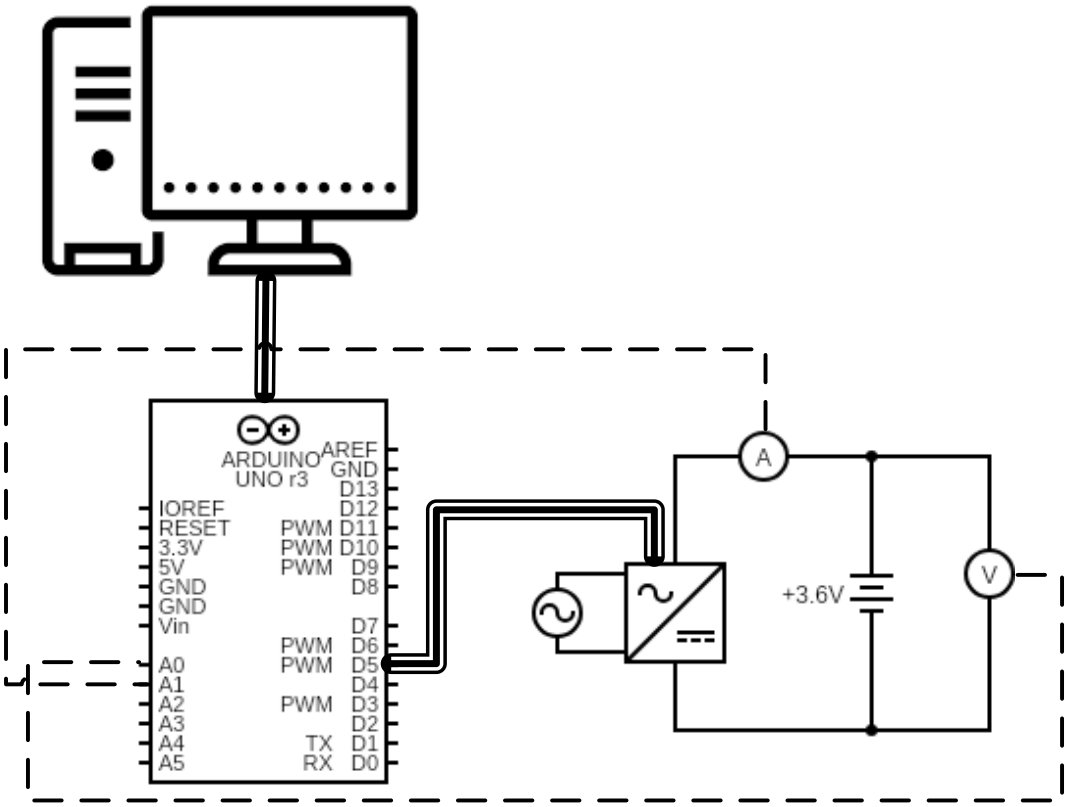

Figure 7.1-2 Real-time multi-objective optimisation implementation setup

Voltage and current measurements (dashed lines in Figure 7.1-2) are taken to capture the battery's status and sent to the Matlab code (wide communication bus). For voltage measurements, the Arduino measurement system was used while current measurements were taken with two N2774A current probes (shown in Figure 7.1-4). The online multi-objective dynamic programming (OMODP) algorithm is run in Matlab and the optimal schedule is communicated to the Arduino board, which transfers it to the charger. The battery charger (AC/DC converter in Figure 7.1-2) was developed by Doshisha University [138] and was lent to Northumbria University for testing. Two current probes have been used to measure positive and negative currents as they only capture currents in the positive direction. An image of the charger is shown in Figure 7.1-3.

Table 7.1-1 Main specifications of MG components

Photovoltaic system	
Simulated 4kWp	
Battery system	
Parameter	**Value**
Technology	Lithium-Ion
Capacity	3.2 Ah
Internal resistance	60 mΩ
Maximum voltage	4.2 V
Minimum voltage	3 V
Battery charger	
Parameter	**Value**
Maximum power	27 W
Maximum voltage	9 V
Maximum current	3 A
Measurements	Voltage, current
Desktop computer	
Parameter	**Value**
Processor	AMD PRO A4-350B R5 3500MHz
RAM	8 GB
Software	Matlab 2018a
Communication	Serial
Arduino Uno R3	
Analog measurements	A_0 voltage, A_1 charging current, A_5 discharging current and D_5 control signal
Measurements	
Current measurements	2xAgilent N2774A current probes

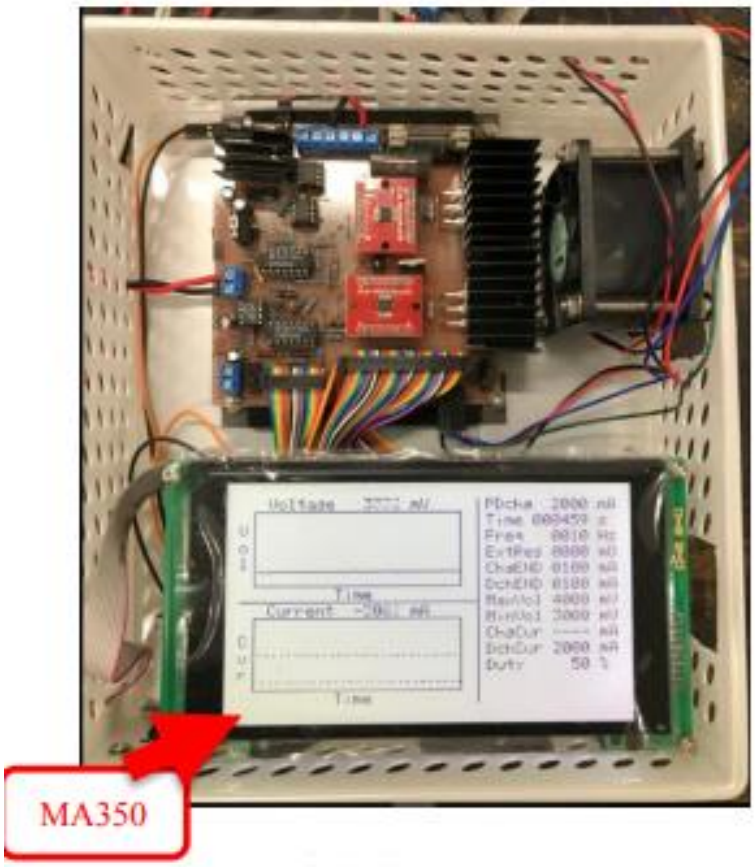

Figure 7.1-3 Bidirectional battery charger

Figure 7.1-4 Agilent current measurement probe

Although the charger is bidirectional, it is not regenerative, which means that the discharged energy is not sent back to the grid but dissipated in the form of heat with the heat sinks, shown in Figure 7.1-3. For this reason, the objective of this chapter is to emulate a MG as often a real MG has a higher rating and is grid-connected. Nevertheless, the proposed algorithm can be easily coupled with a bidirectional regenerative charger, in a MG at any rating, which would then implement real V2G. Furthermore, the Arduino Uno board uses a pulse-width-modulation (PWM) signal to recreate an analogue output, which is not ideal as a regulation/control signal to command the charging/discharging current, as the actual current will oscillate between the maximum value (positive or negative) and zero. To extract only the analogue modulating signal from the PWM, a low pass filter has been employed, which schematic is shown in Figure 7.1-5.

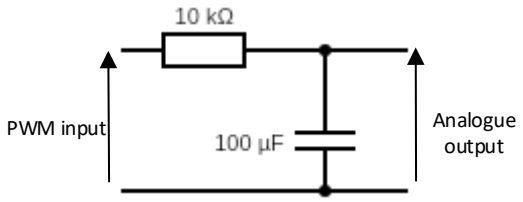

Figure 7.1-5 Low pass filter

As aforementioned, a charging task is built with the information provided by the user through the desktop computer. The list of information required to process the charging task with real-time MOO is provided in Table 7.1-2.

Table 7.1-2 Information provided by the user for MOO

Time of availability	Year-month-day hour:minute (yyyy-mm-dd HH:MM)
Time of next departure	Year-month-day hour:minute (yyyy-mm-dd HH:MM)
Maximum battery energy	Wh
Required energy at departure	Wh
Efficiency of charging/discharging process	%
Priorities of three objectives	Energy cost, battery degradation, grid

This information is then processed and is passed to the next steps, as described Figure 7.1-1. In this work, three main algorithms, fulfilling different tasks, are proposed to effectively control EV charging, and these are:

1) Real-time multi-objective optimisation process based on online multi-objective dynamic programming (OMODP)
2) Adaptive state-of-health estimation algorithm based on particle swarm optimisation
3) Equivalent circuit estimation algorithm based on particle swarm optimisation.

Among the three methods, OMODP performs the principal task of implementing an optimal charging/discharging scheduling, while the latter two modules, inform OMODP on the battery status, hence enabling a more effective scheduling process. It should be noted that this is a modular architecture, where the three modules can be enabled and disabled without compromising the operation of the overall system. This is a crucial feature, as these three algorithms require different computation time, with the latter two being slower than OMODP due to the PSO algorithm. Since the PSO algorithm is a meta-heuristic method its computational burden is significant, as discussed in chapter 5. An efficient parallel computation schedule should be developed to effectively allocate these different tasks, without hindering the operation of the system. In fact, optimal scheduling can be implemented in real-time without simultaneously estimating the battery parameters. In this chapter, the OMODP algorithm will be investigated and an algorithm will be proposed. The algorithms for battery state estimation have been presented in Chapters 4.2.1 and 4.3.1. Although these two modules can be implemented along with OMODP by implementing parallel computing techniques, the latter will require significant time invested purely to draft the code in the Matlab programming language. Due to time limitation, in this research, the validity of OMODP will be proved through experiments, while the battery state estimation algorithms will be validated as a future work. A comprehensive set of experiments implementing different scenarios will be implemented in the experimental setup to validate the effectiveness of OMODP.

7.2 Design of a real-time controller based on Multi-objective dynamic programming

In this Section, the main algorithm for implementing real-time multi-objective optimal scheduling of EV charging/discharging will be discussed. Based on the method proposed in Chapter 6 one could implement the same algorithm with a moving horizon, which is also known as model predictive control (MPC) [154] (as has been implemented in Chapter 6.3.1). Under MPC, measurements of the state of the system under control are taken at the current time-step t, and prediction techniques are used to anticipate the next states within a limited time-horizon $[t, t+T]$. A cost-function is then minimised over the time-horizon to determine the optimal control strategy. Only the action from the current time-step of the control strategy is applied, the time horizon moves to $[t+\Delta t, t+\Delta t+T]$ and measurement and calculations are repeated for the new horizon. The sampling rate adopted for the experiments is 15 minutes based. The main drawback of this approach is the computational burden; for a time-horizon composed by n time-steps, the entire optimisation algorithm is run n times. Consequently, if the state of the system at each time-step of the time horizon is represented by one variable, the optimisation algorithm will have n decision variables (one variable for each time step), and it will be run n times (to update the available information on electricity demand with new measurements). In the specific case of the ANEC algorithm, the computational cost and time depends on the desired resolution of the Pareto front. Having divided the range of values of two objective functions in l and m parts respectively, the optimisation framework is run $l \times m$ times, with constraints being systematically adjusted to limit the feasible space. Furthermore, as the feasible space is constrained towards the minima of the objective functions, the computational time for each calculation will increase. If the energy/power service to be provided requires fast response from the storage assets, then such handling techniques may hinder the normal operation.

To overcome this practical barrier, we proposed a novel multi-objective optimisation algorithm based on dynamic programming (DP) [155]. DP is based on Bellman's principle of optimality [156]. With this approach, the cost function over a time-horizon is divided in sub-

cost-functions defined in each time step. In particular, with the forward induction approach, as the time-horizon advances, the cost function is calculated for each feasible current state and by taking into account the origin state from the previous time step. Ultimately, the optimal trajectory is built iteratively by considering the current and the previous time steps, from the initial state to the final one.

This method can be adapted to the optimal EV charging scheduling task. Upon plugging-in, the initial SOC of the EV is measured (S_A) and a desired SOC is considered as a target (S_B). Let us define the state of the EV at each time step by the discrete SOC of the EV battery, SOC_t^n. The letter n means that the range of SOCs, $[0, \dots, 1]$ has been divided in n steps, i.e. $\mathrm{S}^n = [SOC^1, \dots, SOC^n]$, hence, the SOC at each time-step can only assume one among these n values. At each time-step t, a set of feasible EV states will be considered by the algorithm, defined as F_t^n. Similarly, the set of all root states (states at the previous time step), is F_{t-1}^n. Where:

$$\mathrm{F}_t^n = \left\{ SOC_t^i \in \mathrm{S}^n \middle| \frac{\left|SOC_t^i - SOC_{t-1}^j\right|}{\Delta t} \leq \overline{P_{EV}} \ \cap \ \begin{pmatrix} SOC_t^i \leq S^B + \frac{(T-t)\overline{P_{EV}}}{\Delta t} \\ SOC_t^i \geq S^B - \frac{(T-t)\overline{P_{EV}}}{\Delta t} \end{pmatrix}, \ \forall i, j \right\} \subseteq \mathrm{S}^n \tag{7.1}$$

is the set of feasible EV states at time-step t, such that the maximum SOC variation, from all possible root-SOCs and the desired SOC, is limited by the charger's rating, $\overline{P_{EV}}$. T is the number of time-steps from arrival to departure and S^B is the desired SOC at departure.

Figure 7.2-1 graphically illustrates provides a graphical explanation of the above concept. As time progresses, the set of feasible steps is updated based on the rating of the charger as well as the number of time steps to the next departure. When the next departure time comes, i.e. $T = t$, the feasible set only contains one possible state, $SOC_t^i = S^B$.

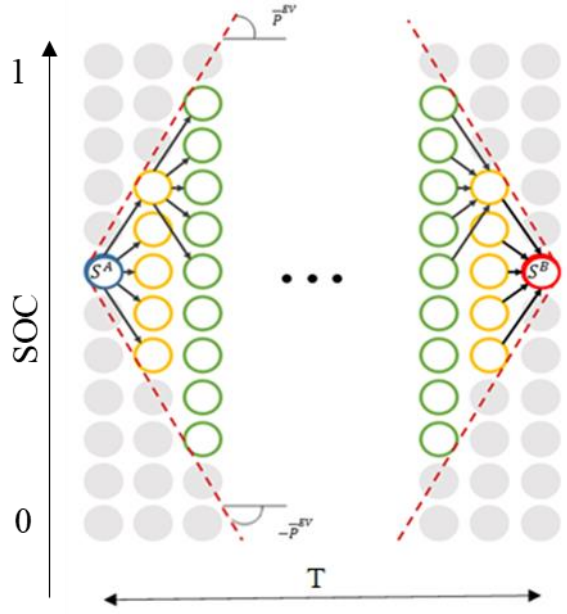

Figure 7.2-1 Illustration of SOC states and feasible set

At each time-step t, the optimal SOC state is chosen in order to minimise the objective function in all the previous and current feasible states, as detailed in the following equation

$$\underset{soc_{t-1}^{i}\in \mathrm{F}_{t-1}^{n}, soc_{t}^{j}\in \mathrm{F}_{t}^{n}}{\operatorname{argmin}} \mathbb{F}\left(SOC_t^i\right) + \mathbb{F}(SOC_t^j), \forall i,j \tag{7.2}$$

As the basic DP strategy has intrinsic shortcomings (discussed below), we further adapt this approach to suit a multi-objective formulation. In fact, DP explores the full search space by comparing every possible combination of states, from the beginning state to the final state. This is a nearly exhaustive search (only the limitation of the feasible states given by the maximum power exchange, as shown in Figure 7.2-1 reduces the number of computations) and is notably demanding in computation effort. As in MOO a Pareto front must be found, which may contain several optimal solutions at each time-step, a pure DP approach would exacerbate the computation time required to evaluate all possible Pareto options. To overcome this obstacle we propose some improvements to the basic DP approach. It is worth pointing out that an effective solution to real-time MOO based on DP is yet to be proposed in literature. In fact, the methods proposed in literature are deterministic and cannot deal with the uncertain nature of many systems in real-life (as it is the case for PV generation) [157], [158]. In this work, we propose an OMODP approach, which makes use of predictions of PV

generation and electricity demand to schedule EV charging in real-time. Prediction of the electricity demand of a single household can be problematic but the method presented in chapter 3.3.2 can provide suitable predictions. The essential steps for OMODP are outlined hereby.

A) Prediction of PV generation and electricity demand

B) Prognostic optimisation for all the objectives using the current SOC state and the forecasts with a MPC approach to determine the SOC set-points for the next time step

C) Determine the range of SOCs by calculating the maximum and minimum SOC set points

D) Determine the feasible range of discretised SOCs by adjusting according to the desired final SOC

E) Calculate the objective functions for all the SOCs in the feasible range and the SOCs at the previous time step

F) Determine the new Pareto frontier.

The pseudo-code of OMODP is presented hereby.

OMODP

Input: predictions $P_2^{PV}, \dots, P_T^{PV}$, $P_2^d, \dots, P_T^d$, measurements P_1^{PV}, P_1^d, SOC^{in} , t^{dep}, SOC^{des}, objectives $\mathbb{F}^1, \dots, \mathbb{F}^m$ and user priorities $\pi^1, \dots, \pi^m$

1: **for** $t \leftarrow 1$ **to** (T) **do**

2: **Initialisation:** MPC optimisation $\begin{cases} \text{argmin}(\mathbb{F}^1) \\ \vdots \\ \text{argmin}(\mathbb{F}^m) \end{cases}$ to determine $\text{SOC}_t^1, \dots, \text{SOC}_t^m$

3: Define $\overline{\text{SOC}_t} = \max(\text{SOC}_t^k)$ and $\underline{\text{SOC}_t} = \min(\text{SOC}_t^k), k \in [1, \dots, m]$

Define feasible SOC range $\text{F}_t^n = \left\{ SOC_t^i \mid SOC_t^i \in \left[\underline{\text{SOC}_t}, \overline{\text{SOC}_t}\right] \cap \right.$

4: $\left. \begin{pmatrix} SOC_t^i \leq S^B + \frac{(T-t)\overline{P_{EV}}}{\Delta t} \\ SOC_t^i \geq S^B - \frac{(T-t)\overline{P_{EV}}}{\Delta t} \end{pmatrix} \right\}$ having divided the $\left[\underline{\text{SOC}_t}, \overline{\text{SOC}_t}\right]$ region in n

steps

5: **if** $t = 1$

6: Compute $\begin{cases} \mathbb{F}^1\left(SOC^{in}, SOC_t^i\right) \\ \vdots \\ \mathbb{F}^m\left(SOC^{in}, SOC_t^i\right) \end{cases}, \forall SOC_t^i \in \mathrm{F}_t^n$

7: **else**

8: Compute $\begin{cases} \mathbb{F}^1\left(SOC_{t-1}^j, SOC_t^i\right) \\ \vdots \\ \mathbb{F}^m\left(SOC_{t-1}^j, SOC_t^i\right) \end{cases}, \forall SOC_t^i \in \mathrm{F}_t^n, \forall SOC_{t-1}^j \in \mathrm{P}_{t-1}^n$

9: Apply non-dominated sorting to determine the Pareto frontier at t, P_t^n

10: **end if**

11: Apply AHP with $\pi^1, \ldots, \pi^m$ to choose $\{SOC_{t-1}^*, SOC_t^*\}$

12: $\begin{cases} P_t^{EV} = \frac{SOC_t^* - SOC_{t-1}^*}{\eta^{ch}} \overline{E}^{EV} & , \boldsymbol{if}\ SOC_t^* - SOC_{t-1}^* \geq 0 \\ P_t^{EV} = \eta^{dis}\left(SOC_t^* - SOC_{t-1}^*\right) \overline{E}^{EV} & , \boldsymbol{if}\ SOC_t^* - SOC_{t-1}^* < 0 \end{cases}$

13: Measure battery voltage V_t^{EV}

14: Calculate current set-point $I_t^{EV} = \frac{P_t^{EV}}{V_t^{EV}}$

15: **end for**

The algorithm requires predictions for the future PV generation and electricity demand, current measurements of PV generation and demand, the objectives to be optimised as well as the requirements for the next departure and priorities of the objectives from the user. In accordance with the next departure, the number of optimisation time-steps is defined and initial predictive optimisations are carried out with MPC. Under this approach, the generation and demand measurements along with predictions over the time horizon are used to determine three SOC set points. The maximum and minimum of these set points constitute the boundaries to constrain the DP method. Once the feasible region has been defined with MPC, DP is implemented to calculate the values of the different objectives in correspondence to all the SOC states in the feasible region. Non-dominated sorting is then carried out to find the Pareto efficient solutions. As described in Section 5.3.1, AHP is implemented to choose a global optimal solution in line with the user priorities. The associated charging/discharging power is calculated by considering the efficiency of the charging/discharging process.

Finally, an optimal current set point is communicated to the bidirectional charger by dividing the power value by the measured battery voltage.

This algorithm has been implemented for real-time control of EV charging, under three cases, representing three different priority choices as will be presented in Section 7.4.

7.3 Graphical user interface

The technique proposed in this chapter serves as a consensus based optimisation approach, where a virtual agent manages the energy/power exchanges in micro-grid in accordance with the user's requirements. A graphical user interface (GUI), developed with the MATLAB 2018a software is used to collect the information necessary to build a charging task. Figure 7.3-1 provides an overview of the GUI.

There are four Sections in the GUI, starting from the User input, where the user can set the charging requirement and the departure time as aforementioned. The scheduling info, such as the electricity demand profile (blue, solid curve), the PV generation (blue, dashed curve), the wholesale electricity price (red, dashed curve) and the current charging/discharging power (blue stems) is depicted in a graph, that is updated each time a new charging/discharging command is issued. Battery measurements, such as battery voltage (blue, diamond shaped scatter), current (blue, circle stems) and capacity (red bars), are taken every minute and displayed in a graph. Any message that informs the user of the status is printed in the dedicated Section of the GUI.

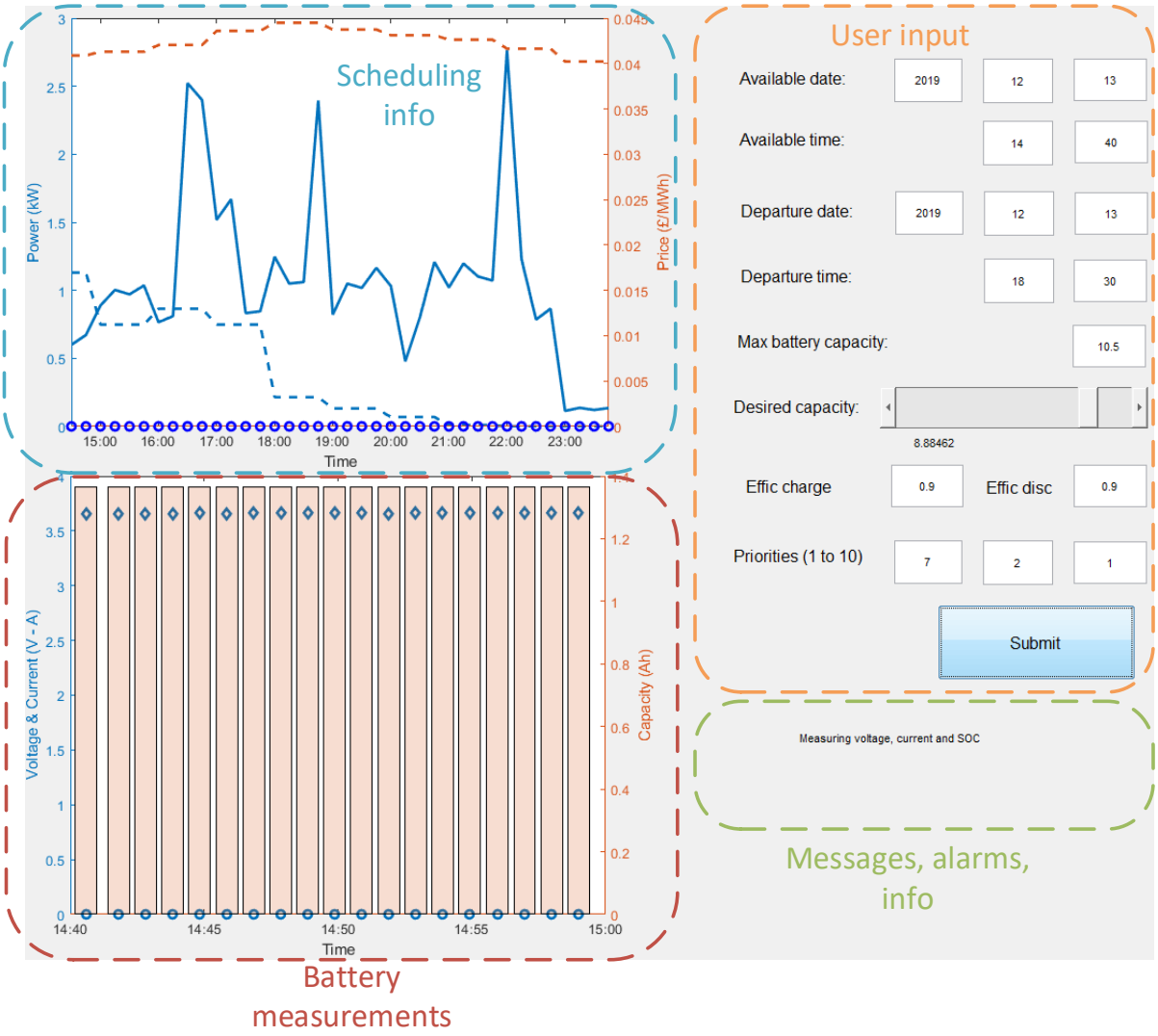

Figure 7.3-1 Graphical user interface to control charging in real-time

In this prototype, the plug-in time can be scheduled to any future time (compared to the task submission time) in accordance to user's availability. Then, departure time, battery maximum energy and required energy must be provided. The charging and discharging efficiency of the battery charger is specified along with the priorities of three key objectives: energy cost, battery degradation and grid impact. The charging task is then submitted to the virtual agent (OMODP) which decides the optimal charging set point and communicates it to the Arduino board controlling the charger, which finally implements the charging task.

7.4 Functional demonstration experiments

To test the validity and operability of the proposed algorithm three case studies have been performed in real-time. The main difference between the three cases are the priorities along the three objectives, the required charge specified by the user, and different demand, generation and price profiles. The details of the three case studies are shown in Table 7.4-1.

Table 7.4-1 Details of the case studies

Parameters	**Case study 1**	**Case study 2**	**Case study 3**
Objective priorities [cost, battery, grid]	[7, 2, 1]	[2, 7, 1]	[1, 2, 7]
Available time (yyyy-mm-dd HH:MM)	2019-12-15 15:15	2019-12-16 10:35	2019-12-14 13:00
Departure time (yyyy-mm-dd HH:MM)	2019-12-15 21:15	2019-12-16 16:45	2019-12-14 19:00
Desired capacity at departure (Ah)	1.8	2.2	2.4

Figure 7.4-1 to Figure 7.4-6 depict the charging schedules and associated Pareto frontiers for the three case studies. In the first case, minimising energy cost, it could be seen that the battery is charged in correspondence of the minimum prices, in the availability window (6 hours, from 3 to 9) and during the period with high-energy price, no charging is initiated. However, it can be seen that the final capacity fell short of 0.2 Ah; this was due to the strict availability period (noticeable from the very limited number of Pareto efficient solutions in Figure 7.4-7.4-2), which meant that the EV left almost as soon as the price spike terminated, not leaving the algorithm enough time to catch the final schedule. This improvement constitutes future works. Also by looking at the Pareto frontiers in Figure 7.4-7.4-2, it could be seen that there was an overall agreement among the three objectives as in most of the time steps, the frontiers were only points.

By looking at the charging current in Figure 7.4-3, it can be seen that in order to minimise the average SOC, the battery is kept uncharged for as long as possible, with charging being initiated only after 2:30 pm. Looking at the Pareto frontiers in Figure 7.4-4, it could be seen that in accordance with the priorities specified, only the solutions characterised with the minimum battery degradation have been issued in the form of charging schedules.

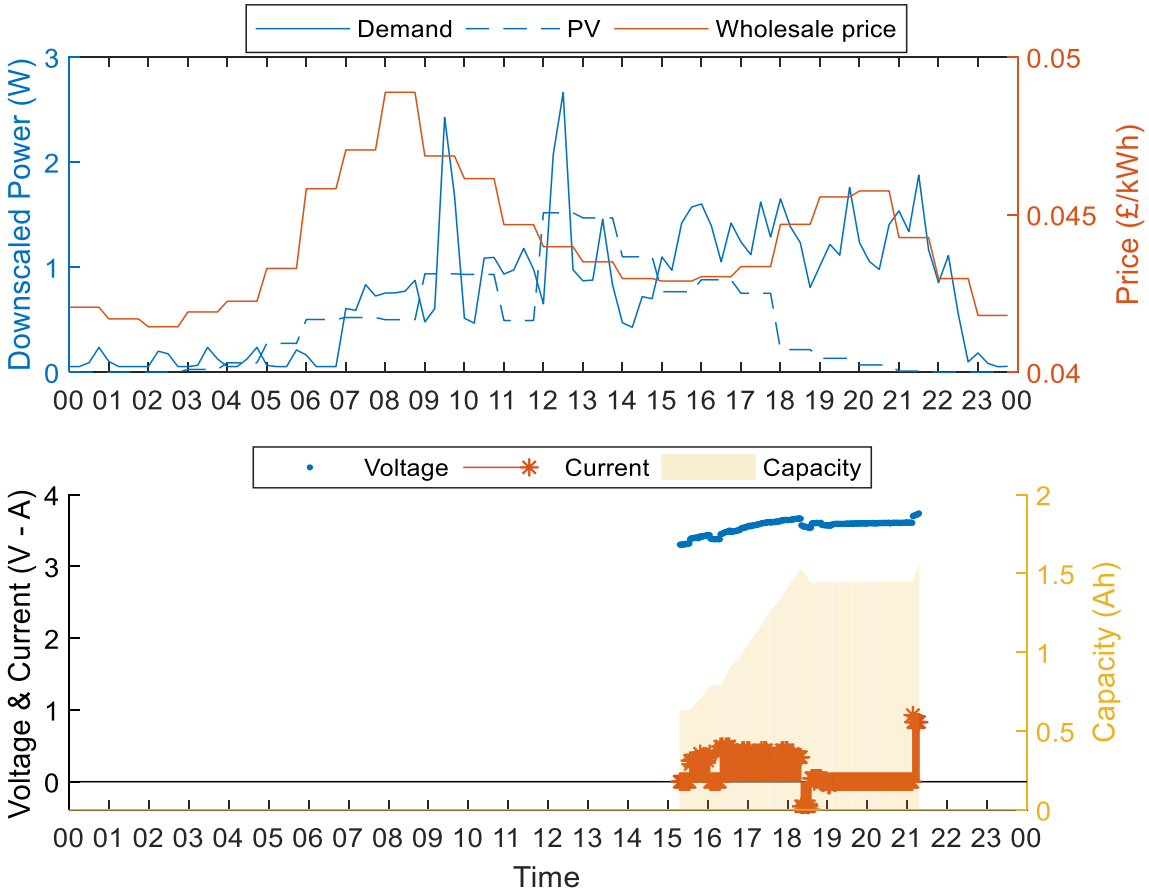

Figure 7.4-1 Real-time charging profile for case study 1

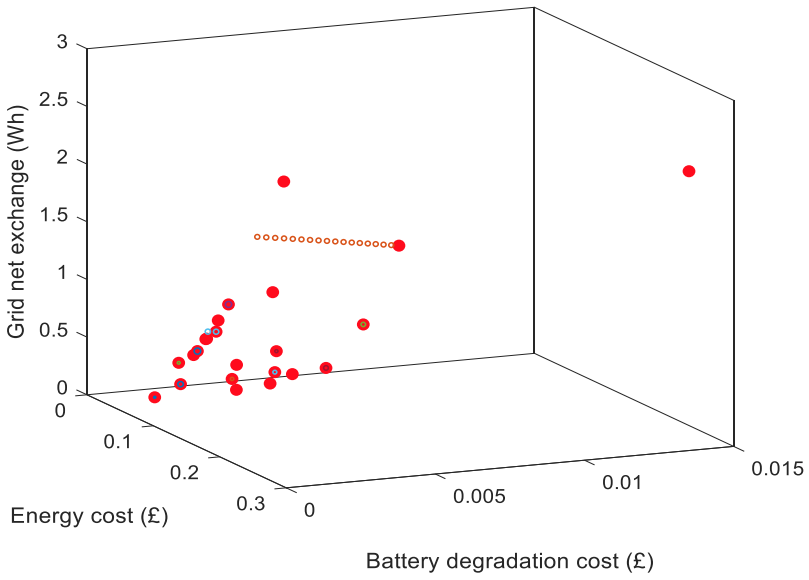

Figure 7.4-7.4-2 Pareto frontiers and chosen solutions in case study 1 (filled dots are the chosen solutions for each time step, empty dots are the Pareto optimal solutions for each time step)

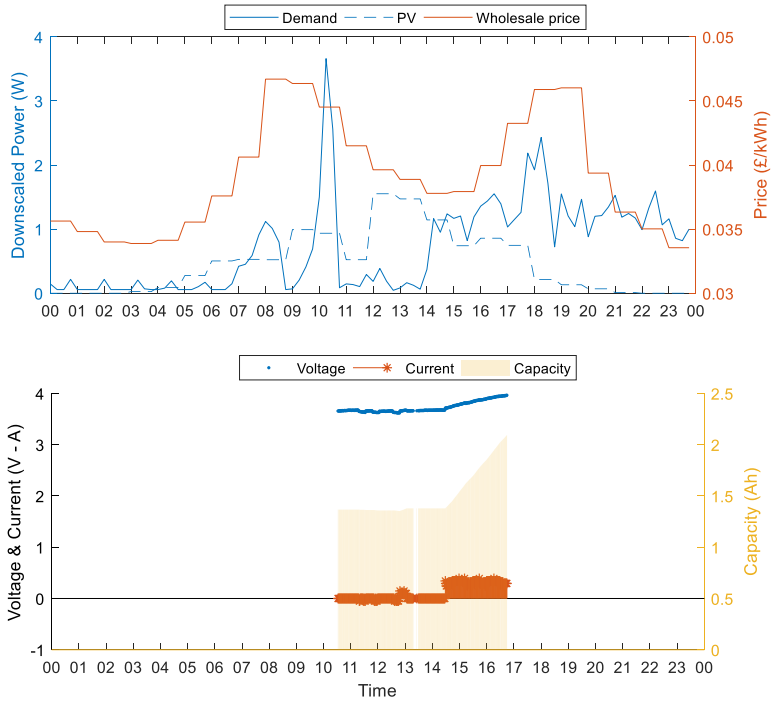

Figure 7.4-3 Real-time charging profile for case study 2

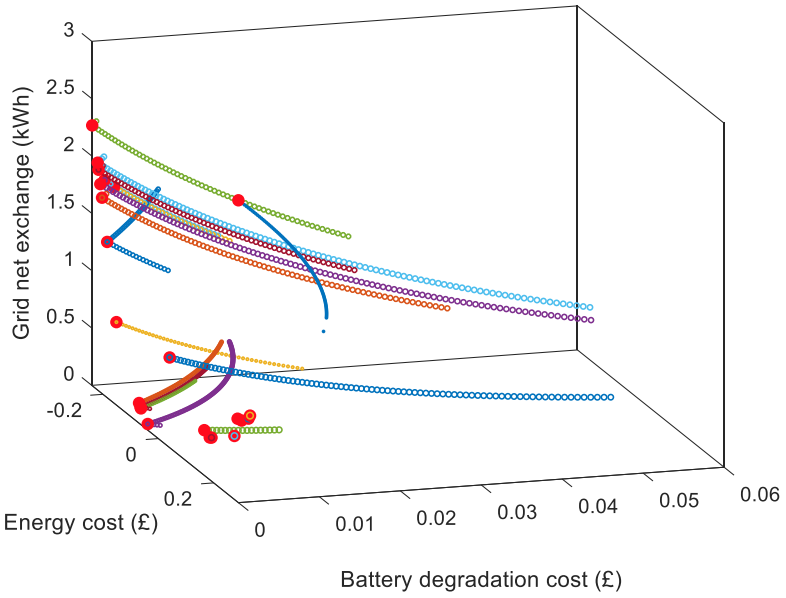

Figure 7.4-4 Pareto frontiers and chosen solutions in case study 2 (filled dots are the chosen solutions for each time step, empty dots are the Pareto optimal solutions for each time step)

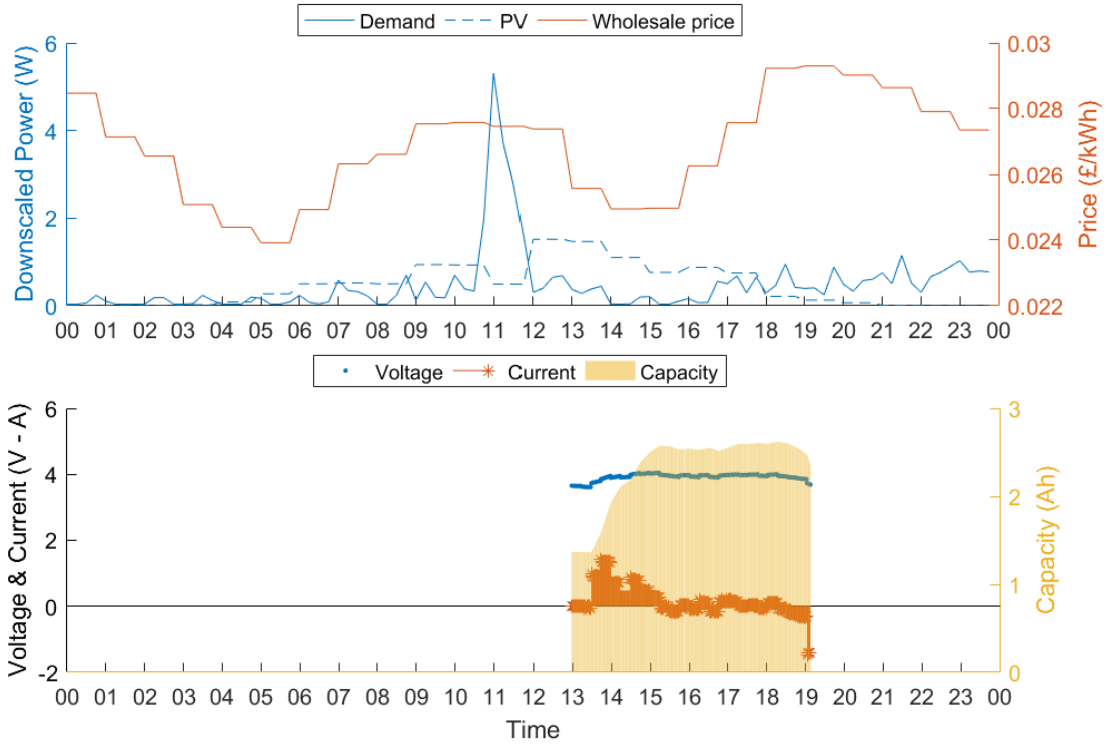

Figure 7.4-5 Real-time charging profile for case study 3

As can be seen, EV charging is scheduled between 13:00 to 19:00 hrs in accordance with the availability specified by the user. At 13:30 hrs there is availability of excess PV generation, since the electricity demand is low, hence the EV is charged, while following the PV generation profile. Charging power is reduced after 3 as the battery exceeds the capacity requested by the user (2.44 Ah). After that moment, the battery is subject to shallow charge and discharge cycles, while following the shape of the electricity demand. After 18:00 hrs the electricity demand is higher than the available PV energy (which is almost negligible), therefore the battery is discharged to provide the demand making use of the additional energy that was charged when PV energy was abundant. Overall, the battery was made available for 6 hours, which corresponds to 24 steps of 15 minutes each. OMODP generated a Pareto frontier for each of these time steps, which are shown in Figure 7.4-6 along with the chosen solutions (red dots).

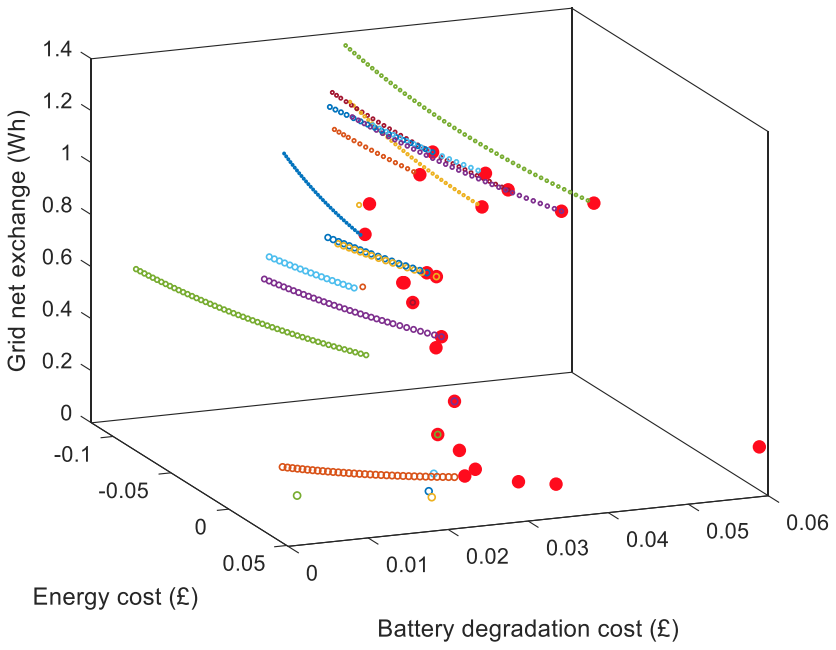

Figure 7.4-6 Pareto frontiers and chosen solutions in case study 3 (filled dots are the chosen solutions for each time step, empty dots are the Pareto optimal solutions for each time step)

It can be seen that OMODP always choses the solution that gives the lowest grid net exchange, in accordance with the priorities set in Table 7.4-1. In addition, it can be noticed

that the Pareto frontiers do not contain the same number of efficient solutions. This is because, the predictive optimisations (see the OMODP algorithm in Section 7.2) and the constraint on requested energy bound the SOC swing allowed by the algorithm (the final steps have only few Pareto members because the algorithm is reaching the required SOC target).

7.5 Comparison between OMODP and ANEC

In this section, the ANEC algorithm and the OMODP method are compared for a generic real-time operation. As the ANEC algorithm is a day-ahead algorithm, it has been adapted to real-time operation with the rolling-window approach described in chapter 7.2. It should be noted that the tested system comprises of a signle household with one EV (30 kWh) and a PV system (4 kWp). The highest priority has been given to the energy cost factor, hence the algorithm that will achieve the lowest cost (highest revenue) in the least amount of time, will be the most suitable for real-time optimisation.

Figure 7.5-1 and Table 7.5-1 present the results for case 4, where the OMODP algorithm has been tested against an established method, like ANEC.

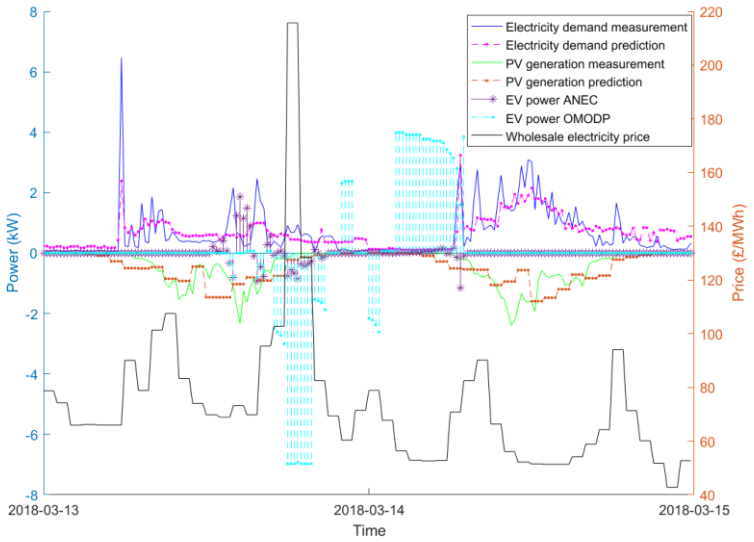

Figure 7.5-1 Comparison between OMODP and ANEC profiles for a generic real-time operation case

Table 7.5-1 Comparison between OMODP and ANEC's performance along three objectives for case 4

Case study 4			
Algorithm	Energy cost (£)	Battery degradation (£)	Grid net exchange (kWh)
ANEC	-0.80	-0.041	67.49
OMODP	0.88	-0.195	230.86

It is evident from Figure 7.5-1 and Table 7.5-1 that the OMODP algorithm is more effective than ANEC in achieving the a lower energy cost, as it is the objective with the highest priority. In fact, OMODP is able to bring a revenue to the HMG owner. This comes at the expense of a higher battery degradation cost, which however is offset by the incurred revenues. It should also be pointed out that this was expected as the main priority was energy cost minimisation and a prioritisation rule that values battery degradation more can be easily set (see case 2). The ability of OMODP of achieving a lower energy cost lies in its capability of better exploring the search space than ANEC, as evidenced by Figure 7.5-2.

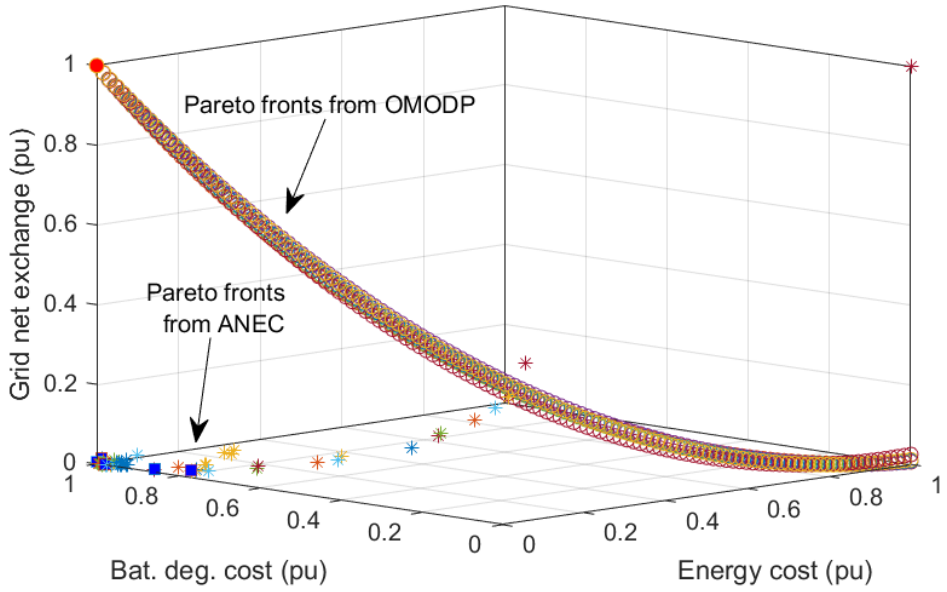

Figure 7.5-2 Comparison between the normalised dynamic Pareto fronts achieved with OMODP (Pareto optimal solutions are scatters and red dots are the chosen solution) and ANEC (Pareto optimal solutions are the asterisks and blue squares are the chosen solutions) for 6 arbitrary time steps.

When assessing the quality of the Pareto frontiers, the major advantage of OMODP lies quite evidently the diversity and regularity of the Pareto optimal solutions, which on the other hand is not achieved by ANEC frontiers. OMODP would therefore allow more flexibility to the decision maker who would be able to make a more informed decision than with ANEC.

Perhaps an even more compelling advantage of OMODP can be seen in Figure 7.5-3, where OMODP overwhelmingly outperforms ANEC in terms of computational time. In fact, in the beginning ANEC can take even more than 150 s to compute the Pareto front, while OMODP would always take less than 5 s. This was due to the inherent computational burden brought by the augmented ε-constraint algorithm implemented in ANEC, which exhibits a quadratic growth as the desired granularity of the Pareto frontier increases. OMODP on the other hand computes a more diverse Pareto front in a fraction of the time, because of the much simpler and more effective heuristic used in evaluating the three objectives for regular SOC steps.

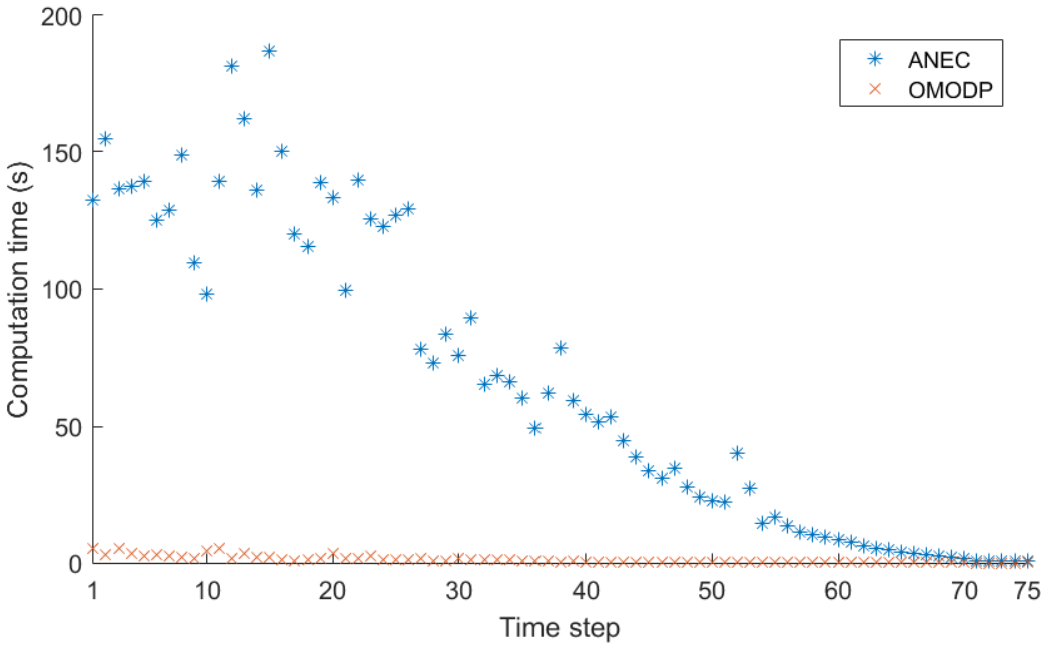

Figure 7.5-3 Comparison between the computational time of OMODP versus ANEC

7.6 Conclusions

In this chapter, a methodology for implementing real-time MOO has been proposed and implemented in an experimental setup. An improved version of the DP approach has been implemented by using predictive optimisation steps. Three cases, characterised by different priorities have been tested and the algorithm has scheduled the charging/discharging process of a battery by satisfying the set priorities. It has been shown that when scheduled to minimise cost, the algorithm avoids charging the battery at peak times and delays charging to periods with lower prices. On the other hand, when scheduled to minimise battery degradation, charging is delayed as close as possible to the departure time, in order to minimise average SOC and consequently minimising battery degradation. When the scheduling is aimed at grid net exchange minimisation, the battery is charged throughout the availability period in order to increase PV generation utilisation and provide the demand peaks. The proposed algorithm has been applied with a 15 minutes resolution but it is fast enough to provide charging schedules every minute. This however comes at the cost of lower accuracy characterised by discrete SOC states that are considered in the algorithm. The performance of the OMODP algorithm has been tested against ANEC, presented in chapter 5.3.1.1, and it has been demonstrated to be a superior method in terms of real-time operation and regularity of the Pareto frontier. The implementation of MOO in a practical experimental setup has been demonstrated, in order to optimise three objectives, energy cost, battery degradation and grid interaction. The results from the experiments demonstrated that the proposed framework can effectively optimise the aforementioned objectives while prioritising user requirements.

Chapter 8 Conclusions and future works

In this thesis we have developed mathematical optimisation algorithms to define EV charging/discharging schedules fulfilling multiple objectives. This particular branch of optimisation, as emphasised in the introduction, has attracted the attention of the research community due to the advent of mainstream electro mobility. This is mainly because, when EVs are to be integrated with RESs and the electricity network in real-life practices, a number of problems/objectives of disparate nature arise/must be fulfilled. These include i) economic objectives, such as energy cost minimisation; ii) technical objectives, i.e. optimal grid utilisation/operation and EV battery degradation minimisation; iii) environmental objectives, such as CO_2 emission minimisation and objectives that have social impact, i.e. EV acceptance. In this thesis, these objectives have been mathematically modelled as close as possible to the real-life phenomena.

In order to promote the adoption of electro mobility while ensuring their efficient integration, the users' transportation requirements must always be fulfilled as a prime priority. It has been shown that in the UK, on average, drivers cover less than 10 miles a day. This leaves a major opportunity to use the EV battery for energy/grid services under the condition that the users' requirements are not violated. To this end, a statistical model depicting vehicle utilisation patterns in the UK has been adopted.

It has been shown that the uncertainty of electricity demand utilisation in households and PV generation constitute a crucial matter when aiming to optimise EV charging. As a result, solutions including regression models, clustering methods and ANNs have been proposed.

Solutions to quantify grid impact of EV charging have been identified. It has been discussed that EVs can help in reducing the overall CO_2 emissions in households, by charging, when available, from PV, or charging in periods when the national electricity grid's CO_2 intensity is low. Ancillary service provision, i.e. frequency regulation, has been modelled as an additional source of income.

As lithium-ion batteries constitute the only energy source in (B)EVs, their optimal utilisation is of pivotal importance. To this end, measures to minimise battery degradation have been proposed in this thesis. Two mathematical models, namely a behavioural and a degradation model have been developed. The former depicts the dynamic behaviour of the battery in terms of the charging voltage and currents with an ECM. The latter models capacity fade due to both calendar and cycling degradation. As only cycling degradation is affected by V2G services, it has been considered as a key objective in the optimisation problems. As in the lifetime of the EVs, they will be subject to diverse utilisation patterns and different lithium-ion chemistries exhibit different behaviour, algorithms to extend these mathematical models in a dynamic and adaptive form have been proposed. These models achieve good accuracy when compared to laboratory and real-life measurements.

A mathematical multi-objective optimisation framework has been developed and adapted to the problem of optimal EV charging. It has been discussed that, depending on the scale and setup of the optimisation problem, the methods will need to be different. In fact, optimisation is carried out in a decentralised manner, data privacy is preserved and the computational burden is shared among the involved agents. On the other hand, the agents have limited knowledge of the overall system variables (and in the worst case none). Furthermore, a distinction between day-ahead optimisation and real-time optimisation has been made as in the latter case, the decision intervals are much shorter compared to the former setup.

To this end, the decentralised MOTEEO algorithm has been developed and implemented to three case studies and improvements along economic, technical and environmental objectives have been achieved when compared with single-objective optimisation. The critical aspect of benefit sharing has been highlighted: the stakeholder that is in charge of managing the

operational framework must ensure that the benefits (profits, cost savings) are fairly shared among the involved stakeholders to encourage participation in these practices. This is because the proposed methods are consensus based and the users' willingness to participate is essential for a successful implementation.

Addressing a wider perspective, a hybrid optimisation framework based on a game theoretical energy-trading system in a local market has been proposed in order to ensure profits/cost savings for the players and ensure optimal network operation. The NIRA algorithm has been implemented in a case study with 10 players (5 EVs and 5 ESSs) and the results demonstrate the capability of the proposed framework in achieving improved economic benefits and reduce network losses. However, as it has been discussed, the computational burden of this approach must be carefully dealt with, trying to simplify the optimisation problem whenever possible with linearization techniques or using meta-heuristic algorithms. Nevertheless, the proposed framework can be generalised to any other unit commitment problem, especially optimal EV charging scheduling.

Finally, a novel real-time optimisation algorithm based on OMODP has been developed and tested in three experimental cases. The measurements show that the algorithm is able to regulate the charging/discharging process in order to achieve three objectives, namely energy cost reduction, battery life improvement and grid net exchange minimisation.

In conclusion, this thesis has provided a range of mathematical models for representing smart grid elements and optimising their interactions in a multi-objective framework. To this end, it is recommended that the suitable approach should be based on the following criteria:

- *Scale:* depending on the number of users, the maximum demand and generation requirements centralised or decentralised can be implemented. This thesis has mainly focused on the latter; an immediate trade-off of these approaches lie in the limited knowledge sharing capability of these frameworks where the agents are unaware of system variables.

- *Type of operation*: it can be day-ahead or real-time optimisation, where the former has more flexible time constraints compared to the latter where decisions must be taken within predefined time limit.
- *Accuracy of the models*: depending on the required level of accuracy, the underlying mathematical models can be non-linear and non-convex. Especially battery degradation and game theoretical frameworks are highly complicated, as they model the interactions between several parameters/players, and if possible the mathematical models should be simplified as much as possible.
- *Available technology:* some of the algorithms developed in this thesis require high computational power. Therefore, for an effective implementation, suitable back office systems, cloud based systems and charging stations should be in place.

8.1 Future works

The methods presented in this thesis can be applied to a wide range of problems and can be extended to include additional phenomena among which some noteworthy ones are listed below:

Additional objectives such as grid stability, grid unbalance minimisation (in a three-phase unbalanced system), can be included in the optimisation framework.

The computational time of the proposed algorithms could be compared with the conventional optimisation strategies, such as genetic algorithm, ant-colony optimisation and distributed algorithms.

The interaction of the electrical system with CHP devices can be developed as an extension towards an integrated electrical and heating system.

References

[1] L. Filho, R. Kotter, “E-Mobility in Europe Trends and Good Practice”, Springer, 2015.

[2] http://www.eea.europa.eu/data-and-maps/indicators/transport-emissions-of-greenhouse-gases/transport-emissions-of-greenhouse-gases-6

[3] G. Putrus, E. Bentley, R. Binns, T. Jiang, D. Johnston, ‘Smart Grids: energising the future’, International Journal of Environmental Studies, Vol. 70, pp. 691-701, 2013.

[4] K. Handberg, G. Owen, ‘Electric Vehicles as Grid Support’, D. Beeton and G. Meyer (eds), Electric Vehicle Business Models. Global perspectives, pp. 129-146, 2015.

[5] Global EV Outlook 2017 - Two million and counting, International Energy Agency, Clean Energy Ministerial, 9 rue de la Fédération 75739 Paris Cedex 15, France.

[6] Western Power Distribution, Innovation, ‘Next Generation Networks: Vehicle to Grid Electric Nation’, November 2017.

[7] B. K. Sovacool, L. Noel, J. Axsen and W. Kempton, ‘The neglected social dimensions to a vehicle-to-grid (V2G) transition: a critical and systematic review’, Environmental Research Letters, January 2018.

[8] http://www.g4v.eu

[9] J. Tomić and W. Kempton, ‘Using fleets of electric-drive vehicles for grid support’, Journal of Power Sources, Vol. 168, pp.459-468, 2007.

[10] K. Mets, T. Verschueren, F. De Turck and C. Develder, "Exploiting V2G to optimize residential energy consumption with electrical vehicle (dis)charging," 2011 IEEE First International Workshop on Smart Grid Modeling and Simulation (SGMS), Brussels, 2011, pp. 7-12.

[11] K. Li and K. J. Tseng, "Energy efficiency of lithium-ion battery used as energy storage devices in micro-grid," IECON 2015 - 41st Annual Conference of the IEEE Industrial Electronics Society, Yokohama, 2015, pp. 5235-5240.

[12] B. Elmegaard and W. Brix, “Efficiency of Compressed Air Energy Storage”, in The 24th International Conference on Efficiency, Cost Optimiztion, Simulation and Environmental Impact of Energy Systems, 2011.

[13] The Boston Consulting Group, Batteries for Electric Cars-Challenges, Opportunities, and the Outlook to 2020, 2009.

[14] M. Dubarry, A. Devie and K. McKenzie, “Durability and reliability of electric vehicle batteries under electric utility grid operations: Bidirectional charging impact analysis”, Journal of Power Sources, vol. 358, pp. 39-49, 2017.

[15] ‘Future Energy Scenarios’, National grid ESO, July 2019.

[16] A. Dubey and S. Santoso, “Electric Vehicle Charging on Residential Distribution Systems: Impacts and Mitigations,” IEEE Access, Vol. 3, pp. 1871–1893, 2015.] [Ir. P. Van Den Bossche, “Conductive Charging Standardisation Issues”, University of Brussel, 2003. http://etec.vub.ac.be/publications/evs17vdb.pdf

[17] https://www.gridwatch.templar.co.uk/download.phphttps://www.ofgem.gov.uk/ofgem-publications/76160/13537-elecgenfactsfspdf

[18] IEA Renewables 2019 Global Status Report https://www.ren21.net/wp-content/uploads/2019/05/gsr_2019_full_report_en.pdf

[19] Feed-In Tariff (FIT) rates, [online] Available at: https://www.ofgem.gov.uk/environmental-programmes/fit/fit-tariff-rates?page=3#block-views-publications-and-updates-block

[20] Solar photovoltaic (PV) cost data, [online] Available at: https://www.gov.uk/government/statistics/solar-pv-cost-data]

[21] UK solar beyond subsidy: the transition, Renewable Energy Association, July 2015.

[22] Solar photovoltaics deployment, [online] Available at: https://www.gov.uk/government/statistics/solar-photovoltaics-deployment

[23] https://www.ofgem.gov.uk/environmental-programmes/fit/fit-tariff-rates

[24] J. A. Gimeno, E. Llera and S. Scarpellini, “Investment Determinants in Self-Consumption Facilities: Characterization and Qualitative Analysis in Spain”, Energies, vol. 11, 2018.

[25] B. Lee, M. Lapides, P. Archambault, I. Matsuhashi, R. Koort, M. Sugiyama, “The Great Battery Race Framing the Next Frontier in Clean Technology – Electrical Energy Storage”, Goldman Sachs, October 2015

[26] Electrifying insights: How automakers can drive electrified vehicle sales and profitability, McKinsey&Company, January 2017. http://www.mckinsey.com/industries/automotive-and-assembly/our-insights/electrifying-insights-how-automakers-can-drive-electrified-vehicle-sales-and-profitability accessed 27 March 2017.

[27] B. Nykvist, M. Nilsson, Rapidly falling costs of battery packs for electric vehicles, Nature Climate Change 5, March 2015, pp 329–332 (2015).

[28] T. Randall, Here’s How Electric Cars Will Cause the Next Oil Crisis, Bloomberg, February 2016. https://www.bloomberg.com/features/2016-ev-oil-crisis/

[29] https://www.bbc.co.uk/news/uk-40726868

[30] https://www.mathworks.com/matlabcentral/fileexchange/47522-matlab-support-package-for-arduino-hardware

[31] A. Briones, J. Francfort, P. Heitmann, M. Schey, S. Schey and J. Smart, ‘Vehicle-to-Grid Power Flow Regulations and Building Codes Review by the AVTA’, Idaho National Laboratory, September 2012.

[32] https://www.ferc.gov/market-oversight/guide/glossary.asp.

[33] G. Fitzgerald, J. Mandel, J. Morris and H. Touati, “The Economics of Battery Energy Storage- How Multi-Use, Customer-Sited Batteries Deliver the Most Services and Value to Customers and the Grid”, Rocky Mountain Institute, October 2015.

[34] J. Geske and D. Schumann, “Willing to participate in vehicle-to-grid (V2G)? Why not!”, Energy Policy, vol. 120, 2018, pp. 392-401.

[35] L. Noel, G. Zarazua de Rubens, J. Kester and B. K. Sovacool, “Beyond emissions and economics: Rethinking the co-benefits of electric vehicles (EVs) and vehicle-to-grid (V2G)”, Transport Policy, vol. 71, 2018, pp. 130-137.

[36] S. Han, S. Han and K. Sezaki, "Economic assessment on V2G frequency regulation regarding the battery degradation," 2012 IEEE PES Innovative Smart Grid Technologies (ISGT), Washington DC, 2012, pp. 1-6, doi: 10.1109/ISGT.2012.6175717.

[37] A.De Los Rios, J. Goentzel, E. Nordstrom, C. W. Siegert, 'Economic Analysis of Vehicle-to-Grid (V2G)- Enabled Fleets Participating in the Regulation Service Market', Innovative Smart Grid Technologies (ISGT), IEEE, April 2012.

[38] A. Schuller, B. Dietz, C. M. Flath and C. Weinhardt, "Charging Strategies for Battery Electric Vehicles: Economic Benchmark and V2G Potential," in IEEE Transactions on Power Systems, vol. 29, no. 5, pp. 2014-2022, Sept. 2014, doi: 10.1109/TPWRS.2014.2301024.

[39] L. Agarwal, W. Peng and L. Goel, "Using EV battery packs for vehicle-to-grid applications: An economic analysis," 2014 IEEE Innovative Smart Grid Technologies - Asia (ISGT ASIA), Kuala Lumpur, 2014, pp. 663-668.

[40] W. Zeng, J. Gibeau and M. Chow, "Economic benefits of plug-in electric vehicles using V2G for grid performance-based regulation service," IECON 2015 - 41st Annual Conference of the IEEE Industrial Electronics Society, Yokohama, 2015, pp. 004322-004327, doi: 10.1109/IECON.2015.7392772.

[41] Y. Shirazi, E. Carr and L. Knapp, "A cost-benefit analysis of alternatively fuelled buses with special considerations for V2G technology", Energy Policy, vol. 87, pp. 591-603, 2015.

[42] D. Ciechanowicz, A. Knoll, P. Osswald and D. Pelzer, "Towards a Business Case for Vehicle-to-Grid-Maximizing Profits in Ancillary Service Markets", a book chapter in Plug-in Electric Vehicles in Smart Grids – Energy Management, Springer, pp. 203-231, 2015.

[43] Y. Zhao, M. Noori and O. Tatari, "Vehicle to Grid regulation services of electric delivery trucks: Economic and environmental benefit analysis", Applied Energy, vol. 170, 2016, pp. 161-175.

[44] C. Peng, J. Zou, L. Lian and L. Li, "An optimal dispatching strategy for V2G aggregator participating in supplementary frequency regulation considering EV driving demand and aggregator's benefits", Applied Energy, vol. 190, 2017, pp. 591-599.

[45] Y. Kuang, Y. Chen, M. Hu and D. Yang, “Influence analysis of driver behaviour and building category on economic performance of electric vehicle to grid and building integration”, Applied Energy, vol. 207, pp. 427-437, 2017.

[46] R. Gough, C. Dickerson, P. Rowley and C. Walsh, ‘Vehicle-to-grid feasibility: A techno-economic analysis of EV-based energy storage’, Applied Energy, Vol. 192, pp 12-23, January 2017.

[47] S. Tamura and T. Kikuchi, "V2G Strategy for Frequency Regulation Based on Economic Evaluation Considering EV Battery Longevity," 2018 IEEE International Telecommunications Energy Conference (INTELEC), Turin, 2018, pp. 1-6, doi: 10.1109/INTLEC.2018.8612431.

[48] J. Liu and C. Zhong, “An economic evaluation of the coordination between electric vehicle storage and distributed renewable energy”, Energy, vol. 186, 2019.

[49] U. Datta, N. Saiprasad, A. Kalam, J. Shi and A. Zayegh, “A price-regulated electric vehicle charge-discharge strategy for G2V, V2H, and V2G”, International Journal of Energy Research, vol. 43, 2019, pp. 1032-1042.

[50] J. Lassila, J. Haakana, V. Tikka and J. Partanen, "Methodology to Analyze the Economic Effects of Electric Cars as Energy Storages," in IEEE Transactions on Smart Grid, vol. 3, no. 1, pp. 506-516, March 2012.

[51] I.G. Unda. P. Papadopoulos, S. S. Kazakos, L. M. Cipcigan, N. Jenkins and E. Zabala, “Management of electric vehicle battery charging in distribution networks with multi-agent systems”, Electric Power Systems Research, vol. 110, pp. 172-179, 2014.

[52] T. Ma, O. A. Mohammed, ‘Economic Analysis of Real-Time Large-Scale PEVs Network Power Flow Control Algorithm With the Consideration of V2G Services’, IEEE Transactions on Industry Applications, Vol. 50, No. 6, December 2014.

[53] K. N. Kumar, B. Sivaneasan, P. H. Cheah, P. L. So and D. Z. W. Wang, "V2G Capacity Estimation Using Dynamic EV Scheduling," in IEEE Transactions on Smart Grid, Vol. 5, No. 2, pp. 1051-1060, March 2014.

[54] M. J. E. Alam, K. M. Muttaqi and D. Sutanto, "Effective Utilization of Available PEV Battery Capacity for Mitigation of Solar PV Impact and Grid Support With Integrated

V2G Functionality," in IEEE Transactions on Smart Grid, Vol. 7, No. 3, pp. 1562-1571, May 2016.

[55] K. Mets, T. Verschueren, W. Haerick, C. Develder and F. De Turck, "Optimizing smart energy control strategies for plug-in hybrid electric vehicle charging," 2010 IEEE/IFIP Network Operations and Management Symposium Workshops, Osaka, 2010, pp. 293-299.

[56] Y. Mu, J. Wu, N. Jenkins, H. Jia and C. Wang, “A Spatial-Temporal model for grid impact analysis of plug-in electric vehicles”, Applied Energy, vol. 114, pp. 456-465, 2014.

[57] R. Lamedica, S. Teodori, G. Carbone and E. Santini, “An energy management software for smart buildings with V2G and BESS”, Sustainable Cities and Society, Vol. 19, pp. 173-183, 2015.

[58] L. Drude, L. C. Pereira Junior and R. Rüther, “Photovoltaics (PV) and electric vehicle-to-grid (V2G) strategies for peak demand reduction in urban regions in Brazil in a smart grid environment”, Renewable Energy, Vol. 68, pp. 443-451, 2014.

[59] J. D. Fitzsimmons *et al.*, "Simulation of an electric vehicle fleet to forecast availability of grid balancing resources," 2016 IEEE Systems and Information Engineering Design Symposium (SIEDS), Charlottesville, VA, 2016, pp. 205-210.

[60] A. Y. S. Lam, K. C. Leung and V. O. K. Li, "Capacity Estimation for Vehicle-to-Grid Frequency Regulation Services With Smart Charging Mechanism," in IEEE Transactions on Smart Grid, Vol. 7, no. 1, pp. 156-166, Jan. 2016.

[61] Y. Wang and D. Infield, Markov Chain Monte Carlo simulation of electric vehicle use for network integration studies, International Journal of Electrical Power & Energy Systems, Vol. 99, pp. 85-94, 2018.

[62] Y. Wang, S. Huang and D. Infield, "Investigation of the potential for electric vehicles to support the domestic peak load," 2014 IEEE International Electric Vehicle Conference (IEVC), Florence, 2014, pp. 1-8.

[63] U. C. Chukwu and S. M. Mahajan, "V2G Parking Lot With PV Rooftop for Capacity Enhancement of a Distribution System," in IEEE Transactions on Sustainable Energy, Vol. 5, No. 1, pp. 119-127, Jan. 2014.

[64] E. Xydas, C. Marmaras, L. M. Cipcigan, A multi-agent based scheduling algorithm for adaptive electric vehicles charging, Applied Energy, Vol. 177, pp. 354-365, 2016.

[65] H. Xing, M. Fu, Z. Lin and Y. Mou, Decentralised Optimal Scheduling for Charging and Discharging of Plug-In Electric Vehicles in Smart Grids, in IEEE Transactions on Power Systems, Vol. 31, no. 5, pp. 4118-4127, Sept. 2016.

[66] G. Binetti, A. Davoudi, D. Naso, B. Turchiano and F. L. Lewis, Scalable Real-Time Electric Vehicles Charging With Discrete Charging Rates, in IEEE Transactions on Smart Grid, Vol. 6, no. 5, pp. 2211-2220, Sept. 2015.

[67] H. N. T. Nguyen, C. Zhang and M. A. Mahmud, Optimal Coordination of G2V and V2G to Support Power Grids With High Penetration of Renewable Energy, in IEEE Transactions on Transportation Electrification, Vol. 1, no. 2, pp. 188-195, Aug. 2015.

[68] M. Tavakoli, F. Shokridehaki, M. Marzband, R. Godina and E. Pouresmaeil, A two stage hierarchical control approach for the optimal energy management in commercial building microgrids based on local wind power and PEVs, Sustainable Cities and Society, Vol. 41, pp. 332-34, 2018.

[69] A. Zakariazadeh, S. Jadid and P. Siano, Multi-objective scheduling of electric vehicles in smart distribution system, Energy Conversion and Management, Vol. 79, pp 43-53, 2014.

[70] K. M. Tan, V. K. Ramachandaramurthy and J. Ying Yong, Optimal vehicle to grid planning and scheduling using double layer multi-objective algorithm, Energy, Vol. 112, pp. 1060-1073, 2016.

[71] W. Yao, J. Zhao, F. Wen, Z. Deng, Y. Xue, Y. Xu, and K. Meng, A Multi-Objective Collaborative Planning Strategy for Integrated Power Distribution and Electric Vehicle Charging Systems, in IEEE Transactions on Power Systems, Vol. 29, no. 4, pp. 1811-1821, July 2014.

[72] S. S. Amiri, S. Jadid and H. Saboori, Multi-objective optimum charging management of electric vehicles through battery swapping stations, Energy, Vol. 165, pp. 549-562, 2018.

[73] J. Li and M. A. Danzer, Optimal charge control strategies for stationary photoVoltaic battery systems, Journal of Power Sources, Vol. 258, pp. 365-373, 2014.

[74] M. J. Morshed, J. B. Hmida and A. Fekih, A probabilistic multi-objective approach for power flow optimization in hybrid wind-PV-PEV systems, Applied Energy, Vol. 211, pp. 1136-1149, February 2018.

[75] J. Li, X. Jin and R. Xiong, Multi-objective optimization study of energy management strategy and economic analysis for a range-extended electric bus, Applied Energy, Vol. 194, pp. 798-807, 2017.

[76] J. García-Villalobos, I. Zamora, K. Knezovic´ and M. Marinelli, Multi-objective optimization control of plug-in electric vehicles in low Voltage distribution networks, Applied Energy, pp. 155-168, 2016.

[77] M. Marzband, M. Javedi, S. A. Pourmousavi and G. Lightbody, An advanced retail electricity market for active distribution systems and home microgrid interoperability based on game theory, Electric Power Systems Research, Vol. 157, pp 187-199, 2018.

[78] H. K. Khanekehdani, M. M. Tafreshi, and M. Khosravi, "Modeling operation of electric vehicles aggregator in reserve services market by using game theory method", Journal of Renewable and Sustainable Energy, vol. 5, 2013.

[79] A. Evans, J. Commings, M. Slocombe and F. Corvaglia, National Travel Survey: England 2017, Department for Transport, July 2018. Accessed online 28/01/2019. Available at (https://assets.publishing.service.gov.uk/government/uploads/system/uploads/attachment_data/file/729521/national-travel-survey-2017.pdf).

[80] A. Cochero, "European electric vehicle fleet: driving and charging behaviours". Accessed online 28/01/2019. Available at (https://upcommons.upc.edu/bitstream/handle/2117/86393/Corchero_AEEE.pdf)

[81] T. Franke and J. F. Krems,'Understanding charging behaviour of electric vehicle users', Transportation Research Part F: Traffic Psychology and Behaviour, vol. 21, 2013, pp. 75-89.

[82] https://www.sciencedirect.com/topics/biochemistry-genetics-and-molecular-biology/gaussian-distribution

[83] https://www.sciencedirect.com/topics/materials-science/weibull-distribution

[84] N. Amjady, F. Keynia, "Short-term load forecasting of power systems by combination of wavelet transform and neuro-evolutionary algorithm", Energy, vol. 34, 2009, pp. 46-57.

[85] https://www.ofgem.gov.uk/ofgem-publications/57017/electricity-demand-profiles.xlsx

[86] E. McKenna and M. Thomson, High-resolution stochastic integrated thermal-electrical domestic demand model, Applied Energy, Vol. 165, pp. 445-461, 2016.

[87] H. Huang, Z. Xu, X. Shao, D. Wismeijer, P. Sun, J. Wang and G. Wu, "Multivariate linear regression analysis to identify general factors for quantitative predictions of implant stability quotient values", PLoS ONE, vol. 12, Oct 2017

[88] https://solcast.com/

[89] K. Y. Lee, Y. T. Cha and J. H. Park, "Short-term load forecasting using an artificial neural network," in IEEE Transactions on Power Systems, vol. 7, no. 1, pp. 124-132, Feb. 1992.

[90] A. Likas, N. Vlassis and J. J. Verbeek, "The global k-means clustering algorithm", Pattern Recognition, vol. 36, 2003, pp. 451-461.

[91] A.D. Sameer, A. Osama, A. Jehad and L. Mohamed, Assessment of Artificial Neural Networks Learning Algorithms and Training Datasets for Solar Photovoltaic Power Production Prediction, Frontiers in Energy Research, vol. 7, 2019, p. 130. DOI=10.3389/fenrg.2019.00130

[92] https://solcast.com/

[93] J. Benesty, J. Chen, Y. Huang and I. Cohen, "Pearson Correlation Coefficient", In: Noise Reduction in Speech Processing. Springer Topics in Signal Processing, vol 2. Springer, Berlin, Heidelberg, 2009.

[94] P.S.R. Murty, Chapter 13 - Graph Theory and Network Matrices, Electrical Power Systems, Butterworth-Heinemann,Pages 277-300, 2017.

[95] A. Monticelli, "Power Flow Equations". In: State Estimation in Electric Power Systems. Power Electronics and Power Systems. Springer, Boston, 1999.

[96] D. Parra, G. S. Walker and M. Gillott, "Modeling of PV generation, battery and hydrogen storage to investigate the benefits of energy storage for single dwelling", Sustainable Cities and Society, Vol. 10, 2014, pp. 1-10.

[97] A. Ben-Israel, "A Newton-Raphson method for the solution of systems of equations", Journal of Mathematical Analysis and Applications, vol. 15, 1966, pp. 243-252.

[98] N. Odeh, N. Hill and D. Forster, 'Current and Future Lifecycle Emissions of Key 'Low Carbon' Technology and Alternatives, Final Report, RICARDO-AEA, April 2013.

[99] http://gridwatch.co.uk/co2-emissions

[100] https://www.nationalgrideso.com/balancing-services

[101] https://www.nationalgrid.com/uk/electricity/balancing-services/frequency-response-services/firm-frequency-response?market-information

[102] S. Bashash, S. J. Moura, J. C. Forman, and H. K. Fathy, "Plug-in hybrid electric vehicle charge pattern optimization for energy cost and battery longevity," Journal of Power Sources, Vol. 196, pp. 541-549, 2011.

[103] http://physicsandsocietybc.files.wordpress.com/2013/04/meriampic.gif, Ed., 2013

[104] C. R. Birkl, M. R. Roberts, E. McTurk, P. G. Bruce and D. A. Howey, "Degradation diagnostics for lithium ion cells", Journal of Power Sources, Vol. 341, 2017, pp. 373-386.

[105] A. Ahmadian, M. Sedghi, A. Elkamel, M. Fowler and M. A. Golkar, "Plug-in electric vehicle batteries degradation modeling for smart grid studies: Review, assessment and conceptual framework", Renewable and Sustainable Energy Reviews, vol. 81, Part 2, 2018, pp. 2609-2624.

[106] M. Ouyang, X. Feng, X. Han, L. Lu, Z. Li and X. He, "A dynamic capacity degradation model and its applications considering varying load for a large format Li-ion battery", Applied Energy, vol. 165, 2016, pp. 48-59.

[107] D. Li, D. L. Danilov, B. Zwikirsch, M. Fichtner, Y. Yang, R. A. Eichel and P. H.L. Notten, "Modeling the degradation mechanisms of C6/LiFePO4 batteries", Journal of Power Sources, vol. 375, 2018, pp. 106-117.

[108] R. Xiong, L. Li, Z. Li, Q. Yu and H. Mu, "An electrochemical model based degradation state identification method of Lithium-ion battery for all-climate electric vehicles application", Applied Energy, vol. 219, 2018, pp. 264-275.

[109] S. Yang, Y. Hua, D. Qiao, Y. Lian, Y. Pan and Y. He, "A coupled electrochemical-thermal-mechanical degradation modelling approach for lifetime assessment of lithium-ion batteries", Electrochimica Acta, vol. 326, 2019.

[110] S. Saxena, Y. Xing, D. Kwon, M. Pecht, "Accelerated degradation model for C-rate loading of lithium-ion batteries", International Journal of Electrical Power & Energy Systems, vol. 107, 2019, pp. 438-445.

[111] K. Uddin, T. Jackson, W. D. Widanage, G. Chouchelamane, P. A. Jennings, J. Marco, “On the possibility of extending the lifetime of lithium-ion batteries through optimal V2G facilitated by an integrated vehicle and smart-grid system”, Energy, Vol. 133, pp. 710-722, 2017.

[112] G. Duleep, H. Van Essen, B. Kampmann, M. Grunig, "Assessment of electric vehicle and battery technology.," CEDelft 2011.

[113] J. Schmalstieg, S. Kabitz, M. Ecker, D.U. Sauer, " From Accelerated Aging Tests to a Lifetime Prediction Model: Analyzing Lithium-Ion Batteries," EVS27, Barcelona, Spain, 2013.

[114] J. Vetter, P. Novák, M. R. Wagner, C. Veit, K. C. Möller, J. O. Besenhard, M. Winter, M. Wohlfahrt-Mehrens, C. Vogler, and A. Hammouche, "Ageing mechanisms in lithium-ion batteries," Journal of Power Sources, Vol. 147, pp. 269-281, 2005.

[115] ZERO, "Taking Charge: Introducing Fast Chargers in Norway," Zero Emission Resource Organisation, Oslo, 2010.

[116] B. Lunz, H. Walz, D. U. Sauer, "Optimizing vehicle-to-grid charging strategies using genetic algorithms under the consideration of battery aging," 2011 IEEE Vehicle Power and Propulsion Conference, Chicago, IL, 2011, pp. 1-7.

[117] S. B. Peterson, J. Apt, J.F. Whitacre, “Lithium-ion battery cell degradation resulting from realistic vehicle and vehicle-to-grid utilization”, Journal of Power Sources, Volume 195, Issue 8, 2010, pp. 2385-2392.

[118] G. Lacey, G. Putrus and E. Bentley, Smart EV charging schedules: supporting the grid and protecting battery life, in IET Electrical Systems in Transportation, Vol. 7, no. 1, pp. 84-91, 3 2017.

[119] G. Ning, R. E. White, B. N. Popov, "A generalized cycle life model of rechargeable Li-ion batteries", Electrochimica Acta, Volume 51, Issue 10, 2006, pp. 2012-2022.]

[120] J. Wehbe, N. Karami, Battery Equivalent Circuits and Brief Summary of Components Value Determination of Lithium Ion, a review, 3rd Conference on Technological Advances in Electrical, Electronics and Computer Engineering (TAEECE), 2015.

[121] G. Lacey, Evaluation of Lithium Ion Battery Degradation and the Implications for the Use of EV batteries in Providing Support to a Smart Grid, a Doctoral thesis, Northumbria University, March 2015.

[122] C. Iclodean et al 2017 IOP Conf. Ser.: Mater. Sci. Eng. 252 012058.

[123] http://www.eco-aesc-lb.com/en/product/liion_ev/

[124] S. Pelletier, O. Jabali, G. Laporte and M. Veneroni, "Battery degradation and behaviour for electric vehicles: Review and numerical analyses of several models", Transportation Research Part B: Methodological, vol. 103, 2017, pp. 158-187.

[125] https://www.openchargealliance.org/

[126] A.A.Ahmadi, "Theory of convex functions", Princeton University press, 2015.

[127] Byrd R.H., Hribar M.E., Nocedal J., SIAM Journal on Optimization, 1999.

[128] H.C. Wu,"The Karush–Kuhn–Tucker optimality conditions in an optimization problem with interval-valued objective function", European Journal of Operational Research, vol. 176, 2007, pp. 46-59.

[129] L. Sun, X. Song and T. Chen, "An Improved Convergence Particle Swarm Optimization Algorithm with Random Sampling of Control Parameters", Journal of Control Science and Engineering, 2019.

[130] C-H. Hwang and AS.M. Masud, Abu, Multiple Objective Decision Making—Methods and Applications: A State-of-the-Art Survey, 1979, 10.1007/978-3-642-45511-7.

[131] C. Deng, N. Liang, J. Tan and G. Wang, Multi-Objective Scheduling of Electric Vehicles in Smart Distribution Network, Sustainability, November 2016.

[132] K. Knezovic, A. Soroudi, M. Marinelli, and A. Keane, Robust Multi-Objective PQ Scheduling for Electric Vehicles in Flexible Unbalanced Distribution Grids, IET Generation Transmission and Distribution, 11(16), pp. 4031-4040, 2017.

[133] G. Mavrotas, Effective implementation of the ε-constraint method in Multi-Objective Mathematical Programming problems, Applied Mathematics and Computation, Vol. 213, pp. 455-465, 2009.

[134] R.W. Saaty, The analytic hierarchy process—what it is and how it is used, Mathematical Modelling, Vol. 9, pp. 161-176, 1987.

[135] G. Platt, The Decentralised Control of Electricity Networks Intelligent and Self-Healing Systems, 2007.

[136] A. Baliyan, K. Gaurav and S. Kumar Mishra, A Review of Short Term Load Forecasting using Artificial Neural Network Models, Procedia Computer Science, Vol. 48, 2015, pp. 121-125.

[137] https://www.ovoenergy.com/electric-cars/vehicle-to-grid-charger

[138] S. Nagamitsu, R. Gondo, N. Nagaoka, A.A.A. Al-karakchi, G. Putrus and Y. Wawng, "A Battery Diagnostic Method for Smart EV Charger Employing a Pulse Current Method for Prolonging Battery Life Time", 53rd International Universities Power Engineering Conference (UPEC), Glasgow, 2018.

[139] https://nuvve.com/

[140] https://innovation.ukpowernetworks.co.uk/projects/transpower-vehicle-to-grid/

[141] https://www.ofgem.gov.uk/data-portal/breakdown-electricity-bill

[142] G. A. Putrus, P. Suwanapingkarl, D. Johnston, E. C. Bentley and M. Narayana, Impact of electric vehicles on power distribution networks, 2009 IEEE Vehicle Power and Propulsion Conference, Dearborn, MI, pp. 827-831, 2009.

[143] https://www.gov.uk/government/statistics/solar-photoVoltaics-deploymen

[144] https://www.gov.uk/government/statistics/energy-consumption-in-the-uk

[145] R. Cleenwerck, Potentieel van een smart grid om de energieautonomie van een stadsgebouw te verhogen: een case study in Kortrijk, a Masters Thesis, 2017.

[146] B. Rotthier, B. Derijcke, R. Leenders, N. Van den Steen, B. Huyck and J. Capelle, Comparison of the contribution of smart charging. V2G and energy demand reduction to the energy autonomy of a Belgian city depot, Electric Vehicle Symposium 31, October 2018.

[147] R. S. Walia, H. S. Shan and P. Kumar, Multi-Response Optimisation of CFAAFM Process Through Taguchi Method and Utility Concept, Materials and Manufacturing Processes, Vol. 21, pp. 907-914, 2006.

[148] G. Kong and D. Zhu, "An Improved NIRA Algorithm of Nash Equilibrium and Its Application," *2007 IEEE International Conference on Automation and Logistics*, Jinan, 2007, pp. 2580-2585.

[149] Krawczyk, Jacek & Zuccollo, James. (2007). NIRA-3: An improved MATLAB package for finding Nash equilibria in infinite games.

[150] https://www.ofgem.gov.uk/consumers/household-gas-and-electricity-guide/consumer-guide-understanding-energy-meters-ofgem

[151] https://domestic.utilitysavingexpert.com/index.html?db=electric

[152] https://www.consumercouncil.org.uk/sites/default/files/2018-06/Economy%207%20Price%20Comparison%20Table%201%20June%202018.pdf

[153] V2GB – Vehicle to Grid Britain – Requirements for market scale-up, Element Energy, June 2019. Public report available at: http://www.element-energy.co.uk/wordpress/wp-content/uploads/2019/06/V2GB_WP-4-report-Requirements-for-market-scale-up.pdf

[154] M. Nikolaou, Model predictive controllers: A critical synthesis of theory and industrial needs, Advances in Chemical Engineering, Academic Press, 2001, vol. 26, pp. 131-204.

[155] D. Huang, Y. Gu, H. Wang, Z. Liu, and J. Chen, “An Incentive Dynamic Programming Method for the Optimization of Scholarship Assignment,” Discrete Dynamics in Nature and Society, 2018.

[156] R. Bellman, The Theory of Dynamic Programming, Bulletin of the Americal Mathematical Society, vol 60, pp. 503-515, 1954

[157] J. Mahmoudimehr and P. Sebghati, "A novel multi-objective Dynamic Programming optimization method: Performance management of a solar thermal power plant as a case study", Energy, vol. 168, 2019, pp. 796-814.

[158] T. Zhao and J. Zhao, “Improved multiple-objective dynamic programming model for reservoir operation optimization”, Journal of Hydroinformatics, vol. 16, 2014.

Appendix A Appendix

A.1 Distribution network modelling

Let us consider the simple network outlined in Figure A.1-1; it has four buses, $n = 4$, interconnected through $n - 1 = 3$ feeders, represented by their admittances, $\overline{Y}_{1\to3}$. The paramters that decide the operational point of the network are the voltages and currents at each bus, namely $\overline{E}_{1\to3}$ and $\overline{I}_{1\to3}$, where the voltages are referred to one phase in a three phase system. Voltages, currents and admittances have been presented using the phasor representation, which implies these are complex dimensions. Although in this example and throughout this thesis only radial networks will be studied, as they are the common layout at low voltage, the methodology presented hereby can be also applied to meshed networks.

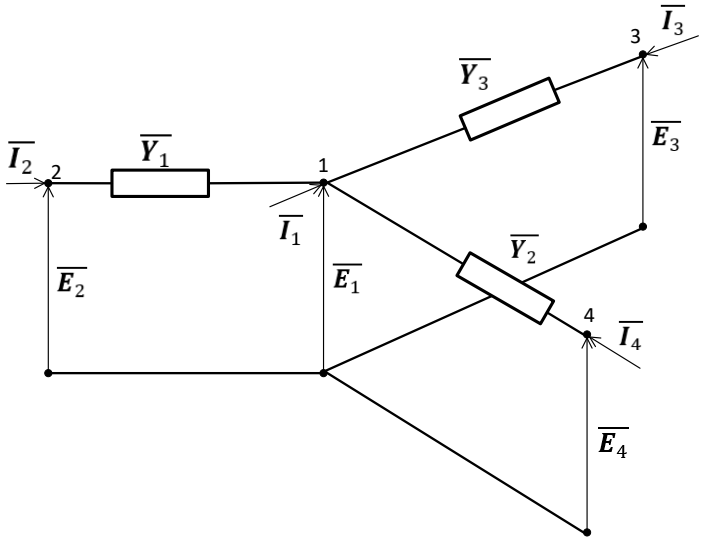

Figure A.1-1 Four buses, three feeders radial network

Next, the bus admittance matrix, or Y-matrix in short, is built, where a number of admittances are used to represent each bus and their interconnection. There are two classes of

admittances, self-admittances and mutual-admittances. Naturally, self-admittances explicate the relationship of one bus with respect to itself, while mutual-admittances model the connections between two buses. With reference to the network represented in Figure A.1-1, the self-admittances can be calculated as:

$$\overline{\boldsymbol{Y}_{11}} = \left(\frac{\overline{\boldsymbol{I}_1}}{\overline{\boldsymbol{E}_1}}\right)_{\overline{\boldsymbol{E}_2},\ \overline{\boldsymbol{E}_3},\overline{\boldsymbol{E}_4}=0} = \overline{\boldsymbol{Y}_1} + \overline{\boldsymbol{Y}_2} + \overline{\boldsymbol{Y}_3} \tag{A.1.a}$$

$$\overline{\boldsymbol{Y}_{22}} = \left(\frac{\overline{\boldsymbol{I}_2}}{\overline{\boldsymbol{E}_2}}\right)_{\overline{\boldsymbol{E}_1},\ \overline{\boldsymbol{E}_3},\overline{\boldsymbol{E}_4}=0} = \overline{\boldsymbol{Y}_1} \tag{A.1.b}$$

$$\overline{\boldsymbol{Y}_{33}} = \left(\frac{\overline{\boldsymbol{I}_3}}{\overline{\boldsymbol{E}_3}}\right)_{\overline{\boldsymbol{E}_1},\ \overline{\boldsymbol{E}_2},\overline{\boldsymbol{E}_4}=0} = \overline{\boldsymbol{Y}_2} \tag{A.1.c}$$

$$\overline{\boldsymbol{Y}_{44}} = \left(\frac{\overline{\boldsymbol{I}_4}}{\overline{\boldsymbol{E}_4}}\right)_{\overline{\boldsymbol{E}_1},\ \overline{\boldsymbol{E}_2},\overline{\boldsymbol{E}_3}=0} = \overline{\boldsymbol{Y}_3} \tag{A.1.d}$$

In this syntax, $\overline{\boldsymbol{Y}_{ii}}$ is the self-admittance of the bus i and is defined as the sum of the admittances of all the feeders that are connected to bus i. The mutual-admittances of the above network can be defined as:

$$\overline{\boldsymbol{Y}_{12}} = \left(\frac{\overline{\boldsymbol{I}_1}}{\overline{\boldsymbol{E}_2}}\right)_{\overline{\boldsymbol{E}_1},\ \overline{\boldsymbol{E}_3},\overline{\boldsymbol{E}_4}=0} = -\overline{\boldsymbol{Y}_1} \tag{A.2.a}$$

$$\overline{\boldsymbol{Y}_{13}} = \left(\frac{\overline{\boldsymbol{I}_1}}{\overline{\boldsymbol{E}_3}}\right)_{\overline{\boldsymbol{E}_1},\ \overline{\boldsymbol{E}_2},\overline{\boldsymbol{E}_4}=0} = -\overline{\boldsymbol{Y}_2} \tag{A.2.b}$$

$$\overline{\boldsymbol{Y}_{14}} = \left(\frac{\overline{\boldsymbol{I}_1}}{\overline{\boldsymbol{E}_4}}\right)_{\overline{\boldsymbol{E}_1},\ \overline{\boldsymbol{E}_2},\overline{\boldsymbol{E}_3}=0} = -\overline{\boldsymbol{Y}_3} \tag{A.2.c}$$

$$\overline{\boldsymbol{Y}_{23}} = \left(\frac{\overline{\boldsymbol{I}_2}}{\overline{\boldsymbol{E}_3}}\right)_{\overline{\boldsymbol{E}_1},\ \overline{\boldsymbol{E}_2},\overline{\boldsymbol{E}_4}=0} = \overline{\boldsymbol{Y}_{24}}, \overline{\boldsymbol{Y}_{24}}, \overline{\boldsymbol{Y}_{34}} = 0 \tag{A.2.d}$$

Where the mutual-admittance $\overline{\boldsymbol{Y}_{ij}}$ is the ratio between the current $\overline{\boldsymbol{I}_i}$ at bus i and the voltage $\overline{\boldsymbol{E}_j}$ at bus j when all the other voltages in the circuit have been shorcircuited. This corresponds to the opposite of the admittance of the feeder that connects the two buses. If the two buses are not connected, than the associated mutual-admittance is nil. The complete bus-admittance matrix for the sample network is therefore defined in the equation below:

$$\overline{\boldsymbol{Y}} = \begin{bmatrix} \overline{\boldsymbol{Y}_1} + \overline{\boldsymbol{Y}_2} + \overline{\boldsymbol{Y}_3} & -\overline{\boldsymbol{Y}_1} & -\overline{\boldsymbol{Y}_2} & -\overline{\boldsymbol{Y}_3} \\ -\overline{\boldsymbol{Y}_1} & \overline{\boldsymbol{Y}_1} & 0 & 0 \\ -\overline{\boldsymbol{Y}_2} & 0 & \overline{\boldsymbol{Y}_2} & 0 \\ -\overline{\boldsymbol{Y}_3} & 0 & 0 & \overline{\boldsymbol{Y}_3} \end{bmatrix} \quad \text{(A.3)}$$

It can be seen that the self-admittances are the diagonal elements of the Y-matrix, whereas the mutual-admittances are the off-diagonal elements. Evidently, the Y-matrix for a radial network will be highly sparse, as the buses are sequentially connected.

Once the Y-matrix is built, power flow analysis is implemented to depict the operation of the network, which will be influenced by the decisions made at the generation and consumption points. The main dimensions used to measure the efficiency of network operation are:

- Bus voltages
- Feeder currents
- Active losses.

In order to calculate these variables, different types of buses are defined, each having a number of variables that are pre-defined. There are three types of buses:

- Generation buses are PV: the supplied powers and voltage magnitudes are fixed. $\overline{\boldsymbol{P}_2}, \dots, \overline{\boldsymbol{P}_h}$ and $\left|\overline{\boldsymbol{E}_2}\right|, \dots, \left|\overline{\boldsymbol{E}_h}\right|$;
- Load buses are PQ: active and reactive powers are fixed. $\overline{\boldsymbol{P}_{h+1}}, \overline{\boldsymbol{Q}_{h+1}}, \dots, \overline{\boldsymbol{P}_n}, \overline{\boldsymbol{Q}_n}$;
- One Slack bus, which is often chosen as the transformer connection point in radial networks: the voltage magnitude is fixed and phase is nil. $\left|\overline{\boldsymbol{E}_1}\right|,\ \theta_1 = 0$.

Finally, the $2n - h - 1$ unknown variables to be determined by the power flow analysis are:

- $n - 1$ voltage phases, $\theta_2, \dots, \theta_n$
- and $n - h$ voltage magnitudes, $\left|\overline{\boldsymbol{E}_{h+1}}\right|, \dots, \left|\overline{\boldsymbol{E}_n}\right|$.

These unknown variables are determined through the resolution of the following system of equations, where at first the currents at each bus is expressed as functions of all bus voltages and the Y-matrix, as presented by

$$\begin{cases} \overline{\boldsymbol{I}_1} = \overline{\boldsymbol{Y}_{11}}\,\overline{\boldsymbol{E}_1} + \cdots + \overline{\boldsymbol{Y}_{1n}}\,\overline{\boldsymbol{E}_n} \\ \vdots \\ \overline{\boldsymbol{I}_n} = \overline{\boldsymbol{Y}_{n1}}\,\overline{\boldsymbol{E}_1} + \cdots + \overline{\boldsymbol{Y}_{nn}}\,\overline{\boldsymbol{E}_n} \end{cases} \tag{A.4}$$

Then, the complex powers at each bus are expressed as follows

$$\begin{aligned} &\overline{\boldsymbol{S}_k} = \overline{\boldsymbol{E}_k}\,\dot{\overline{\boldsymbol{I}_k}} = \overline{\boldsymbol{E}_k}\sum_{i=1}^{n}\dot{\overline{\boldsymbol{Y}_{k\imath}}}\,\dot{\overline{\boldsymbol{E}_\imath}} = \\ &E_k e^{j\theta_k}\sum_{i=1}^{n} Y_{ki}\,E_i e^{j(-\Psi_{ki}-\theta_i)} = E_k\sum_{i=1}^{n} Y_{ki}\,E_i e^{j(\theta_k-\Psi_{ki}-\theta_i)} \end{aligned} \tag{A.5}$$

In the syntax adopted above, $\dot{\overline{x}}$ represents the complex conjugate of the phasor x, Ψ_{ki} are the phase angles of the bus voltages. From equation 3.19, active and reactive powers at the buses are extracted as expressed in the following equations:

$$P_k = E_k\sum_{i=1}^{n} Y_{ki}\,E_i\,\cos(\theta_k - \Psi_{ki} - \theta_i) \tag{A.6.a}$$

$$Q_k = E_k\sum_{i=1}^{n} Y_{ki}\,E_i\,\sin(\theta_k - \Psi_{ki} - \theta_i) \tag{A.6.b}$$

For PV buses there are $h-1$ equations of type (a), while for PQ buses there are $2(\mathrm{n}-\mathrm{h})$ equations of type (a) and (b). Overall, there is a system of $2\mathrm{n}-2\mathrm{h}+h-1 = 2n-h-1$ equations, which being as same as the number of unknown variables, has unique solution.

A variety of numerical methods have been applied in literature for the power flow calculation, with the Newton-Raphson method being the most popular [97]. The steps of this algorithm are briefly outlined in the pseudo-code presented in Table A.1-1.

Table A.1-1 Pseudo-code for Newton-Raphson power flow calculation method

Newton-Raphson method

Input: Bus admittance matrix of the network $\overline{\boldsymbol{Y}}$, active powers and voltages of PV buses, $\overline{\boldsymbol{P}_2}, \dots, \overline{\boldsymbol{P}_h}$ and $|\overline{\boldsymbol{E}_2}|, \dots, |\overline{\boldsymbol{E}_h}|$, active and reactive powers of PQ buses $\overline{\boldsymbol{P}_{h+1}}, \overline{\boldsymbol{Q}_{h+1}}, \dots, \overline{\boldsymbol{P}_n}, \overline{\boldsymbol{Q}_n}$, error tolerance

$toll$

1: **Initialisation**: set $E_1 = E_2 = \cdots = E_n = 1$ and $\theta_1 = \theta_2 = \cdots = \theta_n = 0$

2: **while** $(\Delta \boldsymbol{P}, \Delta \boldsymbol{Q}) > \boldsymbol{toll}$

3: Calculate $(\overline{\boldsymbol{P}_{h+1}}^{*}, \overline{\boldsymbol{Q}_{h+1}}^{*}, \ldots, \overline{\boldsymbol{P}_{n}}^{*}, \overline{\boldsymbol{Q}_{n}}^{*})$ from equations 3.20.a and 3.20.b

4: Determine errors $\Delta \boldsymbol{P} = \begin{bmatrix} \overline{\boldsymbol{P}_{h+1}} - \overline{\boldsymbol{P}_{h+1}}^{*} \\ \vdots \\ \overline{\boldsymbol{P}_{n}} - \overline{\boldsymbol{P}_{n}}^{*} \end{bmatrix}$ and $\Delta \boldsymbol{Q} = \begin{bmatrix} \overline{\boldsymbol{Q}_{h+1}} - \overline{\boldsymbol{Q}_{h+1}}^{*} \\ \vdots \\ \overline{\boldsymbol{Q}_{n}} - \overline{\boldsymbol{Q}_{n}}^{*} \end{bmatrix}$

5: Calculate Jacobian $\boldsymbol{J} = \begin{bmatrix} \frac{\partial \boldsymbol{P}}{\partial \boldsymbol{E}} & \frac{\partial \boldsymbol{P}}{\partial \boldsymbol{\theta}} \\ \frac{\partial \boldsymbol{Q}}{\partial \boldsymbol{E}} & \frac{\partial \boldsymbol{Q}}{\partial \boldsymbol{\theta}} \end{bmatrix}$

6: Determine voltage and phase angle adjustments as $\begin{bmatrix} \boldsymbol{\Delta E} \\ \boldsymbol{\Delta \theta} \end{bmatrix} = \boldsymbol{J}^{-1} \begin{bmatrix} \boldsymbol{\Delta P} \\ \boldsymbol{\Delta Q} \end{bmatrix}$

7: Adjust voltage amplitude and phases $\boldsymbol{E} = \boldsymbol{E} + \Delta \boldsymbol{E}$ and $\boldsymbol{\theta} = \boldsymbol{\theta} + \boldsymbol{\Delta \theta}$

8: **end while**

Under the Newton-Raphson method for the resolution of systems of non-linear equations, voltage magnitudes and phases are initialised to arbitrary values. Active and reactive powers are subsequently calculated using the equations defined above in order to determine an error function. The Jacobian matrix is then employed to calculate the voltage magnitude and phase angle adjustments from the error function. The process stops when the error is below a pre-defined tolerance.

A.2 Definition of a mathematical optimisation problem

Let f be a mathematical function of a variable x defined by the following equation:

$$f(x): \mathbb{R} \rightarrow \mathbb{R} \tag{A.7}$$

Where x belongs to the set of real numbers. The above definition states that f associates one real number to each and every real numbers. In this case the *domain* of f is the whole set of

real numbers, but in general we will consider subsets $X \subset \mathbb{R}$. Now, let us consider the definitions below:

Definition 4.

$$x^* \; is \; global \; minimum \; of \; f: \mathrm{X} \to \mathbb{R} \;\; if \; \forall x \in X \;\; f(x^*) \leq f(x) \tag{A.8}$$

Similarly the definition of *local minimum* is provided hereby.

Definition 5.

$$x^* \; is \; local \; minimum \; of \; f: \mathrm{X} \to \mathbb{R} \;\; if \; \exists \varepsilon > 0 \; s.t. \;\; f(x^*) \leq f(x) \; \forall \{x \in X\} \cap \{|x - x^*| < \varepsilon\} \tag{A.9}$$

Hence, *local minima* are defined in a subregion of X. Now, more details on the function's domain: in general X is an Eucledian space in $\mathbb{R}^n = \mathbb{R} \times \mathbb{R} \times ... \times \mathbb{R} \; n \; times$; it is a finite n-dimensional vector space where the *inner product* among n-dimensional vectors can be computed. Which now means that the variable x is n-dimensional (it is a vector $x \in \mathbb{R}^n$). X is often defined by a set of constraints, in the following forms:

$$A^i x \leq b^i \tag{A.10}$$

$$A^e x = b^e \tag{A.11}$$

The former is a set of m inequality constraints and the latter is a set of m equality constraints, defined by $\boldsymbol{A}_{m \times n}$ matrices and $\boldsymbol{b}_{m \times 1}$ vectors. If the above expressions are verified, we will say that $x \in X$. Next, the definition of a continuous function:

Given a function $f: \mathrm{X} \to \mathbb{R}$, f is *continuous in* $x_0 \in X$ if :

$$\forall \varepsilon > 0 \, , \exists \delta > 0 \; s.t. \; \forall \{x \in X\} \cap \{|x - x_0| < \delta\} \Longrightarrow |f(x) \; - f(x_0) \,| < \varepsilon \tag{A.12}$$

The above definition is important because of the following theorem

Theorem1: Extreme value theorem (Weirstrass)

If f is a real-valued function in a compact space X,then f has at least a maximum and a minimum

The proof of the above theorem is available in any calculus literature hence, it is not provided here. Also, considering that linear programming is widely adopted in mathematical optimisation but not proposed in this research, it is not defined here and instead convex optimisation is brought forward.

Definition 5.

$X \subset \mathbb{R}^n$ is a Eucledian space and it is said to be a *convex set* if

$\forall x, y \in X, \forall t \in [0,1]$ *the following expression holds*, $(1-t)\,x + t\,y \in X$ (A.13)

Subsequently:

Definition 6.

if $X \subset \mathbb{R}^n$ is a *convex set,* $f: \mathrm{X} \to \mathbb{R}$ is *a convex function* if

$\forall x, y \in X, \forall t \in [0,1]$ *the following expression holds,* (A.14)

$f\big((1-t)\,x + t\,y\big) \leq f(x)(1-t) + t\,f(y)$

The above definition, coupled with 5.2 and 5.3 are important because of the following corollary.

Corollary 1.

In an unconstrained optimisation problem, $\underset{x \in \mathbb{R}^n}{argmin}\, f(x)$*, where* f *is convex and differentiable, any point* x^* *that verifies* $\nabla f(x^*) = 0$ *is a global minimum.*

The proof is presented in The proof is provided in [126].

Crucially, if the above is verified, from the Extreme value theorem, there exists a minimum, and it is global. Needles to say that this is a major conclusion that greatly improves the

chances of solving a non-linear optimisation problem. Few last definitions are the following ones:

Definition 7.

$\underset{x\in\mathbb{R}^n}{argmin}\, f(x)$ *is the argument* $x^* \in \mathbb{R}^n$ *that minimises* $f(x)$

Definition 8.

$\underset{x\in\mathbb{R}^n}{min}\, f(x)$ *is the minimum value of* f *when* $x \in \mathbb{R}^n$

$f(x)$ *is called objective function and* x *is the decision variable*

Finally, a major concerning fact is that, if the convexity (concavity) conditions are not met, the existence of a global minimum (maximum) is not guaranteed. Therefore, convex optimisation algorithms will only find local minima, and meta-heuristic algorithms could be used to find global minima.

A.3 Algorithms for mathematical optimisation

Interior point algorithm

Input: Objective function $f(x)$ and set of constraints $c_i(x) = b_i, i = 1,2,\dots,m$

Initialisation: Select feasible starting point $x_0 \in \mathbb{R}^n\ s.t.\ c_i(x) = b_i$ and convergence tolerance ε^{tol}

Set initial iteration $k = 0$ and KKT values, defined by (5.13) – (5.16), as $\mathbf{K} = +\infty$

while $\mathbf{K}_k > \varepsilon^{tol}$ **do**

  $k \leftarrow k + 1$

  $\mu_{k+1} \leftarrow c\,\mu_k, c < 1$

  Define augmented objective function from (5.12)

  Define system of KKT conditions

  Solve system on non-linear equations with Newton-Raphson and obtain $\mathbf{K}_k$

end while

Particle Swarm optimisation

Input: Objective function $f(x)$ and set of constraints $c_i(x) = b_i, i = 1,2, \dots, m$

1: **Initialisation**: Generate random initial population $\mathrm{P}_p = \{x \in \mathbb{R}^n | h(x) = 0 \cap g(x) \geq 0\}$, iteration $k = 0$ and set maximum number of iterations k^{max}. Initialise particles' best personal positions as $p_{i,0} = f(x_{i,0})\ \forall i$ and swarm's global best position as g_0

2: **while** $k < k^{max}$ **do**

3: $k = k + 1$

4: Update $\varphi_{p,k} = 0.99\ \varphi_{p,k}$ and $\varphi_{g,k} = 0.99\ \varphi_{g,k}$ and randomly generate $\xi_p, \xi_g \sim U(0,1)$

5 **for** $i \leftarrow 1$ **to** (p) **do**

6: Update particles' velocity following (5.18)

7: Update particles' position following (5.19)

8: **end for**

9: **end while**

A.4 Setting for case study 2

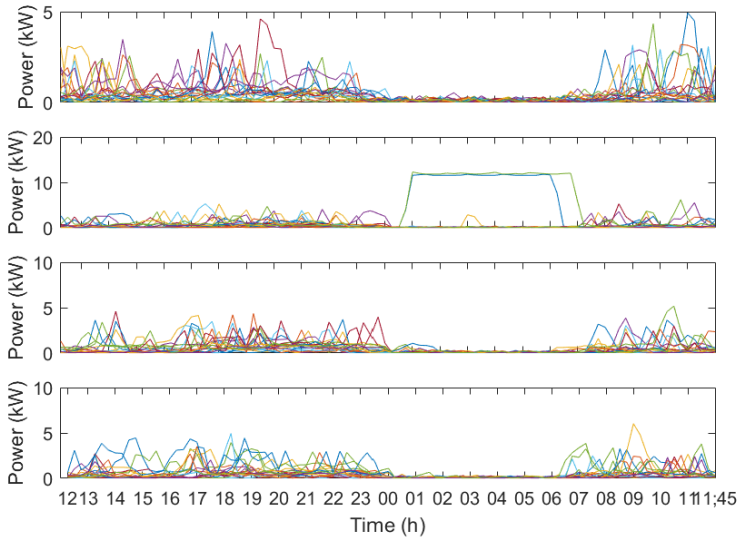

Figure A.4- 1 Electricity demand profiles for 19 houses in winter (weekday and weekend) and spring (weekday and weekend)

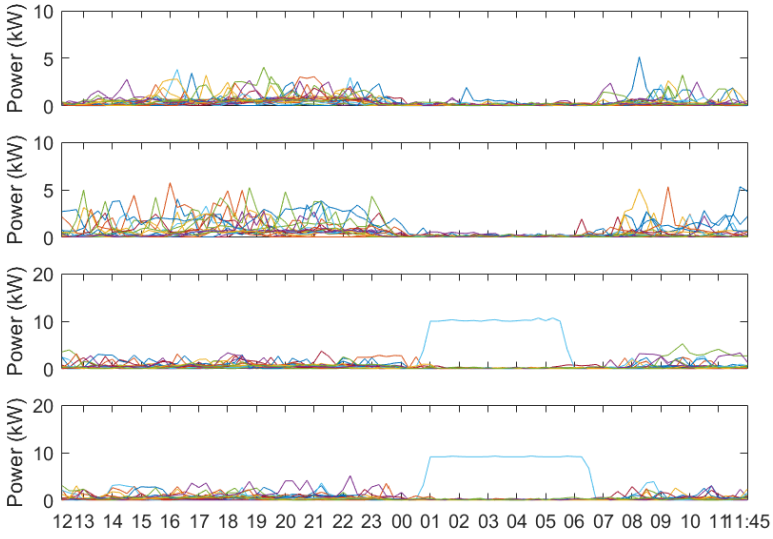

Figure A.4- 2 Electricity demand profiles for 19 houses in summer (weekday and weekend) and autumn (weekday and weekend)

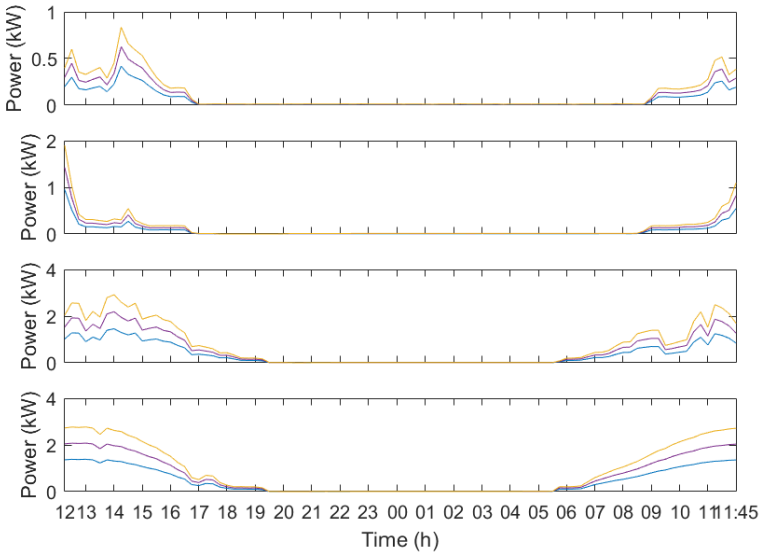

Figure A.4- 3 PV generation profiles for installation sizes 1, 2 and 3 kWp (larger installation provides higher power) in winter (weekday and weekend) and spring (weekday and weekend)

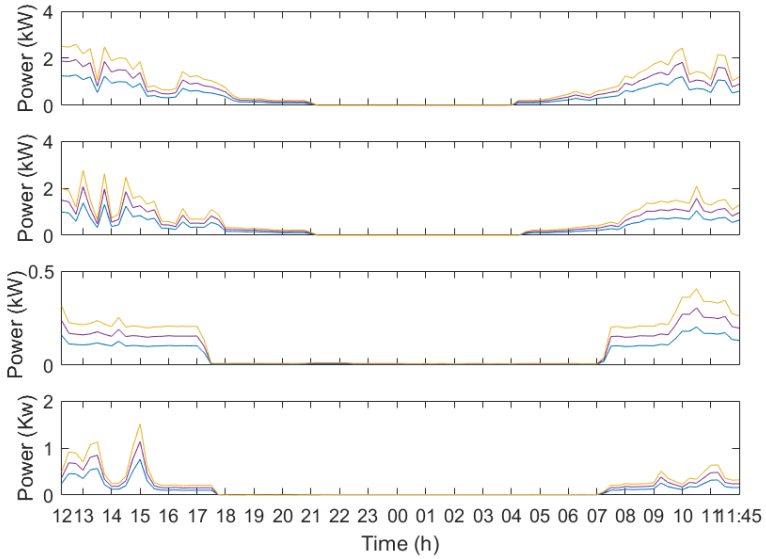

Figure A.4- 4 PV generation profiles for installation sizes 1, 2 and 3 kWp (larger installation provides higher power) in summer (weekday and weekend) and autumn (weekday and weekend)

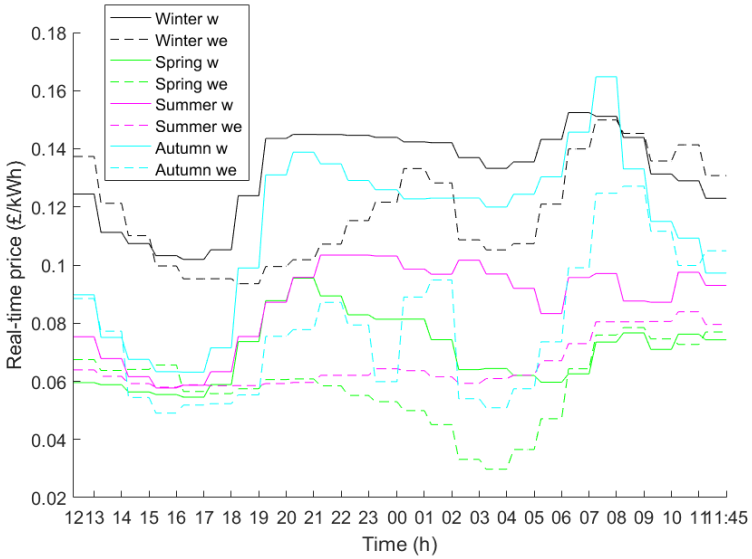

Figure A.4- 5 Electricity price profiles for eight days distributed accross one year

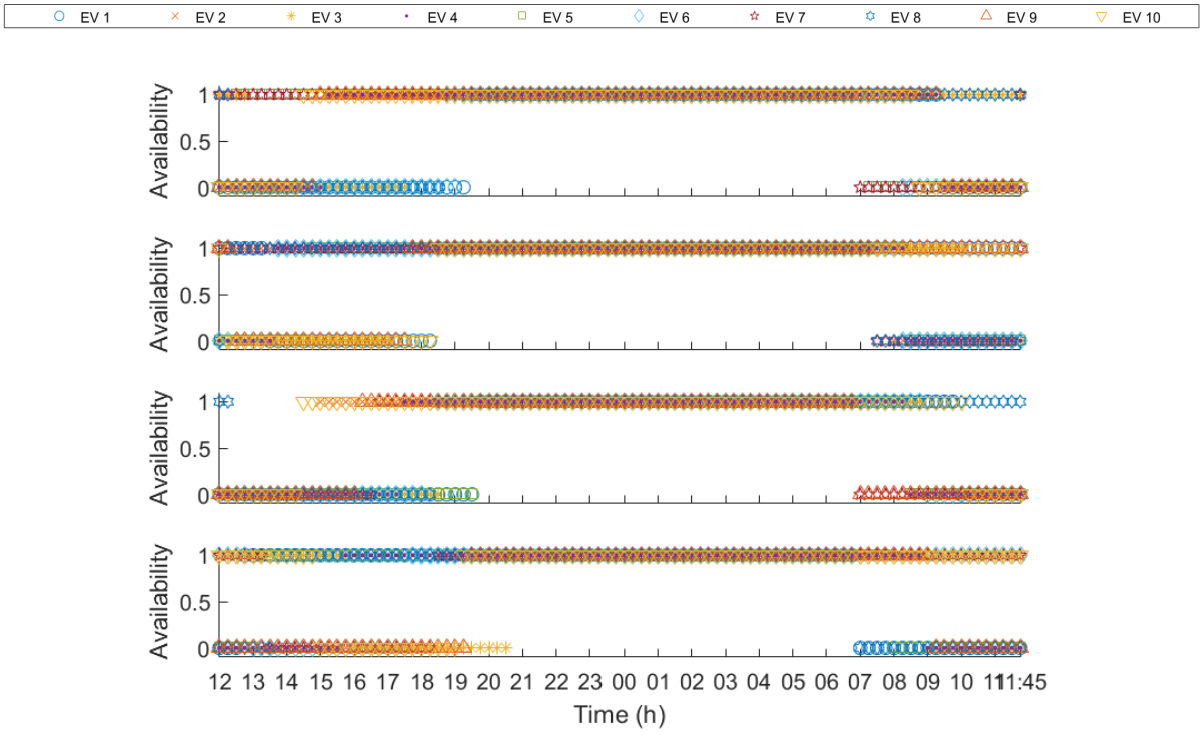

Figure A.4- 6 Availability at home for 10 EVs in winter (weekday and weekend) and spring (weekday and weekend)

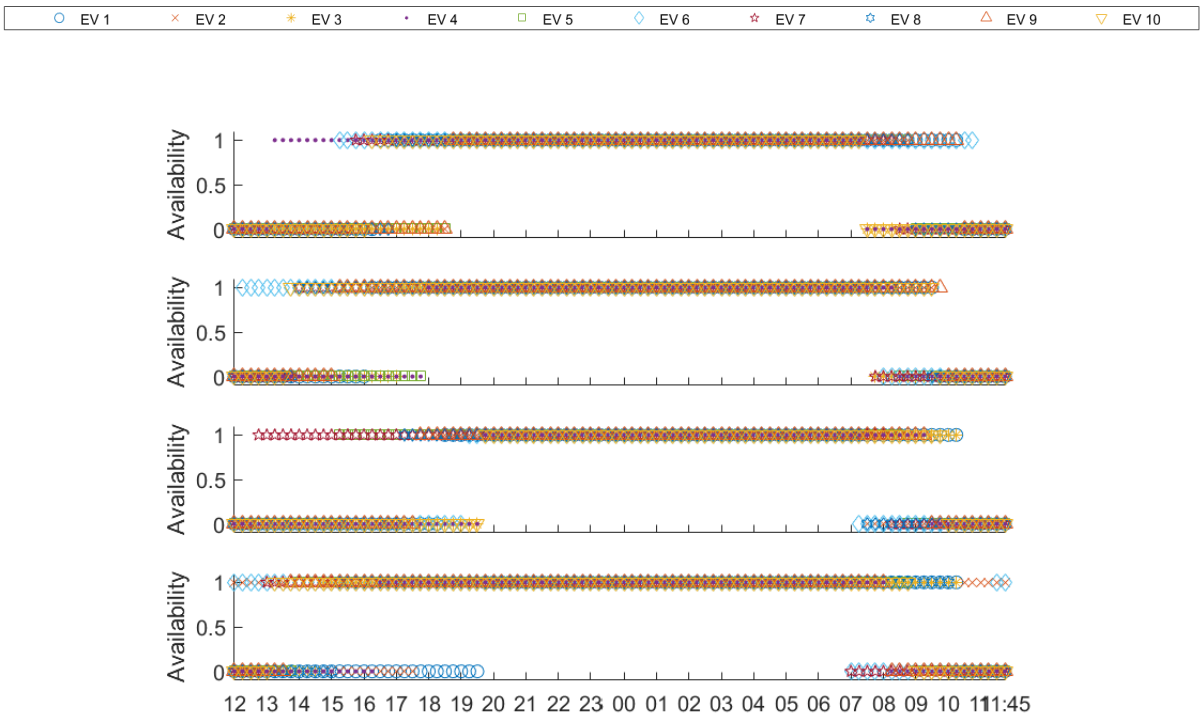

Figure A.4- 7 Availability at home for 10 EVs in summer (weekday and weekend) and autumn (weekday and weekend)

A.5 Decentralised MOO results

Considering the framework proposed in Chapter 6.2, if a PV installation is available, then assuming that the energy generation from the PV system cause zero-emission (life cycle CO_2 emissions are out of scope for this research) it follows that by minimizing grid net exchange CO_2 emission is also minimised. If the PV installation is not available, then emissions are minimised if the EV discharges in periods with high specific CO_2/kWh. In the present work, we assume that a PV system is available. shows the result of the ANEC method minimizing both CO_2 emission and grid net exchange. Given the negligible variation of the two objective functions among the 11 Pareto optimal solutions, we consider grid net exchange and CO_2 emission minimisation to be equivalent.

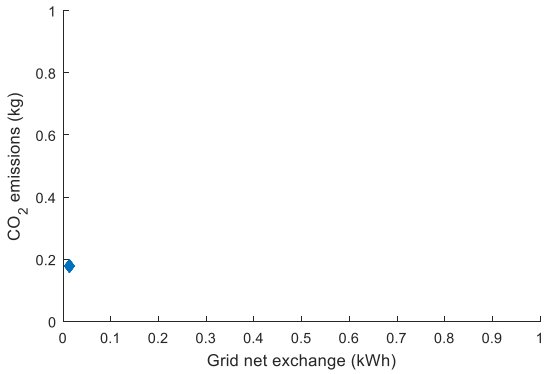

Figure A.5- 1 Bi-objective optimisaiton of CO2 emissions and grid net exchange

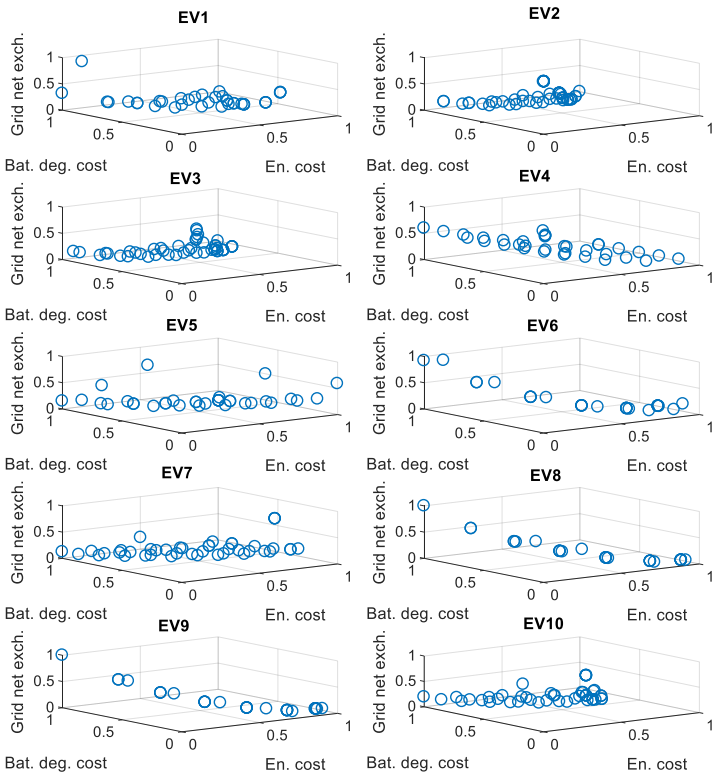

Figure A.5- 2 Pareto fronts for 10 EVs, under scenario 2c) in Chapter 6.2